Università degli Studi di Palermo

AREA QUALITÀ, PROGRAMMAZIONE E SUPPORTO STRATEGICO
SETTORE STRATEGIA PER LA RICERCA
U. O. DOTTORATI

Dottorato in Scienze della Terra e del Mare
DIpartimento di Scienze della TErra e del Mare
Settore Scientifico Disciplinare (GEO-02/03)

Quaternary tectonics from landscape evolution in southern Italy: new clues from a multidisciplinary morphometric approach

IL DOTTORE
Nicolò Parrino

IL COORDINATORE
Prof. Marco Milazzo

IL TUTOR
Attilio Sulli

CO-TUTOR
Pierfrancesco Burrato
Fabrizio Pepe

CICLO XXXIV
ANNO CONSEGUIMENTO TITOLO 2022

Summary

Thesis Introduction

The largest part of the earth surface corresponds to Low Strain Rate regions (LSRr), deforming at a rate less than 1 mm/yr. Such regions can be characterized by both localized and distributed deformation, the second of which often host tectonic structures whose recent activities are not characterized by a well-defined morphological signature. Such "elusive" faults frequently share the tectonic loading between each other, implying that:

a) slip rate can be similar or lower than the erosion rate, and thus, active faults could have no clear morphological signature;
b) active structures can be blind;
c) an imposing structural inheritance could hide their morphological signature;
d) active faults can become dormant for long periods, and thus, their recurrence time could exceed the temporal resolution of historical and instrumental catalogues;
e) a massive quake on one fault could load other remote faults, and thus, such regions could experience episodic and spatially migrating quakes;
f) moreover, further complications may arise if LSRr are located partially offshore, like coastal areas and, thus, not considered offshore or partially offshore. Active faults in such areas can lead to an underestimation of the region's seismic hazard.

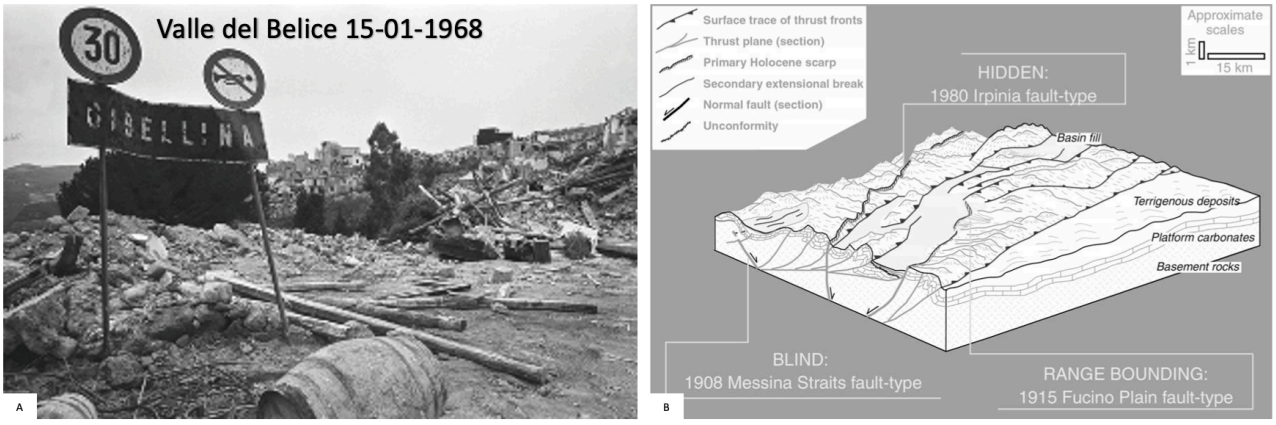

Fig. 1 – A) Picture of the epicentre of the 1968, Mw 6.4 Valle del Belice earthquake whose "elusive" seismogenic source is still debated; B) Types of "elusive" faults from Valensise, G. & Pantosti, D., (2001). Journal of Seismology. https://doi.org/10.1023/A:1011463223440

Despite the low seismic moment release recorded, geodetic and seismological evidence highlights that in such areas, the tectonic forcing is stronger enough to trigger significant but infrequent earthquakes but not enough to overprint the climatic forcing signature. This peculiar feature makes

these regions perfect natural laboratories to analyse how the onshore and offshore landscape evolution (LE) relates to climate and tectonic forcings.

One of the most valuable approaches that overcome these issues and identify active tectonic structures in such areas is to study their geomorphic signal and their LE. It is well known that topography and landscape are the results of two main forcings: a) the climatic and, b) the tectonic forcing.

Considering this, many authors in the last decades tried to understand how the tectonic and climatic forcings drive the LE and how we could use such information to assess the climatic change and seismic related hazards. These authors focused on how:

a) climate change influenced erosion and sedimentation rates,
b) erosion and sedimentation rates link to the LE in active tectonic areas, and
c) erosion and sedimentation products could allow understanding of how much tectonic and climatic forcing drive LE.

The climatic forcing, unlike the tectonic one, is characterized by a significantly broad wavelength, to the point of being almost global and it is well known that the temperatures starting from the beginning of the Quaternary period was characterized on average by a significant decrease and by the establishment of high-frequency oscillations between glacial and interglacial periods.

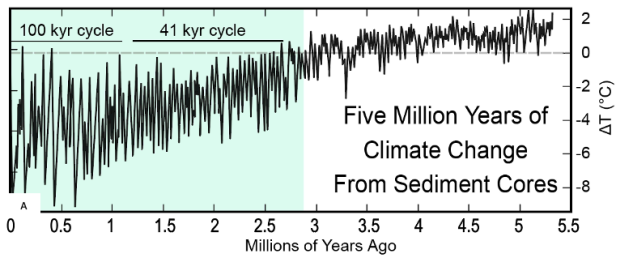

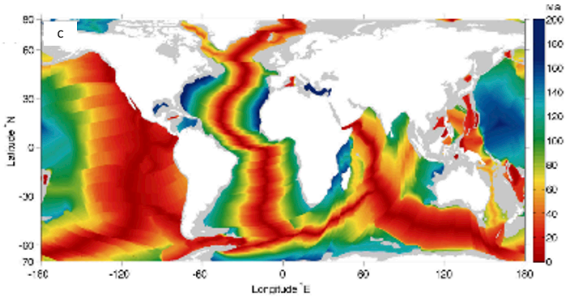

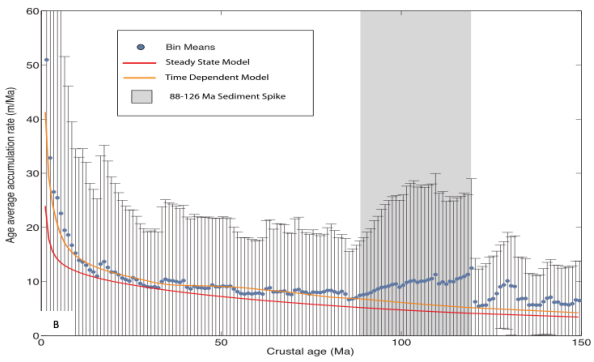

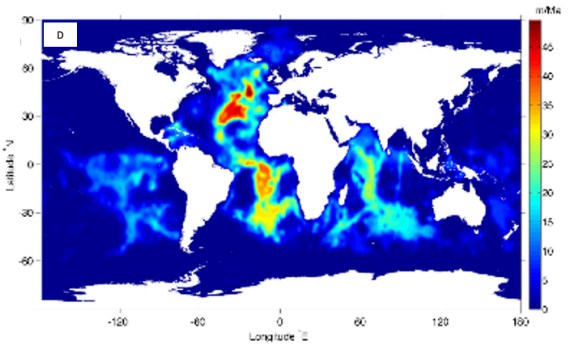

Fig. 2 – A) 5-million-year climate change, modified from Lisiecki, L. E., & Raymo, M. E.(2005). Paleoceanography. https://doi.org/10.1029/2004PA001071; B) Global ocean average sediment accumulation rate versus crustal age from Olson, P., et al. (2016). Geochemistry, Geophysics, Geosystems. https://doi.org/10/f8vk65; C) Age of the ocean crust from Muller, R. D., et al. (2008b), Geochem. Geophys. Geosyst. https://doi.org/10.1029/2007GC001743; D) Present-day global ocean sediment accumulation rate, from Archer, D. E. (1996b), Global Biogeochem. Cycles. https://doi.org/10.1029/96GB01521.

Such glacial and interglacial cycles have systematically changed the relative sea-level forcing the migration of the base level of erosion, that is, the level upstream of which there are erosive processes and downstream of which occur mainly sedimentary processes.

Recent research (see Fig. 2) prove that higher sedimentation rates are recorded in correspondence with the youngest oceanic sediments. Such an increase in sedimentation rates testifies the increase in sedimentary flow and, consequently, the exasperation of both sedimentary processes and erosive processes in onshore areas. Considering the existing relationship between the climate and tectonic forcing in shaping the earth landscape, it is possible to study the climate forcing through approaches independent to the study of the landscape and it is also possible to measure the morphology of the landscape with high accuracy and precision. Consequently, it is possible to isolate the tectonic forcing as the only unknown variable to study it (see Fig. 3).

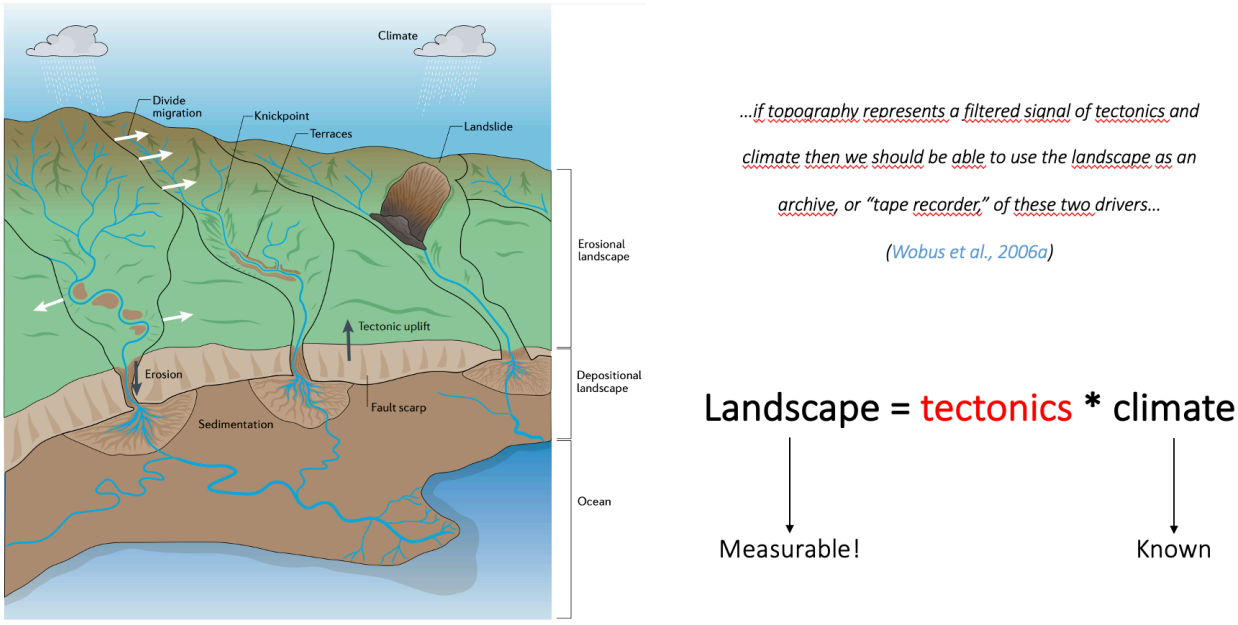

Fig. 3 – Main landscape evolution markers, the study of which allow the understanding of the variation of the main forcings responsible for the nowadays shape of the landscape. Image from Scheingross, J. S., et al., (2020). Nature Reviews Earth & Environment. https://doi.org/10.1038/s43017-020-0096-0.

The presented PhD thesis aims to:

1) develop a morphometric, structural and geophysics approach combining well-known methodologies from different branches of geologic knowledge into an original sequence.

3) tune this approach for LSRr and subsequently test it in areas with low and high deformation rates and offshore environments (Fig. 4).

2) study landscape evolution and the recent fault activity and test it in regions previously studied with standard approaches.

1. Research design: *Workflow implementation*
2. Tuning for *Low Strain Rate regions*
3. Testing in *Low and High Strain Rate regions*
4. *Testing in Offshore Landscapes*

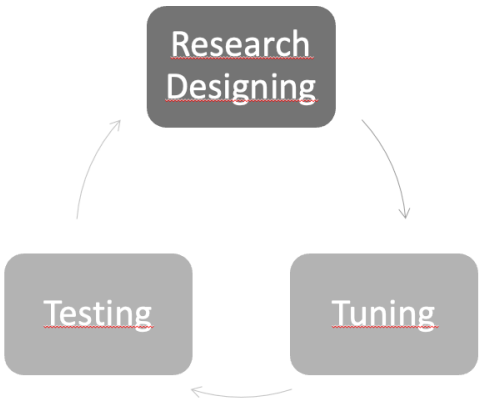

Fig. 4 – Workflow followed in the here presented PhD thesis.

The thus developed morphometric, structural, and geodetic approach is described in the case studies presented in the thesis chapters. In the first chapter of the thesis, a first developed multidisciplinary approach is described, which includes: 1) a morphometric analysis, 2) the reconstruction of a structural geological model of the subsoil through the reconstruction of geological sections and the interpretation of seismic profiles of the subsoil, 3) the analysis of a GNSS velocity field used as an independent variable and 4) the numerical modelling of the deformation produced by the reconstructed structures, carried out to validate the results obtained within an LSRr in NW-Sicily used as a natural laboratory for the tuning of the proposed approach. The second chapter of the thesis presents the application of a widely known approach to the analysis of active deformation to validate the results obtained in the first thesis chapter. The third chapter of the thesis illustrates the test of the multidisciplinary approach proposed in central Calabria (Southern Italy), a high strain rate region characterized by elusive active faults in which the knowledge of the seismotectonic framework has numerous gaps recognized in the literature. The fourth and final chapter describes the application of the multidisciplinary approach proposed in the submarine environment.

Accepted in Tectonophysics

Chapter 1

Elusive active faults in a low strain rate region (Sicily, Italy): hints from a multidisciplinary land-to-sea approach

Authors: Nicolò Parrino[1], Fabrizio Pepe[1], Pierfrancesco Burrato[2*], Gino Dardanelli[3], Marta Corradino[1], Claudia Pipitone[3], Maurizio Gasparo Morticelli[1], Attilio Sulli[1], Cipriano Di Maggio[1]

[1] Dipartimento di Scienze della Terra e del Mare, Via Archirafi 22, Università di Palermo, Italy.
[2] Istituto Nazionale di Geofisica e Vulcanologia, Rome, Italy.
[3] Dipartimento di Ingegneria, Viale delle Scienze, Università di Palermo, Italy.
[*] Corresponding author, e-mail: pierfrancesco.burrato@ingv.it

Keywords: Active deformation; Low strain rate regions; Land-to-sea approach; 3D Fault model; Morphotectonic evolution model; Northern Sicilian continental margin

Highlights

- A land-to-sea approach for identifying active faults in low strain rate regions
- Active faulting evidence along the northern Sicilian continental margin
- New relative GNSS deformation field in the study area
- 3D active fault geometric and kinematic parametrisation
- Landscape morphotectonic evolution model

Abstract

Low Strain Rate regions (LSRrs), i.e., areas undergoing tectonic deformation at rates of 1 mm/yr or less, often host important cities and highly vulnerable anthropogenic assets, and due to their subdued topography and relatively infrequent seismicity, are often considered low seismic hazard areas. Despite this, infrequent but high-magnitude earthquakes in such regions suggest that identifying active structures in the LSRr is one of the primary challenges for both the scientific community and modern societies. In such regions, one of the main issues in identifying active faults is the lack of valuable outcrop data due to erosional/sedimentary rates overwhelming the fault deformation one causing the hidden morphological signature of the tectonic structures.

This work proposes a multidisciplinary approach designed to detect active geological structures and their related deformation in such difficult areas. Our approach consists of quantitative morphotectonic, offshore and onshore tectonostratigraphic and GNSS joint analyses. To test this approach, we selected as a natural laboratory the partially offshore northern Sicilian LSRr (southern Italy), in the coastal sector located between the two major cities of Palermo and Termini Imerese. This area includes the compressional structures of the northern sector of the Apennine-Maghrebian fold and thrust belt, presently accommodating the slow Africa-Europe plate convergence.

The main results we achieved are: 1) new evidence of active tectonic deformation in this region; 2) the 3D modelling of two NNW-trending active faults; 3) the slip rate of a segment of the westernmost of the two detected faults; 4) a newly recorded relative GNSS velocity field; 5) a new morphotectonic map and morphotectonic evolution model of the study area. Our multidisciplinary approach allowed to shed new light on the active tectonic framework of a slowly deforming area that cross the coastline physical limit.

1. Introduction

The activation of previously unknown seismogenic faults in unexpected locations brought the scientific community to pay increasing attention to the seismotectonic of Low Strain Rate regions (LSRrs), i. e., regions deforming at a rate equal or less to 1 mm/yr, hosting previously undetected seismogenic sources and for that reason considered as seismically safe (Landgraf et al., 2017; Stein, 2007). However, significant destructive earthquakes in highly populated LSRrs, such as it is today the New Madrid seismic zone in the Midwestern USA, hit during the 19th century by a sequence of Mw 7 – 8 earthquakes (Newman et al., 1999; Tuttle et al., 2019), and Gujarat in north-western India, hit by the Mw 7.7, 2001 Bhuj earthquake, (Hough, 2002; McCalpin and Thakkar, 2003; Wesnousky et al., 2001), highlighted that the lack of knowledge about active faults in LSRrs does not imply the absence of seismic hazard and related risks (Campbell et al., 2015).

Active faults in LSRrs are usually elusive, and their inherent blind geometry hampers their identification due to their low deformation rates, frequently causing a subdued morphological signature, overprinted by faster climatic and anthropogenic processes. In a region with complex tectonic histories, they may be locally masked by the morphology of the inherited structures (e.g., Valensise and Pantosti, 2001), which, if reactivated, may be the sources of unexpected, destructive earthquakes. Further complications in identifying and mapping active faults may arise in LSRrs extending offshore caused by the necessity of available geophysical data to make up for the lack of directly observable evidence. Finally, the seismological characterisation of the active faults in LSRrs using historical data is not possible due to their long recurrence time that easily exceeds the temporal completeness of historical and instrumental seismic catalogues. An approach to overcome this issue would be using a paleoseismological approach after identifying the target faults (King et al., 2021). However, even in the absence of a detectable morphological signature of the active faults, the deformation related to movements on the fault planes propagate beyond fault tips forcing the landscape evolution (Burbank, D., Anderson, 2001; Wobus et al., 2006). As a consequence, quantitative morphometric analyses of topographic data allow the detection of actively deforming landscapes and, therefore, provide information on the parameters of the underlying controlling source, such as its geographical, geometrical, and stereological properties (Burrato et al., 2003; Goren et al., 2015; Vannoli et al., 2004).

In this work, we test a multidisciplinary land-to-sea approach to identify and parameterise elusive active faults developing in LSRrs. This approach differs from those relating the stratigraphic and structural evidence to the active fault parameters at the outcrop or seismic section scale because

we use fault dislocation modelling to invert the deformation evidence and derive the active fault parameters (De Santis et al., 2021; Meschis et al., 2020; Robertson et al., 2020; Tondi et al., 2021). The deformation data are collected using a multidisciplinary approach integrating morphometric, geological, and geophysical analyses to identify morphotectonic anomalies generated in response to the ongoing tectonic deformation. Geological and geophysical data are also used to detect near-surface secondary tectonic structures formed in response to the current strain field that can provide further information about the primary deformation source.

Although its conspicuous seismic release, due to the relatively low deformation rates, large portions of the Italian peninsula can be considered LSRrs located along the slowly converging African and European plate boundaries (Devoti et al., 2017, Fig. 1). A low seismic moment release characterises our study area along the northern coast of Sicily (southern Italy) in a partially offshore portion of the Sicilian Fold and Thrust Belt (SFTB), whose active shortening is about 1 mm/yr with respect to the foreland reference frame (Devoti et al., 2017; Ferranti et al., 2008; Mastrolembo Ventura et al., 2014). Although numerous authors documented the structural architecture and the recent deformation of this area (Avellone et al., 2011; Billi et al., 2010; Catalano et al., 2013; Del Ben and Guarnieri, 2000; Gasparo Morticelli et al., 2015; Guarnieri, 2004; Gugliotta et al., 2014; Henriquet et al., 2020; Pepe et al., 2005; Sulli et al., 2021; Totaro et al., 2017), the parametrisation of the geological structures accommodating the ongoing deformation still represents an open issue. Due to such uncertainties and its significative potential seismic-induced vulnerability (Cappadonia et al., 2021; Cappadonia and Cafiso, 2019), this area can be considered a natural laboratory for characterising elusive active faults through the inversion of the deformation evidence detected both onshore and offshore.

2. Study area overview

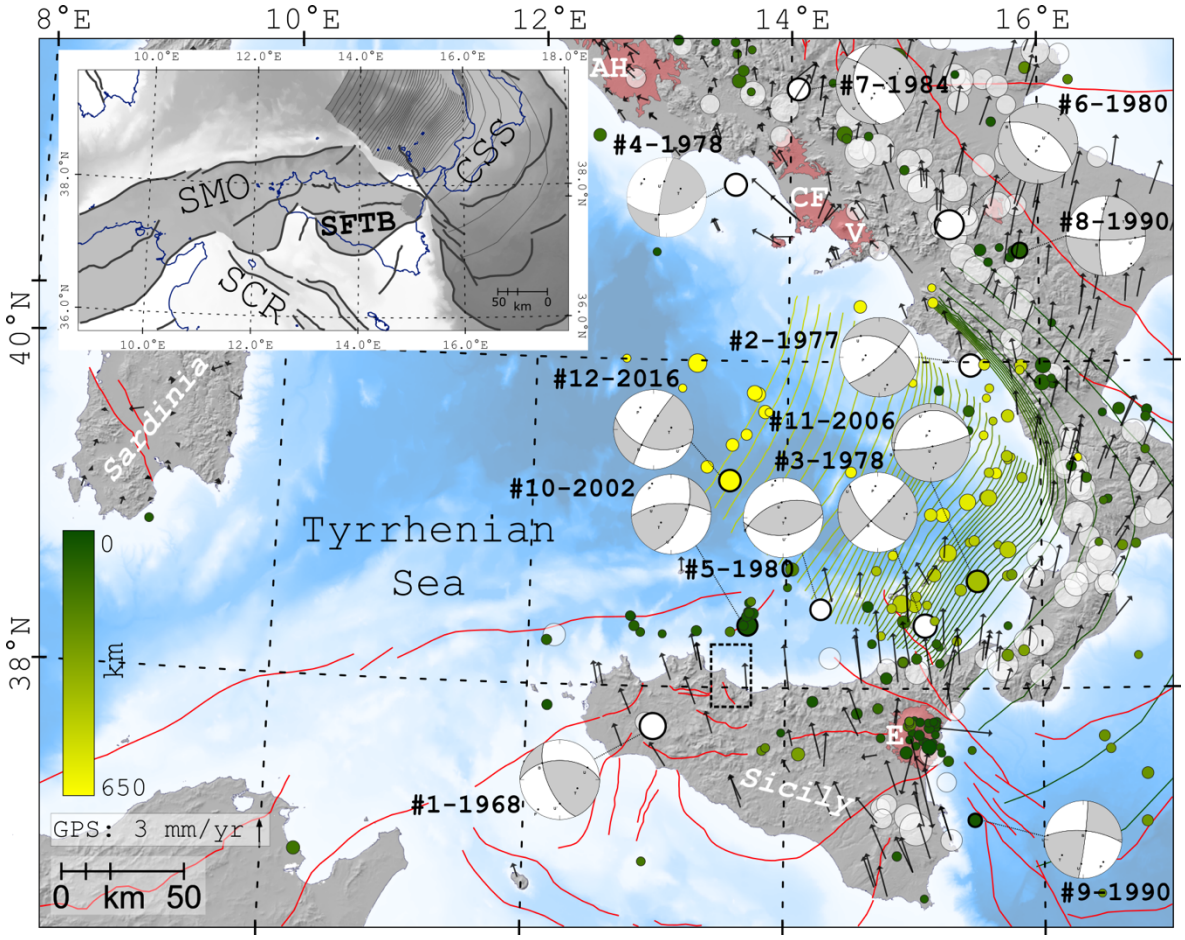

Fig. 1 - Seismotectonic framework of the central Mediterranean region. White circles show historical seismicity of M≥5.5 (Rovida et al., 2020). Green circles show the 1985-2020 INGV instrumental seismicity (ISIDe Working Group, 2007); circles are colour coded according to their hypocentral depth. The size of the circles is scaled to the magnitude of the earthquakes. Focal mechanisms, numbered as in Table S1, are from the Global CMT Catalogue (https://www.globalcmt.org/; Dziewonski et al., 1981; Ekström et al., 2012). The horizontal GNSS velocities in the Eurasian-fixed frame are shown with black arrows (Devoti et al., 2017). Main faults (red lines) and the subduction plane contours (colour coded according to the depth) are modified from the Structural Model of Italy (Bigi et al., 1992), a compilation of recent papers and the DISS database (https://diss.ingv.it/, DISS Working Group, 2021). Key to symbols: AH, Alban Hills; CF, Campi Flegrei; V, Vesuvius; E, Mt. Etna; CSS, Calabrian Subduction System; Sicily Channel Rift; SFTB, Sicilian Fold and Thrust Belt; SMO, Sicilian-Maghrebian Orogeny. Elevation data are from the EU-DEM (http://land.copernicus.eu/), the SRTM (OpenTopography, 2013) and EMODnet (http://www.emodnet-bathymetry.eu).

2.1 Tectonic overview

The study area falls within the central-western sector of the SFTB (Fig. 1) that is the result of two different geodynamic processes: 1) the retreat of the subduction hinge of the Ionian oceanic lithosphere and 2) the post-collisional convergence between Africa and Europe (R. Catalano et al., 2013b; Di Stefano et al., 2015; Faccenna et al., 2004; Sulli et al., 2021). A 25 km thick sequence of 1)

Permian-Paleogene platform-to-pelagic pre-orogenic carbonates, 2) Miocene syn-orogenic deposits covered by 3) Plio-quaternary carbonate and clastic deposits constitute the primary units of the SFTB (Catalano et al., 2002; R. Catalano et al., 2013a), which developed as a collisional system since the early Miocene (Catalano et al., 2013; R. Catalano et al., 2013a; Gasparo Morticelli et al., 2015; Gugliotta et al., 2014; Nigro and Renda, 2001; Roure et al., 1990). The shortening occurred in two subsequent thrusting-model-deformation phases and involved Mesozoic silico-carbonate succession developed on the African passive continental margin: an initial thin-skinned deformation phase was followed by a thick-skinned one (Catalano et al., 2013; Gasparo Morticelli et al., 2015). Two superimposed tectonic events developed during the thin-skinned deformation phase involving different structural levels (Avellone et al., 2010; Gugliotta and Gasparo Morticelli, 2012). The most surficial comprises a stack of thrust sheets composed mainly of deep-water units (Catalano et al., 2013b and c) that overthrusted a thick layer of platform carbonates since the Tortonian. Such carbonate platform rocks constitute the deeper structural level involved in the deformation through deep-seated thrust ramps, re-deforming the pre-existent structural architecture and locally re-activating Mesozoic extensional structures (Avellone et al., 2010; Giunta et al., 2000; Parrino et al., 2019). During this second event, numerous large-wavelength anticlines enucleated while syn-orogenic Tortonian sediments were deposited in wedge top basins (Balestra et al., 2019; Gugliotta et al., 2014; Gugliotta and Gasparo Morticelli, 2012). An extensional phase occurred in the inner sector of the SFTB during the late Pliocene to early Pleistocene (Pepe et al., 2000; Randazzo et al., 2020), causing 1) the formation of E-W trending sin-tectonic sedimentary basin, 2) the thinning of this crustal sector, and 3) a regional uplift process that affected the northern Sicilian continental margin (Di Maggio et al., 2017; Pepe et al., 2004). From about 0.8 Ma ago (Calabrian age), a tectonic reorganisation of the convergent Nubia-Eurasia margin in the central Mediterranean drove a shortening process driven by the Africa-Eurasia lithospheric collision (Billi et al., 2007; Goes et al., 2004; Sulli et al., 2019; Sulli et al., 2021; Zitellini et al., 2020).

The currently ongoing shortening of the central Mediterranean Sea, which still relates to the Africa-Eurasia lithospheric collision, can be depicted through the current GNSS velocity field that suggests a roughly NNW-SSE oriented Africa-Eurasia convergence with a velocity ranging around 1 mm/yr (Devoti et al., 2017; Ferranti et al., 2008; Mastrolembo Ventura et al., 2014, Fig. 1). Well breakouts, mapped active faults and seismological data confirm the kinematic framework depicted by the GNSS velocity field (Heidbach et al., 2018; Mariucci and Montone, 2020). Seismic catalogues show that the study area is a low to moderate seismicity sector with few Mw > 5.5 earthquakes. The most notable ones are the Mw 5.5 1726, the Mw 5.8 1823 and the Mw 5.9 2002 events (Rovida et al.,

2020), all of which occurred offshore in the southern portion of the Tyrrhenian Sea an area where all the recent events were characterised by compressional and transpressional fault plane solutions (Anderson and Jackson, 1987; Pondrelli et al., 2020Fig. 1).

The Neogene compressional events formed the prominent ridges outcropping (Fig. 2; Catalano et al., 2013c; Del Ben and Guarnieri, 2000) and caused the clockwise rotations (Channell et al., 1990; Speranza et al., 2018) accountable for the current orientation of the tectonic structure outcropping in the study area (Avellone et al., 2010; Oldow et al., 1990) through oblique thrusting and block rotation processes (Giunta et al., 2004; Guarnieri, 2004; Nigro and Renda, 2002). These ridges are surrounded by Neogene wedge-top sedimentary deposits that represent the youngest outcrop evidence of deformation available in the area (Gugliotta, et al., 2014; Nigro and Renda, 2001); hence, the only available geological information describing the ongoing tectonic activity are coastal erosional features providing information about a slow regional uplift (Fig. 3, Ferranti et al., 2006).

The first order geological structures outcropping in the study area are those bordering the carbonate reliefs of the Panormide, Trapanese and Imerese units (PaU, TrU, IUa and IUb, see acronyms in Fig. 2) and are mainly NNE-SSW, W-E and NNW-SSE oriented. Such structures superimpose the older carbonate units upon the younger clayey deposits.

The central-western portion of this area hosts mainly high-angle, NNE-SSW trending, reverse faults locally characterised by a left-lateral component of motion and deforming the carbonates of PaU. The EW-oriented structures in the southwestern portion of the study area consist of high-angle reverse faults locally characterised by a right-lateral component of motion. Conversely, the structures located in the south-eastern portion are primarily W-E and WNW-ESE -trending syncline structures bending deposits of the Trb and Ar-Gy (see acronyms in Fig. 2). NNW-SSE -oriented structures are located mainly in the central-eastern portion of the area (Fig. 2) and consist of high angle reverse faults, with a minor lateral component of motion, and anticlines. Anticline hinge zones outcrop both in the carbonate ridge (IUa and IUb) and the clayey hills (NF, see acronyms in Fig. 2). The trend of such structures changes from NNW-SSE to NW-SE moving toward the south.

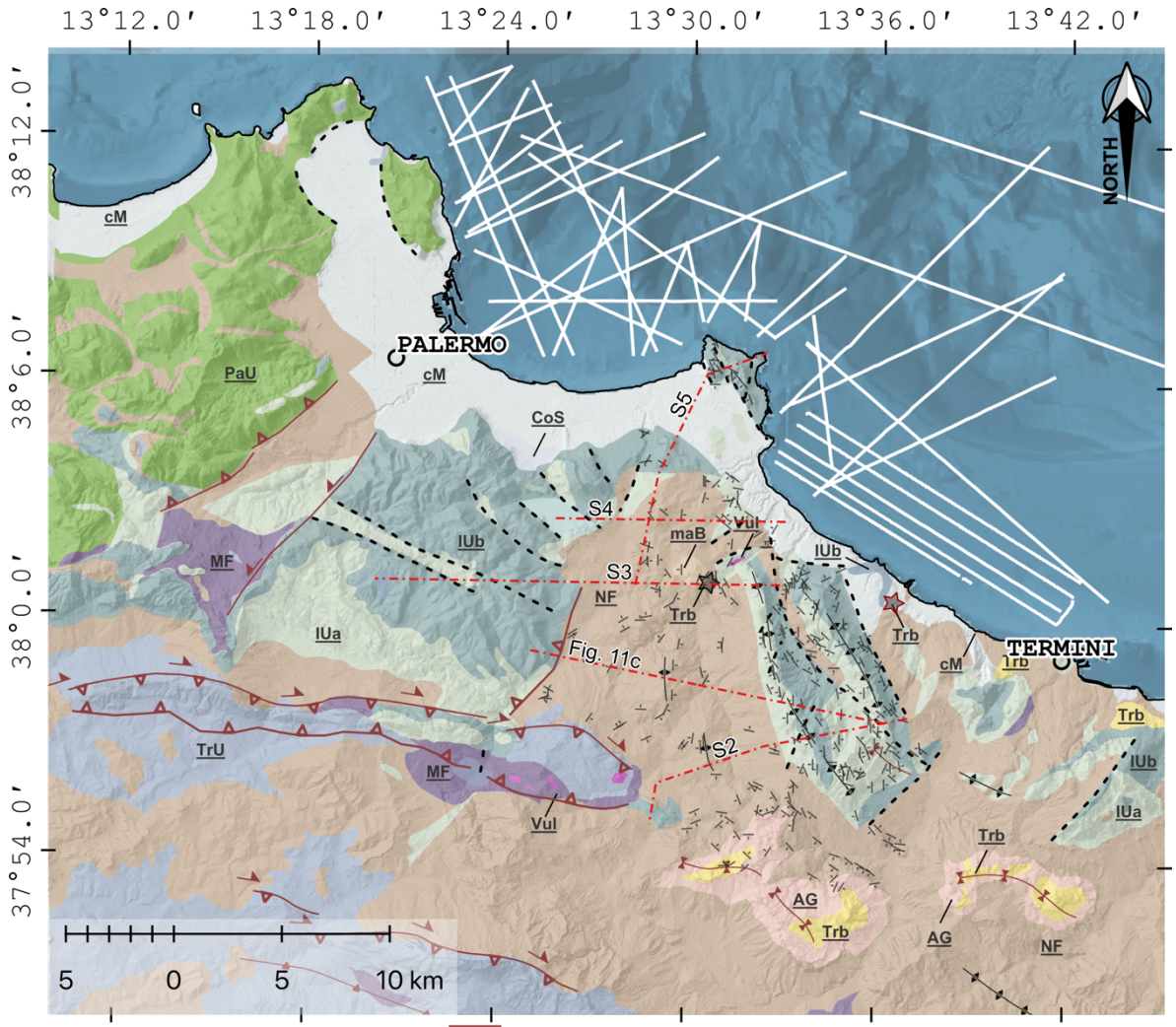

CoS, Continental and shore deposits, Holocene;
Vul, Vulcanites, Pleistocene;
cM, Sandstones and conglomerates, Calcareniti di Marsala Fm., upper Pliocene-lower Pleistocene;
maB, Turbidite sandstones and pelites, Marnoso-Arenacea del Belice Fm., Pliocene-lower Pleistocene;
Trb, Marly limestones, Trubi Fm., lower-middle Pliocene;
AG, Sandstones and marls, Arenazzolo Fm. - Gypsum II cycle, upper Messinian;
NF, Clays, quartz sandstones, Flysh Numidico Fm., upper Oligocene-lower Miocene;
PaU Biolithites, calcarenites, dolomitic limestones and Neptunian Dykes, Panormide units, upper Triassic-lower Cretaceous;
IUa, Marly limestones, calcareous breccias, turbidites, siliceous marls, basaltic pillows lavas, Crisanti Fm. - Caltavuturo Fm. (Imerese units a), lower Jurassic-lower Cretaceous;
IUb, Doloarenites, marly calcilutites, basaltic pillows lavas, Scillato Fm. - Fanusi Fm. (Imerese units b), upper Triassic-lower Jurassic;
MF, Clays, marls, calcilutites, calcarenites, basaltic pillows lavas, Mufara Fm. - Lercara Fm., Permian-upper Triassic;
TrU, Dolomites and Neptunian dykes, basaltic pillows lavas, calcilutites, marls, ammonitic limestones, radiolarites and shales, Trapanese units, upper Triassic-lower Cretaceous.

Fig. 2 - A) Simplified geology of the study area (modified from Catalano et al., 2013a, and reference therein). Black and red stars indicate the maximum elevation reached by Trubi Fm. outcrops. White traces indicate the whole offshore marine geophysical dataset. One of the geological sections is shown in Figure 11c; all the others are in the Supplementary material.

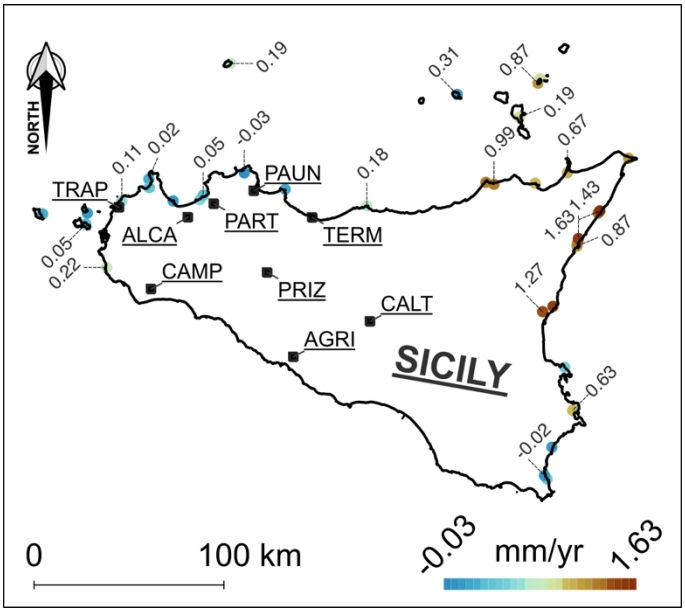

Fig. 3 –Black squares indicate the GNSS location of the UniPa CORS network. Coloured circles indicate the uplift values along the Sicilian coastline from Ferranti et al. (2006).

2.2 Geomorphic overview

The geomorphological evolution of Sicily results from the interaction between uplift, acting to elevate the relief, and river incision/denudation processes, tending to remove the younger upper clastic deposits and exhume the older underlying rocks. A staircase of marine terraces, river terraces and low relief surfaces, and a network of V-shaped valleys and canyons are the result of this interaction. Crustal shortening, thickening and consequent isostatic compensation are the causes of the continuous uplift of Sicily, whose subaerial evolution began between the late Pliocene (post-Trb Fm. deposition, see Fig. 2) and the beginning of the early Pleistocene (Di Maggio et al., 2017). Its geomorphological and topographic settings are characterised by landforms and physical landscapes progressively older from south to north (Hugonie, 1981; Di Maggio et al., 2017).

The study area is part of the central northern and northern zones of Sicily. The central northern zone shows a mountain landscape characterised by prominent landforms due to river downcutting, differential erosion, planation processes (Agnesi et al., 2000; Di Maggio, 2000), karst phenomena (Di Maggio et al., 2014, 2012) and coastal processes (e.g., Mauz et al., 1997). On a smaller scale, the mountain ranges broadly coincide with structural highs of the Mesozoic carbonate units, while the deep and large river valleys coincide with structural lows of the easily erodible Cenozoic deposits (Catalano et al., 2010a, 2010b). The northern coastal zone shows a landscape marked by significant and discontinuous topographic depressions consisting of a flat bottom (coastal plain) opened to the sea

and bounded to the inland by wide tectonically controlled coastal cliffs hundreds of meters tall. Middle-Upper Pleistocene marine terraces along the coastal plains are carved in the Calabrian (1.8 Ma to 0.78 Ma) coastal to neritic deposits and develop from sea level up to about 100-300 m a.s.l. (e.g., Catalano et al., 2010a, 2010c; Di Maggio, 2000). According to Hugonie (1981) and Di Maggio et al. (2017), the genesis of the cliffs can be traced back to an extensional 1.5–0.8 Ma old tectonic phase that triggered normal faulting as the peripheral consequence of the back-arc extension of the Tyrrhenian Sea. These faults resulted in the dismantling and collapse of the northern margin of the Sicilian Mountain belt under the Tyrrhenian Sea, allowing the deposition of the Calabrian deposits and the drowned faulted blocks. Since the Middle Pleistocene, these blocks gradually emerged, producing the present-day successions of marine terraces due to the interplay between coastal processes, uplift, and glacio-eustatic oscillations.

3. Materials and methods

This study is based on the integration of different geophysical, geomorphological, and geological analyses performed on the following datasets: (a) Global Navigation Satellite System (GNSS) data; (b) LIDAR Composite Digital Terrain Model (DTM), (c) single-channel, high-resolution (HR) seismic reflection data, (d) geomorphological, stratigraphic, and structural data from field survey and official maps. In addition, fault dislocation modelling was used to predict the tectonic-related deformation in the area between Palermo and Termini Imerese and its offshore prolongation.

3.1 Morphotectonics and morphometry

We performed field surveys, morphotectonic interpretation on Google Earth satellite imagery and morphometric analyses to recognise landforms directly produced or indirectly controlled by tectonics. Morphometric analysis was performed using a 2 m resolution DTM derived from a LIDAR acquired by the Regione Siciliana over the whole Sicilian territory (Regione Siciliana, 2010).

After a hydrological correction of the DTM through filling and carving algorithms (Schwanghart and Scherler, 2014), we extracted the drainage network, trunk streams, and river catchment areas using the D8 algorithm (O'Callaghan and Mark, 1984) and a threshold area of 20000 m^2 for the minimum channelled outflow.

To quantify the magnitude of the trunk stream lateral shift, we computed the transverse topographic symmetry factor (T-index) for each extracted drainage basin using an in-house developed semi-automated geospatial model following the workflow proposed by Cox, (1994). The T-index metric was computed using the following equation:

$$T = \frac{Da}{Dd} \qquad (1)$$

where Da is the distance between the river trunk stream and the basin midline, and Dd is the distance between the midline and the catchment drainage divide. Shift magnitude values vary from 0 and 1, with higher values indicating river asymmetry.

To assess the degree of iso-orientation of the obtained shift-direction, we computed the dispersion constant K (Fisher k values, Allmendinger et al., 2011; Fisher, 1953) for each river catchment as follows:

$$K = \frac{N-1}{N-R} \qquad (2)$$

where N is the number of poles, and R is the mean resultant vector's length.

We analysed the topography and the relief distribution by extracting swath profiles and calculating nested hypsometric integrals of drainage basins. A swath profile crossing the Eleuterio and Milicia trunk streams, roughly parallel to the coastline and perpendicular to the regional topographic gradient, was used to investigate the geometry of both rivers at roughly the same distance from their base level (i.e., sea level). To analyse the possible tectonic deformation in the area, a second swath profile was computed across the peninsula dividing the gulf of Palermo and Termini Imerese. Swath boxes have a width of 1.5 km, a length of 12 km, and an area of ~18 km^2 and their sampling frequency was set equal to the geometric resolution of the DTM.

The hypsographic curves were obtained by classifying values of elevation and area into 200 bins, normalising elevations by the maximum value of their distributions, and plotting the cumulative distribution of elevation and area against each other. The hypsometric integrals were calculated using the trapezoidal rule, and summing the results as follows:

$$\int_0^1 H_b \approx \sum_{k=0}^{200} \frac{(H_{k+\Delta k} - H_k)}{2} \qquad (3)$$

where Δk is the bin width (0.5) and H_b is the hypsometric integral of drainage basins. Furthermore, we computed two other nested hypsographic curves and hypsometric integrals using the same equation but relative to elevation values of the drainage network and the trunk stream labelled H_n and H_r, respectively (*sensu* Demoulin, 2011).

Two metrics labelled I_b and I_r, describing the morphological response of rivers and drainage basins after a perturbation on their base level, were used to compare the morphological evolution of trunk streams, drainage networks, and drainage basins. The following equations proposed by Demoulin, (2012) were used to calculate the metrics:

$$I_b = \int H_b - H_n \qquad (4)$$

and

$$I_r = \int H_n - H_r \qquad (5)$$

Where I_b describes how much the river network has incised the catchment, while I_r describes how far erosion has affected the drainage network.

We explored the dynamic state and the drainage-divide stability of the studied river basins analysing their current geometry through the computation of the χ-metric and the Divide Asymmetry Index (Scherler and Schwanghart, 2020; Willett et al., 2014). The χ-analysis is an integral approach for solving the stream power law in bedrock rivers (see Perron and Royden, 2013 for further details). The detection of different χ values in a planform view of the river network allows the analysis of the geometric equilibrium across all water divides and their stream piracy tendency. We computed the χ-metrics as follows:

$$\chi = \int_{x_b}^{x} \left(\frac{A_0}{A(x)}\right)^{\frac{m}{n}} dx \qquad (6)$$

where x and x_b are the upstream distance at a generic point along with the river profile and at the base level, respectively, and $A_{(x)}$ and A_0 are the drainages at a generic point along with the river profile and an arbitrary drainage area (which was set as equal to 1, so that slope into χ plot become coincident to the river concavity ϑ).

Similarly, we used the DAI metric to quantify the relief asymmetry across stem drainage divides. Such metric was computed through the eq. proposed by Scherler and Schwanghart, (2020) as follows:

$$DAI = \left|\frac{\Delta HR}{\sum HR}\right| \qquad (7)$$

where ΔHR represents the hillslope relief defined as the elevation difference between two points located on the drainage divide and the river, and ∑HR is the sum of the cross-divide differences in hillslope relief. Moreover, we computed the direction of divide migration tendency as perpendicular to the drainage divide and pointing toward the valley characterised by lower relief values. Finally, we analysed the possible relation between DAI and the bedding dip direction. We selected all DAI values within a 500 meters search radius starting from DIP locations and plotted both values into a 16-direction class confusion matrix.

3.2 GNSS

GNSS data were acquired through the Continuously Operating Reference Stations (CORS) located in western Sicily (UNIPA GNSS CORS, see Dardanelli et al., 2020). This network is included in the Topcon Netgeo GNSS network (http://www.netgeo.it/) and the Rete Dinamica Nazionale 2 (RDN2) which provides the WGS84 datum for Italy in the European Permanent Network since 2013. CORS network consists of eight permanent stations located in Palermo, Termini Imerese, Agrigento, Caltanissetta, Campobello, Partinico, Prizzi and Trapani, equipped with a GNSS Topcon NET-G3 receiver (Fig. 2b).

The horizontal velocities related to the Noto station from CORS stations of Palermo, Termini Imerese, Partinico and Prizzi (PALE, TERM, PART and PRIZ) were recorded, from 2009 to 2011, in RINEX format with a time range of 30 s and a cut-off angle of 10°. Additional parameters include the Earth's rotation, the sun and moon relative ephemerides, the precise ephemerides (sp3 format) and the antenna phase centre position retrieved from the International GNSS Service.

Data processing includes ionospheric error correction using the model proposed by Klobuchar (1996) and tropospheric correction through the Saastamoinen and Niell mapping functions (Niell, 1996; Saastamoinen, 1972). Ocean tidal parameters constraining the values to those of the ocean tide model of Schwiderski, (1980) were also calculated. After that, a single baseline with lengths of 202.76, 213.60, 172.65 and 171.60 km was used to connect the UNIPA GNSS CORS network and the IGS CORS of Noto. At the same time, we estimated the CORS velocities (TERM, PART, PRIZ) stations with respect to the PALE station using a single baseline with lengths of 31.20, 22.14 and 42.54 km. Finally, the zenith troposphere estimation (affecting the baseline coordinates) was performed to process the baselines.

We applied double-differenced observation data combining the wide-lane and ionospheric-free frequencies according to the multi-frequency strategy for a baseline larger than 10 km. The Least-Squares Ambiguity Decorrelation Adjustment (LAMBDA) method was followed to fix the phase ambiguity (Teunissen et al., 1997). The solutions by the Wide-lane observation were determined to estimate the Wide-lane ambiguity and the ionospheric-free observations for estimating the remaining Narrow-lane uncertainty. The CORS coordinates were computed in the International GNSS Service epoch 2008.0 reference frame and in the European Terrestrial Reference Frame of epoch 2008.0 (ETRF2000), using the Altamimi and Boucher equations (Boucher and Altamimi, 2011).

We removed outliers and known discontinuities from the recorded time series and plotted the evolution of the scattered behaviour within the range ± 3σ (Barbarella et al., 2018; Gandolfi et al., 2016). The behaviour of the CORS coordinates can be considered linear (sensu Gülal et al., 2013) and

its time series stationary. We computed the UNIPA GNSS CORS's horizontal velocities using an in-house produced MATLAB script using the non-linear least square algorithm (Roggero, 2015), such analyses were performed in the Frequency Analysis Mapping On Unusual Sampling software (Mignard, 2003).

3.3 Marine geophysics

The dataset consists of 500 km of high-resolution, reflection seismic profiles acquired in June 2004 and May 2017 (Fig. 2), using a 1 kJ Geo-Source Sparker with a multi-tip Sparker array and a single-channel streamer with an active section of a 2.8 m acoustic source for seismic prospecting. The shooting interval was 750 ms with a 500 ms record length and 0.1 ms sampling interval.

Data processing included true amplitude recovery using a T2 spherical divergence correction, band-pass (200–2000 Hz) "finite impulse response" filter using a filter length of 256 samples, swell-filter, deconvolution, multiple attenuations, trace mixing of three traces for enhancing horizontal signal, time-variant gain to boost amplitudes of deeper arrivals and mutes (for the signal noise on the water column). The signal penetration exceeded 250 ms two-way time (t.w.t.), and the vertical resolution was up to 0.5 m in the near sub-seafloor.

We based the reconstruction of the depositional architecture on seismo- and sequence-stratigraphic analysis, coupled with spatial correlations between sedimentary units and tectonic structures inferred from seismic and outcropping data. The sediment thickness and apparent dip of faults were derived from the t.w.t. (ms) to depth (m) conversion using velocities of 1515 m/s, 1650 m/s and 1800 m/s for the water column, post- and pre-Last Glacial Maximum (LGM) deposits, respectively. We derived these values from sound velocity profiles and sonic log data acquired in coeval deposits and similar offshore settings (Ferranti et al., 2019).

We analysed the sedimentary sequences deposited along the fold flanks to discriminate between the periods of activity of the detected folds and used the axial surface orientations to discriminate growth deposits along the fold flanks (Laubach et al., 1999). Finally, we modelled the basal surface of the post-LGM deposits, sampling their bottom depth into the whole seismic datasets through an inverse weight distance approach.

3.4 Subsurface geological model

DIP data, faults traces, lithological thickness and contacts were derived from CARG sheets n. 595 "Palermo" (Catalano et al., 2013b), n. 607 "Corleone" (Catalano et al., 2010b), n. 608 "Caccamo" (Catalano et al., 2010a) and n. 609-596 "Termini Imerese-Capo Plaia" (Catalano et al., 2011) of the

Geological Map of Italy at the 1:50,000 scale (https://www.isprambiente.gov.it/Media/carg/sicilia.html).

The geological model was built by reinterpreting three geological cross-sections (from the CARG database) and creating two unpublished geological cross-sections. We reconstructed the geometry of the strata using bed DIP data through a π-diagram (Ramsay and Huber, 1987) and the Kink method (Suppe, 1983). Fault geometry was first derived from the obtained strata geometry using the constant heave method (White et al., 1986) and subsequently edited through the iterative approach proposed by Santoro et al. (2013, see the paper for further details).

We assumed that a) the mechanical stratigraphy (*sensu* Laubach et al., 2009) of the carbonate layers is the same all over the study area, and b) all the layers were affected by the same loading history. Finally, we computed the pre deformation length of all the cross-section layers, but we assumed that only the volume of the carbonate units was maintained constant during the deformation.

To identify which onshore recognised geologic structures could best connect with the structures detected through the marine seismic profiles, we looked for comparable geographic, geometric, and stereological characteristics and spatial correlations.

3.5 Fault dislocation modelling

The dislocation modelling technique was used following the iterative approach proposed by Santoro et al. (2013, see the paper for details) to predict the best-fit fault geometry and the distribution of expected vertical surficial deformation related to the modelled faults activity. To evaluate the reliability of the proposed model, we compared the deformation observed in the model with the elevation values derived from the DTM, the spatial distribution of the detected morphotectonic anomalies and the folded stratigraphic markers.

Assuming the subsurface as a homogeneous isotropic elastic half-space with the upper limit affected by no shear stress (Okada, 1985), we used Hooke's law to calculate the main stress components related deformation following the procedure proposed by Meade (2007). Furthermore, we assumed a unitary slip on the modelled faults and determined their slip direction compatible with the maximum horizontal stress derived from the GNSS velocity field.

Plotting the vertical component of the computed total displacement, we identified the zero-crossing contour line as the line connecting all the points of zero vertical deformation through the analysis of which we extracted the wavelength of the calculated deformation that we compared with the folded stratigraphic markers and the low pass filtered topography. The low pass topography filter threshold was set equal to the deformation wavelength. The degree of fitting between the expected

vertical deformations, the filtered topography and the morphometric anomalies was quantified in map view and in cross-section computing the absolute value of the difference between the deformation gradient and the river horizontal shifting direction.

4. Results

4.1 Morphotectonics and morphometry

4.1.1 Morphotectonics of the study area

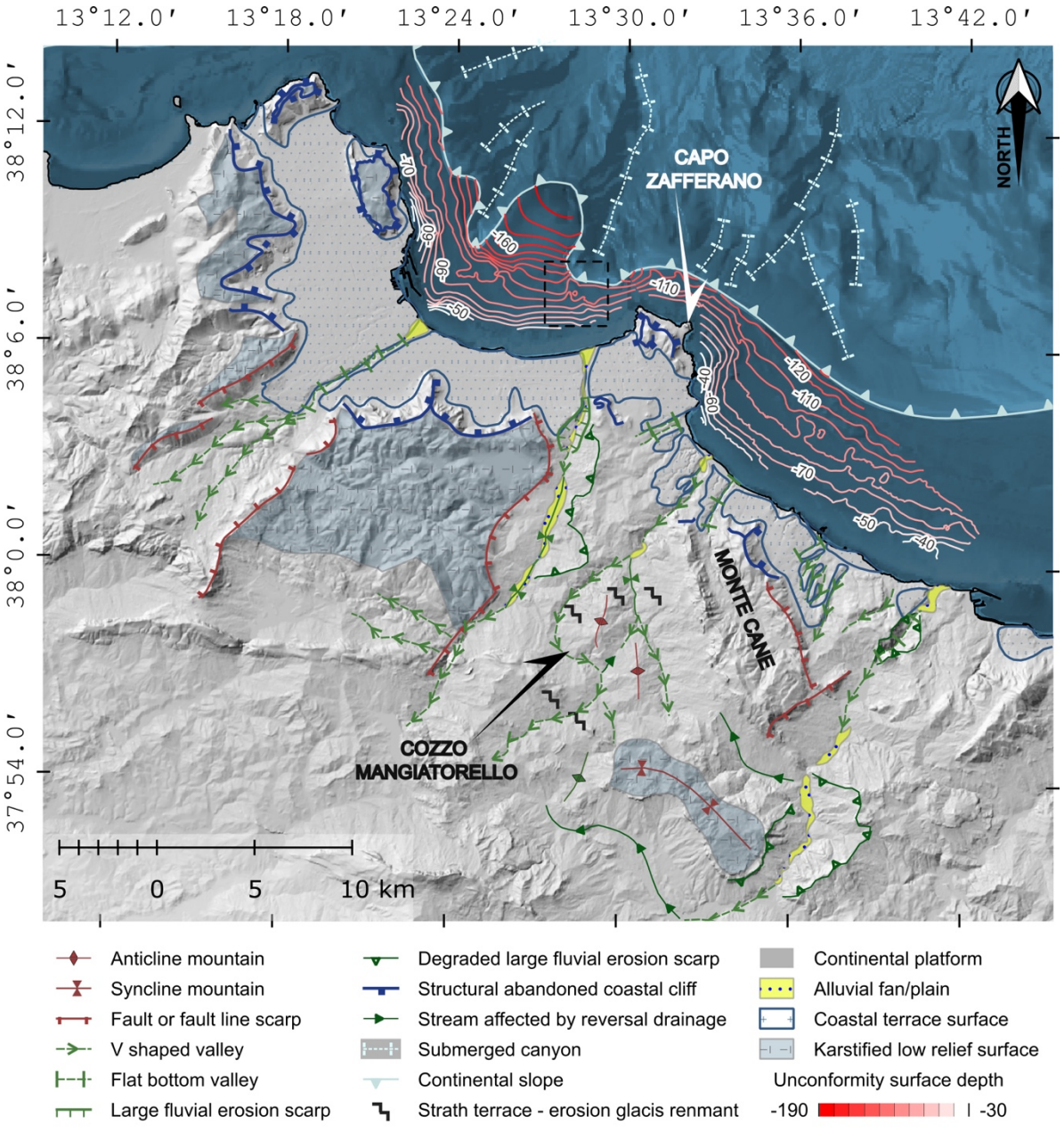

Fig. 4 – Morphotectonic map of the study area. Reddish contour lines represent the local depth of the unconformity at the bottom of the last depositional sequence. Dashed square in the Palermo gulf offshore highlights an abrupt slope change in the unconformity surface.

Geomorphological surveys highlighted coastal, fluvial, hillslope and karst landforms often controlled by differential erosion and tectonics. A staircase of undated uplifted marine terraces, hosted in extensive polycyclic coastal platforms up to 150-180 m a.s.l., testifies for the long-term uplift in the coastal area (Catalano et al., 2010a; Ferranti et al., 2006). These coastal platforms are bordered by large abandoned coastal cliffs hundreds of meters tall (Fig. 4); geological (tectonic units lowered for hundreds of meters along the coastal plains – Catalano et al., 2007) and topographical analysis (their significant vertical development and the meaningful fitting between their directions and fault systems orientation, Di Maggio et al., 2017) suggest structural control as coastal cliffs derived from marine erosion of fault scarps. The marine terraces are carved in the Lower Pleistocene deposits of the cM unit or the Meso-Cenozoic rocks of the older units, suggesting that they formed during mid-late Pleistocene marine highstand stages (Di Maggio et al., 2017 and references therein). Unfortunately, no more detailed age constraints are available in the literature.

A set of deep river valleys separated by ridges, frequently marked by a rounded top, characterise the hilly inland areas where mainly clayey rocks of the NF unit crop out. Generally, both tributaries and trunk stream segments near the catchment head run into V-shaped valleys produced by vertical incisions. The lowest sections of the trunk streams, characterised by a more significant discharge, show a narrow alluvial plain mainly affected by lateral bevelling and, to a lesser extent, by deposition, which gives rise to flat-bottomed valleys cutting the coastal terrace surfaces. Several coalescing coastal plains associated to the last Holocene sea level rise, formed at the river mouths. A larger width, up to 500 m, characterises the alluvial plains of the Eleuterio and San Leonardo rivers cut into the NF soft rocks. On the contrary, the rivers crossing the more resistant Marsala calcarenite rocks (cM in Fig. 2) form narrower alluvial plains (e.g., the downstream reaches of the Oreto, Eleuterio, and Milicia rivers, Figs. 4 and 5). Fluvio-karst canyons coincide with the harder rocks of the IUa and IUb (Eleuterio River near Marineo and San Leonardo River, Figs. 4 and 5).

4.1.2 Morphometric indexes

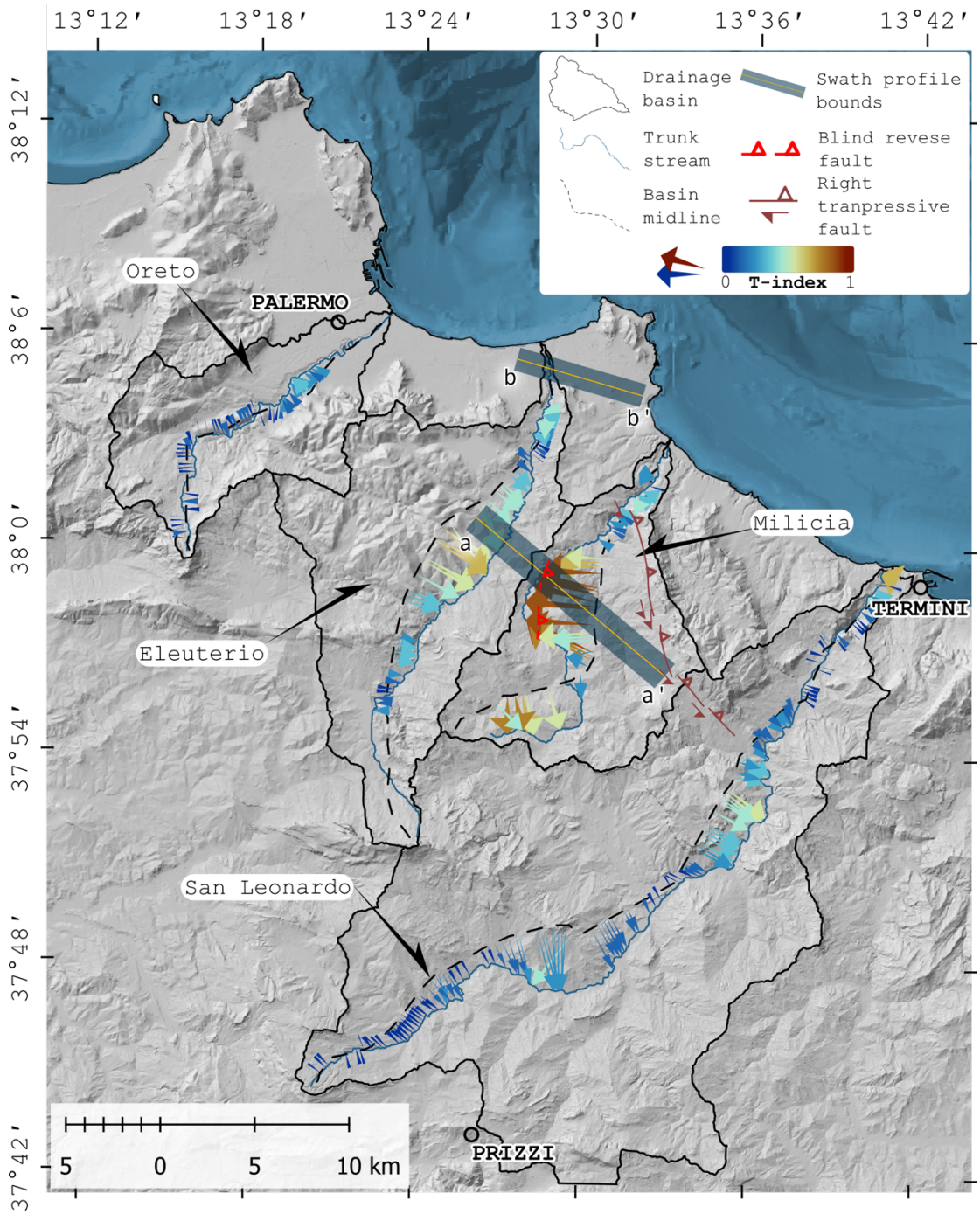

Fig. 5 – Outcomes from the morphometric analyses. Colour coded arrows represents the T-index vectors, and the size of the arrows is proportional to the T-index magnitude. The transparent dark blue boxes represent the swath profile bounding boxes and the yellow lines inside them represent the swath baselines. The thick black lines represent the catchments while, black dashed line represents the basins midline, and the blue thick line represents the rivers trunk stream.

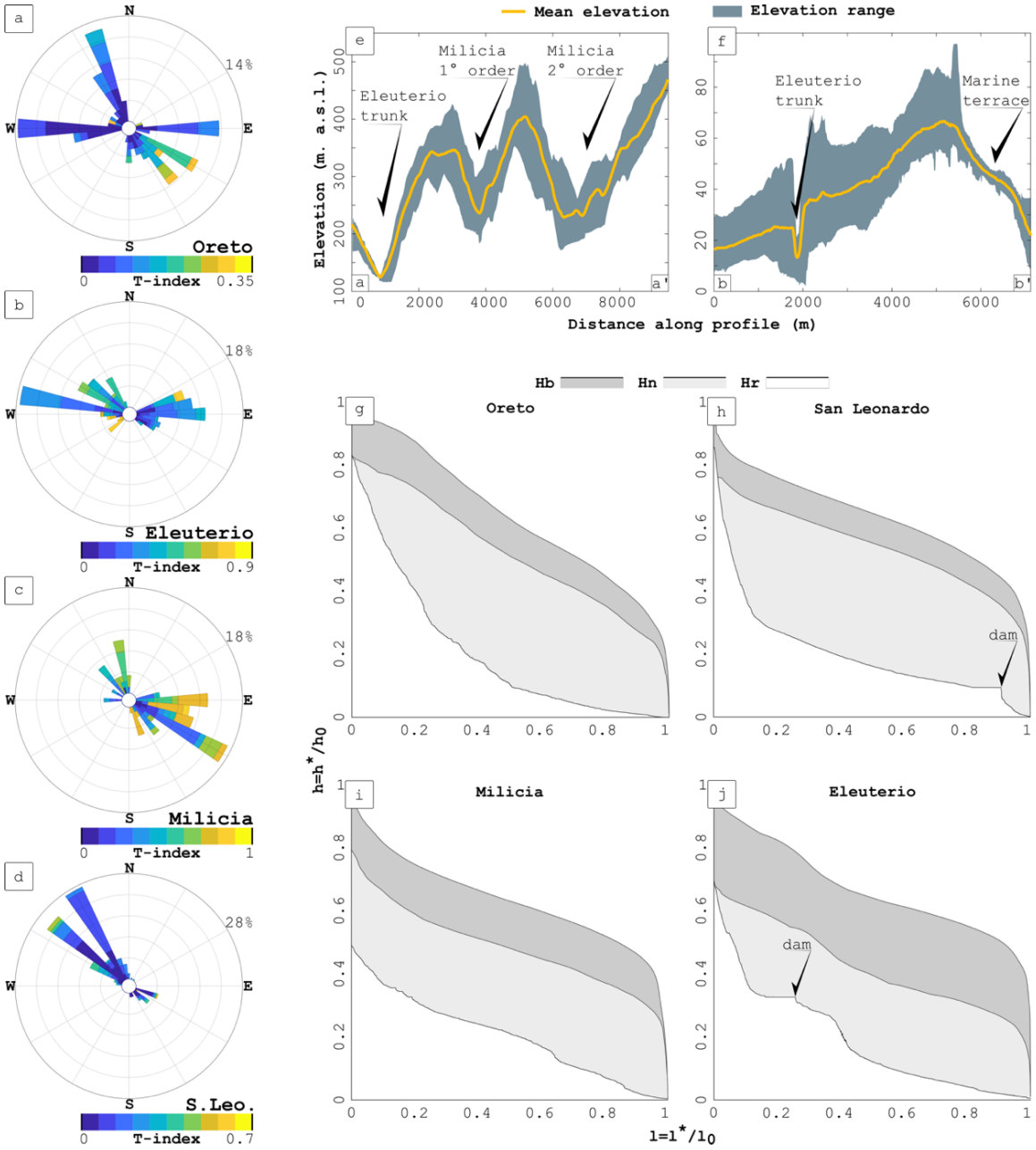

Fig. 6 - Outcomes from morphometric analyses, a – d) Stereographic plots related to the T-index arrows showed in Fig. 5, e – f) Swath profiles related to the swath profile bounds represented in Fig. 5g – j) Nested hypsographic curves related to the drainage basins plotted in Fig. 5.

To characterise ground tilting related to active faulting, we computed 667 basin-asymmetry vectors among all the extracted river catchments (Fig. 5 and Fig. 6a - d, Tab. 1). The Oreto river asymmetry vectors are characterised by the highest K and lowest T-index values, while the vectors computed for the Milicia River are defined by a high K value and the highest T-index values (Tab. 1). The K value of the San Leonardo River asymmetry vectors is the lowest among all the computed ones indicating their random orientation.

T - Index

Nested Hypsometry

Basin	#	K	Min	Max	Mean	Dev st	H_b	H_n	H_r	I_b	I_r
Oreto	110	3.4	0.00013	0.31389	0.09800	0.08131	0.643	0.525	0.205	0.118	0.320
Eleuterio	190	3	0.00046	0.87267	0.35741	0.20552	0.677	0.429	0.188	0.248	0.242
Milicia	99	3.3	0.00079	0.91642	0.52723	0.27914	0.636	0.487	0.203	0.150	0.283
S. Leonardo	276	1.2	0.00140	0.68408	0.15894	0.12255	0.639	0.543	0.204	0.096	0.339

Tab. 1 - T-index and Nested Hypsometry computation for each analysed river basin (see Fig. 5 and 6).

Swath profile in Fig. 6e shows an asymmetrical distribution of the remnant of river terraces and erosional glacis outcropping mainly along the eastern side of the N-S valley of the Milicia trunk stream, while the opposite flank is characterised by high slope values as high as 40° (higher than the friction angle of the NF rocks). The swath profile also highlights that the trunk stream of the Milicia river flows at slightly higher altitudes than the second-order stem of the same river (Fig. 6). Moreover, it shows that Cozzo Mangiatorello hill reaches higher altitudes than the drainage divides, separating the Milicia catchment from the Eleuterio catchment. An asymmetric sigmoid shape characterises all the computed hypsographic curves (Fig. 6g - j). Almost all the trunk stream curves show a positive concavity, excluding the Milicia River, which approaches linearity. Significant knickpoints characterise the trunk stream profiles of both the Eleuterio and San Leonardo rivers (Fig. 6h and j), whereas the Milicia trunk stream longitudinal profile highlights the presence of smaller knickpoints and knickzones (Fig. 6i). The computed hypsometric integral values (Hb, Tab. 1) are quite similar, and suggest a landscape in its youthful stage.

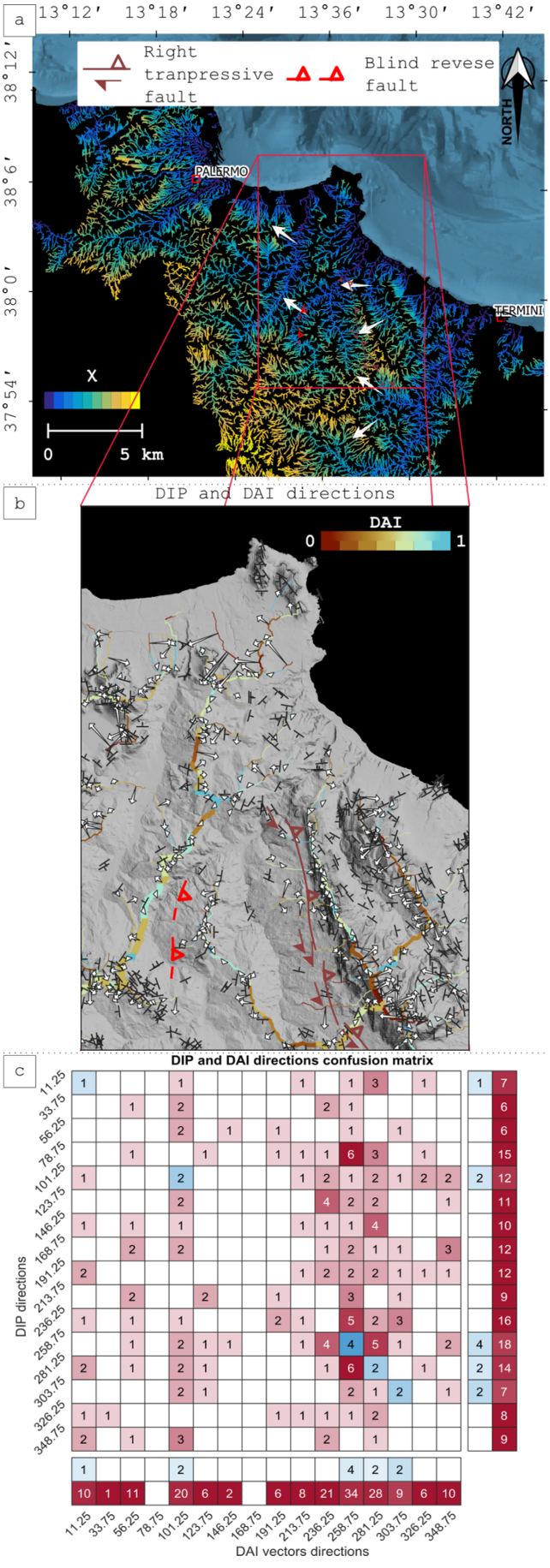
a
13°12′
13°18′
13°24′
13°36′
13°30′
13°42′
38°12′
38°6′
38°0′
37°54′
Right tranpressive fault
Blind revese fault
NORTH
PALERMO
TERMINI
X
0
5 km
b
DIP and DAI directions
DAI
0
1
c
DIP and DAI directions confusion matrix
DIP directions
DAI vectors directions
11.25
33.75
56.25
78.75
101.25
123.75
146.25
168.75
191.25
213.75
236.25
258.75
281.25
303.75
326.25
348.75

Fig. 7 – a) χ space representation of the drainage network extracted in the study area, b) Drainage divide network coloured by DAI values, in black the bed dipping direction. In both figures, white arrows indicate the direction of the drainage divide migration tendency c) confusion matrix of the DIP direction Vs the DAI directions, both classified into 16 classes of orientation. Each class covers an angle of 22.5 degrees.

The χ-space representation (Fig. 7a) shows that starting from the San Leonardo catchment and moving from East to West, the river stems play the role of the aggressor (*sensu* Whipple et al., 2017) when lying on the eastern side of the divide. DAI computation revealed three main areas of anomalous across divide hillslope relief values; such areas are the western flank of Cozzo Mangiatorello, the west side of Monte Cane ridge and the peninsula dividing the two gulfs (Fig. 7b). In these areas, the anomalous drainage divide lies upon uniform lithologies, and the direction of the divide mobility (white arrows in Fig. 7b) is not influenced by the bedding dip directions. The confusion matrix Fig. 7c shows how the cluster of DAI data between classes 11 - 13 spans almost the entire DIP values suggesting an iso-orientation of the DAI data not correlated or anticorrelated to the DIP and STRIKE values (Congalton, 1991).

4.2 GNSS velocity field

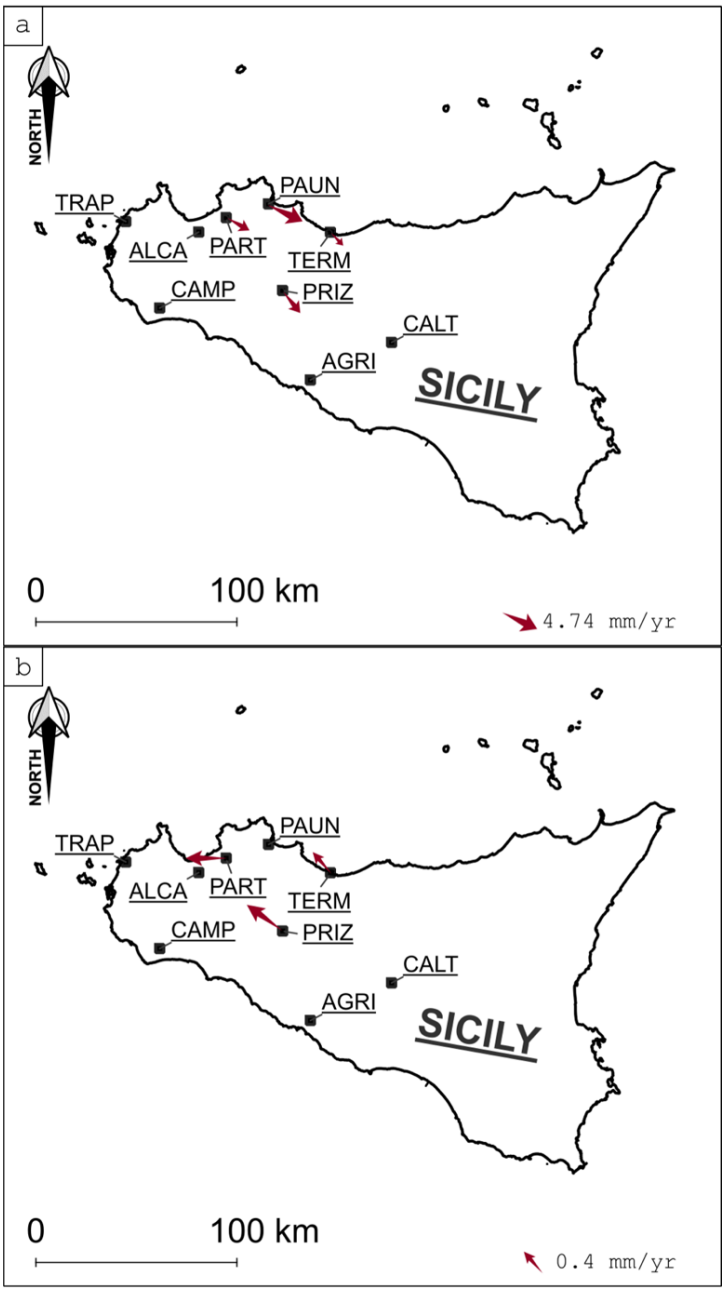

Fig. 8 – a) GNSS velocity field, b) GNSS relative velocity field.

We summarised the CORS station's velocity values averaged for the 2009-2011 period in Tab. 2. The average direction of the CORS velocity vectors is N 128 E (NNW - SSE) and the lowest values were obtained for the station TERM while we obtained the highest velocity values for the PAUN station (Tab. 2, Fig. 8a).

CORS	Easting (Lon)	Northing (Lat)	Elevation (m asl)	Vel_2009 (mm/yr)	Vel_2010 (mm/yr)	Vel_2011 (mm/yr)	Average (mm/yr)	Avg_dir (N deg E)	Sigma_E (mm/yr)	Sigma_N (mm/yr)
PAUN	355202.001	4218813.312	113.562	4.157	2.792	7.162	4.74	115	1.51	1.48

PART	334129.939	4211985.772	247.505	3.033	1.998	4.371	3.13	119	0.88	0.89
PRIZ	362237.034	4175785.685	961.896	3.097	2.716	4.17	3.33	141	0.95	1.13
TERM	386025.285	4204751.839	55.289	2.474	1.781	2.226	2.16	136	0.79	0.86

Tab. 2 Horizontal velocities of the UNIPA GNSS CORS computed in the Noto reference frame. Coordinates are in UTM WGS 84 33N reference system (see fig 2).

The differential velocities of the TERM, PART and PRIZ stations are estimated concerning the PAUN station are minimal but still reliable. Indeed, due to the very short baselines, it was possible to obtain a calculated error of an order of magnitude smaller than the estimated velocities; we summarised such values in Tab. 3 and Fig.8b. Such computed GNSS CORS data and their differentials suggest an active shortening occurring between the PAUN station and the TERM station that move towards each other with a relative velocity of 0.4 mm/yr.

CORS	Easting (Lon)	Northing (Lat)	Elevation (m asl)	Average (mm/yr)	Differential (mm)	Sigma_D	D_dir (N deg E)
PAUN	355202.001	4218813.312	113.562	4.74	--	--	--
PART	334129.939	4211985.772	247.505	3.13	0.4	0,06	270
PRIZ	362237.034	4175785.685	961.896	3.33	0.5	0,08	306
TERM	386025.285	4204751.839	55.289	2.16	0.4	0,05	319

Tab. 3 Differential displacements velocities computed in the Noto reference frame. Those velocities refer to the PART, PRIZ and TERM stations relative to the PAUN station. Coordinates are in UTM WGS 84 33N reference system (see Fig. 5).

4.3 Marine geophysical lines

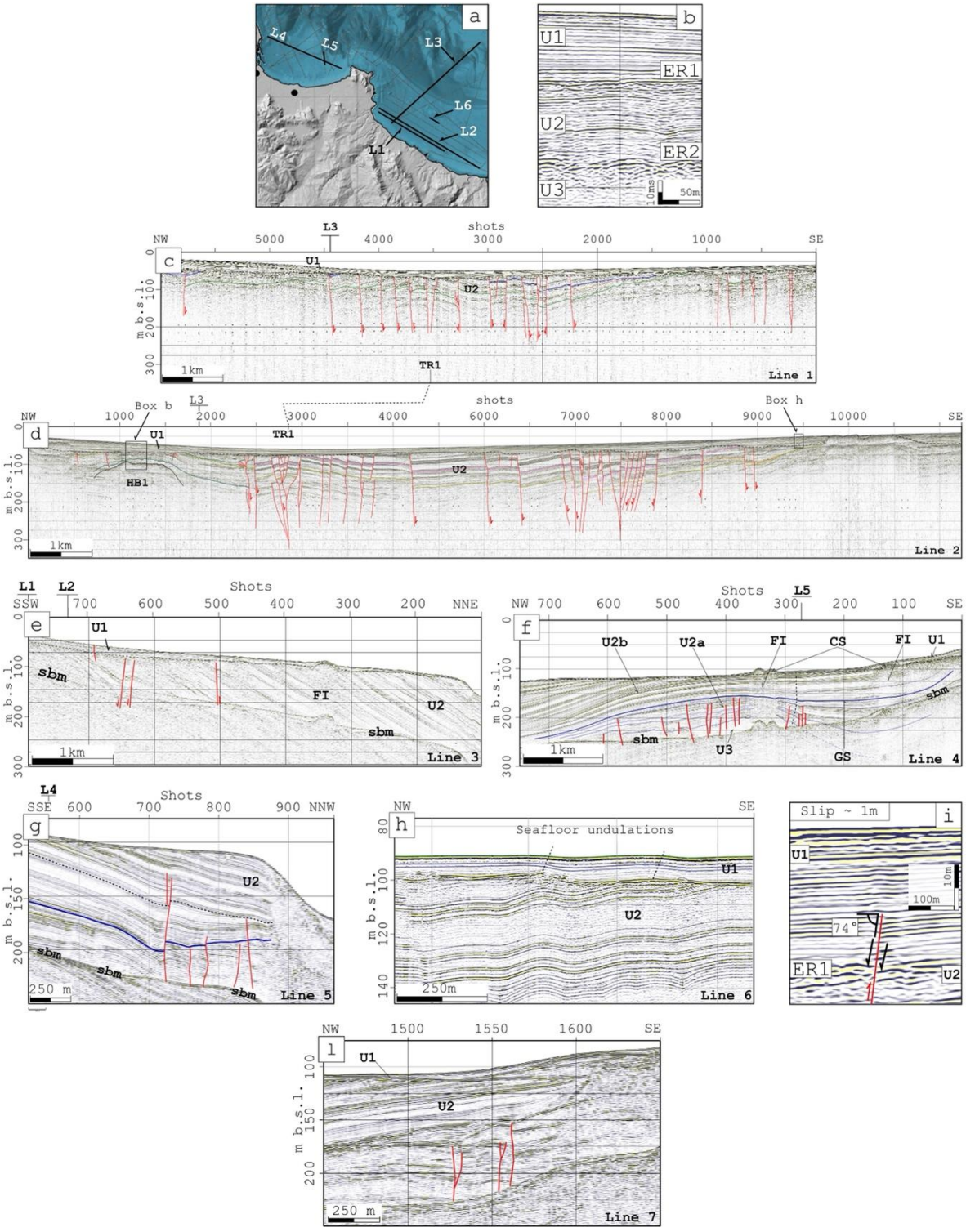

Fig. 9 – a) Locations of the seismic profile shown, black dots indicate borehole locations from Incarbona et al. 2016, b) Seismic stratigraphic units (U3, U2 and U1) and their boundaries (ER2 and ER1) recognised on seismic profiles, c - g) Depth-converted seismic Lines 1-5, and their interpretations. TR1 and An indicate anticlines; HB1 indicates a structural high. L1-5 are the intersections with seismic lines. Abbreviations: CS, cold seep; ES, erosional surface at the top of the structural high HB1; FA, fluid ascent; GS, growth strata; sbm, seabed multiple, h) Part of the depth-converted seismic Line 6 that shows seafloor undulations, i) Zoom of the seismic Line 2 displaying a normal fault that affects upper Quaternary deposits, i) evidence of fault activity younger of 20 ky, l) transpressive faults in the northern offshore the Bagheria area sealed by the U2 deposits.

4.3.1 Seismic stratigraphy

Three seismic stratigraphic units labelled from younger to older as U1, U2 and U3 were recognised basing on their bounding discontinuities, strata architecture and seismic characteristics (e.g., amplitude, lateral continuity, external shape, and frequency of internal reflectors, Fig. 9b). These units were partly calibrated by the outcropping Quaternary sedimentary succession or cores drilled on land close to the study area (Incarbona et al., 2016, drill location in Fig. 9a).

Unit U1 exhibits well-defined, slightly seaward dipping, low- to medium amplitude and laterally continuous reflections with parallel geometry. The upper and lower boundaries of this unit are the seafloor and the basal surface of the last transgression (ER1), respectively (Lo Iacono et al., 2011). The ER1 corresponds to a regional unconformity (*sensu* Pepe et al. 2003 and reference therein), extending along the whole shelf area, carved during the LGM at ~18–23 kyr when the sea level was ~120–130 m the present one (Lambeck et al., 2011). The geometry of such a surface is characterised by anomalous slope break, in the Palermo Gulf (Fig. 4). Considering the age of such surface, we relate the unit U1 with the Upper Pleistocene-Holocene deposits formed during the transgressive and high-stand stages of the last sea level rise. The thickness of unit U1 varies from ~ 30 m to less than 2 meters in the internal and distal sectors of the shelf, respectively and reaches the maximum value of ~40 m in the Capo Zafferano offshore (Fig. 9b and c).

A succession of well-stratified, laterally continuous, high-frequency, medium- to high-amplitude reflections represents the unit U2 (Fig. 9b). Unit U2 exhibits oblique-tangential to parallel reflectors, moving towards the distal part of the shoreline (Fig. 9d and e). We identified the base of this unit with an erosional surface (ER2 in Fig. 9b) that formed in correspondence with structural highs (HB1 in Fig. 9d, blue line in Fig. 9f). Because of the stratigraphic position and seismic signature, we correlate unit U2 with the marine Quaternary deposits overlaying the NF unit drilled in the historical centre of Palermo (Incarbona et al., 2016). Based on their internal geometry we subdivided unit U2 in the Palermo Gulf into two subunits named U2a and U2b. Subunit U2a is characterised by divergent

geometry (Fig. 9f), whereas subunit U2b shows parallel (the distal portion) to oblique-tangential reflectors in the proximal part (Fig. 9f).

Unit U3 is characterised by a reflection-free seismic signature (Fig. 9f) and limited upwards by an erosional truncation (ER2 in Fig. 9b, d, and f). Based on the stratigraphic position, seismic signature and calibration with well-logs (Incarbona et al., 2016), we correlate Unit U3 with the clayey pelites and siltstones of the NF unit. Seismic feature CS displays a mound-shaped feature characterised by transparent to chaotic reflectors and anomalous seismic amplitude (Fig. 9f).

4.3.2 Structural patterns

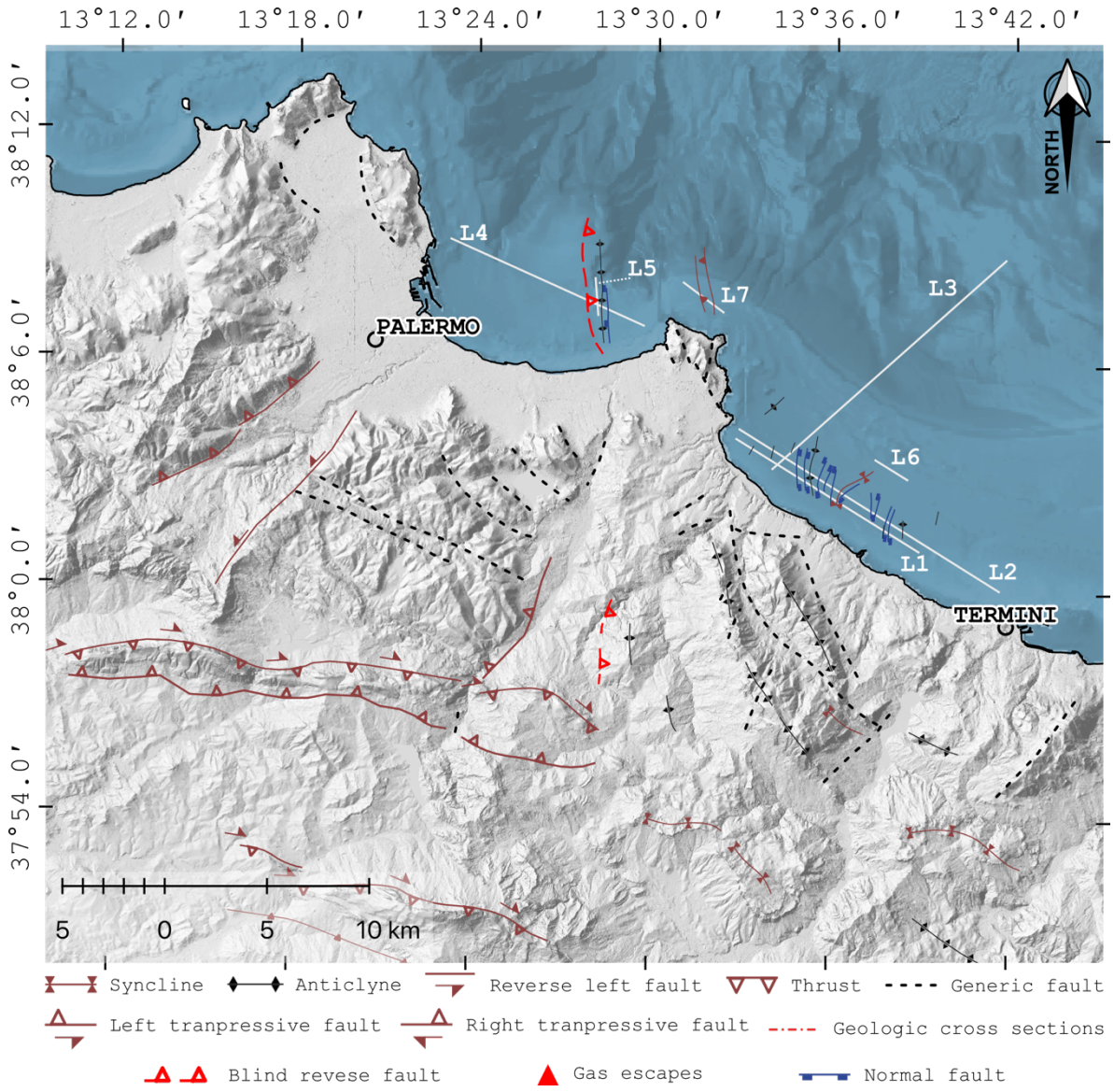

Fig. 10 – Land to sea structural chart of the study area.

We interpreted the Late Quaternary tectonic history of the offshore study area through the analysis of the geometry of the syntectonic strata and the dip of fold axial surfaces.

The U2a subunit shows a thickness variation compatible with a NNW-SSE striking fold west of Capo Zafferano that is spatially correlated with the slope break of the unconformity that we interpreted to be folded, proving the recent activity of this fold (Figs. 4, 9f and 10). The U2 subunit thickness range from ~100 m and reduces to a ~35 m in the fold hinge zone displaying a growth strata geometry (GS in Fig. 9f). The fold hinge orientation is N170E, and its axial surface inferred from the growth strata geometry dips toward the crest of the anticline (lower part of the blue line in Fig. 9f), indicating the syn-tectonic nature of the U2a deposits. West and east-dipping high-angle normal faults affect the flanks of the anticline with displacements up to a few meters (Fig. 9f). Unit U2b overlays the anticline with a variable thickness, and the axial surface within it slightly dips towards the anticline crest (Fig. 9e), indicating the post-tectonic deposition of these sediments. High-angle normal and reverse faults offset reflectors of unit U2b and older deposits in the distal sector of the gulf (Fig. 9g and 10).

Seismic lines 1 and 2 shows that the Termini Imerese Gulf experienced compressive and transpressional deformations during the U3 and U2 deposition time interval (Fig. 9c and d). The growth geometries of U3 along the flanks of the structural-high HB1 suggest that it formed during Late Oligocene – Early Miocene (Fig. 9d). Shortening persisted during the Quaternary period, as suggested by the folding of U2 deposits that formed anticlines and synclines (e.g., TR1 anticline in Figs. 9c and d). The hinge lines of the anticlines strike from ~ N 20° to ~ N 56°. Transtensional faults downthrow the crests (around shot points 3000 and 7500 in Fig. 9d) and limbs (shot points 3500 and 7000 in Fig. 9d) of the anticline (Fig. 10). These structures are characterised by small displacements, lower than the uplift of the hosting anticline, and typically converge at depth into vertical faults.

The seafloor is affected by undulations due to contractional structures with a hundred-meter wavelength (Fig. 9h). Also, one normal fault dipping ~74° to the West and located in the south-eastern sector of the gulf (around shot point 9500 in Fig. 9d) offsets the ER1 of about 1 m (Fig. 9i), demonstrating the tectonic activity during the last 20ka.

We also identified several fluid ascents (FA in Figs. 9e, f and red triangles in Fig. 10), interpreted as gas escapes from cold seeps (CS in Fig. 9f), the latter identified based on their external shape and position along axial tensional faults.

Finally, even the sector between the two analysed gulfs experienced contractional and strike-slip movements recorded by two roughly N-S oriented, transpressional structures detected in the offshore north of the Capo Zafferano area, sealed by the U2 sediments (Fig. 9l and 10).

4.4 Geological model

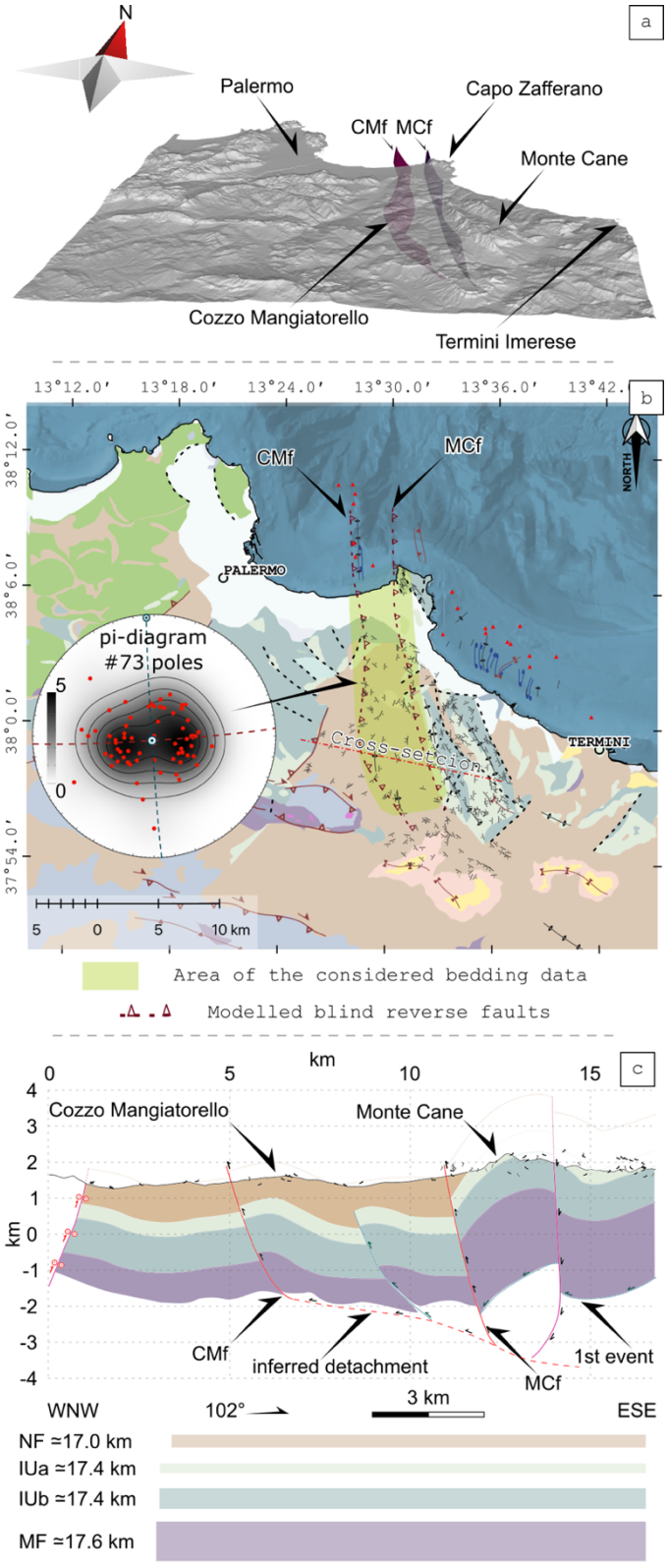

Fig. 11 – a) Reconstructed 3D fault model of the study area showing the geometry of the Cozzo Mangiatorello (CMf) and Monte Cane (MCf) thrusts, b) Simplified geologic map of the study area and π-diagram of bedding poles (1% area contouring, Allmendinger et al., 2011 and reference therein c) Geologic cross-section (see the dashed red line in inset b).

Considering the bedding data, the offshore structural pattern and literature data, the 3D geometry of two thrust faults was reconstructed (Fig. 11a). Analysis of beds attitude data highlighted the presence of a first-order fold structure characterised by an axial plane 265/ 80° and an axis 355/ 03°.

A wavelength of about 5 km and a similar direction characterises both the fold in the Termini Imerese gulf and in the Monte Cane ridge (Fig. 11b). Such similar stereological and geometrical properties, together with the computed T-index metrics, the anomalous relief distribution and drainage divide mobility (Figs. 4, 5 and 6), suggest a possible connection of these structures from land to sea (see Figs. 9a and b). Such stereological and geometrical similarities were not detected across the Gulf of Palermo shoreline. For this reason, to identify the possible geometry of the first-order structure in this area, we used three pieces of evidence from different locations, datasets, and analyses. For the onshore portion, we considered the morphometric anomalies in correspondence with Cozzo Mangiatorello and the stereological analysis of bed attitudinal data in a part of the territory just north of the Mangiatorello hill (Figs. 5, 6, 7 and 11b). For the offshore portion, we have considered the slope anomaly in the unconformity (Fig. 4) spatially correlated with the active fold identified in the Gulf of Palermo (Fig. 9f). The first order detected structures highlight a compressive tectonic regime with faults and folds that develop roughly in the NW-SE direction compatible with the recorded GNSS velocity field (Figs. 8, 10 and 11).

The resulting geological model is characterised by two first-order compressive structures (Fig. 11a, b and c). The eastern one coincides with the ridge of Monte Cane (Monte Cane fault, MCf in Fig. 11c), while the western one is a blind structure located below the low relief of Cozzo Mangiatorello (CMf in Fig. 11c) that lie within a large area characterised by outcropping Numidian Flysh (Fig. 11b). The main parameters of these faults are resumed in Tab. 4. A décollement depth of about 3-5 km within the Mufara Formation characterises both modelled structures (Balestra et al., 2019; Gasparo Morticelli et al., 2015).

Label	Mean Direction (degree)	Depth (m)	Average dip angle (degree)	Length (m)	Modelled slip (m)	Max expected uplift (m)
CMf	N347E	-2877	55	27713	1	0.46
MCf	N359E	-4349	60	25322	1	0.57

Tab. 4 – Main parameters of modelled faults. The expected vertical deformation is shown in Figure 12.

The shortening computable from the geologic cross-sections (Fig. 11c and supplementary materials) is about 1.7 km. Considering the minor but still present strike-slip component of movement, the significant clockwise rotation that occurred in this area (Speranza et al., 2018), and the capacity to preserve volumes during deformation, for the shortening computation, we took into account the carbonate layers only.

4.5 Modelled vertical deformation

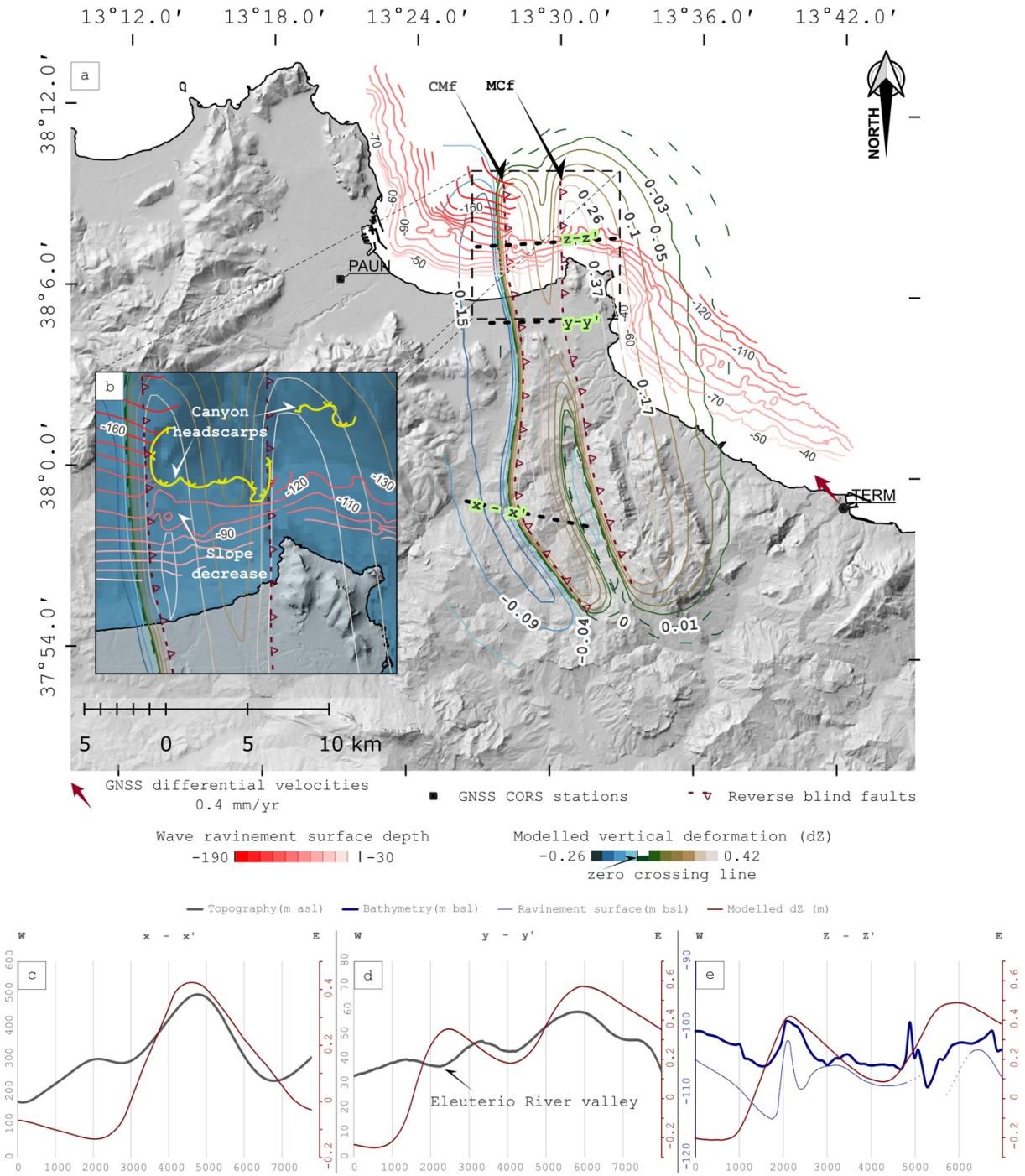

Fig. 12 – a) Colour coded contour line of the modelled vertical deformation, dashed green line represents the zero-crossing line. Reddish lines show the unconformity depth. Red arrows indicate the direction of the computed differential GNSS velocity. Black squares are the locations of CORS GNSS stations. Dashed thick black lines are the cross-sections trace shown in insets c and d. CMf and MCf are the two modelled reverse faults. b) Zoom of the dashed square represented in the inset a showing the abrupt slope change in the eastern part of the Palermo Gulf, in yellow the canyon headscarps from Lo Iacono et al. (2011). c and d) cross-sections showing in thick black the low pass filtered topography and in thin red the modelled vertical component of the deformation. e) cross-sections showing in thick blue the bathymetry, in thin blue the unconformity surface depth and thin red the modelled vertical deformation component. The thin dotted lines in the unconformity surface represent low quality interpolation due to the poor data coverage. The abrupt break in the thin dotted blue line is due to the two different interpolations of the unconformity surface forced by the low density of data in that portion of the study area.

Results of dislocation modelling, consisting of the deformation recorded by a horizontal plane located at sea level, ranges from about 0.6 m of uplift to about -0.3 m of subsidence. The contours of the expected deformation vertical component were superimposed on the digital elevation model of the area (Fig. 12a). The location of maximum uplift values fits the topographic maximums in the analysed area with a reasonable degree of approximation.

The zero-crossing line of the vertical deformation (dashed dark green line in Fig. 12 a) is located at the eastern termination of the city of Palermo and immediately west of the city of Termini Imerese. The wavelength of the modelled deformation (about 3 and 5 km for the CMf and MCf, respectively) is compatible with the wavelength of the deformation observed both in offshore and onshore environments. The modelled CMf deformation is characterized by an excellent spatial correlation with the shape and wavelength of the abrupt slope break in the Palermo Gulf unconformity. Although this slope-break lies closer to the Eleuterio canyon headscarps as mapped by Lo Iacono et al. (2011) using a high-resolution bathymetric dataset, such a portion of the unconformity surface is not influenced by it (Fig. 12b). The uplift computed in the central portion of the study area matches well with the evidence of relative uplift identified at Cozzo Mangiatorello. Such relative uplift was detected through the hypsographic curves (Fig. 7i), the horizontal shift of the river trunk stream (Fig. 5), the asymmetry of the valleys, high slopes of the valley flanks, and the Milicia trunk stream altitude values (see paragraphs 4.1 and Figs. 5, 6, 12a and c). The vertical deformation computed to the south of Capo Zafferano is characterised by two peaks located at about 2500 and 6000 meters from the origin of the section represented in Fig. 12d. The asymmetric slope of the promontory flanks matches the evidence of differential elevation obtained by calculating the relief distribution, slope distribution, and the asymmetry of the drainage divides (Figs. 2, 6f and 7b). The computed peak at 2500 meters appears slightly W-shifted from the topographic one; this apparent shift is due to the Eleuterio valley. Differences between curves are approximately 10% of the wavelength used for filtering the topography and, therefore, entirely within the study's resolution. At about 2000 and 6300 meters from the origin of the section in Fig.12c, two peaks characterise the unconformity surface. The westernmost one aligns

with a bathymetric spike and a peak in the modelled deformation. At the same time, the easternmost one is about 500 meters shifted towards E concerning the peak of the modelled deformation and does not align with any noteworthy bathymetric peak.

5. Discussions

5.1 Morphotectonic evolution model

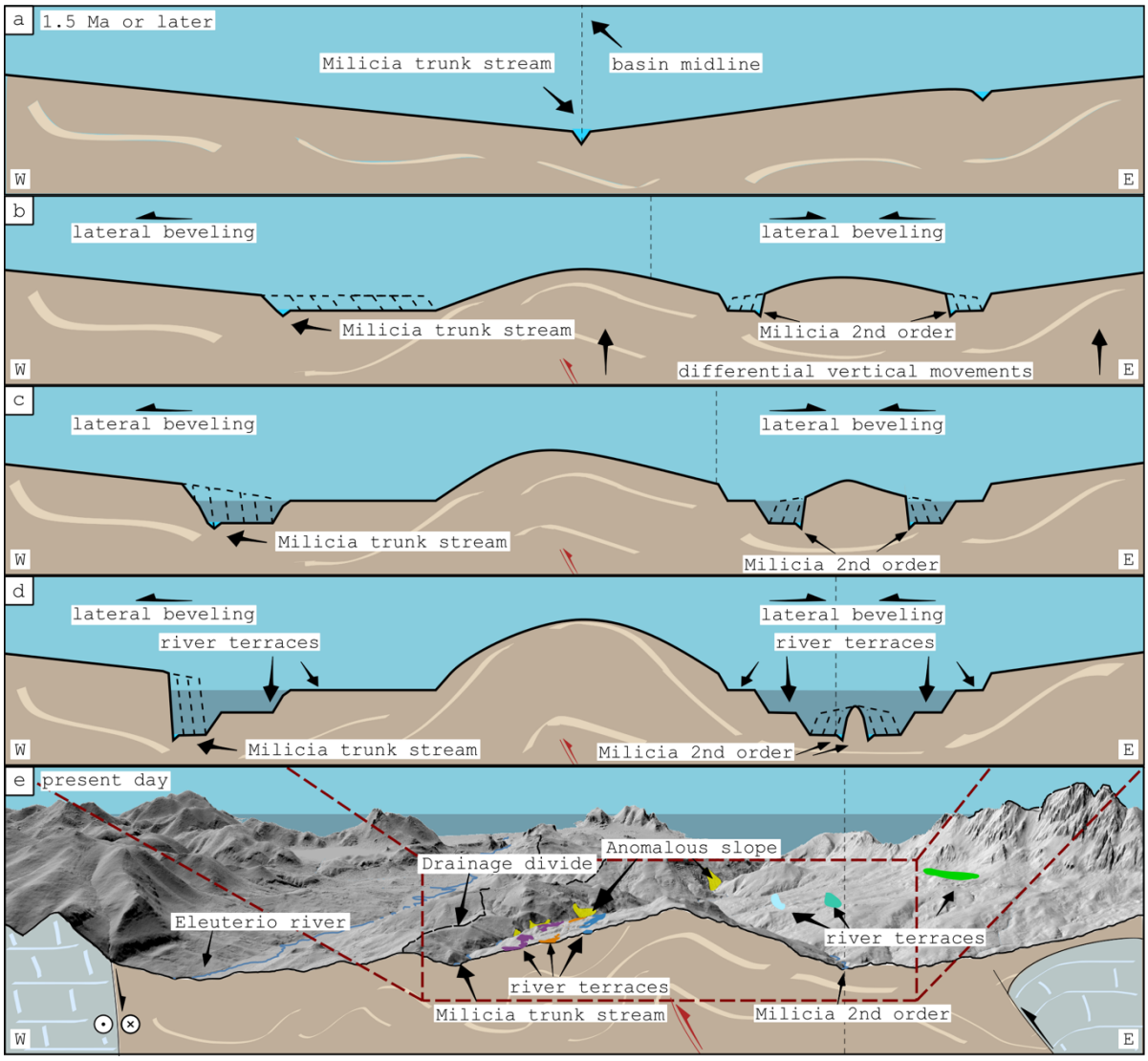

Fig. 13 – Morphotectonic evolution model of the Cozzo Mangiatorello hill area. Cartoons in a – d) represent in cross-section the proposed landscape evolution of the Milicia River network forced by the growth of the modelled structures. Cartoon e) shows a 3D view of the the Cozzo Mangiatorello hill (shaded relief using a 2m DEM); the thick black line represents the actual topographic profile crossing the area (reproducing part of the trace x-x' in Fig. 12a), under which it is represented by a cartoon the subsurface geology.

Morphometric analyses allowed us to identify morphotectonic anomalies used to quantify the deformation field and its modelling to return the fault geometry and kinematics, being the anomalies driven by the differential tectonic surface uplift.

The area of the Cozzo Mangiatorello, along with the Milicia River trunk stream, hosts the most significant number of morphotectonic anomalies such as valley asymmetry with the highest horizontal shift values (T-index), rectilinear river longitudinal profile, slope values exceeding the lithology friction angle, drainage divide migration tendency and others (see paragraph 4.1, Figs. 5, 6 and 7). In this area, the erosion glacis and strath terraces analysis show the long-term incision history and a trend to migrate laterally westwards (trunk stream of the Milicia River) or eastwards and westward (2^{nd} order streams in hydrographic right – Fig. 13). In particular, the abandoned valleys (highlighted in Fig. 4 at the head of the streams affected by reversal drainage) together with the river terrace surfaces along the slopes of Cozzo Mangiatorello suggest that the "original" trunk stream of the Milicia River flowed further East than the current path of its main channel (along the basin midline, Figs. 5, 6e). These relict river landforms were abandoned due to the triggering of prevalent vertical incision, as demonstrated by the staircase of river terraces and the occurrence of V-shaped valleys (Fig. 6e). The asymmetric river terrace distribution and the steep left valleys flank point out that the fluvial down-cutting did not maintain its course according to a vertical superimposition pattern, but it has undergone a westward and eastward/westward shift over time in the trunk stream and 2^{nd} order streams, respectively (Keller and Pinter, 1996). The differential uplift induced undercutting processes that triggered the retreat of the slopes or the preservation of river terraces, according to the valley flank relative position with respect to the underlying growing structures (see dashed lines in Fig. 13b - d). The recognition of erosion glacis and strath terrace surfaces highlights that the morphogenetic phases of lateral fluvial beveling alternated with the vertical incision phases. Such migration occurs through river diversion/piracy and drainage inversion processes, highlighting the sudden relative growth or the incision power of one river stem (Bull, 2009). We relate this relative growth in incision power to a drainage reorganisation triggered by the differential uplift processes induced by faulting on the blind Cozzo Mangiatorello fault (Burrato et al., 2003b; Jaiswara et al., 2019). In this scenario, the geomorphological data suggest that the study area was affected by numerous phases of relative lowering of the river base level, typical of uplifting regions. This indication was also validated by morphotectonic, and geological analyses proposed in the literature (Antonioli et al., 2006; Burbank and Anderson, 2011; Di Maggio et al., 2017; Ferranti et al., 2006, and references therein).

According to the superimposition pattern, a generalised and uniform uplift in a lithologically uniform area would lead the river network to keep its course through the different eroded lithologies

and the tectonic structures that cross as it erodes downward its bedrock (Bull, 2009, 2008; Burbank, D., Anderson, 2001; Keller and Pinter, 1996). The morphometric and morphotectonic analyses showed both first-order streams flowing on syncline depressions and watersheds set on anticline mountains, suggesting that these fluvial processes relate to the growth of anticlines forcedly drove the rivers to their present-day position (Figs. 4, 13).

We produced a morphotectonic evolution model describing the tectonically forced landscape evolution of the study area to explore the cause of these anomalies considering the GNSS velocity directions and the structural style previously identified (as per Tab. 3, Figs. 5, 11 and 12a, b). The cartoons in Fig. 13 (a – e) describe a possible temporal evolution from an initial phase up to the present day. This evolution, started after 0,8 Ma (post cM emersion; see paragraph 5.3), could correlate with the phases of marine abrasion and sea level relative lowering that formed the coastal terraces from middle Pleistocene to Holocene (Di Maggio et al., 2017). In the initial phase, an ancient Milicia River trunk stream flowed along the current midline of the basin, as testified by the abandoned valleys and the first-order river terrace surfaces (Figs. 4, 6e, 13a). The location of the trunk stream along the basin midline indicates that at that period, either the studied area was affected by a uniform regional uplift, or the vertical incision power was much higher than the tectonic activity of local structures producing any potential differential uplift. In the following phases (Fig. 13b - c), downwards and lateral stream migration, suggested by river terrace distribution and slope asymmetry, is due either to the inception of the growth of the Cozzo Mangiatorello anticline or to the decrease of the ratio between regional and local uplift. In the second hypothesis, the Cozzo Mangiatorello anticline was deforming for a long time before. The decreasing vertical erosion power could connect to a lesser local relief produced over time. In these phases, vertical erosion is mainly caused by the uplift of the anticline while its widening triggers the westward (stream in hydrographic left) and eastward (stream in hydrographic right) lateral bevelling (Fig. 13). In the later phases (Figs. 13d - e), the constant growth of the anticline also explains well both the processes of drainage inversion, and the process of fluvial diversion occurred in the river network, as indicated by fluvial elbows, abandoned valleys, wind gaps, horizontal shifting, and asymmetric valley (Figs. 4, 5 and 6e). The development of a growing topographic obstacle has forced the river network to reorganise and adapt to the new geomorphological setting. These changes produced both the truncation of the old trunk stream of the Milicia River and its deviation at the edges of the anticline mountain, along the topographic depressions set on syncline structures. Moreover, the westward migration of the Cozzo Mangiatorello anticline or an eastward tilting of the sector caused the higher altitudes of the Milicia trunk stream than those of its second-order stem (Cox, 1994; Garrote et al., 2008, 2006; Keller and Pinter, 1996). Vertical incision and lateral bevelling to the West (Milicia

River) and the East (Eleuterio River) are also responsible for dismantling the watershed between these two main rivers and its current occurrence at a lower elevation (Fig. 13e). In our model, the growth of the Cozzo Mangiatorello anticline was caused by the activity of the deep blind thrust.

5.2 Research design in LSRr

The proposed approach aims at overcoming the complexities typical of the coastal LSRrs by using integrated land-to-sea analyses. We used quantitative morphotectonic and high-resolution marine geophysics to detect the evidence of ongoing tectonic deformation, i.e., the geomorphic and sedimentary effects of the cumulated uplift and subsidence accrued in the footwall and hangingwall fault blocks. Instead of looking for the direct surface expression of the first order active faults, the tectonically driven surface deformation analysis allows exploiting some of the peculiar characteristics of the investigated environments (geomorphic markers, anomalies and syntectonic growth strata), which can be used as information about first-order faults. Indeed, being the geographical and geometrical distribution of the surface deformation linked to the geometry and kinematics of the active faults, the quantification of its pattern can be used to infer the fault parameters via inverse fault modelling.

Our study area was previously investigated through traditional methods of outcropping geology analysis (Catalano et al., 2013, 2010a; Guarnieri, 2004; Nigro and Renda, 2001) and using a land-to-sea analysis aimed at detecting stratigraphic and structural evidence of primary faulting (Del Ben and Guarnieri, 2000). Both approaches have not detected any evidence of ongoing tectonic activity, concluding that this sector of the SFTB does not host any active fault. Given the non-conservative nature of most of the outcropping lithologies in the onshore portion of the area (Fig. 2), only the less erodible carbonate rocks can preserve stratigraphic and structural evidence of faulting. In addition, due to the age of such carbonate rocks, their analysis can provide information only for the Mio-Pliocene compressional events responsible for setting up the region's current structural architecture (Catalano et al., 2013, 2010a; Gugliotta et al., 2014). Indeed, in this area, the low tectonic strain rates and the substantial rooting depth and blind geometry of the active structures imply little or no primary surficial expression of active faulting, which is also typical of other LSRrs and is a characteristic shared with other Italian areas where the inherited morphological and structural grain hide the active faults morphological signature (Valensise and Pantosti, 2001).

In the offshore, such lack of evidence of recent primary faulting relates to the fact that: a) in LSRrs, the deformation rates are generally lower than the sedimentary ones, and b) a more ductile behaviour characterises the youngest layers of the stratigraphic sequence. Indeed, several authors

documented a strong correlation between the fault propagation to slip ratio with vertical lithological changes, for which the accumulation of slip on the fault plane instead of the vertical propagation of fault tip is enhanced by less competent lithologies (Allmendinger and Shaw, 2000; Livio et al., 2020; Thebian et al., 2018). This implies that the propagation of fault tips hardly reaches the most recent sedimentary levels. Thus, these layers are most likely affected by second-order geological structures accommodating the slow strain caused by more deeply rooted, elusive primary structures (Corradino et al., 2021).

To sum up, the inversion of the deformation field obtained through both the onshore and offshore analyses allow the parameterisation of the active faults responsible for the deformation (Figs. 8 and 9). Moreover, the multidisciplinary approach proposed here is little or not affected by scale-related problems that can lead to an incorrect hierarchisation of the detected geologic structures, a significant misinterpretation of the wavelength of the structures and, thus, to an unreliable overall fault pattern architecture.

5.3 Active fault pattern and slip rate

Through our morphotectonic evolution model, we propose a blind reverse fault causing the growth of Cozzo Mangiatorello and, at the same time, the westward horizontal shift of the Milicia River trunk stream (Fig. 13). We parametrise such structure in the 3D fault model (Tab. 4), proposing a geometrically possible and geologically plausible NNW-SSE, E-dipping, blind reverse fault extending from the Mangiatorello area to the Palermo gulf offshore (Fig. 11a - c). Such reconstruction considers the morphometric anomalies located near Cozzo Mangiatorello, the analysis of bedding and the ongoing folding evidence in the Palermo Gulf (Figs. 5, 6, 9f, 11b, 12a and b). Similarly, we propose a more internal structure linking deformation evidence collected offshore, near the coast and the Mt. Cane ridge (Figs. 5, 6f, 9c – e and h). Indeed, the geographic, geometric, and stereological characteristics of folds in the Gulf of Termini are like the structures in the Monte Cane ridge, such as a wavelength of about 5 km and an NNW-SSE strike direction (Figs. 9c – d, 10, 11b). Together with the detected drainage divide anomalies and fault modelling result (Figs. 5, 6, 7, 12a and c) such similarities suggest the prosecution of this structure from land to sea (Figs. 11b).

Moreover, the different altitudes of marine pelagic deposits of the Trubi formation (Lower Pliocene) outcropping both in the front and in the back of the Mt. Cane anticline (stars in Fig. 2) suggest that the described morphotectonic evolution must frame in a time ranging from late Pliocene (after 3.6 Ma) to the Present-day. According to Di Maggio et al., (2017), numerous slopes of north-western Sicily are wide fault scarps formed during the Calabrian stage (about 1.5 Ma), following faults

lowering large blocks of the northern Sicilian chain below the Tyrrhenian Sea. In this case, our morphotectonic evolution would begin more recently (after 1.5 Ma), partially reactivating favourable oriented, previously formed structures when the ongoing shortening phase began (roughly 0.8 My ago, Sulli et al., 2021). Based on the evidence of post 20 kyr activity of such fault patterns, as shown in Fig. 9 (g - i) and fault dislocation modelling results in Fig. 12b, and, considering that the stress field in this area has not changed during such a period, it is possible to assume that outermost folding is still in progress.

The reconstructed structural architecture in the geological model proposed in Fig. 11a is compatible with the compressive to transpressional thrusting and block rotation processes proposed by Catalano et al., (2013, 2010a), Guarnieri, (2004), Nigro and Renda, (2001). However, outcomes proving the activities of such faults are in contrast with the low seismic moment release of the studied area (e.g., Rovida et al., 2020), suggesting that a possible fault creeping process occurring in the inferred geological structures could currently cause the slow deformation recorded by GNSS. The presence of hydrated phyllosilicates in the mineralogic content of both the Numidian Flysch and the Mufara Fm. (that host the reconstructed décollement surfaces), which may facilitate the creeping processes, support such a hypothesis (Avellone et al., 2010; Balestra et al., 2019; Dongarra and Ferla, 1982; Harris, 2017). In any case, the shallow depth of the décollement of these faults points to a little seismic potential in terms of the maximum magnitude of these active structures.

We used the fold deformation of the late-Pleistocene unconformity mapped in the Gulf of Palermo (Fig. 12e) and fault dislocation model results, to constrain the slip rate of the CMf. We computed a slip rate of 0.84 ± 0.03 mm/yr, considering that: 1) the unconformity is 18 - 23 kyr old, 2) the fold relative uplift is 11.5 m ± 1.0 and 3) our model predicts, for a 55° dipping fault, 0.67 m of relative uplift for every meter of slip on the fault plane. This value implies a horizontal shortening rate of 0.48 ± 0.02 mm/yr that is in agreement with our GNSS results.

Conclusions

Our multidisciplinary land-to-sea approach allowed detecting and parametrising two partially offshore active faults within an area previously considered not actively deforming. The Monte Cane fault is a NNW-SSE, N60E dipping, about 25 km long, reverse fault detaching at about 4 km of depth, while the Cozzo Mangiatorello fault is a NNW-SSE, N55E dipping, about 28 km long reverse fault detaching at about 3 km of depth. For the Cozzo Mangiatorello fault, we computed a late Pleistocene slip rate of 0.84 ± 0.03 mm/yr. Our approach also allowed us to obtain a GNSS deformation field and

a new morphotectonic evolution model of the landscape of the study area from the mid-late Calabrian age to the recent.

Two open questions still to solve are the seismic or aseismic nature of the detected active faults and the possibility that the deformation observed on these faults is triggered by the activity of more deeply rooted structures. In fact, Sulli et al. (2021) proposes a deep, high-wavelength, folding process that would be responsible for the ongoing deformation of the whole north-western Sicilian continental margin, and the existing relationships between the shallow and deep structures are currently still unknown. We believe that an offshore paleoseismological approach and further morphometric analyses on the flight of quaternary marine terraces in a broader coastal area could provide critical information for answering such open questions and giving better constraints to the kinematics of the shallow faults.

Acknowledgements

Marine geophysical data were acquired by the DiSTeM (University of Palermo) on the R/V Urania in the autumn of 2004. We conducted seismic data processing and interpretation using the Geo-Suite AllWorks software package. The Regional Department of Territory and Environment of the Sicilian Region provided LIDAR data. The MATLAB code Topotoolbox (Schwanghart and Scherler, 2014) was used to process DTM data. The Petex, Move software was used for the geological model construction.

The Department of Engineering developed the GNSS CORS network in the frame of the National Interest Research Program (PRIN2005), founded by the Italian Minister of Instruction, University and Scientific Research (MIUR). GPS data were processed in a post-processing phase using the Professional version of NDA software developed by Galileian Plus Ltd., in collaboration with the Polytechnic of Milano and the Italian Space Agency (ASI) and given to the Polytechnic School of Palermo in the evaluation version. This research was developed in the frame of the LEMON project (INQUA – AIQUA framework).

References

Agnesi, v., de cristofaro, d., di maggio, c., macaluso, t., madonia, g., messana, v., 2000. Morphotectonic setting of the madonie area (central northern sicily). Mem. Soc. Geol. It 55, 373–379.

Allmendinger, r.w., cardozo, n., fisher, d.m., 2011. Structural geology algorithms: vectors and tensors, structural geology algorithms: vectors and tensors. Cambridge university press, cambridge. Https://doi.org/10.1017/cbo9780511920202

Allmendinger, r.w., shaw, j.h., 2000. Estimation of fault propagation distance from fold shape: implications for earthquake hazard assessment. Geology 28, 1099–1102.

Anderson, h., jackson, j., 1987. Active tectonics of the adriatic region. Geophysical journal of the royal astronomical society 91, 937–983. Https://doi.org/10/cghqjc

Antonioli, f., kershaw, s., renda, p., rust, d., belluomini, g., cerasoli, m., radtke, u., silenzi, s., 2006. Elevation of the last interglacial highstand in sicily (italy): a benchmark of coastal tectonics. Quaternary international 145–146, 3–18. Https://doi.org/10/c79swt

Avellone, g., gennaro, c., gugliotta, c., barchi, m.r., agate, m., 2011. Tectono-stratigraphic evolution of a basin generated by transpression: the case of the early pliocene lascari basin (northern sicily). Italian journal of geosciences 130, 93–105. Https://doi.org/10/gnwg95

Avellone, g., morticelli, m.g., sulli, a., barchi, m.r., catalano, r., 2010. Interference between shallow and deep-seated structures in the sicilian fold and thrust belt, italy. Journal of the geological society 167, 109–126. Https://doi.org/10/cz5dhx

Balestra, m., corrado, s., aldega, l., morticelli, m.g., sulli, a., rudkiewicz, j.l., sassi, w., 2019. Thermal and structural modeling of the scillato wedge-top basin source-to-sink system: insights into the sicilian fold-and-thrust belt evolution (italy). Bulletin of the geological society of america 131, 1763–1782. Https://doi.org/10/gnwhck

Barbarella, m., gandolfi, s., tavasci, l., 2018. Monitoring of the italian gnss geodetic reference frame, in: new advanced gnss and 3d spatial techniques. Springer, pp. 59–71.

Basili, r., burrato, p., de santis, g.m., fracassi, u., maesano, f.e., tarabusi, g., tiberti, m.m., valensise, g., vallone, r., vannoli, p., 2021. Database of individual seismogenic sources (diss), version 3.3. 0: a compilation of potential sources for earthquakes larger than m 5.5 in italy and surrounding areas. Https://doi.org/10.13127/diss3.3.0

Bigi, g., cosentino, d., parotto, m., sartori, r., scandone, p., 1992. Structural model of italy and gravity map, scale 1: 500.000. Quademi de'la ricera scientifica.

Billi, a., presti, d., faccenna, c., neri, g., orecchio, b., 2007. Seismotectonics of the nubia plate compressive margin in the south tyrrhenian region, italy: clues for subduction inception. Journal of geophysical research: solid earth 112, 1–13. Https://doi.org/10/dr9c7c

Billi, a., presti, d., orecchio, b., faccenna, c., neri, g., 2010. Incipient extension along the active convergent margin of nubia in sicily, italy: cefalù-etna seismic zone. Tectonics 29, n/a-n/a. Https://doi.org/10/bvxppn

Boucher, c., altamimi, z., 2011. Memo: specifications for reference frame fixing in the analysis of a euref gps campaign. Version 8, 5–18.

Bull, w.b., 2009. Tectonically active landscapes, tectonically active landscapes. Https://doi.org/10.1002/9781444312003

Bull, w.b., 2008. Tectonic geomorphology of mountains: a new approach to paleoseismology. Https://doi.org/10.1002/9780470692318

Burbank, d., anderson, r., 2001. Tectonic geomorphology.

Burbank, d.w., anderson, r.s., 2011. Tectonic geomorphology. Wiley online library.

Burrato, p., ciucci, f., valensise, g., 2003a. An inventory of river anomalies in the po plain, northern italy: evidence for active blind thrust faulting. Annals of geophysics 46, 865–882. Https://doi.org/10/gnwg83

Burrato, p., ciucci, f., valensise, g., 2003b. An inventory of river anomalies in the po plain, northern italy: evidence for active blind thrust faulting. Annals of geophysics 46.

Campbell, g.e., walker, r.t., abdrakhmatov, k., jackson, j., elliott, j.r., mackenzie, d., middleton, t., schwenninger, j.-l., 2015. Great earthquakes in low strain rate continental interiors: an example from se kazakhstan. Journal of geophysical research: solid earth 120, 5507–5534. Https://doi.org/10/ggz7fn

Cappadonia, c., cafiso, f., 2019. Landslide inventory and rockfall risk assessment of a strategic urban area (palermo, sicily). Rendiconti online della società geologica italiana 48, 96–105.

Cappadonia, c., cafiso, f., ferraro, r., martinello, c., rotigliano, e., 2021. Rockfall hazards of mount pellegrino area (sicily, southern italy). Journal of maps 17, 29–39. Https://doi.org/10/gn8rzw

Cappadonia, c., di maggio, c., agate, m., agnesi, v., 2020. Geomorphology of the urban area of palermo (italy). Journal of maps 16, 274–284. Https://doi.org/10/gn8rzx

Catalano, avellone, g., basilone, l., contino, a., agate, m., di maggio, c., lo iacono, c., sulli, a., gugliotta, c., gasparo morticelli, m., 2013. Catalano, avellone, g., basilone, l., contino, a., agate, m., 2013b. Carta geologica d'italia alla scala 1: 50.000, foglio 595 palermo. Ispra, servizio geologico d'italia, regione siciliana, assessorato territorio ed ambiente. Https://www.isprambiente.gov.it/media/carg/sicilia.html.

Catalano, r., agate, m., albanese, c., avellone, g., basilone, l., gasparo morticelli, m., gugliotta, c., sulli, a., valenti, v., gibilaro, c., pierini, s., 2013a. Walking along a crustal profile across the sicily fold and thrust belt, geological field trips. Https://doi.org/10.3301/gft.2013.05

Catalano, r., avellone, g., basilone, l., agate, m., sulli, a., barchi, m., bonomo, s., calvi, f., castiglione, d., contino, a., 2007. Foglio 595 palermo.

Catalano, r., avellone, g., basilone, l., contino, a., agate, m., gugliotta, c., di maggio, c., di stefano, e., gennaro, c., arnone, m., 2011. Carta geologica d'italia alla scala 1: 50.000, foglio 609-596 termini imerese - capo plaia. Ispra, servizio geologico d'italia, regione siciliana, assessorato territorio ed ambiente. Https://www.isprambiente.gov.it/media/carg/sicilia.html.

Catalano, r., avellone, g., basilone, l., gasparo morticelli, m., lo cicero, g., gugliotta, c., di maggio, c., contino, a., albanese, c., lena, g., 2010a. Carta geologica d'italia alla scala 1: 50.000, foglio 608 caccamo. Ispra, servizio geologico d'italia, regione siciliana, assessorato territorio ed ambiente. Https://www.isprambiente.gov.it/media/carg/sicilia.html.

Catalano, r., avellone, g., basilone, l., sulli, a., 2010b. Catalano, r., avellone, g., basilone, l., sulli, a., 2010b. Carta geologica d'italia alla scala 1: 50.000, foglio n. 607 corleone ispra, servizio geologico d'italia, regione siciliana, assessorato territorio ed ambiente. Https://www.isprambiente.gov.it/media/carg/sicilia.html.

Catalano, r., merlini, s., sulli, a., 2002. The structure of western sicily, central mediterranean. Petroleum geoscience 8, 7–18. Https://doi.org/10/bd3tss

Catalano, r., valenti, v., albanese, c., accaino, f., sulli, a., tinivella, u., gasparo morticelli, m., zanolla, c., giustiniani, m., 2013b. Sicily's fold-thrust belt and slab roll-back: the si.ri.pro. Seismic crustal transect. Journal of the geological society 170, 451–464. Https://doi.org/10/gnwhcm

Channell, j., oldow, j., catalano, r., d'argenio, b., 1990. Paleomagnetically determined rotations in the western sicilian fold and thrust belt. Tectonics 9, 641–660.

Congalton, r.g., 1991. A review of assessing the accuracy of classifications of remotely sensed data. Remote sensing of environment 37, 35–46. Https://doi.org/10.1016/0034-4257(91)90048-b

Corradino, m., pepe, f., burrato, p., kanari, m., parrino, n., bertotti, g., bosman, a., casalbore, d., ferranti, l., martorelli, e., monaco, c., sacchi, m., tibor, g., 2021. An integrated multiscale method for the characterisation of active faults in offshore areas. The case of sant'eufemia gulf (offshore calabria, italy). Frontiers in earth science 9. Https://doi.org/10/gkjtwn

Cox, r.t., 1994. Analysis of drainage-basin symmetry as a rapid technique to identify areas of possible quaternary tilt-block tectonics: an example from the mississippi embayment. Geological society of america bulletin 106, 571. Https://doi.org/10/c33x73

Dardanelli, g., lo brutto, m., pipitone, c., 2020. Gnss cors network of the university of palermo: design and first analysis of data. Geographia technica 15, 43–69. Https://doi.org/10/ggnxn9

De santis, v., scardino, g., meschis, m., ortiz, j.e., sánchez-palencia, y., caldara, m., 2021. Refining the middle-late pleistocene chronology of marine terraces and uplift history in a sector of the apulian foreland (southern italy) by applying a synchronous correlation technique and amino acid racemization to patella spp. And thetystrombus latus. Italian journal of geosciences 140, 438–463. Https://doi.org/10/gnwhfc

Del ben, a., guarnieri, p., 2000. Neogene transpression in the cefalu basin (southern tyrrhenian): comparison between land and marine data. Memoria della societa geologica italiana 55, 27–33.

Demoulin, a., 2012. Morphometric dating of the fluvial landscape response to a tectonic perturbation. Geophysical research letters 39, 1–5. Https://doi.org/10/gcskzg

Demoulin, a., 2011. Basin and river profile morphometry: a new index with a high potential for relative dating of tectonic uplift. Geomorphology 126, 97–107. Https://doi.org/10/bfwshg

Devoti, r., d'agostino, n., serpelloni, e., pietrantonio, g., riguzzi, f., avallone, a., cavaliere, a., cheloni, d., cecere, g., d'ambrosio, c., falco, l., selvaggi, g., métois, m., esposito, a., sepe, v., galvani, a., anzidei, m., 2017. A combined velocity field of the mediterranean region. Annals of geophysics 60, s0215. Https://doi.org/10/gnwhbs

Di maggio, c., 2000. Morphostructural aspects of the central northern sector of palermo mountains (sicily). Mem. Soc. Geol. It 55.

Di maggio, c., madonia, g., parise, m., vattano, m., 2012. Karst of sicily and its conservation. Journal of cave and karst studies 74, 157–172. Https://doi.org/10/f4bhtw

Di maggio, c., madonia, g., vattano, m., 2014. Deep-seated gravitational slope deformations in western sicily: controlling factors, triggering mechanisms, and morphoevolutionary models. Geomorphology 208, 173–189. Https://doi.org/10/gngn27

Di maggio, c., madonia, g., vattano, m., agnesi, v., monteleone, s., 2017. Geomorphological evolution of western sicily, italy. Geologica carpathica 68, 80–93. Https://doi.org/10/gk5qqf

Di stefano, p., favara, r., luzio, d., renda, p., cacciatore, m.s., calò, m., napoli, g., parisi, l., todaro, s., zarcone, g., 2015. A regional-scale discontinuity in western sicily revealed by a multidisciplinary approach: a new piece for understanding the geodynamic puzzle of the southern mediterranean. Tectonics 34, 2067–2085. Https://doi.org/10/gjpq57

Dongarra, g., ferla, p., 1982. Le argille di portella colla e del flysch numidico auct. (m. Madonie - sicilia). Aspetti deposizionali e diagenetici. Rendiconti della societa italiana di mineralogia e petrologia 38, 1119–1133.

Dziewonski, a.m., chou, t., woodhouse, j.h., 1981. Determination of earthquake source parameters from waveform data for studies of global and regional seismicity. Journal of geophysical research: solid earth 86, 2825–2852. Https://doi.org/10/dq766t

Ekström, g., nettles, m., dziewoński, a.m., 2012. The global cmt project 2004–2010: centroid-moment tensors for 13,017 earthquakes. Physics of the earth and planetary interiors 200, 1–9. Https://doi.org/10/gctpdx

Faccenna, c., piromallo, c., crespo-blanc, a., jolivet, l., rossetti, f., 2004. Lateral slab deformation and the origin of the western mediterranean arcs. Tectonics 23. Https://doi.org/10/bmz2qd

Ferranti, l., antonioli, f., mauz, b., amorosi, a., dai pra, g., mastronuzzi, g., monaco, c., orrù, p., pappalardo, m., radtke, u., renda, p., romano, p., sansò, p., verrubbi, v., 2006. Markers of the last interglacial sea-level high stand along the coast of italy: tectonic implications. Quaternary international 145–146, 30–54. Https://doi.org/10/bsmjmv

Ferranti, l., oldow, j.s., d'argenio, b., catalano, r., lewis, d., marsella, e., avellone, g., maschio, l., pappone, g., pepe, f., sulli, a., 2008. Active deformation in southern italy, sicily and southern sardinia from gps velocities of the peri-tyrrhenian geodetic array (ptga). Bollettino della societa geologica italiana 127, 299–316.

Ferranti, l., pepe, f., barreca, g., meccariello, m., monaco, c., 2019. Multi-temporal tectonic evolution of capo granitola and sciacca foreland transcurrent faults (sicily channel). Tectonophysics 765, 187–204. Https://doi.org/10/gnwhcd

Fisher, r., 1953. Dispersion on a sphere. Proceedings of the royal society a: mathematical, physical and engineering sciences 217, 295–305. Https://doi.org/10/djwjf3

Gandolfi, s., tavasci, l., poluzzi, l., 2016. Improved ppp performance in regional networks. Gps solutions 20, 485–497. Https://doi.org/10/f8s73x

Garrote, j., cox, r.t., swann, c., ellis, m., 2006. Tectonic geomorphology of the southeastern mississippi embayment in northern mississippi, usa. Bulletin of the geological society of america 118, 1160–1170. Https://doi.org/10/dwjjm7

Garrote, j., garzón heydt, g., cox, r.t., 2008. Multi-stream order analyses in basin asymmetry: a tool to discriminate the influence of neotectonics in fluvial landscape development (madrid basin, central spain). Geomorphology 102, 130–144. Https://doi.org/10/fxfm3d

Gasparo morticelli, m., valenti, v., catalano, r., sulli, a., agate, m., avellone, g., albanese, c., basilone, l., gugliotta, c., 2015. Deep controls on foreland basin system evolution along the sicilian fold and thrust belt. Bulletin de la société géologique de france 186, 273–290. Https://doi.org/10/f7r2pz

Giunta, g., luzio, d., tondi, e., de luca, l., giorgianni, a., d'anna, g., renda, p., cello, g., nigro, f., vitale, m., 2004. The palermo (sicily) seismic cluster of september 2002, in the seismotectonic framework of the tyrrhenian sea-sicily border area. Annals of geophysics 47, 1755–1770. Https://doi.org/10/gjpq5w

Giunta, g., nigro, f., renda, p., 2002. Inverted structures in western sicily. Bolletino della societa geologica italiana 121, 11–17.

Giunta, g., nigro, f., renda, p., giorgianni, a., 2000. The sicilian-maghrebides tyrrhenian margin: a neotectonic evolutionary model. Bollettino della società geologica italiana 119, 553–565.

Goes, s., jenny, s., hollenstein, c., kahle, h.g., geiger, a., 2004. A recent tectonic reorganization in the south-central mediterranean. Earth and planetary science letters 226, 335–345. Https://doi.org/10/b4j2gb

Goren, l., castelltort, s., klinger, y., 2015. Modes and rates of horizontal deformation from rotated river basins: application to the dead sea fault system in lebanon. Geology 43, 843–846. Https://doi.org/10/f7n84g

Group, isid.w., 2007. Italian seismological instrumental and parametric database (iside).

Guarnieri, p., 2004. Structural evidence for deformation by block rotation in the context of transpressive tectonics, northwestern sicily (italy). Journal of structural geology 26, 207–219. Https://doi.org/10/c264mn

Gugliotta, c., 2011. Partitioning between "wedge-top" river- and wave-dominated successions: an example from the late tortonian - early messinian terravecchia formation (nw sicily). Central european journal of geosciences 3, 235–259. Https://doi.org/10/db4cxs

Gugliotta, c., gasparo morticelli, m., 2012. Using high-resolution stratigraphy and structural analysis to constrain polyphase tectonics in wedge-top basins: inferences from the late tortonian scillato basin (central-northern sicily). Sedimentary geology 273–274, 30–47. Https://doi.org/10/gnwg94

Gugliotta, c., gasparo morticelli, m., avellone, g., agate, m., barchi, m.r., albanese, c., valenti, v., catalano, r., 2014. Middle miocene–early pliocene wedge-top basins of nw sicily (italy): constraints for the tectonic evolution of a 'non-conventional' thrust belt, affected by transpression. Journal of the geological society 171, 211–226. Https://doi.org/10/gnwg93

Harris, r.a., 2017. Large earthquakes and creeping faults. Reviews of geophysics 55, 169–198. Https://doi.org/10/f94gwb

Heidbach, o., rajabi, m., cui, x., fuchs, k., müller, b., reinecker, j., reiter, k., tingay, m., wenzel, f., xie, f., ziegler, m.o., zoback, m.l., zoback, m., 2018. The world stress map database release 2016: crustal stress pattern across scales. Tectonophysics 744, 484–498. Https://doi.org/10/gff69f

Henriquet, m., dominguez, s., barreca, g., malavieille, j., monaco, c., 2020. Structural and tectono-stratigraphic review of the sicilian orogen and new insights from analogue modeling. Earth-science reviews 208, 103257. Https://doi.org/10/gnwhc9

Hough, s.e., 2002. The 26 january 2001 m 7.6 bhuj, india, earthquake: observed and predicted ground motions. Bulletin of the seismological society of america 92, 2061–2079. Https://doi.org/10/dg8c85

Incarbona, a., contino, a., agate, m., bonomo, s., calvi, f., di stefano, e., giammarinaro, m.s., priulla, a., sprovieri, r., 2016. Biostratigraphy, chronostratigraphy and paleonvironmental reconstruction of the palermo historical centre quaternary succession. Italian journal of geosciences 135, 512–525. Https://doi.org/10/f87dw7

Jaiswara, n.k., pandey, p., pandey, a.k., 2019. Mio-pliocene piracy, relict landscape and drainage reorganization in the namcha barwa syntaxis zone of eastern himalaya. Scientific reports 9, 17585. Https://doi.org/10/gnwhc3

Keller, e.a., pinter, n., 1996. Active tectonics. Prentice hall upper saddle river, nj.

King, t.r., quigley, m., clark, d., zondervan, a., may, j.h., alimanovic, a., 2021. Paleoseismology of the 2016 mw 6.1 petermann earthquake source: implications for intraplate earthquake behaviour and the geomorphic longevity of bedrock fault scarps in a low strain-rate cratonic region. Earth surface processes and landforms 46, 1238–1256. Https://doi.org/10/gnwhd3

Klobuchar, j.a., 1996. Ionospheric effects on gps. Global positioning system: theory and application.

Lambeck, k., antonioli, f., anzidei, m., ferranti, l., leoni, g., scicchitano, g., silenzi, s., 2011. Sea level change along the italian coast during the holocene and projections for the future. Quaternary international 232, 250–257. Https://doi.org/10/csft3s

Landgraf, a., kübler, s., hintersberger, e., stein, s., 2017. Active tectonics, earthquakes and palaeoseismicity in slowly deforming continents. Geological society special publication 432, 1–12. Https://doi.org/10/gnwhc4

Laubach, s.e., olson, j.e., cross, m.r., 2009. Mechanical and fracture stratigraphy. Aapg bulletin 93, 1413–1426. Https://doi.org/10/bbkb4h

Laubach, s.e., schultz-ela, d.d., tyler, r., 1999. Differential compaction of interbedded sandstone and coal. Geological society, london, special publications 169, 51–60. Https://doi.org/10/fm44fx

Livio, f.a., ferrario, m.f., frigerio, c., zerboni, a., michetti, a.m., 2020. Variable fault tip propagation rates affected by near-surface lithology and implications for fault displacement hazard assessment. Journal of structural geology 130. Https://doi.org/10/gnwhdv

Lo iacono, c.l., sulli, a., agate, m., lo presti, v., pepe, f., catalano, r., 2011. Submarine canyon morphologies in the gulf of palermo (southern tyrrhenian sea) and possible implications for geo-hazard. Marine geophysical research 32, 127–138. Https://doi.org/10/d5ffzn

Mariucci, m.t., montone, p., 2020. Database of italian present-day stress indicators, ipsi 1.4. Scientific data 7, 1–11. Https://doi.org/10/gnwhfn

Mastrolembo ventura, b., serpelloni, e., argnani, a., bonforte, a., bürgmann, r., anzidei, m., baldi, p., puglisi, g., 2014. Fast geodetic strain-rates in eastern sicily (southern italy): new insights into block tectonics and seismic potential in the area of the great 1693 earthquake. Earth and planetary science letters 404, 77–88. Https://doi.org/10/f6m3tw

Mauz, b., buccheri, g., zöller, l., greco, a., 1997. Middle to upper pleistocene morphostructural evolution of the nw-coast of sicily: thermoluminescence dating and palaeontological-stratigraphical evaluations of littoral deposits. Palaeogeography, palaeoclimatology, palaeoecology 128, 269–285. Https://doi.org/10/db7qrr

Mccalpin, j.p., thakkar, m.g., 2003. 2001 bhuj-kachchh earthquake: surface faulting and its relation with neotectonics and regional structures, gujarat, western india. Annals of geophysics 46, 937–956. Https://doi.org/10/gnwhdq

Meade, b.j., 2007. Algorithms for the calculation of exact displacements, strains, and stresses for triangular dislocation elements in a uniform elastic half space. Computers and geosciences 33, 1064–1075. Https://doi.org/10/bkt97r

Meschis, m., scicchitano, g., roberts, g.p., robertson, j., barreca, g., monaco, c., spampinato, c., sahy, d., antonioli, f., mildon, z.k., scardino, g., 2020. Regional deformation and offshore crustal local faulting as combined processes to explain uplift through time constrained by investigating differentially uplifted late quaternary paleoshorelines: the foreland hyblean plateau, se sicily. Tectonics 39. Https://doi.org/10/gnwhfg

Mignard, f., 2003. Famous. Frequency analysis mapping on unusual sampling,(oca cassiopee), software.

Newman, a., stein, s., weber, j., engeln, j., mao, a., dixon, t., 1999. Slow deformation and lower seismic hazard at the new madrid seismic zone. Science 284, 619–621. Https://doi.org/10/c6c67p

Niell, a.e., 1996. Global mapping functions for the atmosphere delay at radio wavelengths. Journal of geophysical research: solid earth 101, 3227–3246. Https://doi.org/10/d4bw9r

Nigro, f., renda, p., 2002. From mesozoic extension to tertiary collision: deformation patterns in the units of the north-western sicilian chain. Boll. Soc. Geol. It. 121, 87–97.

Nigro, f., renda, p., 2001. Oblique-slip thrusting in the maghrebide chain of sicily (*). Boll. Soc. Geol. It. 187–200.

O'callaghan, j.f., mark, d.m., 1984. The extraction of drainage networks from digital elevation data. Computer vision, graphics, and image processing 28, 323–344. Https://doi.org/10/drcwbw

Okada, b., 1985. Surface deformation due to shear and tensile faults in a half-space. International journal of rock mechanics and mining sciences & geomechanics abstracts 23, 128. Https://doi.org/10/bnnwk6

Oldow, j., channell, j., catalano, r., d'argenio, b., 1990. Contemporaneous thrusting and large-scale rotations in the western sicilian fold and thrust belt. Tectonics 9, 661–681. Https://doi.org/10/fhk6b6

Parrino, n., agosta, f., di stefano, p., napoli, g., pepe, f., renda, p., 2019. Fluid storage and migration properties of sheared neptunian dykes. Marine and petroleum geology 102, 521–534. Https://doi.org/10/gnwhbj

Pepe, f., bertotti, g., cella, f., marsella, e., 2000. Rifted margin formation in the south tyrrhenian sea: a high-resolution seismic pofile across the north sicily passive continental margin. Tectonics 19, 241–257. Https://doi.org/10/d6mz59

Pepe, f., bertotti, g., cloetingh, s., 2004. Tectono-stratigraphic modelling of the north sicily continental margin (southern tyrrhenian sea). Tectonophysics 384, 257–273. Https://doi.org/10/bjdzpf

Pepe, f., sulli, a., bertotti, g., catalano, r., 2005. Structural highs formation and their relationship to sedimentary basins in the north sicily continental margin (southern tyrrhenian sea): implication for the drepano thrust front. Tectonophysics 409, 1–18. Https://doi.org/10/csh74t.

Perron, j.t., royden, l., 2013. An integral approach to bedrock river profile analysis. Earth surface processes and landforms 38, 570–576. Https://doi.org/10/f4wdkp.

Pondrelli, s., visini, f., rovida, a., d'amico, v., pace, b., meletti, c., 2020. Style of faulting of expected earthquakes in italy as an input for seismic hazard modeling. Nat. Hazards earth syst. Sci., 20, 3577–3592, https://doi.org/10.5194/nhess-20-3577-2020, 2020.

Ramsay, j.g., huber, m.i., 1987. The techniques of modern structural geology: folds and fractures. Academic press.

Randazzo, v., le goff, j., di stefano, p., reijmer, j., todaro, s., cacciatore, m.s., 2020. Carbonate slope re-sedimentation in a tectonically-active setting (western sicily cretaceous escarpment, italy). Sedimentology 67, 2360–2391.

Regione siciliana, 2010. Modello digitale del terreno (mdt) 2m x 2m regione siciliana-ata 2007-2008 [www document]. Url http://www. Sitr. Regione. Sicilia. It.

Robertson, j., roberts, g.p., iezzi, f., meschis, m., gheorghiu, d.m., sahy, d., bristow, c., sgambato, c., 2020. Distributed normal faulting in the tip zone of the south alkyonides fault system, gulf of corinth, constrained using 36cl exposure dating of late-quaternary wave-cut platforms. Journal of structural geology 136. Https://doi.org/10/gnwhff

Roggero, m., 2015. Extensive analysis of igs repro1 coordinate time series, in: viii hotine-marussi symposium on mathematical geodesy. Springer, pp. 81–89. Https://doi.org/10/gnwhdz

Roure, f., howell, d.g., müller, c., moretti, i., 1990. Late cenozoic subduction complex of sicily. Journal of structural geology 12, 259–266. Https://doi.org/10/d6cj6r

Rovida, a., locati, m., camassi, r., lolli, b., gasperini, p., 2020. The italian earthquake catalogue cpti15, bulletin of earthquake engineering. Springer netherlands. Https://doi.org/10.1007/s10518-020-00818-y

Saastamoinen, j., 1972. Atmospheric correction for the troposphere and stratosphere in radio ranging satellites. The use of artificial satellites for geodesy 15, 247–251.

Santoro, e., ferranti, l., burrato, p., mazzella, m.e., monaco, c., 2013. Deformed pleistocene marine terraces along the ionian sea margin of southern italy: unveiling blind fault-related folds contribution to coastal uplift. Tectonics 32, 737–762. Https://doi.org/10/f45j2g

Scherler, d., schwanghart, w., 2020. Drainage divide networks - part 2: response to perturbations. Earth surface dynamics 8, 261–274. Https://doi.org/10/gnwhcr

Schwanghart, w., scherler, d., 2014. Short communication: topotoolbox 2 - matlab-based software for topographic analysis and modeling in earth surface sciences. Earth surface dynamics 2, 1–7. Https://doi.org/10/gb9b74

Schwiderski, e.w., 1980. On charting global ocean tides. Reviews of geophysics 18, 243–268. Https://doi.org/10/ccg599

Speranza, f., hernandez-moreno, c., avellone, g., gasparo morticelli, m., agate, m., sulli, a., di stefano, e., 2018. Understanding paleomagnetic rotations in sicily: thrust versus strike-slip tectonics. Tectonics 37, 1138–1158. Https://doi.org/10/gdtcn9

Stein, s., 2007. Approaches to continental intraplate earthquake issues. Special paper of the geological society of america 425, 1–16. Https://doi.org/10/d3v6tj

Sulli, a., gasparo morticelli, m., agate, m., zizzo, e., 2021. Active north-vergent thrusting in the northern sicily continental margin in the frame of the quaternary evolution of the sicilian collisional system. Tectonophysics 802. Https://doi.org/10/gnwhds

Sulli, a., morticelli, m.g., agate, m., zizzo, e., 2019. Hinterland-verging thrusting in the northern sicily continental margin: evidences for a late collisional stage of the sicilian fold and thrust belt?, in: the structural geology contribution to the africa-eurasia

geology: basement and reservoir structure, ore mineralisation and tectonic modelling. Springer, pp. 251–253. Https://doi.org/10.1007/978-3-030-01455-1_54

Suppe, j., 1983. Geometry and kinematics of fault-bend folding., american journal of science. Https://doi.org/10.2475/ajs.283.7.684

Teunissen, p.j.g., de jonge, p.j., tiberius, c., 1997. The least-squares ambiguity decorrelation adjustment: its performance on short gps baselines and short observation spans. Journal of geodesy 71, 589–602. Https://doi.org/10/d3kz3q

Thebian, l., najjar, s., sadek, s., mabsout, m., 2018. Numerical investigation of dip-slip fault propagation effects on offshore seabed sediments. Engineering geology 237, 149–167. Https://doi.org/10/gc4nhz

Tondi, e., blumetti, a.m., čičak, m., di manna, p., galli, p., invernizzi, c., mazzoli, s., piccardi, l., valentini, g., vittori, e., volatili, t., 2021. 'conjugate' coseismic surface faulting related with the 29 december 2020, mw 6.4, petrinja earthquake (sisak-moslavina, croatia). Scientific reports 11. Https://doi.org/10/gnwhfd

Totaro, c., kukarina, e., koulakov, i., neri, g., orecchio, b., presti, d., 2017. Seismotomographic detection of major structural discontinuity in northern sicily. Italian journal of geosciences 136, 389–398. Https://doi.org/10/gnwg9v

Tuttle, m.p., wolf, l.w., starr, m.e., villamor, p., lafferty, r.h., morrow, j.e., scott, r.j., forman, s.l., hess, k., tucker, k., 2019. Evidence for large new madrid earthquakes about ad 0 and 1050 bc, central united states. Seismological research letters 90, 1393–1406. Https://doi.org/10/gnwhd6

Valensise, g., pantosti, d., 2001. The investigation of potential earthquake sources in peninsular italy: a review, journal of seismology.

Vannoli, p., basili, r., valensise, g., 2004. New geomorphic evidence for anticlinal growth driven by blind-thrust faulting along the northern marche coastal belt (central italy). Journal of seismology 8, 297–312. Https://doi.org/10/d4r78d

Wesnousky, s.g., seeber, l., rockwell, t.k., thakur, v., briggs, r., kumar, s., ragona, d., 2001. Eight days in bhuj: field report bearing on surface rupture and genesis of the 26 january 2001 earthquake in india. Seismological research letters 72, 514–524. Https://doi.org/10/cw8snk

Whipple, k.x., dibiase, r.a., ouimet, w.b., forte, a.m., 2017. Preservation or piracy: diagnosing low-relief, high-elevation surface formation mechanisms. Geology 45, 91–94. Https://doi.org/10/f9vc5f

White, n.j., jackson, j.a., mckenzie, d.p., 1986. The relationship between the geometry of normal faults and that of the sedimentary layers in their hanging walls. Journal of structural geology 8, 897–909. Https://doi.org/10/fvzvgs

Willett, s.d., mccoy, s.w., taylor perron, j., goren, l., chen, c.y., 2014. Dynamic reorganization of river basins. Science 343. Https://doi.org/10/gbfspk

Wobus, c., whipple, k.x., kirby, e., snyder, n., johnson, j., spyropolou, k., crosby, b., sheehan, d., 2006. Tectonics from topography: procedures, promise, and pitfalls. Special paper of the geological society of america 398, 55–74. Https://doi.org/10/cqhm6q

Zitellini, n., ranero, c.r., loreto, m.f., ligi, m., pastore, m., d'oriano, f., sallares, v., grevemeyer, i., moeller, s., prada, m., 2020. Recent inversion of the tyrrhenian basin. Geology 48, 123–127. Https://doi.org/10/gnwhfh

To be submitted

Chapter 2

Quaternary coastal landscape evolution of North-Western Sicily

Authors: Nicolò Parrino[1], Pierfrancesco Burrato[2], Attilio Sulli[1], Maurizio Gasparo Morticelli[1], Mauro Agate[1], Eshaan Srivastava[3], Javed N. Malik[3], Cipriano Di Maggio[1*]

[*]Corresponding author

[1]Dipartimento di Scienze della Terra e del Mare, Università di Palermo, Italy.
[2]Istituto Nazionale di Geofisica e Vulcanologia, Rome, Italy.
[3]Indian Institute of Technology Kanpur, Earth Sciences, India.

Keywords: Marine terraces, low strain rate region, coastal landscape evolution, Quaternary, sea-level change

Abstract:

Broad polycyclic surfaces or staircase distributions of paleoshorelines are the outcomes of the interplay of climate and tectonic forcings on the coastal landscape evolution both at the regional or local scale. These forcings drive coastal landscape evolution globally through vertical differential movements and eustatic sea-level variations, resulting in relative land uplift or subsidence at variable rates. As a result, paleoshorelines are often encoded in the topography of coastal areas as a staircase sequence of several orders of marine terraces or as few and large polycyclic coastal platforms resulting from the reoccupation of old terrace surfaces where a relatively stable sea level or a slow uplifting rate occurred. These landforms can be used as geomorphologic markers to provide a critical dataset for quantifying tectonic and climatic forcings; therefore, understanding their topographical signatures is crucial for decoding the Late Quaternary evolution of coastal landscapes.

The coastal sector of the northern Sicilian continental margin alternates mountains and plains in its western and central portions and ridges with steep slopes in its eastern termination. This sector is a puzzling region resulting from the interaction of two different geodynamic processes. The western and central parts of the margin are characterized by the Africa-Europa collision, in which African thinned continental crust subducted beneath the European Sardinian and Kabylian-Calabrian units. Differently, its rapidly uplifting eastern portion results from the subduction of the Ionian oceanic lithosphere beneath the European Calabrian Arc.

Several studies investigated the differential vertical movements in the eastern sector of the margin, analyzing Quaternary marine terrace staircases, drainage networks, offshore morphobatimetric setting and the sedimentary architecture; conversely, there are still few attempts to investigate the uplift history in the central-western sector of this margin. This sector hosts considerable outcrop evidence of the Neogene shortening processes that affected the northern Sicilian continental margin, such as prominent ridges (structural highs) formed during the two late Serravallian - early Tortonian compressional events. These now exhumed ridges are surrounded by syn-orogenic ductile lithologies that cannot record any outcrop-scale evidence of recent deformation. The youngest yet described outcrop evidence of the ongoing tectonic activity consists of coastal erosional features suggesting a slow regional uplift.

This paper aims to contribute to the knowledge about the ongoing deformation and landscape evolution in the central-western sector of the northern Sicilian continental margin. In pursuing such an aim, we performed quantitative morphometric and field analysis of a flight of Quaternary marine terraces, including a wide polycyclic surface, along the Palermo and Termini Imerese coastal sector

(NW-Sicily, southern Italy). The achieved outcomes summarized in a geomorphological map can improve the knowledge about the framework of active processes along the Africa-Europe plate boundary and its seismotectonic setting.

1. Introduction

The evolution of the coastal landscape is driven by the constant interaction between tectonics and climate. These two forcings shape the present-day landscape through the tectonically induced differential vertical movements and the glacio-eustatically induced migration of the base level of the erosion. Considering the above, the landscape topography can be assumed as the envelope of the tectonics and climate signals and, thus, an archive hosting information about the variation of these two drivers through time.

Some of the primary markers resulting from the interaction of these two signals are paleoshorelines, marine terrace sequences and the Unconformity-Bounded Stratigraphic Units (UBSUs, sensu CHANG, 1975). The joint analyses of these markers allow the reconstruction of the landscape evolution and, in case, the quantification of the differential vertical movements providing valuable data for tectonic dynamics and seismic hazard assessment (e.g., Ferranti et al., 2021; Sulli et al., 2013).

The partially offshore sector of the western Northern Sicilian Continental Margin (NSCM) is a low strain rate region located along the plate boundary of the slowly converging African and European plates. This sector is characterized by a low seismic moment release, an active shortening of about 1 mm/yr and by elusive active faults whose behavioural parameters are still not fully constrained yet (Basili et al., 2021; Devoti et al., 2017; Parrino et al., 2022; Rovida et al., 2021; Sulli et al., 2021). Such sector shows a landscape marked by wide and discontinuous low relief coastal plains interspersed with mountain ranges matching with Mesozoic carbonate structural highs (Di Maggio et al., 2017). Such low relief coastal plains host Plio-Quaternary marine and continental deposits in which broad polycyclic marine terrace surfaces, extending from sea level up to about 100-300 m a.s.l., are carved (Agate et al., 2017; Catalano, Avellone, Basilone, Gasparo Morticelli, et al., 2010; Catalano, Avellone, Basilone, & Sulli, 2010; Di Maggio, 2000).

Despite the significant number of studies in the area, the age of most of the surfaces and Quaternary deposits and, thus, its recent landscape evolution is still a matter of debate (Agate et al., 2017; Antonioli et al., 2006, 2018, 2018; Catalano et al., 2013, 2011; Catalano, Avellone, Basilone, Gasparo Morticelli, et al., 2010; Catalano, Avellone, Basilone, & Sulli, 2010; D'Angelo et al., 2006; Di Maggio et al., 2008; Ferranti et al., 2006). To fill this knowledge gap, we present a review of the

most up to date literature together with a new morphometric dataset extracted from the study area's digital elevation model. The proposed dataset could represent a valuable tool for new studies on seismic hazard assessment and landscape evolution forecasting scenarios.

2. Geological overview

2.1 Stratigraphy

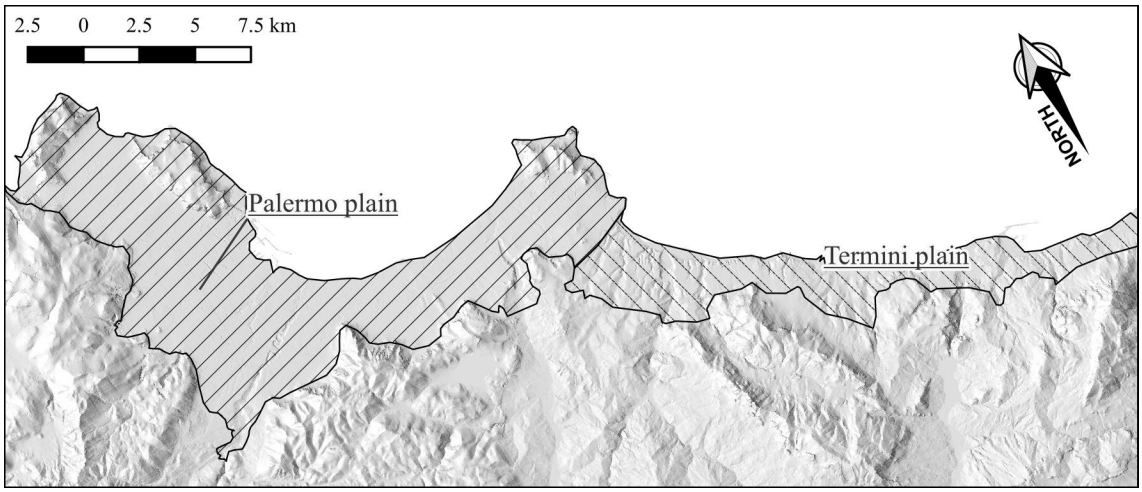

Fig. 1 – The polygons whit different patterns represent the nowadays extent of the Palermo and Termini plains.

The lithologic successions of the Palermo and Termini plain characterize two significant different Upper Neogene to Quaternary basins in the studied area (Fig. 1, Agate et al., 2017; Contino et al., 2006; Di Maggio et al., 2008; Dominici et al., 2020; Incarbona et al., 2016; Lo Iacono et al., 2014; Martorana et al., 2018; Milia et al., 2021).

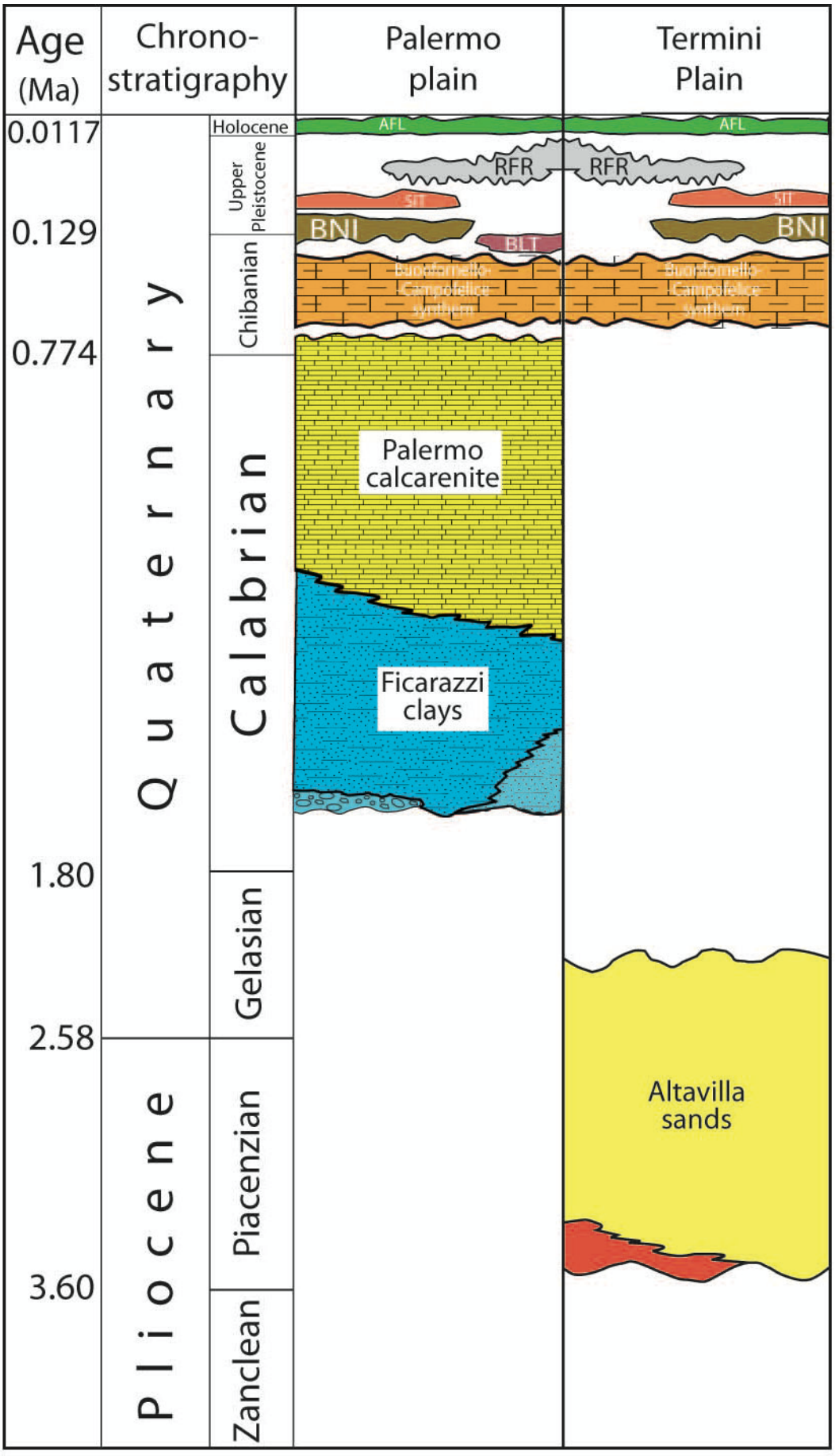
Age (Ma)
Chrono-stratigraphy
Palermo plain
Termini Plain
0.0117
0.129
0.774
1.80
2.58
3.60
Quaternary
Pliocene
Holocene
Upper Pleistocene
Chibanian
Calabrian
Gelasian
Piacenzian
Zanclean
AFL
RFR
SIT
BNI
BLT
Palermo calcarenite
Ficarazzi clays
Altavilla sands

Fig. 2 – a) Stratigraphic log of the Palermo plain from Incarbona et al., 2016; b) Stratigraphic log of the Termini plain from Dominici et al., 2020.

The Palermo plain comprises a Quaternary succession extending partially offshore and consisting of deposits discordantly overlaying the Triassic to Miocene substrate. The lithologies at the base of the succession are members d and e of the Marsala synthem, the Ficarazzi Clays, and the Palermo Calcarenites (Calabrian, 1.5 – 0.8 Ma), respectively (see Fig. 2 for details). The Ficarazzi clays consist of 40-50 meters of bluish clay with sandy-silty horizons/layers with a conglomerate level at the base. Differently, the Palermo Calcarenites are roughly 20 m of yellowish calcarenites and sands with interbedded microconglomerates. The succession continues upwards with about 4 m of middle-late Pleistocene coastal and marine deposits of carbonate, sandy and silty conglomerates unconformably overlaying the previously described units of the Barcarello synthem. The top of the succession is constituted by Holocene continental deposits up to 20 meters thick reddish quartz silty sands with siliceous and carbonate lenses of the Capo Plaia synthem (Martorana et al., 2018).

The sea-level fluctuations had significantly driven the depositional history of the Palermo plain, made up of discontinuous and repeated episodes of marine proximal shelf sedimentation delimited by unconformities. During the Holocene high-stand (7.0 and 8.0 ka), the basins recorded continental and transitional sedimentation that persisted until historical times (Incarbona et al., 2016 and reference therein).

The Termini plain is an NNW-SSE partially offshore Plio-Quaternary basin adjacent to the eastern termination of the Palermo plain basin. Sediments in this basin are arranged in two 80 meters thick, large-scale units of alluvial conglomerates, deltaic sandstones, deltaic-pebbly sandstones, and inner-shelf mudstones eluvium-colluvium continental deposits pertaining to the Sabbie di Altavilla recognized as a member of the Marnoso Arenacea del Belice Fm. The lower part of the succession shows a deepening upward arrangement from alluvial fans to delta front to open shelf paleoenvironment. Evidence of subaerial flood-dominated fluvio-deltaic deposition suggests high slope values of sediment source areas similar to the modern topography. Thin mudstone intervals coarse-grained sediments of the proximal delta, paleosoils, and alluvial fan deposits in the upper part of the succession highlight an initial sediment bypass to deeper marine settings followed by an accommodation space decrease (Dominici et al., 2020). The syn-depositional tectonic activity in this basin is supported by significant unconformities and the difference in dip values between the lower and upper parts of the succession, N345E and N10E, respectively. The latter also highlights the tectonic forcing on the fluvial drainage geometry through which a fluvial system, flowing towards the

NW during Pliocene times, deflected NE during early Pleistocene times. The top of the succession is unconformably covered by a few meters of coastal and marine deposits of the Benincasa synthem.

2.2 Tectonics

The study area falls within the central-western sector of the NSCM (Fig. 1) in which two different geodynamic processes such as the Ionian oceanic crust subduction hinge retreat and Africa - Europe convergence (Catalano et al., 2013c; Di Stefano et al., 2015; Faccenna et al., 2004; Sulli et al., 2021). The collisional system developed since the early Miocene through two subsequent thin and thick-skinned thrusting phases involved the Mesozoic silico-carbonate succession developed on the African passive continental margin re-deforming the pre-existent structural architecture and locally re-activating Mesozoic extensional structures (Avellone et al., 2010; Catalano, Valenti, et al., 2013; Gasparo Morticelli et al., 2015; Gugliotta et al., 2014; Gugliotta & Gasparo Morticelli, 2012; Parrino et al., 2019). Fault controlled structural highs, resulting from such late Miocene–early Pliocene shortening phases, bounded a series of intraslope basins formed in response to the progressive retreating of the Ionian slab toward the SE, starting from the early Pliocene (Kastens et al., 1988; Lo Iacono et al., 2014). Starting from about 0.8 Ma ago (Calabrian age), a tectonic reorganization of the convergent Nubia-Eurasia margin occurred in the central Mediterranean. These reorganizations triggered the ongoing shortening process and the regional uplift driven by the Africa-Eurasia lithospheric collision (Di Maggio et al., 2017; Goes et al., 2004; Sulli et al., 2021; Zitellini et al., 2020). The computed GNSS velocity fields together whit coastal erosional features provide information highlight a slow NNW-SSE oriented convergence with a velocity ranging around 1 mm/yr and a slow regional uplift of about 0 to 24 mm/kyr in the area (Devoti et al., 2017; Ferranti et al., 2006).

2.3 Geomorphology

The study area shows a landscape marked by significant and discontinuous topographic depressions consisting of a flat bottom (coastal plain) opened to the sea and bounded inland by vast tectonically controlled coastal cliffs hundreds of meters tall. The present-day topography results from the interaction between differential uplift, river incision and eustatic processes. Such processes influenced by the previously formed structural and lithological architectures driven the landscape evolution of this area (Di Maggio et al., 2017). The result of such evolution consists of a staircase of marine terraces alternated with broad polycyclic marine surfaces near the coast and mountain ranges to the inland (Di Maggio et al., 2017; Hugonie, 1981; Mauz et al., 1997). The landforms in the inland portion highlight that river downcutting, karst phenomena, differential erosion and planation processes

characterizes the active processes in this mountain landscape (Agnesi et al., 2000; Di Maggio, 2000; Di Maggio et al., 2012, 2014). Middle-Upper Pleistocene marine terraces, whose raiser develop parallel to the modern coastline, outcrop along the coastal plains due to coastal processes, differential uplift and glacio-eustatic oscillations. Such surfaces are carved in the Gelasian (2.6 to 1.8 Ma) and Calabrian (1.8 Ma to 0.78 Ma) coastal to neritic deposits and develop from sea level up to about 100-300 m a.s.l. (e.g., Catalano et al., 2010a, 2010c; Di Maggio, 2000).

3. Methods

The here presented cartography is the result of the review of recent literature (Agate et al., 2017; Catalano, Avellone, et al., 2013; Catalano, Avellone, Basilone, Gasparo Morticelli, et al., 2010; Catalano et al., 2011; Di Maggio et al., 2008; Dominici et al., 2020 and reference therein), field survey and morphometric analyses performed on a LiDAR-derived digital elevation model provided by the Regione Siciliana over the whole Sicilian territory (Regione Siciliana, 2010).

Morphometric analyses were performed following the TerraceM approach (Jara-Muñoz et al., 2019) to detect the shoreline angles location into 53 swath profiles oriented roughly perpendicular to the coastline covering almost the entire study area.

The obtained dataset was integrated and validated by investigating the altitude and slope variations along topographic profiles oriented towards the maximum slope direction. Furthermore, an additional dataset validation was performed comparing the extracted shoreline angle locations and elevations with the lithological boundaries of the Plio-Quaternary succession outcropping in the study area, such as the upper limits of the Marsala Formation, Sabbie di Altavilla, Benincasa and Barcarello synthems.

We analyzed the elevation of the validated shoreline angle dataset into a distance VS elevation chart to check the data reliability and exclude remaining outliers through an in-house developed semi-automatic geospatial model. To minimize the perspective distortion in the resulting chart, we projected each point along the coastline through the minimum distance connection between each point and the coastline. Then we computed the distance between each projected point and the coastline starting point.

In the distance VS elevation chart, we checked the reliability of shoreline elevation outlier values through satellite imagery interpretation (Google Earth imagery, freely accessible at: https://earth.google.com/web/).

Detailed field reliefs were performed using published base maps (1:10,000 scale map of the Carta Tecnica Regionale, CTR, provided by the Regione Siciliana and accessible at: https://www.sitr.regione.sicilia.it/cartografia/carta-tecnica-regionale/) aiming at the validation of the

shoreline elevation orders collecting both lithological and geomorphic evidence of paleo-sea levels into critical sectors of the study area. Moreover, field survey allowed the discrimination of paleo-sea levels orders in sectors that are not characterized by easily recognizable morphometric signatures of relatively uplifted shoreline angles.

4. Results

The computed dataset consists of 210 recognized shoreline angles elevation and location extracted from an initial dataset of 334 values. Among the eight recognized levels, only six are characterized by a reliable continuity along the investigated area (see Fig. 3).

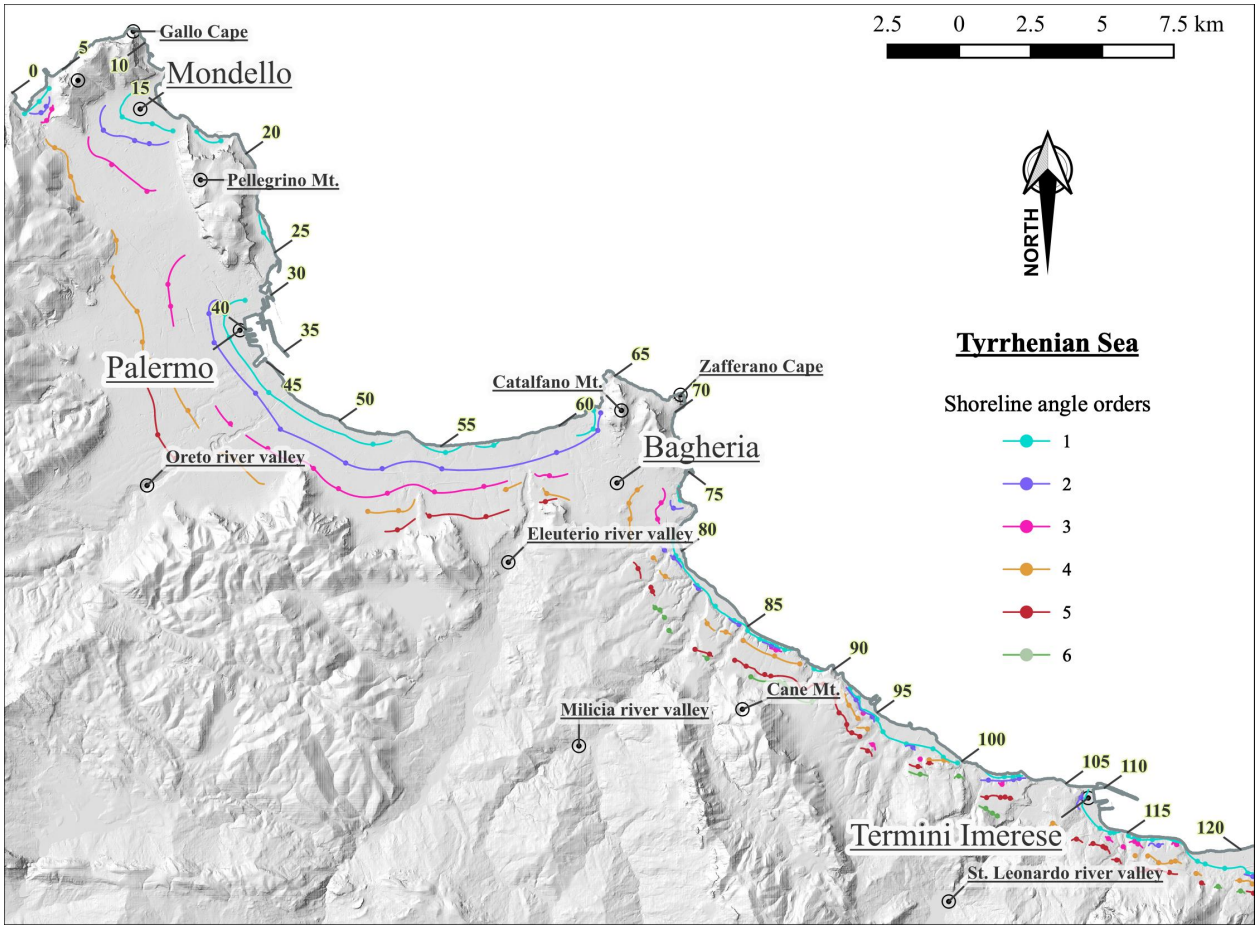

Fig. 3 – Map view of the detected shoreline angles orders in the study area. The yellow bordered numbers represent the distance along the coastline (km).

Statistical parameters of the detected shoreline angles elevation orders are summarized in Tab. 1.

Level (#)	Num (#)	Min (m asl)	Max (m asl)	St. Dev. (#)	Linear regression eq.	Correlation coeff. (#)	Regression line slope (°)
1.0	57	5.0	23.0	4.6	y = 0.0301x + 7.929	0.0579	1.7

2.0	30	14.0	35.8	7.8	y = 0.2119x + 10.201	0.8548	12.0
3.0	26	23.0	53.7	8.6	y = 0.2232x + 24.92	0.907	12.6
4.0	41	50.0	86.5	12.3	y = 0.3208x + 42.654	0.8326	17.8
5.0	40	80.0	116.0	10.0	y = 0.4027x + 62.969	0.8039	21.9
6.0	16	108.5	133.9	7.5	y = 0.5719x + 64.913	0.9195	29.8

Tab. 1 – Statistical parameters of the shoreline angles elevation dataset.

In the Palermo plain, the shoreline angles elevation points of the 4th and 5th order roughly corresponds to the upper limit of the Marsala calcarenites (the highest mapped limit of Quaternary deposits, 1.8 Ma). Differently, in the Termini plain, shorelines angle points of the 5th and 6th order are located in the surrounding of the Benincasa synthem upper limit, which is often interested by two or three orders of shoreline angles elevation (Fig. 3). Points of the 1st order lie near the Barcarello synthem upper limit along the coast of the whole study area (Fig. 3).

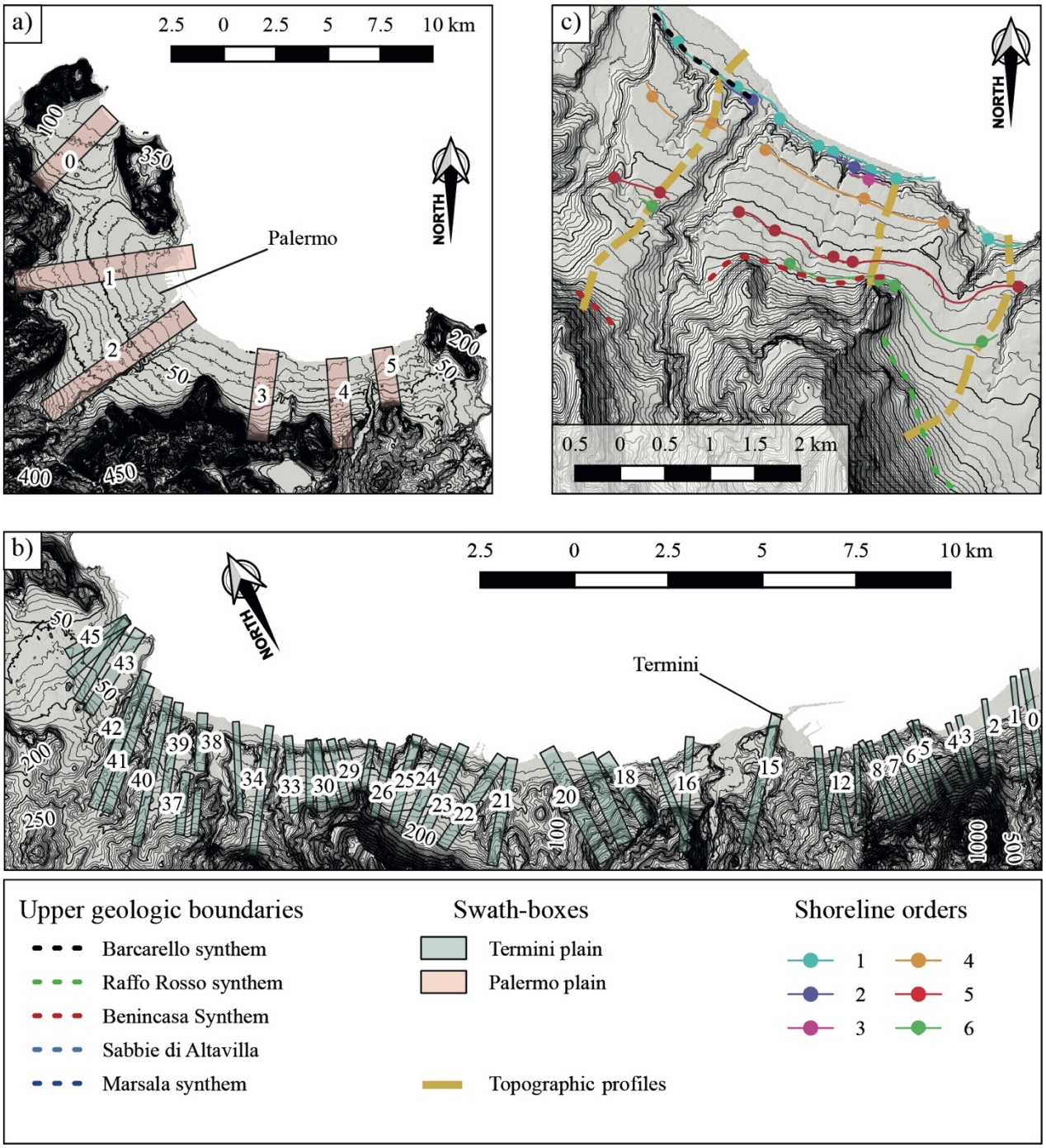

Fig. 3 – a) Computed swath profile boxes in the Palermo plain; b) Computed swath profile boxes in the Termini plain; c) The thick yellow dashed line represents some of the extracted topographic profiles oriented toward the maximum slope direction. Thin dashed lines represent the upper boundaries of Plio-Pleistocene deposits. Coloured circles are the location of the shoreline angles detected evidence, while the coloured lines represent the envelope of the different orders of shorelines.

Field surveys allowed the detection of 29 evidence of paleo-sea level from 7 different locations in a rocky coast sector of Termini plain whose morphologies do not show enough constraints to be interpreted solely by morphometric techniques. Such evidence that consists of tidal notches, marine

sedimentary bodies, marine fossils, and marine fossil traces (see Fig. 4) allowed us to validate the first 5 of the 6 shoreline angles orders morphometrically recognized in the whole study area.

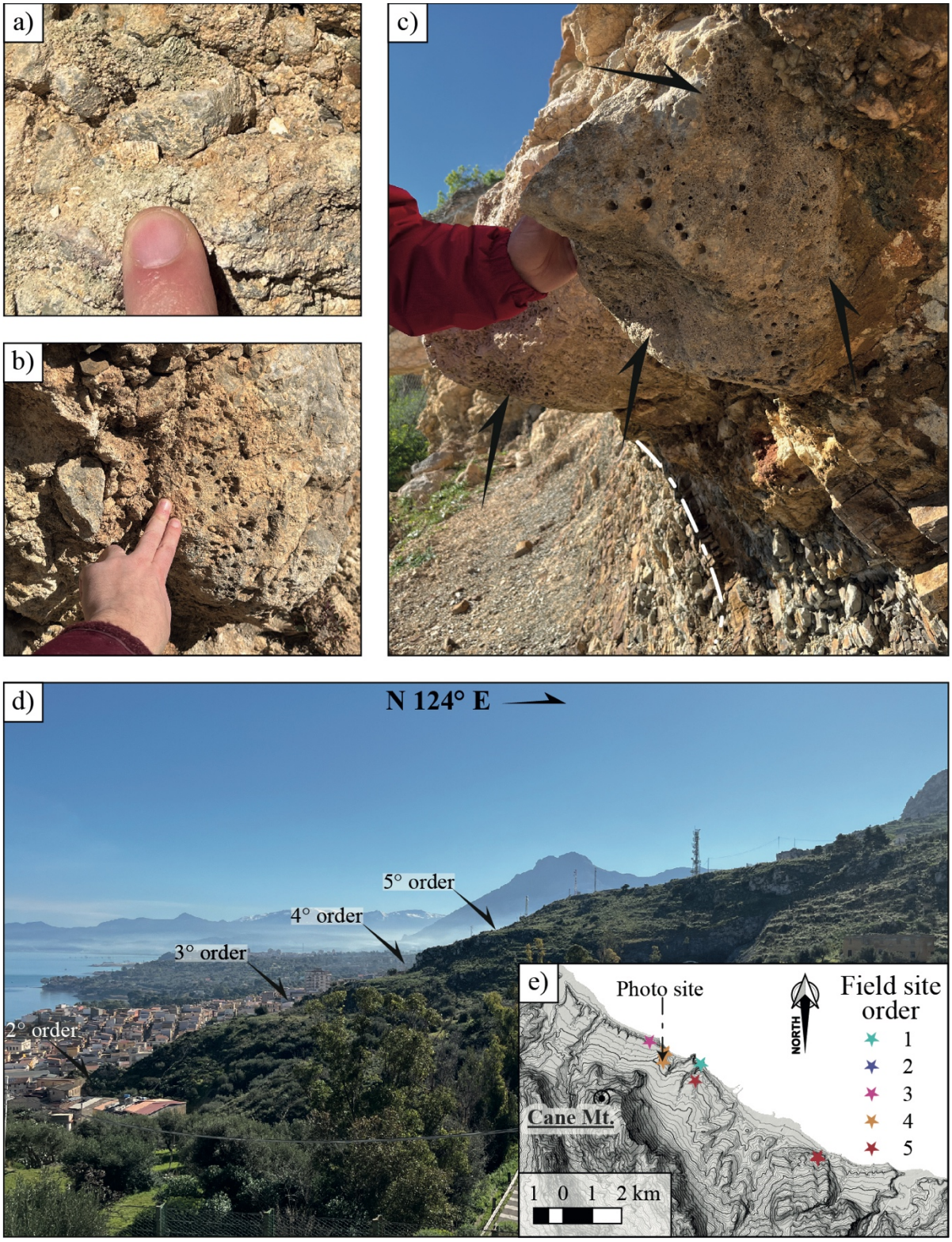

Fig. 4 – a) Fragmented marine fossils; b) Evidence of Lithophaga holes; c) The black arrows point traces of Clione Vastifera orange sponges, which are also interested by Lithophaga holes. The white dashed line highlights the morphology of the studied smoothed tidal notch (sensu Antonioli et al., 2018); d) Panoramic view of the 2° up to the 5° of shoreline angles orders; e) The stars represent the map view of surveyed sites. Colour code highlights the five shoreline angle orders in the inset e and d.

The slope of the shoreline angles elevation data regression lines highlights that almost all the detected orders recorded higher uplift rates in the Termini plain than those recorded in the Palermo one (Fig. 5).

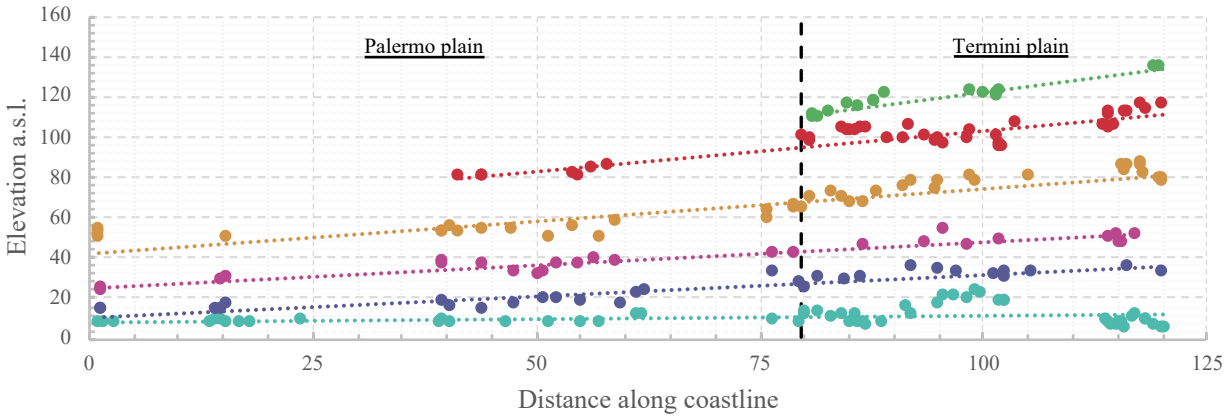

Fig. 5 – Shoreline angles orders elevation VS distance along the coastline (see Fig. 3 for the map view of these data).

5. Discussion and conclusions

The analysis of the obtained results allows us to state that, despite being geographically contiguous, the plain of Palermo and the plain of Termini have been characterized by significantly different evolutions of their coastal landscape. These evolutions can be reconstructed from the upper Pliocene to the late Quaternary and are summarized in Tab. 2. They are reflected both in the stratigraphic logs of the two plains and in the number and elevations of the identified shoreline angles orders.

Period	Palermo plain	Termini plain
Upp. Pleistocene – Present	Partially submerged (different uplift rate from shoreline orders)	
Mid. Pleistocene – Calabrian (1.5 – 0.8 Ma)	Submerged	Emerged
Low. Pleistocene – Gelasian (2.5 – 1.8 Ma)	? (emerged / eroded)	Submerged
Upp. Pliocene (3.6 – 2.5 Ma)	? (emerged / eroded)	Submerged

Tab. 2 – Summary of the coastal evolution of the Palermo and Termini plains.

The horizontal distance between the shorelines in the Palermo plain is, on average, more significant than the same distance in the Termini plain. This characteristic, which is recognizable in all the elevation orders but is particularly evident for the shorelines of the first three orders, could be due to different pre-existing paleo-morphologies. Based on the interpretation of the shape of these shorelines and to its known structural pattern, the paleo-morphology of the Palermo plain can be interpreted as a partially submerged flat area whose filling could be associated with the filling processes of the thrust top basins as documented in surrounding area. In a completely different way, both the interpretation of the geometry of the paleoshorelines and its sedimentary record highlight that the paleo-morphology of the Termini plain had to be characterized by significant paleo slopes as in the present days. Such high slope values could probably be related to the fact that this coast was incised upon an area characterized by a more significant regional uplift partially re-activating previously enucleated structures, whose structuring over time has forced the evolution of this coastal landscape. Such an interpretation fits the landscape evolution proposed by Parrino et al. (2022) and provides new clues about the recent tectonic activity of this coastal sector.

Numerous authors in the literature identify the Marine Isotope Stage (MIS) 5e (roughly 125 ka) in correspondence to the first order of the shoreline elevation detected. The evidence of such MIS described in the literature has been detected in the vicinity of the localities of Gallo cape and Zafferano cape (see Fig. 3) and do not provide any data on the Termini plain area. Assuming that the first order of shorelines elevation was recorded during MIS 5e, the uplift rates for the Palermo plain are approximately 0.01 mm/yr. Such rate agrees with those proposed in the literature for the Palermo plain, which vary from -0.03 mm/yr to 0. 01 mm/yr (Antonioli et al., 2006b, 2018; Ferranti et al., 2006). Similarly, the uplift rates for the Termini plain, which are four times larger than those calculated for the Palermo plain (0.04 mm/yr), well fit with the regional increase in uplift rates recorded from W to E along the coast of the NSCM.

Considering the above, the two areas of the analyzed NSCM coastal sector were characterized by different paleo morphologies and, also, by different uplift rates, which, together with the Quaternary eustatic oscillations, drove two significatively different landscape evolutions in adjacent sectors. The presented dataset and uplift rates are consistent with the previous studies in the Palermo plain area and provide new information regarding the Termini plain area. Moreover, the overall vision allowed by the review work carried out made it possible to reconstruct for the first time the coastal landscape evolution of this coastal sector of the NSCM. The results obtained are helpful information that fills the knowledge gap about the recent landscape evolution and tectonic forcings and represents a critical tool for parametrising active geological structures in the area.

Software

QGIS 3.22.1-Białowieża, MATLAB, TopoToolbox (Schwanghart & Scherler, 2014) and TerraceM-2 were used for the morphometric analyses, while Adobe Illustrator was used for the vector-based production of the Map.

Acknowledgements

This research was developed in the **L**andscape **E**volution **M**arker **O**nline **N**etwork (**LEMON**) project (**LEMON**) project (Multi-year Project INQUA – AIQUA).

Declaration of interest

The authors reported no potential competing interests.

References

Agate, M., Basilone, L., Di Maggio, C., Contino, A., Pierini, S., & Catalano, R. (2017). Quaternary marine and continental unconformity-bounded stratigraphic units of the NW Sicily coastal belt. Journal of Maps, 13(2), 425–437. https://doi.org/10/gjpq6b

Agnesi, V., De Cristofaro, D., Di Maggio, C., Macaluso, T., Madonia, G., & Messana, V. (2000). Morphotectonic setting of the Madonie area (central northern Sicily). Mem. Soc. Geol. It, 55, 373–379.

Antonioli, F., Ferranti, L., Stocchi, P., Deiana, G., Lo Presti, V., Furlani, S., Marino, C., Orru, P., Scicchitano, G., Trainito, E., Anzidei, M., Bonamini, M., Sansò, P., & Mastronuzzi, G. (2018). Morphometry and elevation of the last interglacial tidal notches in tectonically stable coasts of the Mediterranean Sea. Earth-Science Reviews, 185(June), 600–623. https://doi.org/10/gfngcv

Antonioli, F., Kershaw, S., Renda, P., Rust, D., Belluomini, G., Cerasoli, M., Radtke, U., & Silenzi, S. (2006a). Elevation of the last interglacial highstand in Sicily (Italy): A benchmark of coastal tectonics. Quaternary International, 145–146, 3–18. https://doi.org/10/c79swt

Antonioli, F., Kershaw, S., Renda, P., Rust, D., Belluomini, G., Cerasoli, M., Radtke, U., & Silenzi, S. (2006b). Elevation of the last interglacial highstand in Sicily (Italy): A benchmark of coastal tectonics. Quaternary International, 145–146, 3–18. https://doi.org/10/c79swt

Avellone, G., Morticelli, M. G., Sulli, A., Barchi, M. R., & Catalano, R. (2010). Interference between shallow and deep-seated structures in the Sicilian fold and thrust belt, Italy. Journal of the Geological Society, 167(1), 109–126. https://doi.org/10/cz5dhx

Basili, R., Burrato, P., De Santis, G. M., Fracassi, U., Maesano, F. E., Tarabusi, G., Tiberti, M. M., Valensise, G., Vallone, R., & Vannoli, P. (2021). Database of Individual Seismogenic Sources (DISS), Version 3.3. 0: A compilation of potential sources for earthquakes larger than M 5.5 in Italy and surrounding areas. https://doi.org/10.13127/diss3.3.0

Catalano, Avellone, G., Basilone, L., Contino, A., Agate, M., Di Maggio, C., Lo Iacono, C., Sulli, A., Gugliotta, C., & Gasparo Morticelli, M. (2013). Catalano, Avellone, G., Basilone, L., Contino, A., Agate, M., 2013b. Carta geologica d'italia alla scala 1: 50.000, Foglio 595 Palermo. ISPRA, Servizio Geologico d'Italia, Regione Siciliana, Assessorato Territorio ed Ambiente.

Https://www.isprambiente.gov.it/Media/carg/sicilia.html.

Catalano, R., Avellone, G., Basilone, L., Contino, A., Agate, M., Gugliotta, C., Di Maggio, C., Di Stefano, E., Gennaro, C., & Arnone, M. (2011). Carta geologica d'italia alla scala 1: 50.000, Foglio 609-596 Termini Imerese—Capo Plaia. ISPRA, Servizio Geologico d'Italia, Regione Siciliana, Assessorato Territorio ed Ambiente. Https://www.isprambiente.gov.it/Media/carg/sicilia.html.

Catalano, R., Avellone, G., Basilone, L., Gasparo Morticelli, M., Lo Cicero, G., Gugliotta, C., Di Maggio, C., Contino, A., Albanese, C., & Lena, G. (2010). Carta Geologica d'Italia alla scala 1: 50.000, Foglio 608 Caccamo. ISPRA, Servizio Geologico d'Italia, Regione Siciliana, Assessorato Territorio ed Ambiente. Https://www.isprambiente.gov.it/Media/carg/sicilia.html.

Catalano, R., Avellone, G., Basilone, L., & Sulli, A. (2010). Catalano, R., Avellone, G., Basilone, L., Sulli, A., 2010b. Carta Geologica d'Italia alla scala 1: 50.000, Foglio n. 607 Corleone ISPRA, Servizio Geologico d'Italia, Regione Siciliana, Assessorato Territorio ed Ambiente. Https://www.isprambiente.gov.it/Media/carg/sicilia.html.

Catalano, R., Valenti, V., Albanese, C., Accaino, F., Sulli, A., Tinivella, U., Gasparo Morticelli, M., Zanolla, C., & Giustiniani, M. (2013). Sicily's fold-thrust belt and slab roll-back: The SI.RI.PRO. seismic crustal transect. Journal of the Geological Society, 170(3), 451–464. https://doi.org/10/gnwhcm

CHANG, K. H. (1975). Unconformity-bounded stratigraphic units. GSA Bulletin, 86(11), 1544–1552. https://doi.org/10.1130/0016-7606(1975)86<1544:USU>2.0.CO;2

Contino, A., Giammarinaro, M. S., Vallone, P., Varsalona, S., & Zuccarello, A. (2006). Analisi stratigrafico geotecnica del settore meridionale della città di Palermo finalizzata alla caratterizzazione di fattori di pericolosità sismica in esso presenti. 16.

D'Angelo, U., Ribaudo, R., & Vernuccio, S. (2006). Evidence of Middle and Upper Pleistocene shorelines in the area between Capo Mongerbino (Bagheria) and Piano Sperone (Altavilla Milicia), NC Sicily.

Devoti, R., D'Agostino, N., Serpelloni, E., Pietrantonio, G., Riguzzi, F., Avallone, A., Cavaliere, A., Cheloni, D., Cecere, G., D'Ambrosio, C., Falco, L., Selvaggi, G., Métois, M., Esposito, A., Sepe, V., Galvani, A., & Anzidei, M. (2017). A combined velocity field of the mediterranean region. Annals of Geophysics, 60(2), S0215. https://doi.org/10/gnwhbs

Di Maggio, C. (2000). Morphostructural aspects of the central northern sector of Palermo Mountains (Sicily). Mem. Soc. Geol. It, 55(8).

Di Maggio, C., Agate, M., Contino, A., Basilone, L., & Catalano, R. (2008). Quaternary deposits within the National Geologic Maps of Northwestern Sicily: Climatic, environmental and tectonic implications. Rendiconti Online Societa Geologica Italiana, 3(1).

Di Maggio, C., Madonia, G., Parise, M., & Vattano, M. (2012). Karst of Sicily and its conservation. Journal of Cave and Karst Studies, 74(2), 157–172. https://doi.org/10/f4bhtw

Di Maggio, C., Madonia, G., & Vattano, M. (2014). Deep-seated gravitational slope deformations in western Sicily: Controlling factors, triggering mechanisms, and morphoevolutionary models. Geomorphology, 208, 173–189. https://doi.org/10/gngn27

Di Maggio, C., Madonia, G., Vattano, M., Agnesi, V., & Monteleone, S. (2017). Geomorphological evolution of western Sicily, Italy. Geologica Carpathica, 68(1), 80–93. https://doi.org/10/gk5qqf

Di Stefano, P., Favara, R., Luzio, D., Renda, P., Cacciatore, M. S., Calò, M., Napoli, G., Parisi, L., Todaro, S., & Zarcone, G. (2015). A regional-scale discontinuity in western Sicily revealed by a multidisciplinary approach: A new piece for understanding the geodynamic puzzle of the southern Mediterranean. Tectonics, 34(10), 2067–2085. https://doi.org/10/gjpq57

Dominici, S., Benvenuti, M., Garilli, V., Uchman, A., Pollina, F., & David, A. (2020). Pliocene-pleistocene stratigraphic

paleobiology at altavilla milicia (palermo, sicily): Tectonic, climatic and eustatic forcing. Bollettino Della Societa Paleontologica Italiana, 59(1), 57–83. https://doi.org/10/gnwhdg

Faccenna, C., Piromallo, C., Crespo-Blanc, A., Jolivet, L., & Rossetti, F. (2004). Lateral slab deformation and the origin of the western Mediterranean arcs. Tectonics, 23(1). https://doi.org/10/bmz2qd

Ferranti, L., Antonioli, F., Mauz, B., Amorosi, A., Dai Pra, G., Mastronuzzi, G., Monaco, C., Orrù, P., Pappalardo, M., Radtke, U., Renda, P., Romano, P., Sansò, P., & Verrubbi, V. (2006). Markers of the last interglacial sea-level high stand along the coast of Italy: Tectonic implications. Quaternary International, 145–146, 30–54. https://doi.org/10/bsmjmv

Gasparo Morticelli, M., Valenti, V., Catalano, R., Sulli, A., Agate, M., Avellone, G., Albanese, C., Basilone, L., & Gugliotta, C. (2015). Deep controls on foreland basin system evolution along the Sicilian fold and thrust belt. Bulletin de La Société Géologique de France, 186(4–5), 273–290. https://doi.org/10/f7r2pz

Goes, S., Jenny, S., Hollenstein, C., Kahle, H. G., & Geiger, A. (2004). A recent tectonic reorganization in the south-central Mediterranean. Earth and Planetary Science Letters, 226(3–4), 335–345. https://doi.org/10/b4j2gb

Gugliotta, C., & Gasparo Morticelli, M. (2012). Using high-resolution stratigraphy and structural analysis to constrain polyphase tectonics in wedge-top basins: Inferences from the late Tortonian Scillato Basin (central-northern Sicily). Sedimentary Geology, 273–274, 30–47. https://doi.org/10/gnwg94

Gugliotta, C., Gasparo Morticelli, M., Avellone, G., Agate, M., Barchi, M. R., Albanese, C., Valenti, V., & Catalano, R. (2014). Middle Miocene–Early Pliocene wedge-top basins of NW Sicily (Italy): Constraints for the tectonic evolution of a 'non-conventional' thrust belt, affected by transpression. Journal of the Geological Society, 171(2), 211–226. https://doi.org/10/gnwg93

Hugonie, G. (1981). Mouvements tectoniques et variations de la morphogenèse au Quaternaire en Sicile septentrionale. Revue de Géologie Dynamique et de Géographie Physique Paris, 23(1), 3–14.

Incarbona, A., Contino, A., Agate, M., Bonomo, S., Calvi, F., Di Stefano, E., Giammarinaro, M. S., Priulla, A., & Sprovieri, R. (2016). Biostratigraphy, chronostratigraphy and paleonvironmental reconstruction of the Palermo historical centre Quaternary succession. Italian Journal of Geosciences, 135(3), 512–525. https://doi.org/10/f87dw7

Industry-leading vector graphics software | Adobe Illustrator. (n.d.). Retrieved February 14, 2022, from https://www.adobe.com/products/illustrator.html

Jara-Muñoz, J., Melnick, D., Pedoja, K., & Strecker, M. R. (2019). TerraceM-2: A Matlab® Interface for Mapping and Modeling Marine and Lacustrine Terraces. Frontiers in Earth Science, 7(October), 1–18. https://doi.org/10/gnwhbp

Kastens, K., Mascle, J., Auroux, C., Bonatti, E., Broglia, C., Channell, J., Curzi, P., Emeis, K.-C., Glaçon, G., & Hasegawa, S. (1988). ODP Leg 107 in the Tyrrhenian Sea: Insights into passive margin and back-arc basin evolution. Geological Society of America Bulletin, 100(7), 1140–1156. https://doi.org/10/b3zx63

Lo Iacono, C., Sulli, A., & Agate, M. (2014). Submarine canyons of north-western Sicily (Southern Tyrrhenian Sea): Variability in morphology, sedimentary processes and evolution on a tectonically active margin. Deep-Sea Research Part II: Topical Studies in Oceanography, 104, 93–105. https://doi.org/10/f59hw5

Martorana, R., Agate, M., Capizzi, P., Cavera, F., & D'Alessandro, A. (2018). Seismo-stratigraphic model of "La Bandita" area in the Palermo Plain (Sicily, Italy) through HVSR inversion constrained by stratigraphic data. Italian Journal of Geosciences, 137(1), 73–86. https://doi.org/10/gczwv4

Mauz, B., Buccheri, G., Zöller, L., & Greco, A. (1997). Middle to Upper Pleistocene morphostructural evolution of the NW-

coast of Sicily: Thermoluminescence dating and palaeontological-stratigraphical evaluations of littoral deposits. Palaeogeography, Palaeoclimatology, Palaeoecology, 128(1–4), 269–285. https://doi.org/10/db7qrr

Milia, A., Iannace, P., & Torrente, M. M. (2021). The meeting place of backarc and foreland rifting: The example of the offshore western Sicily (Central Mediterranean). Global and Planetary Change, 198(February 2020), 103408. https://doi.org/10/gnwhdh

Parrino, N., Agosta, F., Di Stefano, P., Napoli, G., Pepe, F., & Renda, P. (2019). Fluid storage and migration properties of sheared Neptunian dykes. Marine and Petroleum Geology, 102, 521–534. https://doi.org/10/gnwhbj

Regione Siciliana. (2010). Modello digitale del terreno (MDT) 2m x 2m Regione Siciliana-ATA 2007-2008 [WWW Document]. URL Http://Www. Sitr. Regione. Sicilia. It. http://www.sitr.regione.sicilia.it/geoportale/mobile/record.html?id=r_sicili:449a45a2-9c31-4dfe-8013-90c4dd19f8a2

Rovida, A. N., Locati, M., Camassi, R. D., Lolli, B., & Gasperini, P. (2021). Catalogo Parametrico dei Terremoti Italiani CPTI15, versione 2.0.

Schwanghart, W., & Scherler, D. (2014). Short Communication: TopoToolbox 2—MATLAB-based software for topographic analysis and modeling in Earth surface sciences. Earth Surface Dynamics, 2(1), 1–7. https://doi.org/10/gb9b74

Sulli, A., Gasparo Morticelli, M., Agate, M., & Zizzo, E. (2021). Active north-vergent thrusting in the northern Sicily continental margin in the frame of the quaternary evolution of the Sicilian collisional system. Tectonophysics, 802. https://doi.org/10/gnwhds

Zitellini, N., Ranero, C. R., Loreto, M. F., Ligi, M., Pastore, M., D'Oriano, F., Sallares, V., Grevemeyer, I., Moeller, S., & Prada, M. (2020). Recent inversion of the Tyrrhenian Basin. Geology, 48(2), 123–127. https://doi.org/10/gnwhfh

To be submitted

Chapter 3

Recent tectonics in the Catanzaro Trough (Calabria, southern Italy) from morphotectonic and morphometric analyses

Authors: Pirrotta C.[1], **Parrino N.[4*]**, Pepe F.[4], Tansi C.[5], Monaco C.[1,2,3]

[1] Dipartimento di Scienze Biologiche Geologiche e Ambientali, Università di Catania, Catania, Italy
[2] CRUST – Interuniversity Center for 3D Seismotectonics with territorial applications, Italy
[3] Istituto Nazionale di Geofisica e Vulcanologia, Osservatorio Etneo—Sezione di Catania, Catania, Italy
[4] Dipartimento di Scienze della Terra e del Mare, Via Archirafi 22, Università di Palermo, Italy
[5] CNR-IRPI, Rende (CS), Italy
[*]*Corresponding author:* nicolo.parrino@unipa.it

Keywords: Calabrian Arc; Active tectonics; Geomorphology; Morphotectonics; Fluvial morphometry.

Abstract

In this work, we investigate the landscape response to the recent activity of the faults of the Catanzaro Trough, a seismically active structural basin that developed transversally to the Calabrian Arc (Southern Italy) during the Neogene-Quaternary. We mapped Quaternary faults and performed a geomorphological and morphometric study of the drainage networks and basins intercepted by the faults. Results indicate that the fault systems located to the north of the Catanzaro Trough are still active: a WNW-ESE oriented, strike-slip fault system (here named South Sila Piccola Fault System) accommodates the different SE-ward advancement of the upper crustal sectors of the orogen; a south-dipping WNW-ESE oriented fault system (the Lamezia Catanzaro Fault System), which has a more evident normal component of movement, accommodates the transition from the strike-slip regime at north to the extensional one at south. Inside the Catanzaro Trough, we detected for the first time a NNE-SSW trending, WNW dipping fault system, named Caraffa Fault System. This system represents the northern prolongation of the Serre Fault, a large extensional structure extending longitudinally to the Calabrian Arc. The recent activity of the Caraffa Fault System is testified by the differential uplift and tilting of discrete areas inside the basin, as revealed by the morphometric indexes and by published geodetic and seismological data. Given its location, geometry and kinematics, the Caraffa Fault System could be responsible for the occurrence of large historical earthquakes.

1. Introduction

Starting from Pliocene times, an extensional and strike-slip tectonics phase, whose deformation was superimposed on the pre-existing contractional framework, affected the Calabrian Arc (southern Italy, Fig. 1A, Monaco et al., 1996). Such a tectonics phase triggered the formation of basins oriented longitudinally and transversally to the orogenic arc (Ghisetti and Vezzani, 1982). The Catanzaro Trough is a transversally elongated basin located between the longitudinal Crati Basin in the western sector of the Sila Massifs, to the north and the longitudinal Mesima Basin, west of the Serre Mts., to the south (Tortorici et al., 1995; Monaco and Tortorici, 2000; Tansi et al., 2005; 2007) (Fig. 1A).

The definition of the current tectonic setting of the sector of the Calabrian Arc hosting the Catanzaro Trough represents a challenging task hampered by its inherited structural complexity. Despite the geological studies carried out in the Catanzaro Trough and surrounding areas (Tortorici et al., 1995; Monaco and Tortorici, 2000; Van Dijk et al., 2000; Tansi et al., 2007; Brutto et al., 2016; Pirrotta et al., 2021; Punzo et al., 2021), the landscape response to tectonics is not consistently constrained yet. Particularly, the role and the recent activity of the WNW-ESE fault systems bordering

to the north and south the Catanzaro Trough (Brutto et al., 2016; Moretti, 2000; Tansi et al., 2007) and the extensional processes in it (Gullà et al. 2005, Pirrotta at al., 2021) are still poorly defined or matter of debate.

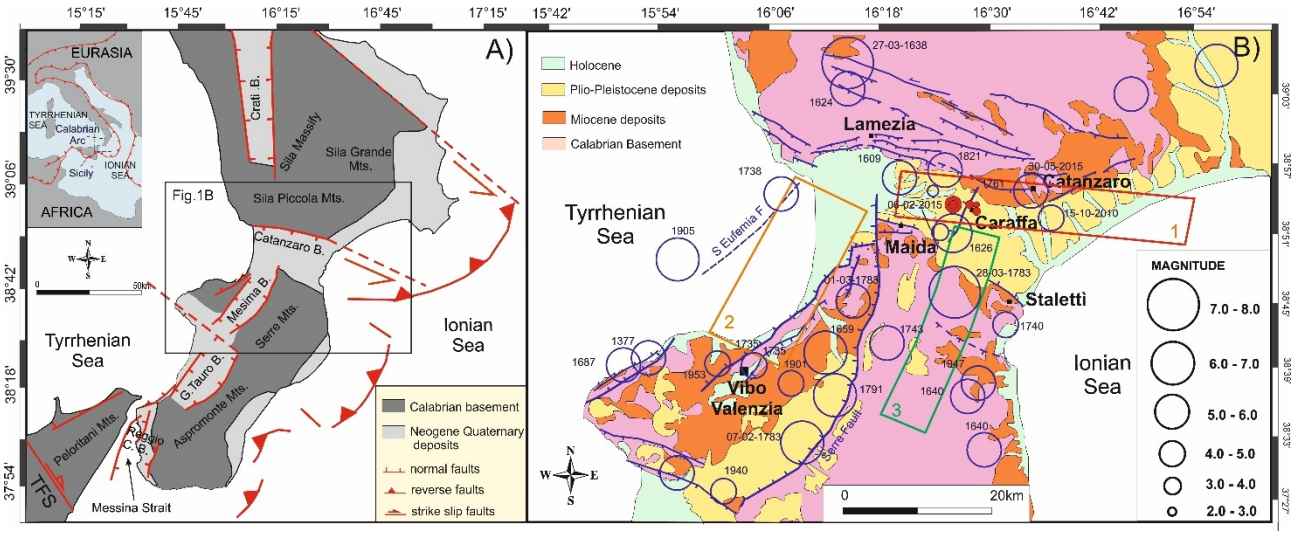

Fig. 1: A) Simplified map showing the main structural elements of the Calabrian Arc (from Pirrotta et al., 2021 modified); TFS, Tindari Fault System; inset shows the Eurasia-Africa convergence and the central Mediterranean orogen. B) Geological map of the Catanzaro Trough and surrounding area showing the Quaternary faults from literature (see Fig. 1A for location); circles are the historical and instrumental epicentres of earthquakes with magnitude higher than 4.8 (CPTI, Rovida et al., 2021); red balls represent the seismic sequence of October 2019; rectangles are modelled seismogenic sources: 1, ITCS068; 2, ITCS110 (both proposed by the DISS Working Group, 2021); 3, ITES002 (modelled by Akinci et al., 2017).

During historical times, several destructive earthquakes, with Mw up to 7.5 and maximum intensity of 11, occurred in the Catanzaro Trough (Rovida et al., 2021) (Fig. 1B), such as the 1626 event (Io IX and Mw = 6.07, Rovida et al., 2021) and the March 28, 1783 event (Io XI and Mw = 7.03, Rovida et al., 2021), the latter the last of a seismic sequence that destroyed the southern Calabria. Notwithstanding the several seismogenic sources parametrized in the central Calabrian Arc (see DISS Working Group, 2021), only the NNE-SSW exploratory source modelled by Akinci et al. (2017) (ITES002; see Fig. 1b) might be suitable for these events. However, at the state, it remains a working hypothesis based on regional geological data and geodynamic considerations not constrained by structural field evidence or by a clear morphometric signature.

Morphometric analysis has proved to be particularly efficient in detecting the tectonic forcing on the landscape evolution, highlighting the activity of blind or elusive faults located where the intense erosion rapidly erases their morphological signature (Cox, 1994; Burrato et al., 2003; Hare and Gardner, 1985; Valensise and Pantosti 2001; Snyder et al., 2000). Numerous authors successfully applied morphometric approaches, based on the drainage network hierarchy evaluation, the computation of catchment and drainage pattern metrics, the relief distribution and the river longitudinal

profiles analyses, to highlight recent differential vertical movements (Snyder al., 2000; Whipple, 2004; Guarnieri and Pirrotta, 2008; Pedrera et al., 2009; Figueroa and Knott, 2010; Demoulin, 2011; Camafort et al., 2020; Pirrotta and Barbano, 2020), even in the northern and southern sectors of the Calabrian Arc (Molin et al., 2004; Pirrotta et al., 2016; Roda-Boluda and Whittaker, 2017).

In this work, we decipher recent fault activity and define potential seismogenic sources, in the Catanzaro Trough, through: i) a morphostructural study to define fault patterns; ii) qualitative geomorphological and quantitative morphometric investigations of the drainage network and related basins; iii) computation of hierarchical parameters and geomorphic indices (e.g., hypsometric integrals and normalized stream-length gradient); iv) critical review and new interpretation of the most up to date published geodetic and seismological dataset.

2. Geological setting

2.1. Geodynamic framework

The geodynamic evolution of the Calabrian Arc and its adjacent offshore sectors (Fig. 1) is controlled by the north-westward subduction of the oceanic Ionian lithosphere that, confined between two continental sectors (the Apulian block, to the north and the Pelagian block, to the south), has led the bowing of this sector of the Apennine-Maghrebian Chain and the development of a complex Neogene-Quaternary backarc/forearc/trench system in the central Mediterranean (Carminati et al., 1998; Faccenna, 2005; Carminati and Doglioni, 2005; Guarnieri, 2006; Pepe et al., 2010; Tiberti et al., 2017; Corradino et al., 2020; Corradino et al., 2021). Currently, the subduction of the Ionian lithosphere continues only in a small internal segment of the arc between the Tindari Fault System (TFS in Fig. 1A) and the Catanzaro Trough (Orecchio et al., 2014; Maesano et al., 2017; Scarfì et al., 2018; Barreca et al., 2019). North of the Catanzaro Trough, the subduction interface ends on a lateral ramp that acts as a gradual transition from subduction in the Calabrian Arc to collision in the Southern Apennines (Wortel and Spakman, 2000; Guarnieri, 2006; Maesano et al., 2017; Scarfì et al., 2018; De Ritiis et al., 2019).

Pliocene-Quaternary post-orogenic extension, perpendicular to the arc, and coeval regional uplift, likely due to asthenosphere flow or wedging (Westaway, 1993; Wortel and Spakman, 2000; Doglioni et al., 2001), caused the development of several systems of normal faults (Ghisetti and Vezzani, 1982; Miyauchi et al., 1994; Monaco et al., 1996; Monaco and Tortorici, 2000; Pepe et al., 2014; Brutto et al., 2016; Monaco et al., 2017). Such a tectonics phase triggered the formation of basins oriented longitudinally to the orogenic trend, e.g., Crati, Mesima, Gioia Tauro and Messina Strait,

interrupted by transversal basins, e.g., Sibari, Reggio Calabria and the Catanzaro Trough (Ghisetti and Vezzani, 1982) (Fig. 1A). The Catanzaro Trough is a WNW-ESE trending, Late Neogene to Quaternary structural basin that separates the northern and southern parts of the Calabrian Arc (Van Dijk et al., 2000; Tansi et al., 2005; 2007). Recently, the Catanzaro Trough has been interpreted as a semigraben structured by the polyphase activity of the Lamezia Catanzaro Fault System that bounds the basin to the north and represents the surface expression of the deep tear-fault (Guarnieri, 2006; Pirrotta et al., 2021), delimiting the transition from the subduction domain to the collisional one.

2.2. Geological, geomorphological, and structural features of the Catanzaro Trough

The Neogene to Quaternary deposits of the Catanzaro Trough unconformably lie on the structural units of the Calabrian Arc (Fig. 1B), made up of metamorphic and magmatic rocks of the Hercynian basement, Mesozoic calcareous platform, and Cenozoic terrigenous units (Amodio-Morelli et al., 1976; Gullà et al., 2005). From the bottom, the sedimentary succession is composed of a Middle-Upper Miocene transgressive sequence (Colella et al., 1995), including thin and discontinuous limestone–gypsum strata of the Messinian sequence, delimited at the top by a Pliocene conglomerate and marly deposits (Roda, 1964; Ferrini and Testa, 1997; Zecchin et al., 2015). The sedimentary sequence continues upwards with cross-stratified sand and sandstones, up to 60 m thick (Chiarella et al., 2012; Longhitano et al., 2014). In areas where the clayey predominates, instability phenomena are widely present, such as generalized degradation for widespread erosion or large size landslides (Gullà et al., 2005). The top of the sedimentary succession includes five orders of Middle-Upper Pleistocene marine terraces made of siliciclastic sands and sandstones (Gullà et al., 2005; Brutto et al., 2016, Fig. 2B). Due to the activity of the bordering faults to the north and south of the basin, the terraced deposits lie at increasing altitudes. An extensive system of coalescent fans covers the terraced deposits in the north-western sector of the Catanzaro Trough (Fig. 2B).

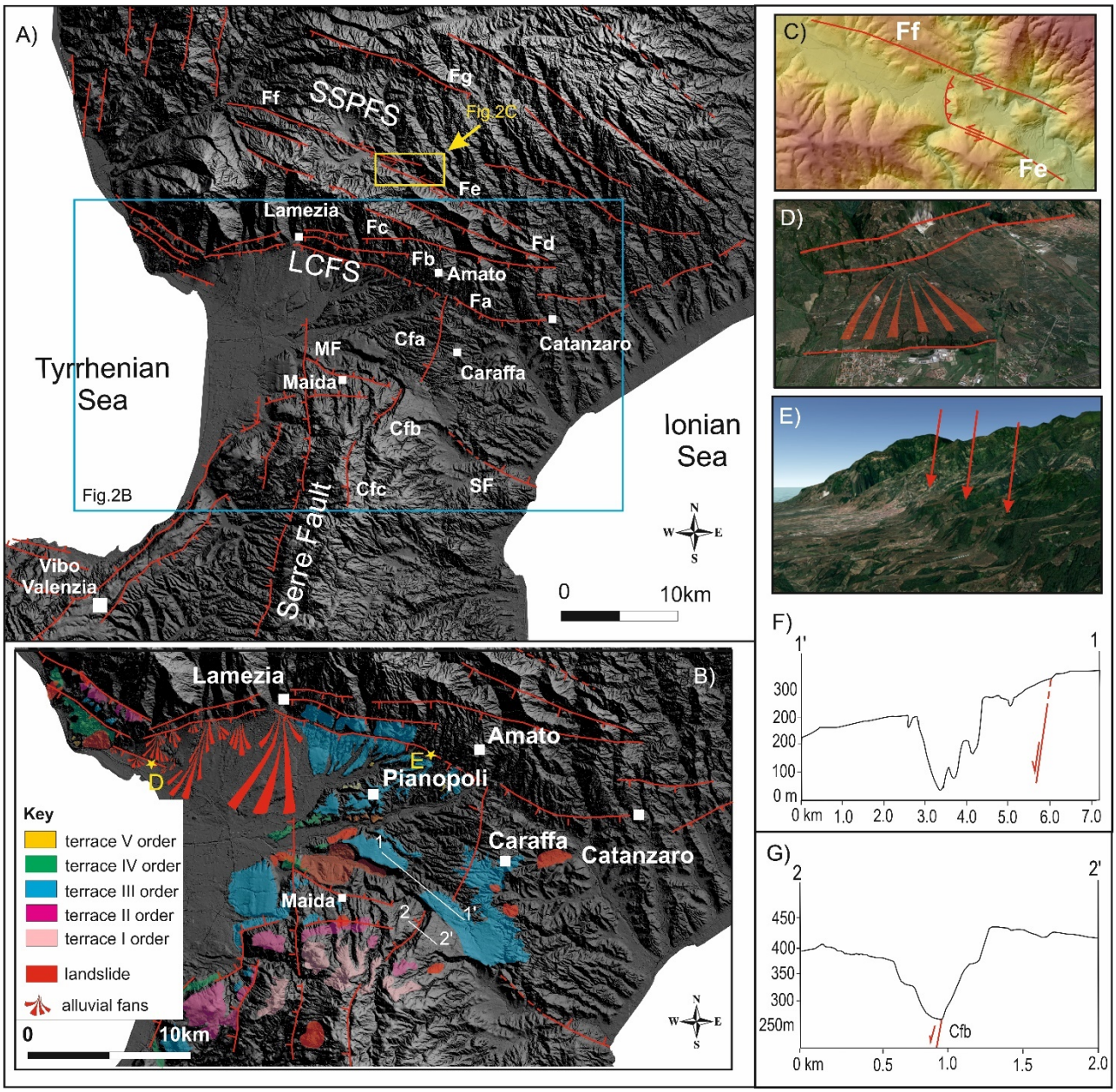

Fig. 2: A) DTM hillshade and fault pattern of the Catanzaro Trough area: SSPFS, South Sila Piccola Fault System; LCFS, Lamezia Catanzaro Fault System; MF, Maida, Fault; SF, Staletti Fault; Cfa, Cfb and Cfc are the segments of the Caraffa Fault System. B) DTM hillshade (see Fig. 2A for location) showing alluvial fans, faults (dashed where inferred) and colour coded upper Middle-Upper Pleistocene terraces (modified from Gullà et al., 2005 and Brutto et al., 2016); stars are the location of Fig. 2D and 2E. C) Push-up ridge between Fe and Ff at the Serrastretta locality (see Fig. 2A for location). D) Dislocated alluvial fan. E) Trapezoidal facets created by Fa north of Pianopoli. F) Schematic geological profile showing the III order terrace warped and tilted by the Caraffa Fault System; G) Schematic geological profile showing the Cfb scarp and the asymmetric valley.

The Lamezia Catanzaro Fault System borders the Catanzaro Trough to the north and separates the Calabrian Arc units from the Neogene-Quaternary sequences (Fig. 2). It is roughly 50 km long and constituted by minor 10-15 Km long WNW-ESE and WSW-ENE strike/oblique-slip faults locally arranged in a left-stepping en-echelon pattern (Gullà et al., 2005; Brutto et al., 2016). Pirrotta et al.

(2021) observed a left-lateral component of motion along the WNW-ESE striking fault planes and a prevalent normal motion, slightly right-lateral, along the WSW-ENE oriented planes. According to these authors, the system is characterized by long-term left-lateral transtension, even though morphological evidence highlights a prevalence of normal faulting during the late Pleistocene. Inside the Catanzaro Trough, N-S to NNE-SSW normal faults, with a weak right-lateral component of motion and limited displacement at the surface, offset Tortonian to Pliocene and Pleistocene deposits (Gullà et al., 2005). Minor north dipping normal faults, about 9-10 km long and WNW-ESE oriented, characterize the southern margin of the trough, the most developed of which are the Maida Fault and the Stalettì Fault (Fig. 2A). North of the Catanzaro Trough, a strike-slip fault system affects the southern sector of the Sila Piccola Massif. It belongs to a Middle Miocene-Middle Pleistocene left-lateral strike-slip shear zone (Sellia-Decollatura fault zone of Van Dijk et al., 2000; Amantea-Gimigliano fault of Tansi et al., 2007).

In the northern and central Catanzaro Trough areas, the fault activity is testified by clusters of earthquakes and by geodetic data indicating left lateral motion along of the Lamezia Catanzaro Fault System and extension inside the trough (Pirrotta et al., 2021). In particular, these data support the presence of an inferred NNE-SSW oriented extensional fault that should belong to the alignment of the Serre Fault (Fig. 2A), a major structure that accommodates the extension orthogonal to the Calabrian Arc (Pirrotta et al., 2021).

3. Methods and analysis

Our research involved the following methods: 1) joint interpretation of aerial photos and Digital Terrain Models (DTM) to detect morphological imprints of active faults; 2) geomorphological and morphometric investigations of the drainage networks and hydrographic basins to analyse the landscape response to the tectonic forcing of active faults; 3) a combined review of the seismicity catalogues and the GNSS velocity field to validate the activity of the mapped faults.

In order to review the active faults previously mapped in literature (Gullà et al., 2005; Tansi et al., 2007; Brutto et al., 2016; Pirrotta et al., 2021) and to check the accuracy of their position, we analysed the 5 m geometrical resolution LIDAR-derived DTM (Digital Terrain Model) provided by the Regione Calabria (http://geoportale.regione.calabria.it/, projected in WGS 1984 UTM Zone 33N) and the aerial stereopairs provided by the Italian Military Geographical Institute (1:33.000 scale, https://www.igmi.org/it/descrizione-prodotti/aerial-photography/black-and-white-or-colour-aerial-photographs).

The qualitative geomorphological analysis was focused on the geomorphological markers indicating landscape response to tectonic forcing, such as offset, tilted and warped terraces, morphological scarps and fluvial deflections and piracies in correspondence of faults (Ouchi, 1985; Molin et al., 2004; Guarnieri and Pirrotta, 2008; Pirrotta and Barbano, 2020). We analysed these markers both in map view and on landscape profiles. In detail, we extracted two profiles along alignments of drainage divide tracts: one orthogonal to the Catanzaro Trough and parallel to the Calabrian Arc (A-A' in Figs. 3A and 4A) and the other longitudinal to the trough (B-B' in Figs. 3A and 4B). The main advantage of the investigation of the drainage divide is that along its track the landscape is less influenced by erosional processes and the effects of tectonic perturbation are more evident. Also, we reconstructed a 6 km width, 35 km length, W-E trending swath profile extending from the Tyrrhenian coast towards the Ionian coast (C-C' in Figs. 3A and 4C). Additionally, we extracted the path profile of minor river channels, for evaluations at more local scale (R1-R5 in Figs. 3C and 5A-E). These profiles were smoothed by applying a first-order polynomial loess filter with the nearest neighbour's bandwidth method and a 0.1 sampling proportion.

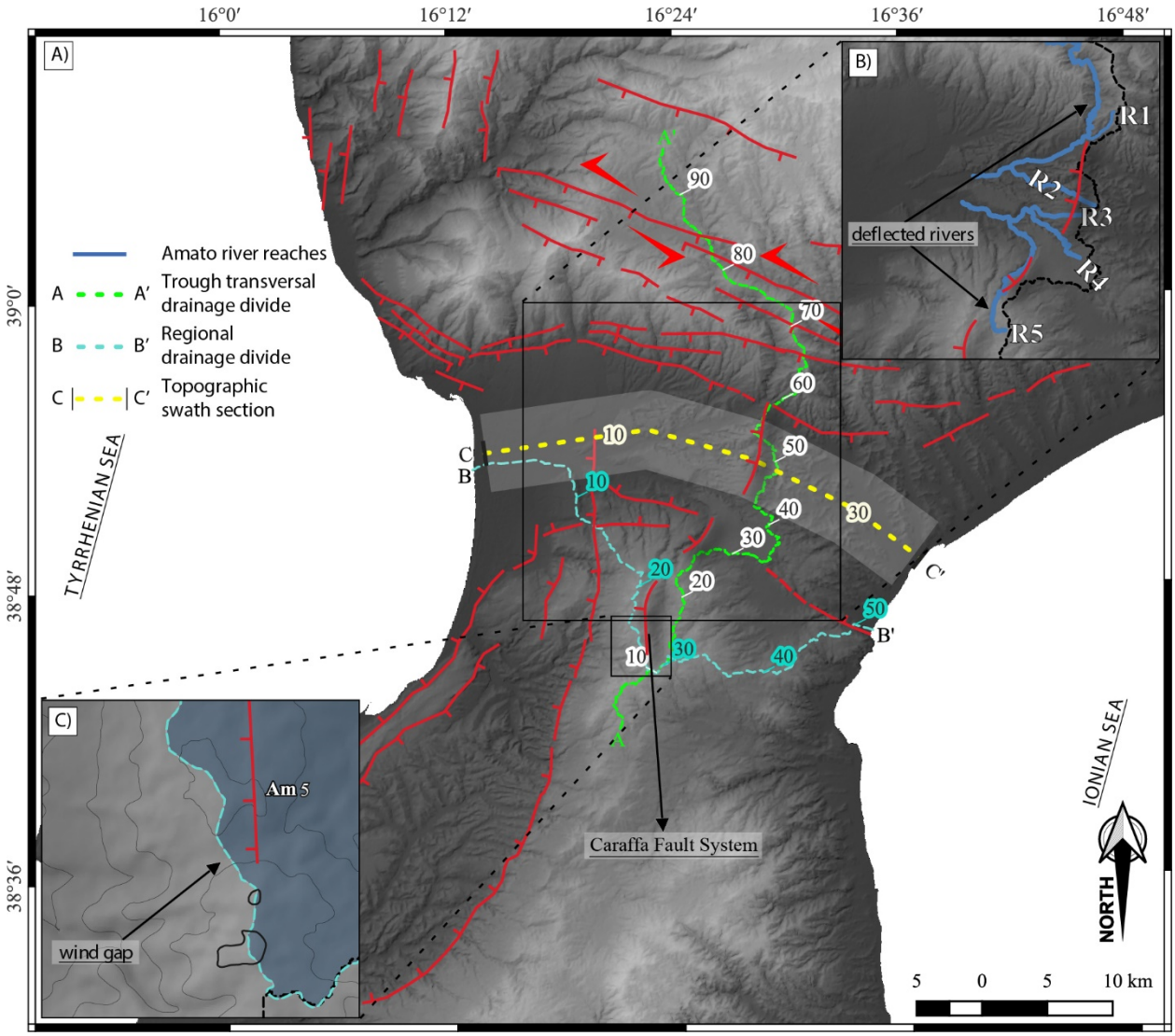

Fig. 3: A) Hillshade visualisation of the Digital Elevation Model (DEM) of the Central Calabria. The green dashed line A-A' indicates the trace of the drainage divide transversal with respect to the Catanzaro Trough (the profile is plotted in Fig.4A); the cyan dashed line B-B' is the trace of the regional drainage divide crossing out the Catanzaro Trough (the profile is plotted in Fig.4B). The yellow dashed line C-C' and the semi-transparent white polygon represent, respectively, the baseline and the area sampled by the topographic swath profile plotted in Fig.4C. Numbers indicate the along trace distance expressed in km. B) Map view of the main reaches of the Amato River crossed out or deflected by the Caraffa Fault System; the profiles of the reaches R1 – R5 are plotted in Figs. 5A-E. C) Map view of a significant wind gap along the trace B-B' (see also Fig.4B).

The quantitative morphometric analysis focuses on 17 sub-basins extracted from six main basins flowing into the Catanzaro Trough, selecting as outlets each intersection between rivers stems and the 50 m a.s.l. contour line (Figs.6A and B). The digital network of the drainage was obtained using the D8 approach (O'Callaghan and Mark, 1984) and a minimum mappable outflow of 20.000 square meters. For the extracted sub-basins we computed some landscape parameters, such as slope degree and local relief, by using a square moving window of 500 m per side (Figs. 6C and 6D) and some geomorphic indexes such as the normalized steepness index, K_{sn} and the transverse topographic

basin asymmetry index T-factor (Figs. 6B and 6E; see Table 1 for the description). To compare with literature data, we computed the sub-basin averaged K_{sn} values using a reference concavity of 0.45. The T-factor was extracted following the Cox's (1994) methodology through an in-house developed geospatial model, sampling the basin midlines every 100 m.

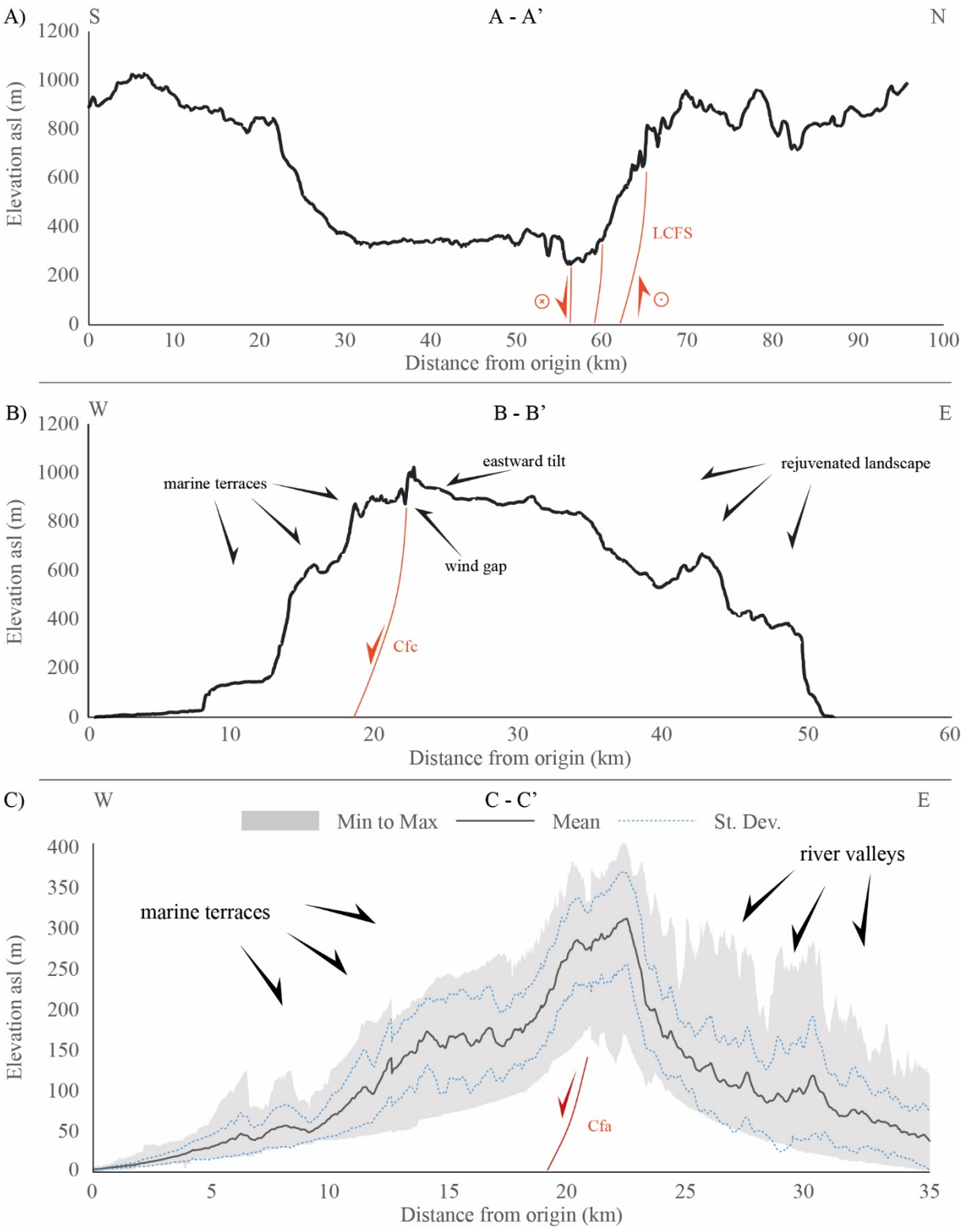

Fig 4: A) Topographic profile along the A-A' trace. B) Topographic profile along the B-B' trace. The map view of both profiles is reported in Fig. 3A. C) Swath profile across the Catanzaro Trough (see Fig. 3A for the trace).

We applied a further quantitative investigation to three sub-basins: the Am4 and the C2, in the northern boundary of the trough (Figs 6F, 7 and 8), and the A1, in the southern boundary of the trough (Figs. 6F and 10). For this analysis, Am4 and C2 were extracted selecting as outlets the slope break of the South Sila Piccola massif. We calculated the hierarchical drainage parameters (Strahler order; Bifurcation ratio; Direct bifurcation ratio; Bifurcation index, R and Anomaly parameter, An) and geomorphic indexes (Asymmetry factor, AF; Basin Elongation Ratio, Re; Sinuosity index, S; Hypsometric integral curve; see Table 1 for the descriptions) and extracted the path profile of the main river trunk.

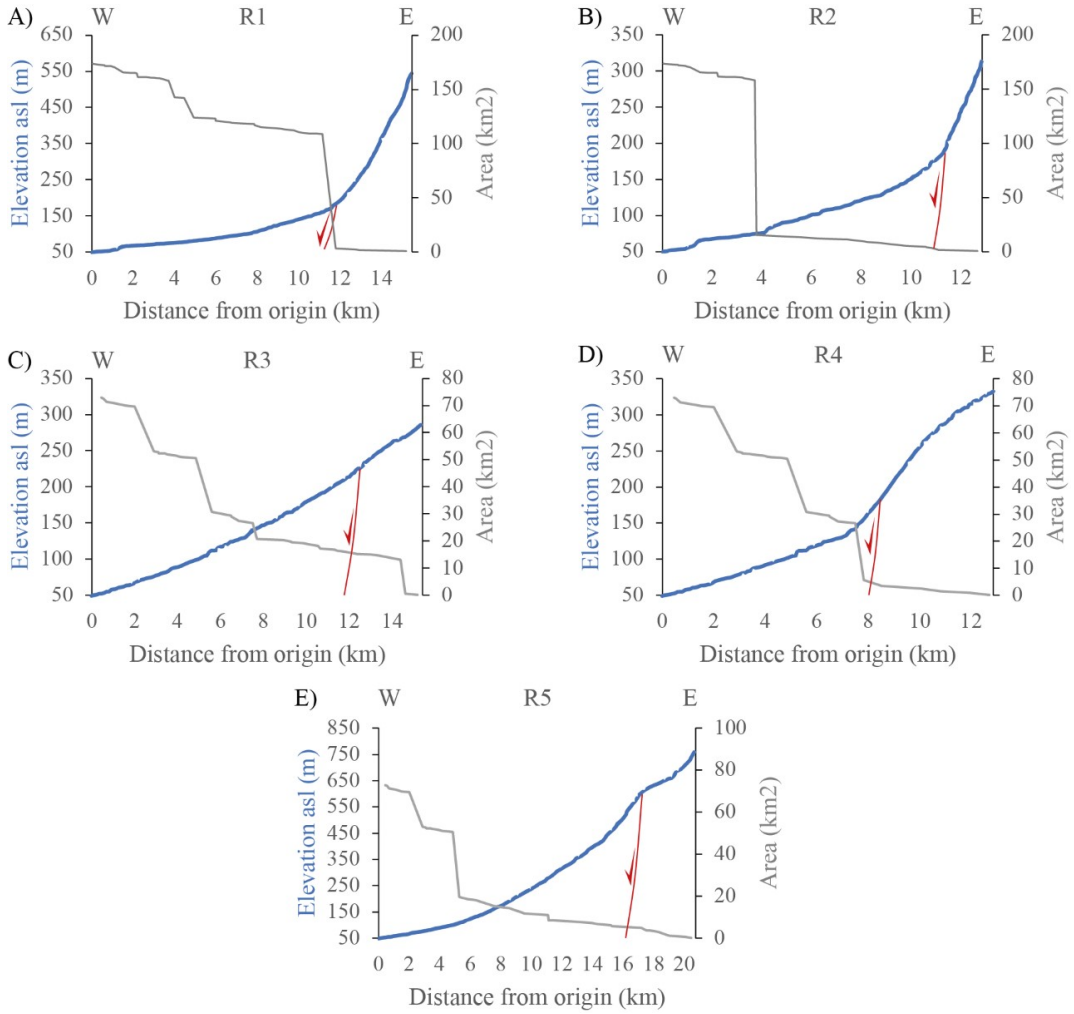

Fig 5: A-E) longitudinal profiles (blue lines) of the R1 - R5 channels of the Amato River and catchment area (grey lines) (see Fig. 3B for the traces).

Fault activity and movement were validated through a roughly E to W velocity profile, by using the GNSS dataset of the Istituto Geografico Militare Italiano (IGM) (https://www.igmi.org/it/Home,

accessed on September 1, 2021), previously elaborated by Pirrotta et al. (2021). The profile highlights differences in the movements of crustal blocks composing the trough (Fig. 11 and 12A). Finally, we plotted both in section and in map view the 1985 – 2022 instrumental seismicity from the seismic database provided by the Istituto Nazionale di Geofisica e Vulcanologia (INGV, http://terremoti.ingv.it/, ISIDE Working Group, 2007) (Fig. 12B).

Table 1. Hierarchical parameters and geomorphic indexes.

Parameters	Description	References
Strahler order	It indicates the phase of maturity of the hydrographic network. The fluvial drainage is subdivided into several segments going from a flow junction to the successive one. An order, indicated by a roman number, is associated with each segment of the hydrographic network. The headwater tributaries have the first (I) order. Then, when two segments of the same order meet, the successive fluvial segment reaches a higher order than the previous. Thus, two I order channels produce a II order segment; two II orders provide a III order, and so on. The hierarchical number is the highest order of the stream network.	Horton, 1945; Strahler, 1952
Bifurcation ratio	It describes the degree of branching of the hydrographic network and highlights possible hierarchical anomalies. $R_{b(u-u+1)} = N_u/N_{u+1}$ $\mathbf{N_u}$ is the number of fluvial segments of a given order; $\mathbf{N_{u+1}}$ is the number of fluvial segments of the immediately higher order. It considers how many segments of a given order are, concerning the highest order.	Horton, 1945; Avena et al., 1967; Strahler, 1952
Direct bifurcation ratio	It describes the degree of branching of the hydrographic network and highlights possible hierarchical anomalies. Rbd = Ndu/Nu+1 ***Ndu*** represents the number of fluvial segments of a given order that flow into higher order segments; ***Nu+1*** is the number of segments of the next higher order. It considers how many segments of a given order flow into the highest order.	
Bifurcation index (R)	It describes the degree of branching of the hydrographic network and highlights possible hierarchical anomalies. R = Rb – Rdb ***Rb*** encompasses all the segments of a given order, including the anomalous drainage, while ***Rbd*** considers only the not anomalous segments.	

	For a well-organized basin, ***(Rb ≈ Rbd***) R must approach zero; on the contrary, high R values indicate that the fluvial network does not have an excellent hierarchical organization.	
Anomaly parameter	It indicates the fluvial anomalies. An i.e., a river segment of a given order u flowing into a segment of order u+2. It is calculated for each u order.	Avena et al., 1967
Geomorphic indexes	Description	Reference
Asymmetry factor	It allows evaluating the asymmetry of the basin that can be due to broad lateral tilting or uplift and subsidence of discrete blocks. AF= 100(Ar/At) where ***Ar*** is the basin area on the hydrographic right, to the main river trunk segment; ***At*** is the area of the entire drainage basin. ***AF*** value greater than 50 indicates shifting towards the hydrographic left, whereas a value lower than 50 indicates rightwards shifting.	Cox, 1994; Hare and Gardner, 1985; Molin et al., 2004; Pinter, 2005
Transverse Topographic Symmetry factor	It allows evaluating the asymmetry of the basin that can be due to broad lateral tilting or uplift and subsidence of discrete blocks. T= Da/Dd where ***Da*** is the distance from the main river trunk to the basin midline; ***Dd*** is the distance from the basin watershed to the basin midline. This metric was computed by automating the methodology proposed by Cox, (1994), through in-house developed scripts and geospatial models The basin must be divided into constant intervals. Stability is indicated by low ***T*** values (***Da*** approaches zero); on the contrary, ***T*** values approaching one indicate basin asymmetry and, thus, tilting.	Cox, 1994;
Basin elongation Ratio (Re)	It describes the planimetric shape of the basin and its phase of maturity; a mature basin, draining on a stable area, has a shape similar to a circle, whereas a basin draining on an area characterized by a rapid uplift shows an elongated narrow shape. Re = (2√A:√Π)/Lb Where ***A*** is the basin area, ***Lb*** is the length of the basin parallel to the main drainage line. The basin area is considered a circle, and its hypothetic diameter is compared to the basin length. High values indicate a shape approaching a circle; on the contrary, low values indicate elongated basins whose shape depends on the tectonic control.	Bull and McFadden, 1977; Molin et al., 2004

Sinuosity index	It indicates the response of a fluvial channel to slope steepening with a meandering sinuosity increase. Sinuosity is the ratio of channel length over valley length. S = L / Sl_Dist ***Sl_Dist*** is the straight-line distance from the catchment startpoint to the endpoint and L is the total length of the line segments. The sinuosity of a straight line is 1. If the line is closed (startpoint equals endpoint), the sinuosity is 0. As the line gets curvier, the sinuosity increases.	Woolderink et al., 2021 and reference therein
Hypsometric integral	It quantifies the areal distribution of the relief elevation in the basin, describing the stage of the drainage basin or part of it, if youthful, mature, or old. This parameter highlights possible local or more widely areal rejuvenation due to regional uplift or fault dip movement. Hypsometric integral is measured for an interval of elevation. The relative area (**a/A** ratio, with A total area and the basin area above a given elevation h, and the relative elevation (**h/H** ratio, with H maximum basin elevation and h topographic elevation), are represented in the Cartesian graph as a curve. The curve shape indicates the evolution stage of the basin: an upward convex curve indicates a juvenile stage, a sigmoidal curve a mature stage and finally an upward concave curve a senile stage.	Strahler, 1952
Normalized steepness index (K_{sn})	It represents a measure of the river channel slope normalized to the drainage area directly proportional to the uplift rates. $$k_{sn} = \frac{S}{A^{-\theta_{ref}}}$$ S represent the slope, A the drainage area and θ_{ref} represent the normalized channel concavity set equal to 0.45 following the Kirby and Whipple, (2012) approach. The normalized steepness index (K_{sn}) allows the comparison of stream profiles characterized by wildly varying drainage areas. Higher values indicate higher uplift rate values.	Duvall et al., 2004; Lague and Davy, 2003; Kirby and Whipple, 2012; Snyder et al., 2000; Wobus et al., 2006

4. Geomorphological and morphometric evidence of fault activity

4.1. Structural pattern

The mapped fault systems are the following: 1) the WNW-ESE to ESE-WNW trending, south-dipping, Lamezia Catanzaro fault system (LCFS: Fa, Fb and Fc in Fig. 2A) and the WNW-ESE striking South Sila Piccola Fault System (SSPFS: Fd, Fe, Ff and Fg in Fig. 2A), both running along the northern bound of the Catanzaro Trough; 2) the WNW-ESE trending, north-dipping, Maida Fault (MF in Fig.

2 A) and Staletti Fault (SF in Fig. 2A), both bordering the basin to the south; 3) a newly detected NNE-SSW trending, WNW dipping, fault system in the central portion of the basin, here named Caraffa Fault System (Fig. 2A). This system extends south with a segmented pattern (Cfa, Cfb and Cfc in Fig. 2A) and a total length of about 17 km. The southern segment shows a N-S direction, parallel to the major Serre Fault (Figs. 2A, B).

4.2. The South Sila Piccola and Lamezia Catanzaro fault systems

The SSPFS shows evidence of recent left-lateral transtensional activity at the Serrastretta locality where, during the middle-late Pleistocene, two over-stepping en-echelon fault segments (Fe and Ff in Fig. 2C) gave rise to a NNE-SSW-trending restraining sector (push-up structure), obstructing the drainage network and causing the formation of the Decollatura paleo-lake, characterized by middle-late Pleistocene lacustrine deposits.

In the north-western sector of the study area, the LCFS is characterized by a set of fault steps that offsets both upper Pleistocene marine terraces and alluvial fans (Figs. 2B and D). Triangular and trapezoidal facets characterize the escarpment of Fa (Fig. 2E) north-east of Pianopoli town (Fig. 2B), suggesting a recent normal reactivation of this WNW-ESE trending segment of the LCFS. The A-A' topographic profile (Figs. 3A and 4A) shows the landscape imprint of the LCFS characterized by morphological scarp and rejuvenation of the slope between the fault traces.

The activity of the SSPFS and the LCFS is testified by the morphometric analysis of the sub-basins flowing in the northern sector of the trough (i.e., B1-3, Am 1-4 and C1) (Figs. 6A and 6F) that show the most significative among the multiple river flow deflections that characterize the drainage network of the Catanzaro Trough (roughly 180° in the North Amato sub-basin, Fig. 7A). These sub-basins are characterized by medium to high values of K_{sn} (Fig. 6B) and by increases in the values of slope and local relief at the footwall of the LCFS and, moderately, of the SSPFS (Figs. 6C and D), testifying the recent normal dip-slip activity of these faults.

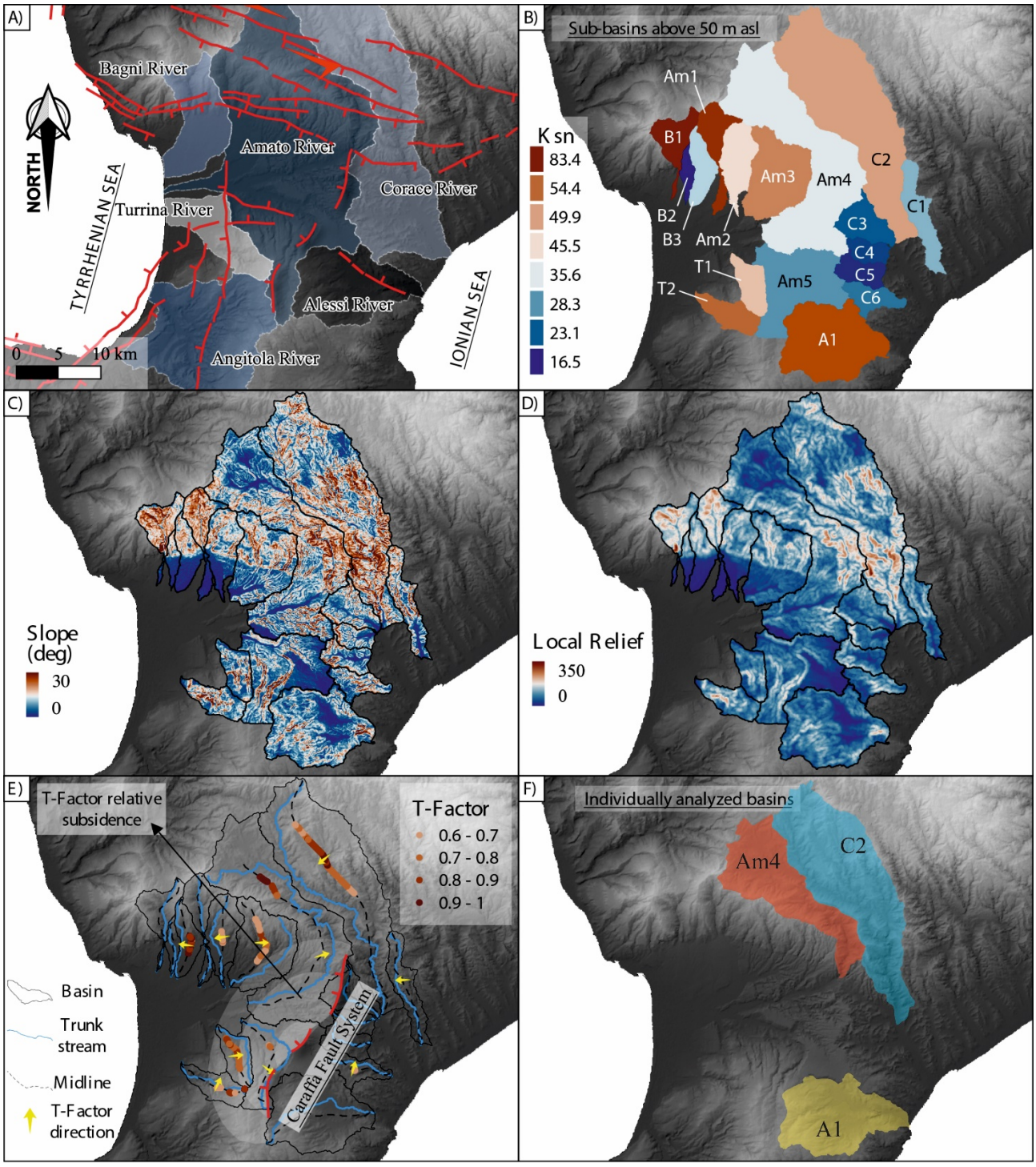

Fig. 6: *A) Hillshade visualisation of the Digital Elevation Model (DEM) of the analysed river basins considered for the analysis; B) Sub-basins: B1-3, sub-basins of the Bagni River; Am1-4 sub-basins of the Amato River; C1-6, subbasins of the Corace River; T1-2, sub-basins of the Turrina River; A1, subbasins of the Alessi River); K_{sn} values measured for each sub-basins. C) Slope analysis; values are in degree. D) Local relief trend. E) T-factor represented by coloured bars; yellow arrows indicate the direction of migration of the main river trunk. F) Sub-basins further analysed through a morphometric approach: Am4, C2 and A1.*

As it concerns the analysis of the Am4 and C2 sub-basins, the values of the AF index (Table 2) and T-factor (Fig. 6E) highlight a strong asymmetry and an anomalous shifting and convergence

between the two main river trunks, in the sector where the drainage is intercepted by the LCFS and the SSPFS, indicating differential movements and tilting of discrete blocks in this area. The values of the Re index of the Am4 and C2 sub-basins (Table 2) indicate an anomalously elongated shape suggesting, along with the high values of the S index (Table 2), a tectonic control and fast local uplift of the LCFS and SSPFS footwall area.

The computed hierarchical parameters characterizing the Am4 and C2 sub-basins, such as the R_b, $R_{bd,}$ R and An value (Tab. 2), suggest a scant organization of the fluvial network, typical of recently rejuvenated drainage patterns. The Hypsometric curve of these sub-basins confirms such rejuvenation at the footwall of the SSPFS and of the LCFS (Figs. 7B and 8B). Additionally, the shape of the path profiles of these two rivers shows an increase of the slope in correspondence of the LCFS and a flat shape in the upper reach where the main river trunks flow parallel to the Fe and Fd belonging to the SSPFS (Figs. 7 C and 8C). Such evidence confirms the prevalent normal motion of the LCFS and the transcurrent kinematics of the SSPFS.

Table 2: Hierarchical parameters and geomorphic indexes of the three major river drainage networks.

Am4	number	Rb	Rbd	R=(Rb-Rbd)	An	AF	Re	S
ord 1	742	5,7	3,7	1,9	255	58,40	0,184	1,62
ord 2	131	4,0	2,8	1,2	39			
ord 3	33	3,7	2,6	1,1	10			
ord 4	9	4,5	3,5	1,0	2			
ord 5	2	2,0	2,0	0,0	0			
ord 6	1							

C2	number	Rb	Rbd	R=(Rb-Rbd)	An	AF	Re	S
ord 1	1117	5,6	3,6	2,0	395	25,82	0,171	1,58
ord 2	199	4,6	3,0	1,6	68			
ord 3	43	8,6	6,8	1,8	9			
ord 4	5	5,0	5,0	0,0	0			
ord 5	1							

A1	number	Rb	Rbd	R=(Rb-Rbd)	An	AF	Re	S
ord 1	609	6,6	3,9	2,7	247	52,97	0,308	1,47
ord 2	92	5,4	3,9	1,5	26			
ord 3	17	4,3	3,0	1,3	5			
ord 4	4	2,0	2,0	0,0	0			
ord 5	2	2,0	2,0	0,0	0			
ord 6	1							

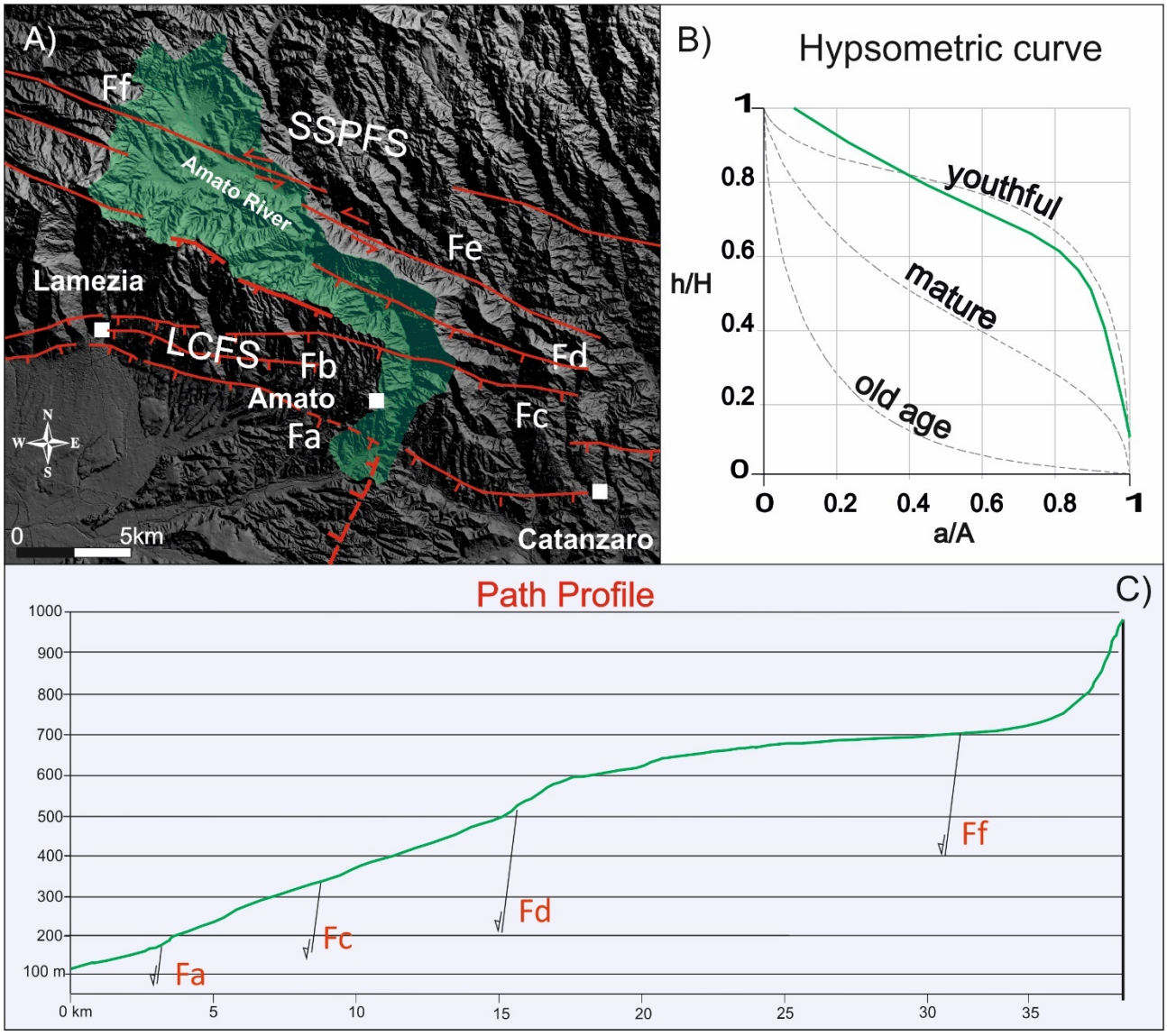

Fig. 7: A) DTM hillshade showing the Am4 sub-basin and faults crossing the area. B) Hypsographic curve of the Am4 sub-basin. C) Path profile of the main river trunk of the Am4 sub-basin and faults.

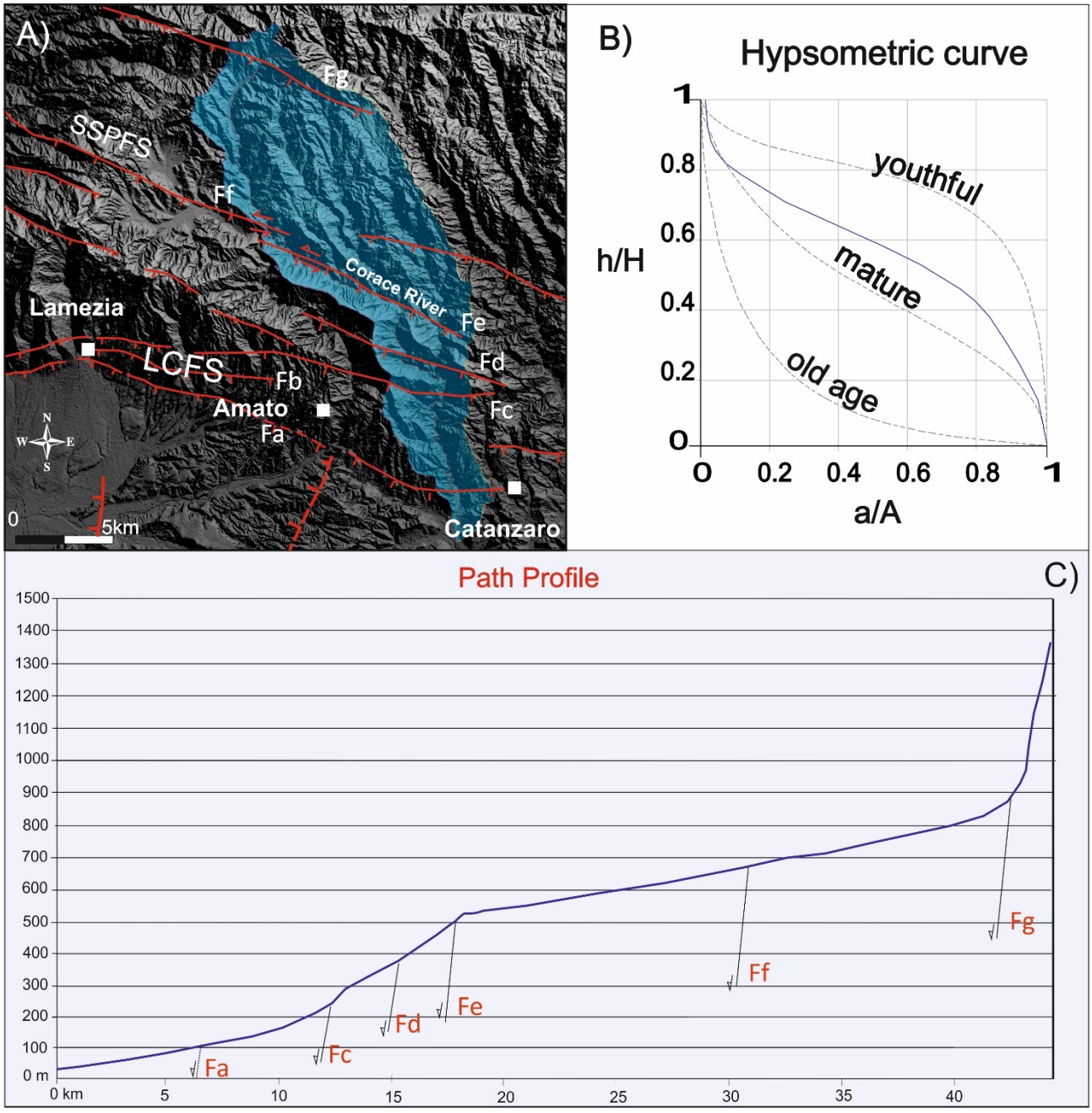

Fig. 8: A) DTM hillshade showing the C2 sub-basin and faults crossing the area. B) Hypsometric curve of the C2 sub-basin. C) Path profile of the C2 sub-basin and faults.

The recent activity of the SSPFS and the LCFS is also testified by a double fluvial capture of the fluvial network of the Am4 sub-basin at the expense of two old tributaries of the C2 sub-basin (Fig. 9). The first capture occurred where the Am4 is crossed by the Fc and should be related to the relative uplift of the Fa and Fc footwall, triggering a faster head retreat of the young Am4 drainage, up to intercept the old sector of the C2 (Figs. 9A and 9B). This piracy event is testified by wind gaps / suspended valleys, representative of the abandoned drainage reaches of the C2 (see Figs. 9C and 9D). The second capture event happened in response to the footwall uplift of the SSPFS causing the

progressive northward erosion of the Am4 fluvial network, intercepting the old C2 fluvial network and causing the Decollatura paleo-lake empty (Fig. 9E and 9F). Such fluvial captures produced the clockwise deflection of the Am4 sub-basin (about 180 degrees).

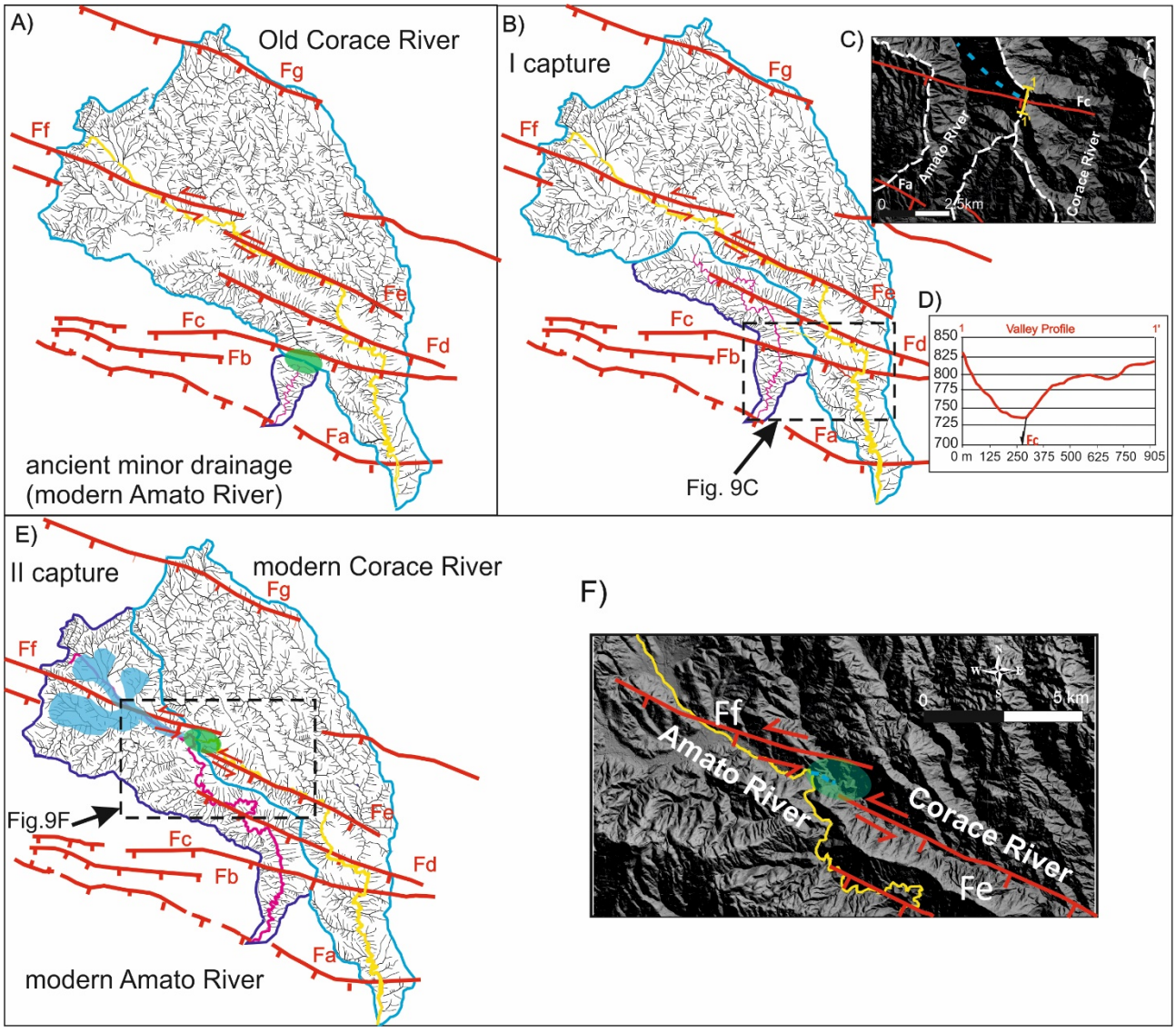

Fig. 9: Reconstruction of the evolution of the fluvial network of Am4 sub-basin (blue polygon is the watershed, the pink line is the main river course) and fluvial network of C2 sub-basin (cyan polygon is the watershed, the yellow line is the main river course). A) Ancient Am4 fluvial network (blue polygon), initially formed by minor drainage and ancient C2 fluvial network (cyan polygon); the zone of the fluvial catchment is indicated by the green ellipse. B) fluvial network configuration after the first capture of the minor drainage (old Am4 fluvial network) at the expense of the old C2 fluvial network. C) Detail of the fluvial capture of the old C2 fluvial network (see Fig. 9B for location); blue dashed line is the track of the suspended valley. D) profile of the watershed (see trace 1-1' in Fig. 1C) showing the suspended valley and the track of Fc. E) Second capture of the old C2 fluvial network and present-day configuration of the two rivers; green ellipse is the area of push-up and obstruction of the old C2 fluvial network; cyan polygon represents the Decollatura paleo-lake. F) Detail of the northern capture, the cyan line is the old, abandoned C2 drainage (see Fig. 9E for location).

4.3. The Maida and Stalettì faults

In the southern side of the Catanzaro Trough, the Maida and Stalettì faults show intensely eroded, low steep scarps, displacing Pliocene-Middle Pleistocene deposits and discouraging any interpretation of the recent activity of those faults. The Maida and Stalettì faults cross out the T1, Am5 and A1 sub-basins characterized by low to moderate values of K_{sn}, low slope and low local relief values at the interception with these faults (Figs. 6A-D). Outcomes from T-Factor analysis indicate an eastward shifting of the main river trunk of the river flowing in the western sector, not compatible with the expected kinematics of the Maida and Stalettì faults.

A1 is the most developed basin intercepted by the Stalettì Fault (Fig. 10A). Outcomes from hierarchical parameters, T-factor, AF, Re and S indexes suggest that the Alessi River is relatively stable (Table 2). The stability of this river is testified by a mature stage of the Hypsometric curve and an eroded and mature profile of the main river trunk in correspondence to the Stalettì Fault (Figs. 10B and 10C).

The wholeness of the geomorphological and morphometric evidence indicates weak or nil recent activity of the Maida and Stalettì faults.

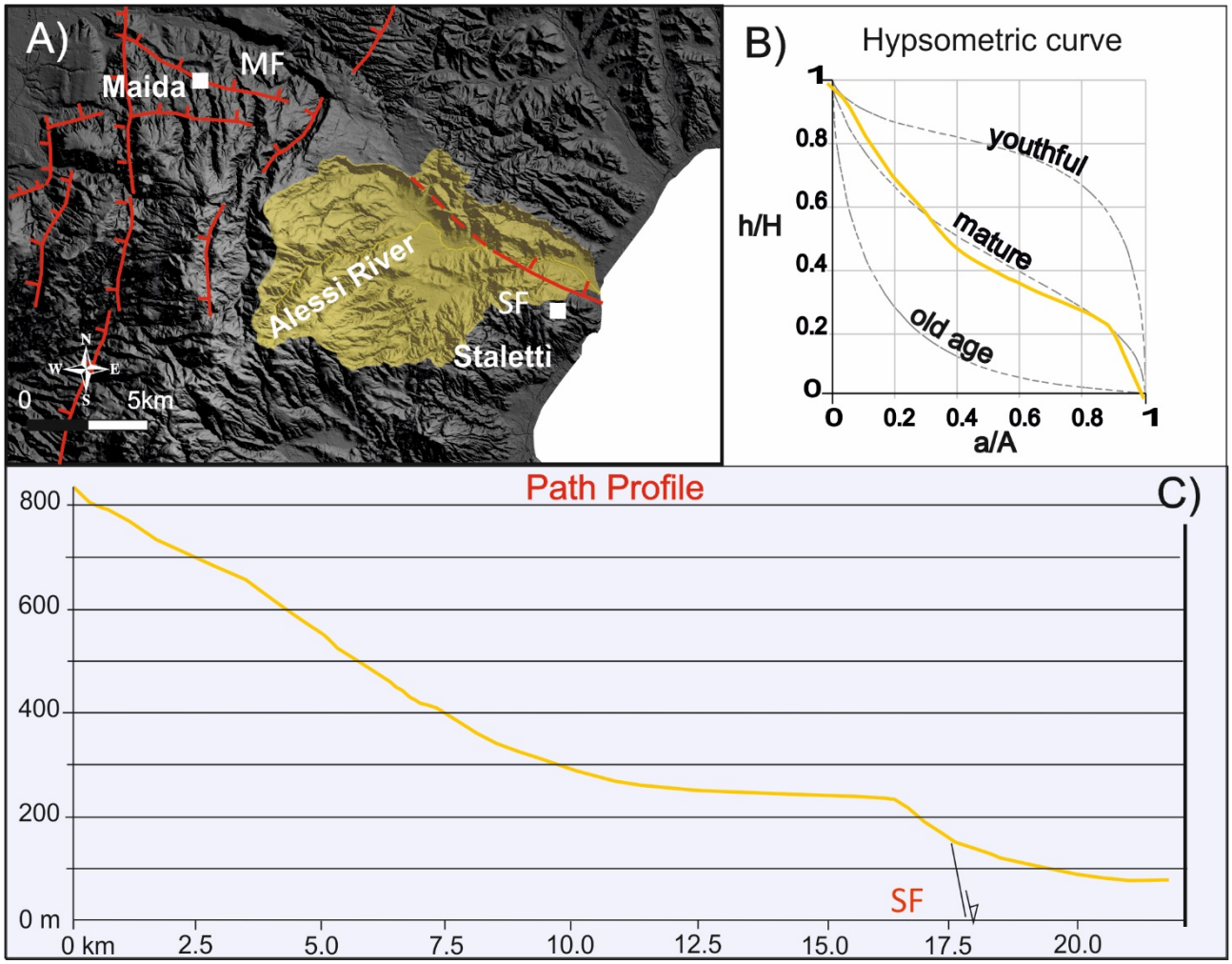

Fig. 10: A) DTM hillshade showing the Alessi sub-basin and faults crossing the area. B) Hypsometric curve of the Alessi sub-basin. C) Path profile of the main river trunk of the Alessi sub-basin and faults.

4.4. The Caraffa Fault System

Even though characterized by weak outcrop scale structural evidence, the Caraffa Fault System gives rise to geomorphological markers indicating its recent activity. The northernmost segments of the system (Cfa and Cfb) are responsible for up-faulted and down-faulted blocks in the central sector of the Catanzaro Trough (Fig. 2B). The Cfa segment is responsible of the tilting and warping of the III order marine terrace south-west of the Caraffa town (Fig. 2F). The Cfb segment dislocates a morphological platform and causes the rejuvenation of the eastern side of a valley (Fig. 2G). The morphological imprint of the Cfc segment is evident in the B-B' profile (Figs. 3A and 4B) that shows marine terraces in the western side at the hangingwall of the Caraffa Fault System, a west dipping morphological scarp in correspondence of the Cfc fault track, landscape tilting with eastward downfaulting and landscape rejuvenation with deeply incised V-shaped fluvial valleys in the eastern side of the Catanzaro Trough, at the footwall of the Cfc segment.

The swath profile along the C-C' track (Figs. 3A and 4C) confirms the substantial variation in the relief distribution between the Tyrrhenian and the Ionian sectors of the Catanzaro Trough, passing from the hangingwall to the footwall of the Caraffa Fault System. In this profile, the lower standard deviation values, together with the more continuous topography of the western side, highlight a landscape currently related to the vertical movement and resulting from the interplay of eustatic forcing and regional uplift that caused the formation of the staircase of marine terraces. Differently, the high standard deviation values of the eastern side of the trough and the presence of numerous V-shaped valleys suggest faster relative uplift of this sector.

The longitudinal profiles of the R1-R5 reaches of the Amato River show slope break and increases in correspondence of the Caraffa Fault System (Figs. 5A-E), indicating its persisting activity not correlated to the values of the catchment area. The geometry of the R1and R5 river reaches shows significative deflections (roughly 90° degree) in the fault surrounding that bend the river network from a fault-perpendicular flow direction towards a fault-parallel flow direction (Fig. 3B). Diffuse wind gaps, such as that observed between the Amato and Angitola rivers (Figs. 3C) testify the persisting activity of the northernmost segment of the System.

Additionally, T-factor values of the sub-basins located inside the trough highlight that, in the nearness of the Caraffa Fault System, the main river trunks are anomalously shifted toward E, against the track of this fault, indicating the presence of a depocenter in correspondence of it (see T1-2 and Am3-5 in Fig. 6E).

5. Seismotectonic implications

As depicted by the GNSS velocity field and its cross section, the GNSS station in the Ionian side of the Catanzaro Trough are characterized by migration velocities toward ESE greater than the GNSS station in the Tyrrhenian side of the basin. Such velocity difference highlights the observation of an ongoing extension process characterized by a rate of roughly 1 mm/yr compatible with the presence of the NNE-SSW trending extensional Caraffa Fault System (Figs. 11 and 12A).

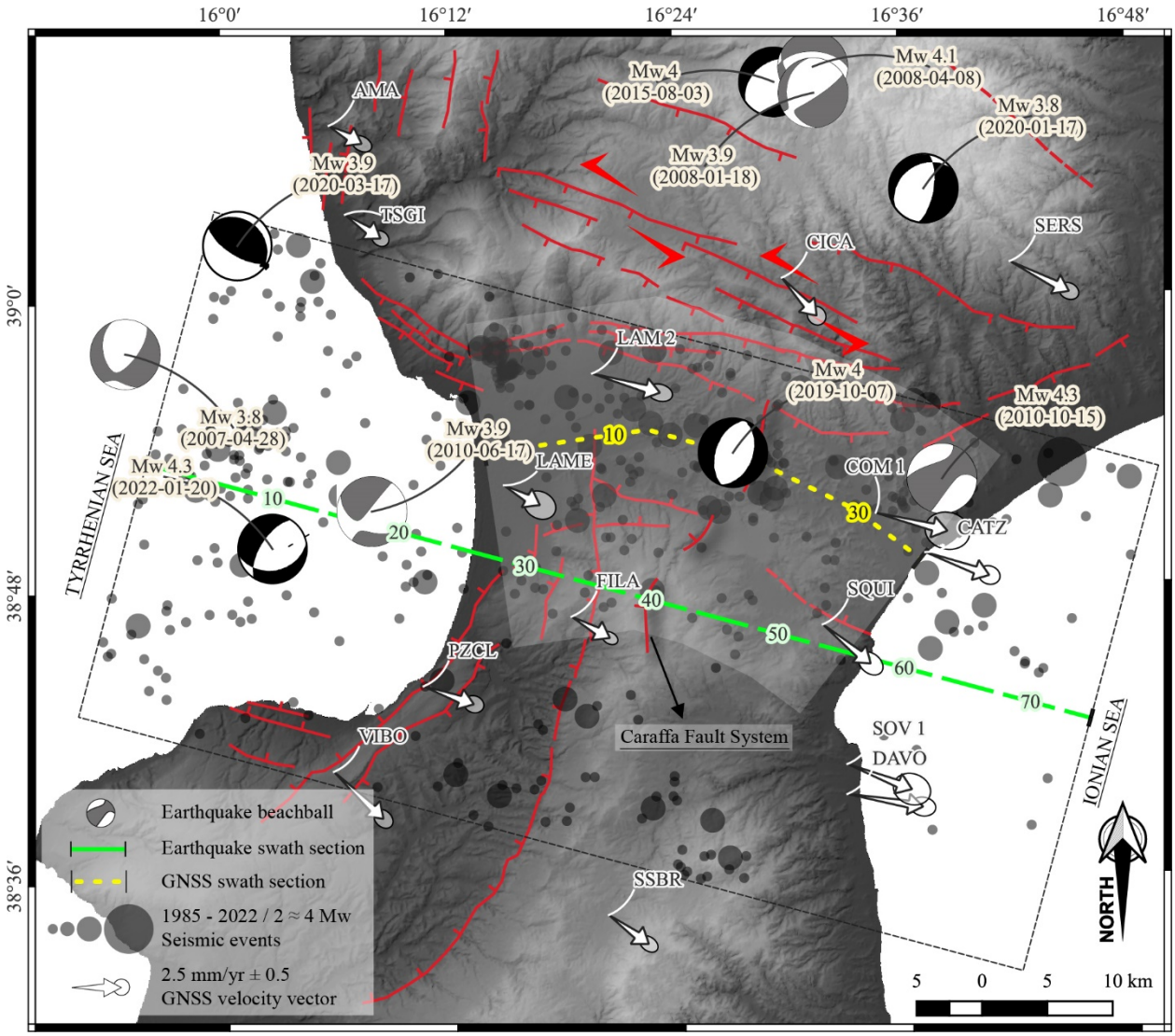

Fig. 11: Seismotectonic map of the Catanzaro Trough. The beachballs and black dots indicate the 1985 – 2022 instrumental and parametric seismicity of the area (from the ISIDE Working Group, 2007). White arrows represent the GNSS velocity field (from Pirrotta et al., 2021). The yellow dashed line together with the whitish transparent polygon represent the swath baseline and the swath area of the GNSS velocity cross section plotted in Fig. 12A. The green dashed line and the black dashed polygon represent the swath baseline and area of the seismicity cross section plotted in Fig. 12B. The yellow and light green buffered numbers along the two dashed lines represent the distance along the line expressed in km.

The projection of the hypocenters of the instrumental earthquakes acquired in the span of time 1985 – 2022 along a section roughly parallel to the Catanzaro Trough, shows that the seismogenic layer results thicker in the eastern side of the basin, likely due to the presence of the Ionian plate below the Calabrian Arc, rather than in the western side where the Ionian plate dips below the continental crust into the mantel (Fig. 12B). In correspondence of the Caraffa Fault System, a vertical alignment of hypocenters deepens up to the limit of the seismogenic layer, almost up to the continental/oceanic crust transition, testifying the seismic activity of such structure.

The 2019 seismic sequence (up to 4.3 Mw) occurred west of the Caraffa village (red circles in Fig. 1B); the map projection of the mainshock focal mechanism (Figs. 11 and 12B) reveals N-S oriented normal fault planes that well matches with the geometry and kinematics of the Caraffa Fault System.

As regards the large historical earthquakes occurred in the Central Calabrian Arc, those of 1626 A.D. and March 28, 1783 were located respectively in the central and southern sector of the Catanzaro Trough (Rovida et al., 2021, Fig. 1B). In this area only two seismogenic sources have been modelled: the ITCS110 located in the western margin of the trough and related to the 1905 earthquake that likely occurred in the Tyrrhenian offshore; the ITCS068 that bounds the basin to the north and should be suitable to generate earthquakes with a magnitude up to 7.1 (DISS Working Group, 2021) (Fig. 1B). The latter source partially coincides with the Lamezia Catanzaro Fault System that, according to Pirrotta et al. (2021), could be responsible for the historical and instrumental seismicity of the area, given the presence of earthquake clusters nucleated on these faults. However, due to their location and geometry, these sources are not consistent with many of the earthquakes occurred in the central-southern sectors of the Catanzaro Trough such as the 1626 A.D. and the March 28, 1783. Akinci et al. (2017) modelled a NNE-SSW seismogenic source (ITES002) in the central sector of the trough (Fig. 1B) inferred on the basis of geodynamic considerations, despite it is not yet constrained by field evidence. The seismic potential (roughly Mw 7 according to Akinci et al., 2017), its location and geometry make this source suitable with the large historical earthquakes of the Catanzaro Trough and with the seismic sequence of 2019. Considering its location, geometry and kinematics, the Caraffa Fault System well matches with the ITEES002 seismogenic source. This system is long about 17 km at the surface; however, it could have a length at the sub-surface up to about 24 km, considering that the sub-surface rupture length (RLD) of a fault is generally longer than the rupture length at the surface (SRL) up to 35–45% (Wells and Coppersmith, 1994; Boncio et al., 2004). Thus, the Caraffa Fault System should be capable of generating earthquakes with a magnitude up to 6.7.

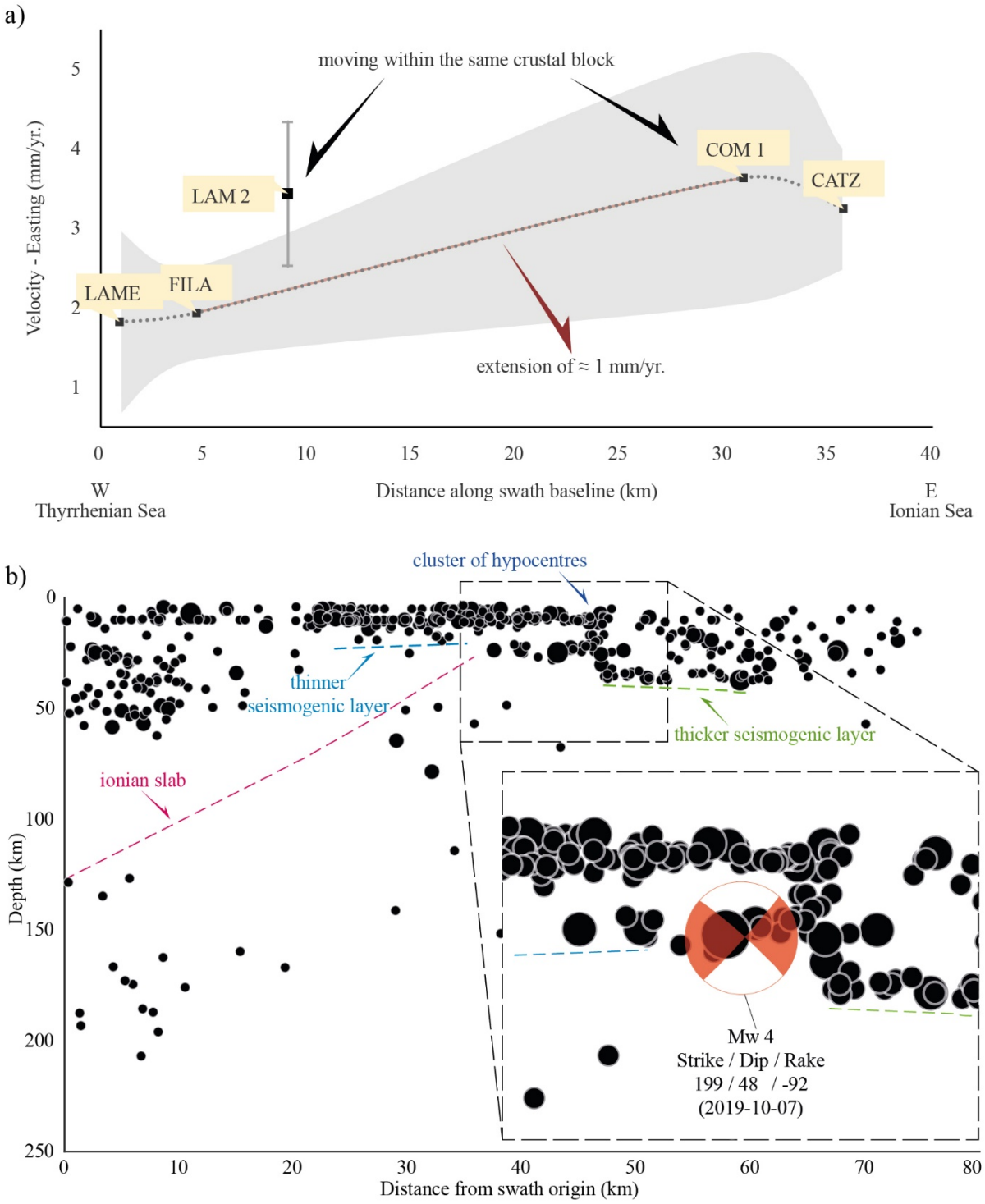

Fig. 12: A) GNSS velocity cross section along the Catanzaro Trough showing a current extension in the Catanzaro Trough of roughly 1 mm/yr (section trace is plotted in Fig. 11). B) Swath cross section showing the Catanzaro Trough earthquake hypocentre distribution (section trace is plotted in Fig. 11). The beachball refers to the 2019 Mw 4 earthquake, whose epicentre was located near the Caraffa village (see Figs. 1 and 11 for location).

The evidence of seismic activity of this fault, testified by the alignment of earthquakes at depth (Fig. 12B), and its parametrization (location, geometry and kinematics) make the Caraffa Fault System to be a good candidate as source responsible for the historical and instrumental seismicity of this sector

of the Catanzaro Trough, enclosed the 1626 and the March 28, 1783 events and the seismic sequence of 2019 (Fig. 1B). The macroseismic epicentre of the March 28, 1783 event has been located more to the southeast respect to the Caraffa Fault System (Rovida et al., 2021). However, the location of this event could be mistaken, and it could be located more at north inside the Catanzaro Trough because its macroseismic field includes the localities already seriously damaged by the preceding shocks of the 1783 seismic sequence, mainly located in southern Calabria. The uncertainty of the epicentral position of this event could be hampered by the deeper location of its nucleation point with respect to the previous earthquakes of the 1783 seismic sequence, that makes the isoseismal gradient scantly steep and the felt area wide (Jacques et al., 2021).

6. Conclusions

The presented geomorphological and morphometric study of the Catanzaro Trough and surrounding areas allowed us to improve the knowledge on the active tectonics and the landscape evolution of this crucial sector of the Calabrian Arc. The South Sila Piccola Fault System and the Lamezia Catanzaro Fault System show the most significant evidence of Quaternary activity. These systems show transtensional left-lateral kinematics, with a more marked left-lateral motion along the South Sila Piccola Fault System, which accommodates the different SE-ward advancement of the upper crustal sectors of the orogen, and a more prevalent normal component of motion along the Lamezia Catanzaro Fault System that accommodates the transition from the strike-slip regime, at the north, to the extensional one, at the south. Conversely, the normal faults bounding the Catanzaro Trough to the south (the MS and SF) don't show evidence of recent movement. Outcomes from the relief distribution and morphometric analyses made it possible to detect for the first-time the morphological signature of the Caraffa Fault System, a NNE-SSW trending WSW dipping extensional structural alignment extending from the central portion of the Catanzaro Trough to the south. The Caraffa Fault System probably represents the northern prosecution of the Serre Fault, a major extensional structure that accommodates the WNW-ESE oriented extension of the Calabria Arc (Gullà et al., 2005; Pirrotta et al., 2021). Given its location, geometry and kinematics, the Caraffa Fault System could be responsible for the historical and instrumental seismicity of this sector of the Calabrian Arc, including the 1626 A.D., the March 28, 1783 earthquakes and the seismic sequence of the 2019.

Acknowledgements

This work was funded by the **MUSE 4D** project – Overtime tectonic, dynamic and rheologic control on destructive multiple seismic events – Special Italian Faults & Earthquakes: from real 4D cases to models in the frame of PRIN 2017. Part of the research presented was performed in the **L**andscape **E**volution **M**arker **O**nline **N**etwork (**LEMON**) project (INQUA – AIQUA framework).

References

Akinci, A., Vannoli, P., Falcone, G., Taroni, M., Tiberti, M. M., Murru, M., Burrato, P., Mariucci, M. T. (2017). When time and faults matter: towards a time-dependent probabilistic SHA in Calabria, Italy. Bulletin of Earthquake Engineering, 15(6), 2497-2524.

Amodio Morelli, L., Bonardi, G., Colonna, V., Dietrich, D., Giunta, G., Ippolito, F., Liguori, V., Lorenzoni, S., Paglionico, A., Perrone, V., Piccarreta, G., Russo, M., Scandone, P., Zanettinlorenzoni, E., Zuppetta, A. 1976. L'Arco Calabro-Peloritano nell'orogene Appenninico-Maghrebide. Memorie della Società Geologica Italiana, 17, 1-60.

Avena, G. C., Giuliano, G., Lupia Palmieri, E. 1967. Sulla valutazione quantitativa della gerarchizzazione ed evoluzione dei reticoli fluviali. Bollettino della Società Geologica Italiana, 86, 781–796.Barreca, G., Scarfì, L., Gross, F., Monaco, C., De Guidi, G. 2019. Fault pattern and seismotectonic potential at the south-western edge of the Ionian Subduction system (southern Italy): New field and geophysical constraints. Tectonophysics, 761, 31-45, doi:10.1016/j.tecto.2019.04.020.

Boncio, P., Lavecchia, G., Pace, B., 2004. Defining a model of 3D seismogenic sources for seismic hazard assessment applications: the case of central Apennines (Italy). J. Seismol. 8 (3), 407–425. doi:10.1023/B:JOSE. 0000038449.78801.05

Brutto, F., Muto, F., Loreto, M.F., De Paola, N., Tripodi, V., Critelli, S., Facchin, L. 2016. The Neogene-Quaternary geodynamic evolution of the central Calabrian Arc: A case study from the western Catanzaro Trough basin. J. Geodynamics, 102, 95–114, doi: 10.1016/j.jog.2016.09.002.

Bull, W. B., McFadden, L. 1977. Tectonic geomorphology north and south of the Garlock Fault, California. Geomorphology in arid regions. Editor D. O. Doering (Binghamton, NY: State University of New York, Binghamton), 115–138.

Burrato, P., Ciucci, F., Valensise, G. 2003. An inventory of river anomalies in the Po Plain, Northern Italy: evidence for active blind thrust faulting. Annals of Geophysics, 46(5).

Camafort, M., Pérez-Peña, J. V., Booth-Rea, G., Melki, F., Gràcia, E., Azañón, J.M., Galve, J.P., Marzougui, W., Gaidi, S., Ranero, C.R. 2020. Active tectonics and drainage evolution in the Tunisian Atlas driven by interaction between crustal shortening and mantle dynamics. Geomorphology, 351, 106954. https://doi.org/https://doi.org/10.1016/j.geomorph.2019.106954

Carminati, E., Doglioni, C. 2005. EUROPE|Mediterranean tectonics.

Carminati, E., Wortel, M. J. R., Spakman, W., Sabadini, R. 1998. The role of slab detachment processes in the opening of the western–central Mediterranean basins: Some geological and geophysical evidence. Earth and Planetary Science Letters, 160 (3–4), 651–665.

Chiarella, D., Longhitano, S.G., Muto, F. 2012. Sedimentary features of the lower Pleistocene mixed siliciclastic-bioclastic tidal deposits of the Catanzaro Strait (Calabrian Arc, south Italy). Rendiconti Online Società Geologica Italiana, 21, 919–920.

Colella, A. 1995. Sedimentation, deformational events and eustacy in the perityrrhenian Amantea Basin: Preliminary synthesis. Giornale Di Geologia, 57 (1–2), 1193–1779.

Corradino, M., Pepe, F., Bertotti, G., Picotti, V., Monaco, C., and Nicolich, R. (2020). 3-D Architecture and Plio-Quaternary Evolution of the Paola Basin: Insights into the Forearc of the Tyrrhenian-Ionian Subduction System. Tectonics 39. Doi:10.1029/2019tc005898

Corradino, M., Pepe, F., Burrato, P., Kanari, M., Parrino, N., Bertotti, G., Bosman, A., Casalbore, D., Ferranti, L., Martorelli, E., et al. 2021. An integrated multiscale method for the characterisation of active faults in offshore areas. The case of Sant'Eufemia Gulf (Offshore Calabria, Italy). Froniers in Earth Science, 9, 670557. DOI: 10.3389/feart.2021.670557

Cox, R. T. 1994. Analysis of drainage basin symmetry as a rapid technique to identify areas of possible Quaternary tilt-block tectonics: an example from the Mississippi Embayment. Geological Society America Bulletin, 106, 571–581. DOI: 10.1130/0016-7606(1994)106<0571:AODBSA>2.3.CO,2

DISS Working Group, 2021. Database of Individual Seismogenic Sources (DISS), Version 3.3.0: A compilation of potential sources for earthquakes larger than M 5.5 in Italy and surrounding areas. Istituto Nazionale di Geofisica e Vulcanologia (INGV). https://doi.org/10.13127/diss3.3.0

Doglioni, C., Innocenti, F., Mariotti, G. 2001. Why Mt. Etna? Terra Nova, 13, 25–31.

Duvall, A., Kirby, E., Burbank, D. 2004. Tectonic and lithologic controls on bedrock channel profiles and processes in coastal California. Journal of Geophysical Research: Earth Surface, 109. https://doi.org/https://doi.org/10.1029/2003JF000086

Faccenna, C. 2005. Constraints on mantle circulation around the deforming Calabrian slab. Geophysical Research Letters, 32, doi:10.1029/2004gl021874.

Ferranti, L., Palano, M., Cannavò, F., Mazzella, M.E., Oldowc, J.S., Gueguen, E., Mattia, M., Monaco, C. 2014. Rates of geodetic deformation across active faults in southern Italy. Tectonophysics 621, 101–122. http://dx.doi.org/10.1016/j.tecto.2014.02.007.

Ferrini, G, Testa, G., 1997. La successione miocenica superiore della Stretta di Catanzaro, dati preliminari. In Abstracts of the Gruppo di Sedimentologia del CNR, Ed. Critelli, S., Annual Meeting, 474, 13–17 October 1997, Arcavacata di Rende, (Italy), pp. 53–55.

Figueroa, A.M., Knott, J.R., 2010. Tectonic geomorphology of the southern Sierra Nevada Mountains (California): Evidence for uplift and basin formation. Geomorphology, 123, 34–45. https://doi.org/doi:10.1016/j.geomorph.2010.06.009.

Forte, A.M., Whipple, K.X. 2018. Criteria and tools for determining drainage divide stability. Earth and Planetary Science Letters, 493, 102–117. https://doi.org/10.1016/j.epsl.2018.04.026

Ghisetti, F. 1979. Evoluzione neotettonica dei principali sistemi di faglie della Calabria centrale. Bollettino della Società Geologica Italiana, 98, 387–430.

Ghisetti. F., Vezzani, L. 1982. Different styles of deformation in the Calabrian arc (southern Italy): implications for a seismotectonic zoning. Tectonophysics, 85, 149- 165.

Guarnieri, P. 2006. Plio-Quaternary segmentation of the south Tyrrhenian forearc basin. Int. J. Earth Sci. (Geol Rundsch), 95, 107–118. DOI: 10.1007/s00531-005-0005-2

Guarnieri, P., Pirrotta, C. 2008. The response of drainage basins to the late Quaternary tectonics in the Sicilian side of the Messina Strait (NE Sicily). Geomorphology, 95, 260–273. Doi:10.1016/j.geomorph.2007.06.013

Gullà, G., Antronico, L., Sorriso-Valvo, M., Tansi, C. 2005. Proposta metodologica per la valutazione di indicatori di pericolo e rischio da frana a scala intermedia: l'area della Stretta di Catanzaro (Calabria, Italia). Geologica Romana, 38, 97-12.

Hare, P. W., Gardner, T. W. 1985. Geomorphic indicators of vertical neotectonism along converging plate margins, Nicoya Peninsula, Costa Rica. In Tectonic geomorphology. Proceedings of the 15th annual Binghamton geomorphology symposium. Editors M. Morisawa and J. T. Hack (Boston, MA: Allen & Unwin), 123–134.

Horton, R. E. 1945. Erosional development of streams and their drainage basins. Hydro-physical approach to quantitative morphology. Geological Society of America Bulletin, 56 (3), 275–370. Doi:10.1130/0016-7606(1945)56[275:EDOSAT]2.0.CO,2

ISIDe Working Group. 2007. Italian Seismological Instrumental and Parametric Database (ISIDe). Istituto Nazionale di Geofisica e Vulcanologia (INGV). https://doi.org/10.13127/ISIDE

Jacques, E., Monaco, C., Tapponnier, P., Tortorici, L., Winter, T. 2001. Faulting and earthquake triggering during the 1783 Calabria seismic sequence. Geophysical Journal International, 147, 499–516.

Kirby, E., Whipple, K.X., 2012. Expression of active tectonics in erosional landscapes. Journal of Structural Geology, 44, 54–75. https://doi.org/10.1016/j.jsg.2012.07.009

Lague, D., Davy, P., 2003. Constraints on the long-term colluvial erosion law by analyzing slope-area relationships at various tectonic uplift rates in the Siwaliks Hills (Nepal). Journal of Geophysical Research: Solid Earth 108. https://doi.org/https://doi.org/10.1029/2002JB001893

Longhitano, S.G., Chiarella, D., Muto, F. 2014. Three-dimensional to two-dimensional cross-strata transition in the lower Pleistocene Catanzaro tidal strait transgressive succession (southern Italy). Sedimentology, 61, 2136–2171, doi: org/10.1111/sed.12138.

Maesano, F.E., Tiberti, M.M., Basili, R. 2017. The Calabrian Arc: three-dimensional modelling of the subduction interface. Scientific Reports, 7:8887, doi:10.1038/s41598-017-09074-8.

Miyauchi, T., Dai Pra, G., Labini, S.S. 1994. Geochronology of Pleistocene marine terraces and regional tectonics in the Tyrrhenian coast of south Calabria, Italy. Il Quaternario, 7, 17–34.

Molin, P., Pazzaglia, F. J., Dramis, F. 2004. Geomorphic expression of the active tectonics in a rapidly-deforming forearc, Sila Massif, Calabria, Southern Italy. Am. J. Sci., 304, 559–589. doi:10.2475/AJS.304.7.559.

Monaco, C., Tortorici, L. 2000. Active faulting in the Calabrian arc and eastern Sicily. Journal of Geodynamics, 29, 407–424, doi: 10.1016/S0264-3707(99)00052-6.

Monaco, C., Barreca, G., Di Stefano, A. 2017. Quaternary marine terraces and fault activity in the northern mainland sectors of the Messina Straits (southern Italy). Italian Journal of Geosciences, 136 (3), 337-346, doi:10.3301/IJG.2016.10.

Monaco, C., Tortorici, L., Nicolich, R., Cernobori, L., Costa, M. 1996. From collisional to rifted basins: An example from the southern Calabrian arc (Italy), Tectonophysics, 266, 233–249, doi:10.1016/S0040-1951(96)00192-8.

Moretti, A. 2000. Il database delle faglie capaci della Calabria: stato attuale delle conoscenze. Le ricerche del GNDT nel campo della pericolosità sismica (1996–1999), 219-226.

O'Callaghan, J.F., Mark, D.M., 1984. The extraction of drainage networks from digital elevation data. Computer vision, graphics, and image processing 28, 323–344. https://doi.org/https://doi.org/10.1016/S0734-189X(84)80011-0

Orecchio, B., Presti, D., Totaro, C. Neri, G. 2014. What earthquakes say concerning residual subduction and STEP dynamics in the Calabrian Arc region, south Italy. Geophysical Journal International, 199, 1929–1942, doi:10.1093/gji/ggu373.

Ouchi, S. 1985. Response of alluvial rivers to slow active tectonic movement. Geological Society of America Bulletin, 96, 504–515. doi:10.1130/0016-7606(1985)96<504:ROARTS>2.0.CO,2

Pedrera, A, Pérez-Peña, J.V., Galindo-Zaldívar, J., Azañón, J.M. and Azor, A. 2009. Testing the sensitivity of geomorphic indices in areas of low-rate active folding (eastern Betic Cordillera, Spain). Geomorphology, 105, 218-231. DOI: 10.1016/j.geomorph.2008.09.026.

Pepe, F., Bertotti, G., Ferranti, L., Sacchi, M., Collura, A.M., Passaro, S., Sulli, A. 2014. Pattern and rate of post-20 ka vertical tectonic motion around the Capo Vaticano Promontory (W Calabria, Italy) based on offshore geomorphological indicators. Quaternary International, 332, 85–98. http://dx.doi.org/10.1016/j.quaint.2013.11.012.

Pinter, N. 2005. Applications of tectonic geomorphology for deciphering active deformation in the Pannonian Basin Hungary. In Proceedings of the workshop on "applications of GPS in plate tectonics in research on fossil energy resources and in earthquake hazard assessment," Occasional Papers of the Geological Institute of Hungary. Editors L. Fodor and K. Brezsnyánszky, 204, 25–51.

Pirrotta, C., Barbano, M. S., Monaco, C. 2016. Evidence of active tectonics in Southern Calabria (Italy) by geomorphic analysis: the examples of the Catona and Petrace rivers. Italian Journal of Geoscience 135 (1), 142–156. doi:10.3301/IJG.2015.20

Pirrotta, C. M. S. Barbano, 2020. New Macroseismic and Morphotectonic Constraints to Infer a Fault Model for the 9 (Mw6.1) and 11 January (Mw7.3) 1693 Earthquakes (Southeastern Sicily). Frontiers in Earth Sciences. doi: 10.3389/feart.2020.550851.

Pirrotta, C., Barberi, G., Barreca, G., Brighenti, F., Carnemolla, F., De Guidi, G., Monaco, C., Pepe, F., Scarfì, L. 2021. Recent Activity and Kinematics of the Bounding Faults of the Catanzaro Trough (Central Calabria, Italy): New Morphotectonic, Geodetic and Seismological Data. Geosciences, 11, 405. https://doi.org/10.3390/geosciences11100405

Roda-Boluda, D.C., Whittaker, A.C., 2017. Structural and geomorphological constraints on active normal faulting and landscape evolution in Calabria, Italy. Journal of the Geological Society 174, 701–720. https://doi.org/10/gbnqrt

Rovida, A., Locati, M., Camassi, R., Lolli, B., Gasperini, P., Antonucci, A. 2021. Italian Parametric Earthquake Catalogue (CPTI15), version 3.0. Istituto Nazionale di Geofisica e Vulcanologia (INGV), 2021, https://doi.org/10.13127/CPTI/CPTI15.3.

Scarfì, L., Barberi, G., Barreca, G., Cannavò, F., Koulakov, I., Patanè, D. 2018. Slab narrowing in the Central Mediterranean: The Calabro-Ionian subduction zone as imaged by high resolution seismic tomography. Scientific Reports, 8:5178, doi:10.1038/s41598-018-23543-8.

Scherler, D., Schwanghart, W. 2020. Drainage divide networks - Part 2: Response to perturbations. Earth Surface Dynamics, 8, 261–274. https://doi.org/10.5194/esurf-8-261-2020

Schwanghart, W., Scherler, D., 2014. Short Communication: TopoToolbox 2 - MATLAB-based software for topographic analysis and modeling in Earth surface sciences. Earth Surface Dynamics, 2, 1–7. https://doi.org/10.5194/esurf-2-1-2014

Schumm, S.A. 2005. River Variability and Complexity. Cambridge University Press, New York.

Snyder, N.P., Whipple, K.X., Tucker, G.E., Merritts, D.J. 2000. Landscape response to tectonic forcing: Digital elevation model analysis of stream profiles in the Mendocino triple junction region, northern California. Geological Society of America Bulletin, 112, 1250–1263. https://doi.org/https://doi.org/10.1130/0016-7606(2000)112<1250:LRTTFD>2.0.CO,2

Strahler, A. N. 1952. Hypsometric (area-altitude) analysis of erosional topography. Geological Society of America Bulletin, 63, 1117–1142. doi:10.1130/0016- 7606(1952)63[1117:HAAOET]2.0.CO,2

Tansi C., Iovine G., Fòlino-Gallo M. 2005. Tettonica attiva e recente, e manifestazioni gravitative profonde, lungo il bordo orientale del graben del Fiume Crati (Calabria settentrionale). Boll. Soc. Geol. It., 124, 563-578.

Tansi, C., Muto, F., Critelli, S., Iovine, G. 2007. Neogene-Quaternary strike-slip tectonics in the central Calabria Arc (southern Italy). Journal of Geodynamics, 43, 397–414.

Tiberti M.M., Vannoli P., Fracassi U., Burrato P., Kastelic V., Valensise G. 2017. Understanding seismogenic processes in the Southern Calabrian Arc: a geodynamic perspective. Italian Journal of Geosciences, 136(3), 365-388

Tortorici, L., Monaco, C., Tansi, C., Cocina O. (1995). Recent and active tectonics in the Calabrian arc (Southern Italy). Tectonophysics, 243, 37-55.

Valensise, G., & Pantosti, D. (2001). The investigation of potential earthquake sources in peninsular Italy: a review. Journal of Seismology, 5(3), 287-306

Van Dijk, J.P., Bello, M., Brancaleoni, G.P., Cantarella, G., Costa, V., Frixa, A., Golfetto, F., Merlini, S., Riva, M., Torricelli, S., Toscano, C., Zerilli, A. 2000. A regional structural model for the northern sector of the Calabrian Arc (southern Italy). Tectonophysics, 324, 267–320. DOI: 10.1016/S0040-1951(00)00139-6.

Wells, D., Coppersmith, K., 1994. New empirical relationships among magnitude, rupture length, rupture width, rupture area, and surface displacement. Bull. Seismol. Soc. Am. 84, 974–1002.

Westaway, R. 1993. Quaternary uplift of southern Italy. Journal of Geophysics Research, 98, B12,741–772.

Whipple, K.X. 2004. Bedrock rivers and the geomorphology of active orogens. Annual Review of Earth and Planetary Sciences, 32, 151-185. https://doi.org/10.1146/annurev.earth.32.101802.120356

Wobus, C., Whipple, K.X., Kirby, E., Snyder, N., Johnson, J., Spyropolou, K., Crosby, B., Sheehan, D., 2006. Tectonics from topography: procedurses, promise, and pitfalls. Geological Society of America Special Paper 398, 55–74. https://doi.org/10.1130/2006.2398(04).

Woolderink, H.A.G., Cohen, K. M., Kasse, C., Kleinhans, M. G., Van Balen, R.T. 2021. Patterns in river channel sinuosity of the Meuse, Roer and Rhine rivers in the Lower Rhine Embayment rift-system, are they tectonically forced? Geomorphology, 375, 107550. DOI:10.1016/j.geomorph.2020.107550

Wortel, R., Spakman, W. 2000. Subduction and slab detachment in the Mediterranean-Carpathian region. Science, 290, 1910–1917. DOI: 10.1126/science.290.5498.1910.

Zecchin, M., Praeg, D., Ceramicola, S., Muto, F. 2015. Onshore to offshore correlation of regional unconformities in the Plio-Pleistocene sedimentary successions of the Calabrian Arc (central Mediterranean). Earth Science Reviews, 142, 60–78. DOI: 10.1016/j.earscirev.2015.01.006

Front. Earth Sci., 11 June 2021 https://doi.org/10.3389/feart.2021.670557

Chapter 4

An Integrated Multiscale Method for the Characterisation of Active Faults in Offshore Areas. The Case of Sant'Eufemia Gulf (Offshore Calabria, Italy)

Authors: Corradino M.[1,2], Pepe F.[1*], Burrato P.[3], Kanari M.[4] **Parrino N.**[1], Bertotti, G.[5], Bosman, A.[6], Casalbore, D.[7], Ferranti L.[3,8,9], Martorelli E.[6], Monaco C.[2,9,10], Sacchi M.[11], Tibor G.[4]

[1]Dipartimento di Scienze della Terra e del Mare, Università di Palermo, Palermo, Italy
[2]Dipartimento di Scienze Biologiche, Geologiche ed Ambientali, Università di Catania, Catania, Italy.
[3]Istituto Nazionale di Geofisica e Vulcanologia, Roma, Italy
[4]Department of Marine Geology and Geophysics, Israel Oceanographic & Limnological Research, Haifa, Israel
[5]Department of Civil Engineering and Geosciences, Delft University of Technology, Delft, Netherlands,
[6]Istituto di Geologia Ambientale e Geoingegneria, Consiglio Nazionale delle Ricerche (IGAG-CNR), Roma, Italy
[7]Dipartimento Scienze della Terra, Sapienza Università di Roma, Roma, Italy
[8]Dipartimento di Scienze della Terra, dell'Ambiente e delle Risorse, Università di Napoli "Federico II", Napoli, Italy;
[9]CRUST-DiSTAR, Centro inteRUniversitario per l'analisi SismoTettonica tridimensionale con applicazioni territoriali, Università G. d'Annunzio, Chieti Scalo, Italy
[10]Istituto Nazionale di Geofisica e Vulcanologia, Osservatorio Etneo, Catania, Italy
[11]Consiglio Nazionale delle Ricerche - Istituto di Scienze Marine, Sede secondaria di Napoli, Napoli, Italy
***Correspondence:** Prof. Fabrizio Pepe (fabrizio.pepe@unipa.it)

Keywords: Active tectonics, Southern Tyrrhenian, Calabrian Arc, STEP fault, High-resolution seismic data, Morphotectonic

Abstract

Diagnostic morphological features (e.g. rectilinear seafloor scarps) and lateral offsets of the Upper Quaternary deposits are used to infer active faults in offshore areas. Although they deform a significant seafloor region, the active faults are not necessarily capable of producing large earthquakes as they correspond to shallow structures formed in response to local stresses. We present a multiscale approach to reconstruct the structural pattern in offshore areas and distinguish between shallow, non-seismogenic, active faults, and deep blind faults, potentially associated with large seismic moment release. The approach is based on the interpretation of marine seismic reflection data and quantitative morphometric analysis of multibeam bathymetry, and tested on the Sant'Eufemia Gulf (southeastern Tyrrhenian Sea). Data highlights the occurrence of three major tectonic events since the Late Miocene. The first extensional or transtensional phase occurred during the Late Miocene. Since the Early Pliocene, a right-lateral transpressional tectonic event caused the positive inversion of deep (> 3 km) tectonic features, and the formation of NE-SW faults in the central sector of the gulf. Also, NNE-SSW to NE-SW trending anticlines (e.g. Maida Ridge) developed in the eastern part of the area. Since the Early Pleistocene (Calabrian), shallow (< 1.5 km) NNE-SSW oriented structures formed in a left-lateral transtensional regime. The new results integrated with previous literature indicates that the Late Miocene to Recent transpressional/transtensional structures developed in an ~E-W oriented main displacement zone that extends from the Sant'Eufemia Gulf to the Squillace Basin (Ionian offshore), and likely represents the upper plate response to a tear fault of the lower plate. The quantitative morphometric analysis of the study area and the bathymetric analysis of the Angitola Canyon indicate that NNE-SSW to NE-SW trending anticlines were negatively reactivated during the last tectonic phase. We also suggest that the deep structure below the Maida Ridge may correspond to the seismogenic source of the large magnitude earthquake that struck the western Calabrian region in 1905. The multiscale approach contributes to understanding the tectonic imprint of active faults from different hierarchical order and the geometry of seismogenic faults developed in a lithospheric strike-slip zone orthogonal to the Calabrian Arc.

1. Introduction

Identifying seafloor scarps in bathymetry and the offset of Middle to Upper Quaternary marine deposits in seismic images are typically used in offshore areas to infer active faults and derive their geometric and kinematic characteristics that are necessary to parametrise seismogenic sources. Among the geophysical methodologies used to detect active faults, the high-resolution seismic reflection

imaging provides a powerful tool to unravel the Late Quaternary activity of faults, to measure the displacements along the fault planes and to correlate the onshore with the offshore segments (e.g., Barreca et al., 2014, 2018; Corradino et al., 2021; Cultrera et al., 2017a; Ferranti et al., 2014). Standard methods for qualitative morphotectonic analysis that use multibeam high-resolution bathymetric data consist of tracing in plan-view the faults that offset the seafloor and in recognising morphological features close to the tectonic structures, such as rectilinear canyons, scarps or seafloor undulations (e.g. Di Bucci et al., 2009; Cultrera et al., 2017b; Fracassi et al., 2008; Loreto et al., 2013; Loreto et al., 2021). However, a limitation in reconstructing complex structural pattern in offshore areas is caused by the difficulty in mapping faults in areas not fully covered by geophysical data, by the low preservation potential of fault scarps and, often, by the blind nature of the tectonic deformation occurring when the structures do not produce detectable deformation at shallow depth (due to their geometry and depth). Consequently, an approach that includes only observation of the seafloor and superficial deposits can be insufficient and misleading for identifying the primary active faults associated with the most significant seismic moment release. Most shallow faults may be secondary features formed in response to local stresses (e.g. bending moment normal faults that occur on the top of a reverse structure) and are not the direct surface expressions of primary structures. Besides, the primary active faults can exploit inherited faults in response to a change of the regional stress regime, further complicating the interpretation. The question tackled in this work is what is the correct approach in the offshore area to identify and characterise primary active faults that can be potentially seismogenic?

We test a multiscale and multidisciplinary approach to detect surficial and blind active faults, and distinguish the tectonic imprint of active faults from different hierarchical orders. Our method is based on the integration of seismic reflection data with different resolution/penetration and the quantitative morphometric analysis of a high-resolution multibeam bathymetric dataset. The approach significantly differs from the standard because the quantitative analysis of the bathymetry can identify seafloor areas in a transient state caused by fault-related deformation, even if these areas are not fully covered by seismic reflection data.

The site chosen for testing the method is the Sant'Eufemia Gulf (Tyrrhenian offshore the central Calabrian Arc, Figure 1a and b) because it can be considered as a natural laboratory to investigate the complex relationships between regional and local processes due to the presence of a slab tear in the Calabrian subduction system (Maesano et al., 2017; Neri et al., 2009; Rosenbaum et al., 2008; Scarfì et al., 2018) and, at shallower levels, of crustal faults that controlled the Plio-Quaternary tectonic evolution (Brutto et al., 2016; Del Ben et al., 2008; Loreto et al., 2013). This

region was also the epicentral area of the Mw 7.0, 1905 central Calabria destructive earthquake (Rovida et al., 2020). The seismogenic source of this event is still poorly constrained and debated (DISS Working Group, 2018) due to its offshore location and the limited seismic instrumental records.

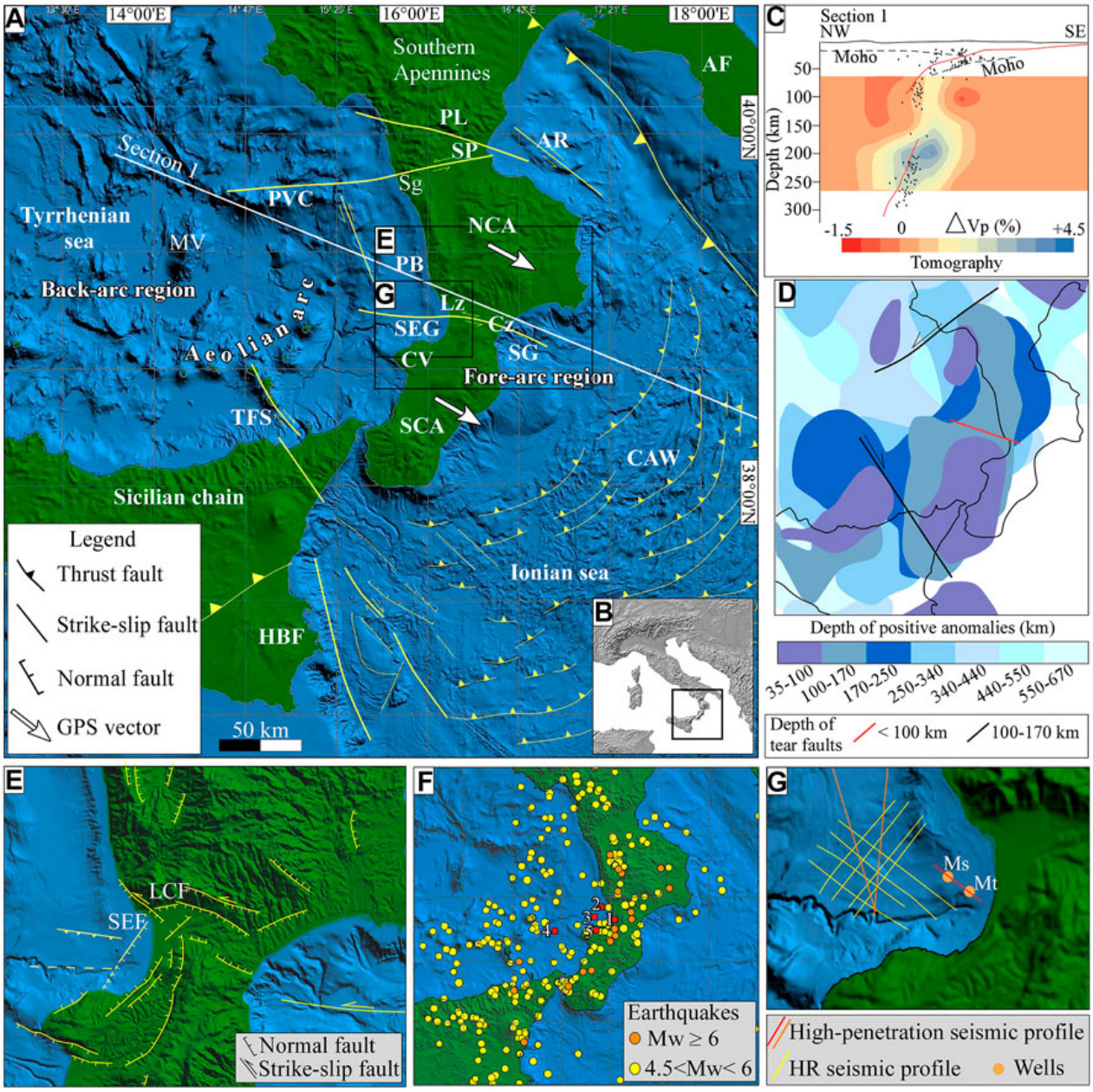

FIGURE 1. (A) Schematic tectonic map of the Tyrrhenian-Ionian subduction system. AF, Apulian foreland; AR, Amendolara ridge; CAW, Calabrian accretionary wedge; CV, Capo Vaticano; Cz, Cosenza; HBF. Hyblean foreland; Lz, Lamezia; MV, Marsili volcano; NCA, northern Calabrian Arc; PB, Paola basin; PL, Pollino; PVC, Palinuro volcano complex; SCA, southern Calabrian Arc; SEG, Sant'Eufemia Gulf; Sg, Sangineto; SG, Squillace Gulf, SP, Sibari Plain; TFS, Tindari fault system. (B) Location of the area shown in panel a. (C) Section across the slab (modified from Maesano et al., 2017). Redline is the position of the subduction interface. Black dots are the earthquakes collected in 10-km wide buffers around the section trace. The dashed black line is the position of the Moho from Scrocca et al., 2003. Tomographic data are from Neri et al., 2009. (D) Upper mantle structure based on positive P wave seismic anomalies (modified from Rosenbaum et al., 2008). The coloured areas represent positive anomalies at different depth ranges. Rosenbaum et al., 2008 interpreted these areas as remnant subducting slabs, separated by tear faults (black and red lines). (E) Schematic tectonic map of the central Calabrian Arc (modified from Monaco and Tortorici, 2000; Brutto et al., 2016) and offshore (modified from Loreto et al., 2013; Del Ben et al., 2008). LCF, Lamezia-Catanzaro Fault; SEF, Sant'Eufemia Fault. (F) Distribution of instrumental earthquakes recorded since 1985 up-to-date, from INGV Seismic Bulletin (ISIDe Working Group, 2007; http://iside.rm.ingv.it). Red squares indicate the 1905 epicentral location proposed by (1) Rizzo, (1906), (2) Riuscetti and Schick, (1975), (3) Camassi et al. (1997), (4) Michelini et al. (2006), (5) Guidoboni et al. (2007). (G) Grid of high-penetration and high-resolution (HR) seismic profiles used for this study. Ms, Marisa well; Mr, Marta well.

2. Geological setting

2.1 SE Tyrrhenian basin and the Adjacent Calabrian Arc

The Tyrrhenian basin developed since Late Miocene within the frame of Europe-Africa convergence and was mainly controlled by the westward and northwestward subduction of the Adriatic and Ionian lithosphere (Carminati et al., 1998; Faccenna et al., 2001; Carminati and Doglioni, 2005). The upper plate of the subduction system, from west to east, consists of back-arc basins that appear younger southeastwards (Vavilov and Marsili basins; Carminati and Doglioni, 2005; Faccenna et al., 2007, 2001), an arc-shaped volcanic ridge (i.e., Aeolian islands), and a forearc region including the Calabrian Arc and the Calabrian accretionary wedge (Corradino et al., 2020; Pepe et al., 2010; Figure 1a and b).

The subducting lithosphere dips ~ 70–80° northwestward (Wortel and Spakman, 2000; Piromallo and Morelli, 2003; Chiarabba et al., 2008; Scarfì et al., 2018). Seismic tomography data highlights positive P wave anomalies (Lucente et al., 1999) in the subducting lithosphere, interpreted as the signature of slab breakoff beneath the northern Calabrian Arc (Neri et al., 2009; Maesano et al., 2017; Scarfì et al., 2018, Figure 1c), and sub-vertical tears in the slab that propagates perpendicular to its strike (Rosenbaum et al., 2008, Figure 1d). Tearing and segmentation of subducting oceanic lithosphere are common processes in subduction systems (Carminati et al., 1998; Chatelain et al., 1992; Lallemand et al., 2001; Levin et al., 2002; Miller et al., 2006; Wortel and Spakman, 2000). These processes can be consequent to (i) changes in the velocity of subduction rollback (Govers and Wortel, 2005), (ii) the lateral variation of nature (continental or oceanic) or thickness of the slab (Argnani, 2009), (iii) local collisional events (Sacks and Secor, 1990). E-W trending deep tear faults (greater

than 340 km) were detected in the northern Tyrrhenian sea. These tear faults continue at slightly shallower depths (< 340 km) beneath the north and central Apennines with a NNE-SSW orientation (see Fig. 5 in Rosenbaum et al., 2008). Shallower (between 100 km and 340 km) NE-SW and NW-SE trending tear faults were interpreted beneath the southern Apennines and eastern Sicily, respectively (Figure 1d). These tear faults accommodate vertical or oblique to horizontal motion (or both) between the two blocks of the subducting slab across their strike and dip- to strike-slip movements in the upper plate (Govers and Wortel, 2005; Rosenbaum et al., 2008; Baes et al., 2011). At the edges of the subducting lithosphere, Subduction-Transform Edge Propagator (STEP, also called tear) faults occur (Gallais et al., 2013; Orecchio et al., 2014; Gutscher et al.,

2016; Maesano et al., 2020). STEP faults produce tearing in the slab and generally propagate perpendicular to the subduction strike (Nijholt and Govers, 2015). Most of them show vertical motion between the two blocks of the underthrusting plate at both sides of the STEP fault and normal to strike-slip movements in the upper plate (Baes et al., 2011; Govers and Wortel, 2005).

The Calabrian Arc is an allochthonous block of continental crust (Calabria–Peloritani terrane after Bonardi et al., 2001) that connects the southern Apennines with the Sicilian-Maghrebides chain (Figure 1a). Its arcuate shape can be attributed to the Apennine belt's diachronous collision with the Apulian foreland to the north and with the Hyblean foreland to the south (Malinverno and Ryan, 1986; van Dijk et al., 2000). Strike- slip fault systems developed both oblique and perpendicular to the orogenic belt. These fault zones caused the fragmentation of the Calabrian Arc in NW-SE elongated blocks that have moved independently southeastwards with different displacements and rotations (Knott and Turco, 1991; van Dijk and Okkes, 1991; van Dijk, 1992; van Dijk and Scheepers, 1995). The major strike-slip fault systems are the Pollino and Sangineto system to the north and their offshore prolongations (Ferranti et al., 2009, 2014; De Ritis et al., 2019), the Lamezia-Catanzaro line in the central sector (Neri et al., 1996; Tansi et al., 2007; Del Ben et al., 2008), and the Tindari line in the north-eastern Sicily (Figure 1a; Billi et al., 2006; Cultrera et al., 2017b). Both the northern and the southern strike-slip zones represent the upper plate expression of the Ionian slab STEP faults (De Ritis et al., 2019; Doglioni et al., 2001; Govers and Wortel, 2005; Maesano et al., 2020; Polonia et al., 2016; Rosenbaum et al., 2008; Figure 1a and d).

NNW-SSE strike-slip fault systems also affected both the Tyrrhenian and Ionian offshore of the northern Calabrian Arc (i.e. Paola Basin in the Tyrrhenian offshore, and the Amendolara Ridge in the Ionian offshore, PB and AR in Figure 1a) during the Late Pliocene – Early Pleistocene (Ferranti et al., 2014; Corradino et al., 2020).

2.2 The Lamezia-Catanzaro system and surroundings offshore areas

The Lamezia-Catanzaro system is a WNW-ESE trending strike-slip fault system (Figure 1a and e) that separates the northern and southern parts of the Calabrian Arc (van Dijk et al., 2000; Tansi et al., 2007). In the western offshore of the Catanzaro trough (Sant'Eufemia Gulf in Figure 1a), Loreto et al. (2013) recognise three main tectonic features affecting the Plio-Quaternary basin infill. These structures are 1) a ~13 km long, N31o striking normal fault that offsets seismic reflectors up to the seafloor (SEF in Figure 1e), 2) a WNW-striking polyphase fault system, and 3) a likely E-W trending lineament (Figure 1e). Two deep wells were drilled in the Sant'Eufemia Gulf (Marisa and Marta, Mr and Mt in Figure 1g). The stratigraphic succession indicates a metamorphic basement covered by Messinian deposits, overlain by Pliocene fine-grained deposits (mudstone and claystone), and Pleistocene coarser deposits (sandstone and siltstone).

Brutto et al., (2016) based on structural data acquired in the western Catanzaro basin and its offshore prolongation in the Sant'Eufemia Gulf, document 1) a left lateral NW-SE oriented fault system that affects upper Miocene deposits, 2) right-lateral NE-SW oriented faults that involve Piacenzian-Lower Pleistocene units and led to the development of structural highs in the eastern sector of the gulf and 3) NE-SW and, subordinately, N-S oriented normal faults that affect Middle Pleistocene to Recent deposits.

Based on the analysis of the depth variation of the edges of Infralittoral Prograding Wedges, Pepe et al., (2014) documented difference in the post-Last Glacial Maximum vertical tectonic movements between the SW and NE offshore sectors of the Capo Vaticano promontory (western Calabria, southern Italy). Offshore of Capo Vaticano promontory, Pleistocene intrusive, and off-arc volcanic activities occurred (De Ritis et al., 2010; Loreto et al., 2015). The uprising of magma was favoured by Pliocene NW- and Pleistocene NE-trending normal fault systems.

The eastward offshore prolongation of the Lamezia-Catanzaro line lies in the Squillace Gulf (Figure 1a and e). Here, a W-E trending, transtensional basin developed during the Pliocene (Del Ben et al., 2008).

2.3 Seismotectonic framework

The western margin of the central Calabrian Arc is an area of large seismic moment release (Figure 1f; CFTI5Med, Guidoboni et al., 2018; CPTI15, Rovida et al., 2020; 2021), where destructive historical earthquakes have been generated by onland crustal seismogenic sources (Tiberti et al., 2017; DISS Working Group, 2018). The seismogenic activity of the Ionian subducting lithosphere is highlighted by the deep seismicity down to ~ 600 km beneath the Tyrrhenian Sea (Chiarabba and

Palano, 2017). Despite the evidence of seismogenic activity, no large inter-plate historical or instrumental earthquakes have been documented so far, being the deep seismicity interpreted as intraslab events (Figure 1c; Chiarabba et al., 2015). Only the 1905 earthquake has been tentatively interpreted by some authors as a plate interface event (e.g. Galli and Molin, 2009; Presti et al., 2017). However, this earthquake is still poorly documented, and it has uncertain magnitude estimates and epicentral locations, most of them offshore (Figure 1f, see Sandron et al., 2015 for a review of the studies on the 1905 earthquake). Nonetheless, modelling of GPS velocities shows that the subduction may be locked and capable of large magnitude earthquakes with long return times (Carafa et al., 2018).

The INGV instrumental catalogue shows that the largest seismic events in the past 35 years have epicentres located in the Tyrrhenian offshore and hypocentre deeper than 100 km (maximum Mw 5.8, October, 26, 2006 earthquake at 221 km of depth; ISIDe Working Group, 2007). Conversely, the onland seismicity is located up to 20 km depth (maximum Mw 3.9). Only shallow, scattered events were localised in the Ionian offshore.

The historical seismicity indicates that the Calabrian Arc is one of the most seismic areas of the whole Italian territory. The area between the Messina Straits and the Catanzaro trough was affected by several large earthquakes (Mw >6), among these, the 1783 seismic events (February 5, Mw 7.1, February 7, Mw 6.7, and March 28, Mw 7.0), 1905 (Mw 7.0) and 1908 (Mw 7.1) events, which were generated by crustal faults (DISS Working Group, 2018).

Active deformation data (GPS, Devoti et al., 2017; focal mechanisms, Totaro et al., 2016, Pondrelli et al., 2020; active stress indicators, IPSI database, Mariucci and Montone, 2020) show that the central sector of the Calabrian Arc is characterised by an NW-SE oriented extensional tectonic regime, responsible for large magnitude earthquakes (e.g., Galli and Peronace, 2015). Towards the east, the Ionian offshore area undergoes a transcurrent regime due to the oblique plate convergence (Totaro et al., 2016), and is affected by active compressional structures related to the Calabrian subduction complex (e.g. Gutscher et al., 2017; Polonia et al., 2011)

The seismotectonic interpretation of the seismicity may be broadly divided into two alternative models (see Tiberti et al., 2017 for a review). The first model, described as the “Siculo-Calabrian Rift Zone” (Tortorici et al., 1995; Monaco and Tortorici, 2000), considers a system of W-dipping high-angle surface normal faults as the source of the largest earthquakes. The second one, named as “Subduction-top model” (Tiberti et al., 2017) and implemented in the DISS database (DISS Working Group, 2018), highlights the role of east-dipping, low angle, blind normal faults, antithetic to the subduction system, located along the Tyrrhenian side of the Calabrian Arc. In the latter model, the longitudinal normal fault systems are dissected by strike-slip faults zone crossing the Calabria Arc.

The transversal faults have deemed the sources of earthquakes occurring at the edges of the longitudinal seismogenic segments. The W-dipping faults are considered shallow antithetic faults respect to the E-dipping ones, as shown, for example, in the Messina Straits area (Bonini et al., 2011).

3. Data and Methods

3.1. Multibeam Bathymetry

The high-resolution Digital Elevation Model (DEM) is a part of the multibeam bathymetric dataset acquired and processed by the National Research Council (IGAG) between 2010 and 2013. Bathymetric data were collected using multibeam systems at different frequencies. In shallow water, the Kongsberg EM 3002D (300 kHz), EM 710 (10-100 kHz) and Reson SeaBat 7111 (100 kHz) systems were used, while in deep waters, Reson SeaBat 7160 (44 kHz) was used.

During the bathymetric surveys, multibeam transducers' calibration in areas close to the survey zone was performed together with sound velocity profiles. The Caris Hips & Sips hydrographic software processed all bathymetric datasets. Data processing included: a) patch test on calibration lines, b) tide corrections, c) statistical and geometrical filters to remove coherent and incoherent noise, d) manual removal of spikes.

Processed data were gridded, generating DEMs with cell size varying from 0.5–1 m in shallow water (<100 m) to 10 m in intermediate water (100–500 m) and 15–20 m in deep water (>500 m). In this work, the DEM was at 15 m gridded resolution, and the bathy-morphological map was projected in UTM 33N - Datum WGS84.

3.2. Seismic Reflection Data Acquisition and Processing

Over 500 km of multichannel high-penetration reflection seismic data (Airgun) and high resolution (HR) multichannel seismic reflection data (Geo-Source Sparker) were recorded in the Sant'Eufemia Gulf in 1999 and 2019, respectively (orange and yellow lines in Figure 1g). Airgun profiles are oriented from NNW–SSE to NNE–SSW directions. Geo-Source Sparker inline profiles are primarily oriented in the NW–SE to N–S directions, with crossline seismic profiles acquired along the NE–SW direction. A DGPS system controlled the navigation positioning for all datasets. This paper presents a subset of these data consisting of seismic lines oriented from NW-SE to NE-SW.

A high-resolution 48-channel seismic reflection system with slant streamers and group spacing varying from 1 to 2 m recorded the signals generated by an innovative multi-tip (400) Sparker array in a dual-source Sparker system based on negative discharge technology. The shooting interval was

2.0s, with a 1.5 s record length and 0.1ms sampling interval. An innovative differential GPS positioning system was used to perform all necessary computations to determine real-time positions of sources and receivers. The processing sequence included the following operations: geometry assignment by 2D CDP profiles binning, DC removal, signature deconvolution, F-K filter, trace stacking, static corrections, velocity analysis, multiple attenuation, post-stack Kirchhoff time migration, receiver deghosting, time-variant bandpass filtering and automatic gain control removal to restore the True Amplitude. Signal penetration exceeds 500 ms two-way time (t.w.t). Vertical resolution reached up to 0.25 m near the seafloor.

The Geo-Suite AllWorks software package was used to process single-channel reflection seismic data and for seismic interpretation. Seismo- and sequence stratigraphy based analysis facilitated the reconstruction of the depositional architecture of seismic-stratigraphic units.

An additional MCS profile from Vi.DE.PI database (red line in Figure 1g, https://www.videpi.com/videpi/sismica/sismica.asp) was used for this study. The MCS section was converted from raster to SEG-Y format using the GeoSuite AllWorks software. The geodetic reference system is the WGS84 with a UTM 33 N projection.

3.3 Morphotectonic analysis

Two grids of 50 swath profiles covering roughly 1,000 km2 were used to analyse the relief distribution and the topographic response to tectonic forcing (Figure 2a). Swath profiles sample topographic information from rectangular areas and include such information into an elevation profile by stacking multiple topographic profiles. The trace of these topographic profiles, here labelled as profile lines, are equally spaced and oriented perpendicularly to the swath profile baselines (Fig. 2a and b). The same length characterises all the profile lines.

A 2 km swath width was adopted to highlight tectonic signals at the kilometric scale for detecting the primary faults in the study area. Two grids with N-S, E-W, NNW-ESE and ENE-WSW oriented segments define the baselines for the swath profiles (Figure 2a). The swath profiles were computed using a code wrapper employing the algorithms proposed by Schwanghart and Scherler, (2014). We extracted and listed endpoint coordinates of each grid segment, sampled two pairs of coordinates simultaneously, and computed the swath profiles between those extracted points. A grid of swath profiles oriented along with the directions of the segments above described, and the diagonal joining two adjacent segments was obtained (Figure 2a). For example, the first swath profile was created using the two coordinates labelled A and B, the second one using the coordinates B and C, and going in this way until using all the stored coordinates. The maximum, minimum, and mean values of

bathymetric depth were sampled along each profile line (Figure 2b) and arranged as a matrix of 146,071 georeferenced points. The coordinates of each point correspond to the intersection between the profile lines and swath baselines (Figures 2b). The dataset was used to compute the local relief for each point as the difference between the maximum and minimum value sampled for each profile. This value corresponds to the local relief along the profile. Finally, the local relief was normalised dividing the data distribution by its maximum value, so the result values range from one to zero. Considering that values approaching one represents the maximum computed relief, the 75° percentile of this distribution was considered as the minimum threshold to detect the areas with the highest relief values (Figure 2c). The mean elevations approaching the maximum ones were detected within these areas to infer the bathymetric response to the tectonic forcing (Burbank and Anderson, 2011). To do this, we computed the mid-to-max value and filtered the dataset using the following equations:

$$\text{midtomax} = \text{max bathymetry} - \text{min bathymetry} \quad \text{Eq. 1}$$

$$\text{anomalous} = (\text{max bathymetry} - \text{min bathymetry})/2 \quad \text{Eq. 2}$$

The distribution of mid-to-max values ranging from one to zero was obtained by normalisation. The values approaching zero are areas controlled by the tectonic forcing. A threshold of values lower than the 75° percentile was applied to select the Anomalous Mid-To-Max (AMTM) values from this distribution. The resulting points (14,815) of AMTM values coincide in correspondence of high-relief areas where the submarine landscape responds to recent tectonic forcing (Figure 2d).

The bathymetric map and swath profiles were qualitatively analysed to identify morphologic signature related to nearby tectonic structures (Figures 2d). In particular, the upstream portion of the Angitola Canyon was analysed through a ~ 22 km-long trunk longitudinal profile and 23 bathymetric cross profiles. Such profiles were placed along the canyon to capture changes in the canyon aspect ratio by computing the height to width ratio (H/W). Finally, the spatial correlation among slope changes of the trunk stream long profile, H/W values, and the geographic and stereological properties of the main geologic structures detected closely were analysed to infer the possible response of the Angitola Canyon to the tectonic forcing.

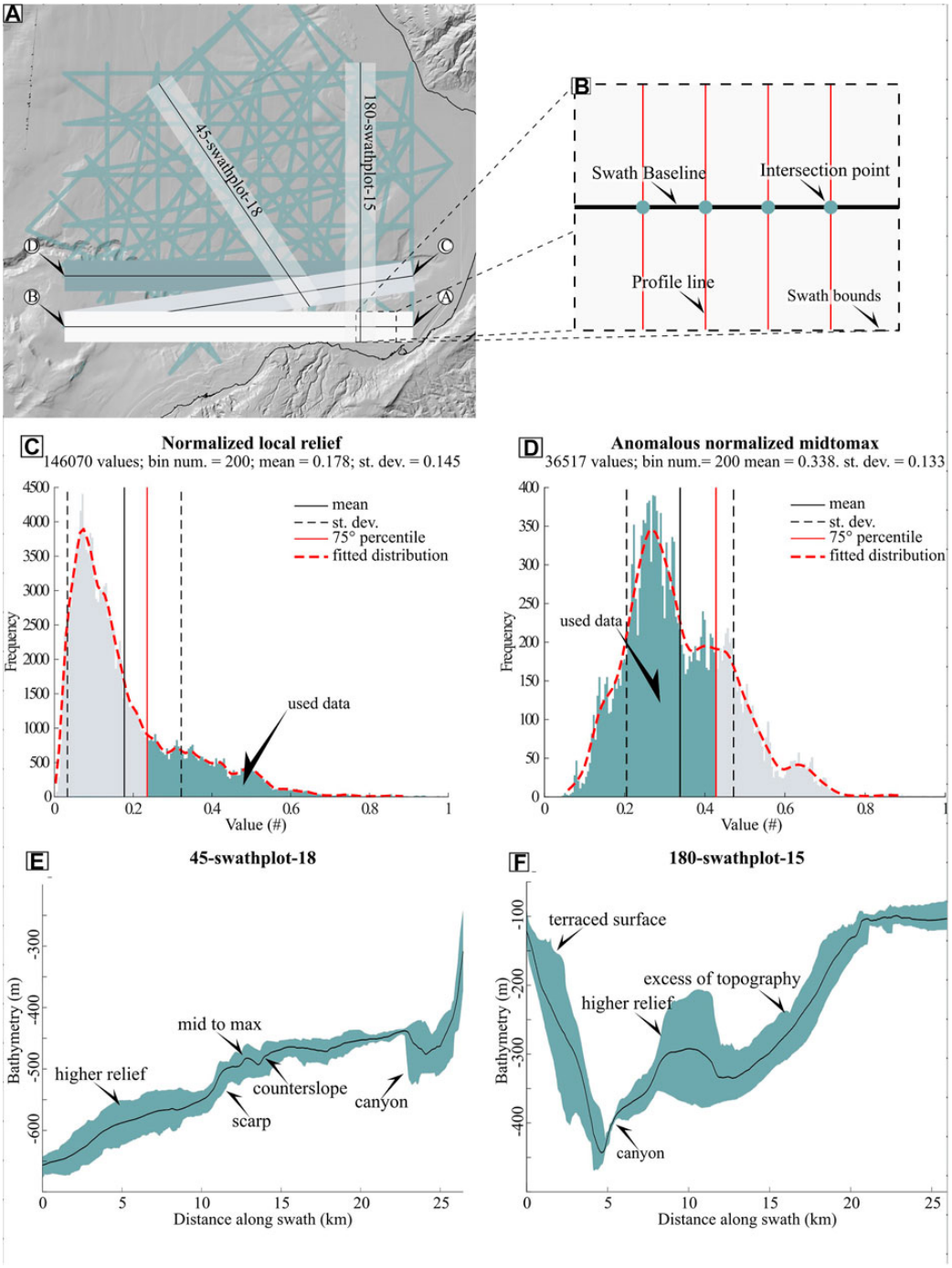
A
45-swathplot-18
180-swathplot-15
D
C
B
A
B
Swath Baseline
Intersection point
Profile line
Swath bounds
C
Normalized local relief
146070 values; bin num. = 200; mean = 0.178; st. dev. = 0.145
mean
st. dev.
75° percentile
fitted distribution
used data
Frequency
Value (#)
D
Anomalous normalized midtomax
36517 values; bin num.= 200 mean = 0.338. st. dev. = 0.133
mean
st. dev.
75° percentile
fitted distribution
used data
Frequency
Value (#)
E
45-swathplot-18
higher relief
mid to max
counterslope
scarp
canyon
Bathymetry (m)
Distance along swath (km)
F
180-swathplot-15
terraced surface
excess of topography
higher relief
canyon
Bathymetry (m)
Distance along swath (km)

FIGURE 2. A) Map view of the swath profile grid used for the seafloor morphometric analyses. The two swath profiles labelled "45-swathplot-18" and "180-swathplot-15", shown in (C and D), respectively, are highlighted with the white transparent band. Capital letters, from A to D, into white circles, represent the edges of the swath profile segments in white, light grey, and light green. (B) Conceptual sketch representing the zoom of the initial portion of the white swath profile of the previous inset. The thick black line represents the swath profile baseline, the dashed black line represents the swath profile bounds, and the thin red lines represent the topographic profile lines. The light green circles represent the intersection points between the profile lines and baseline. (C) Frequency histogram of the normalised local relief data distribution. Values higher than the 75% percentile, in light green, represent the highest computed local relief values. (D) Frequency histogram of the anomalous normalised mid-to-max data distribution. Values lower than the 75% percentile relate to areas where the mean bathymetry significantly approaches higher bathymetry values. (E) Swath profile labelled 45-swathplot-18 highlighting the presence of a scarp and a counter-slope area in the Gulf central sector. (F) Swath profile labelled 180-swathplot-15 evidencing a significantly higher relief detected in correspondence of a bathymetric ridge.

6. Results

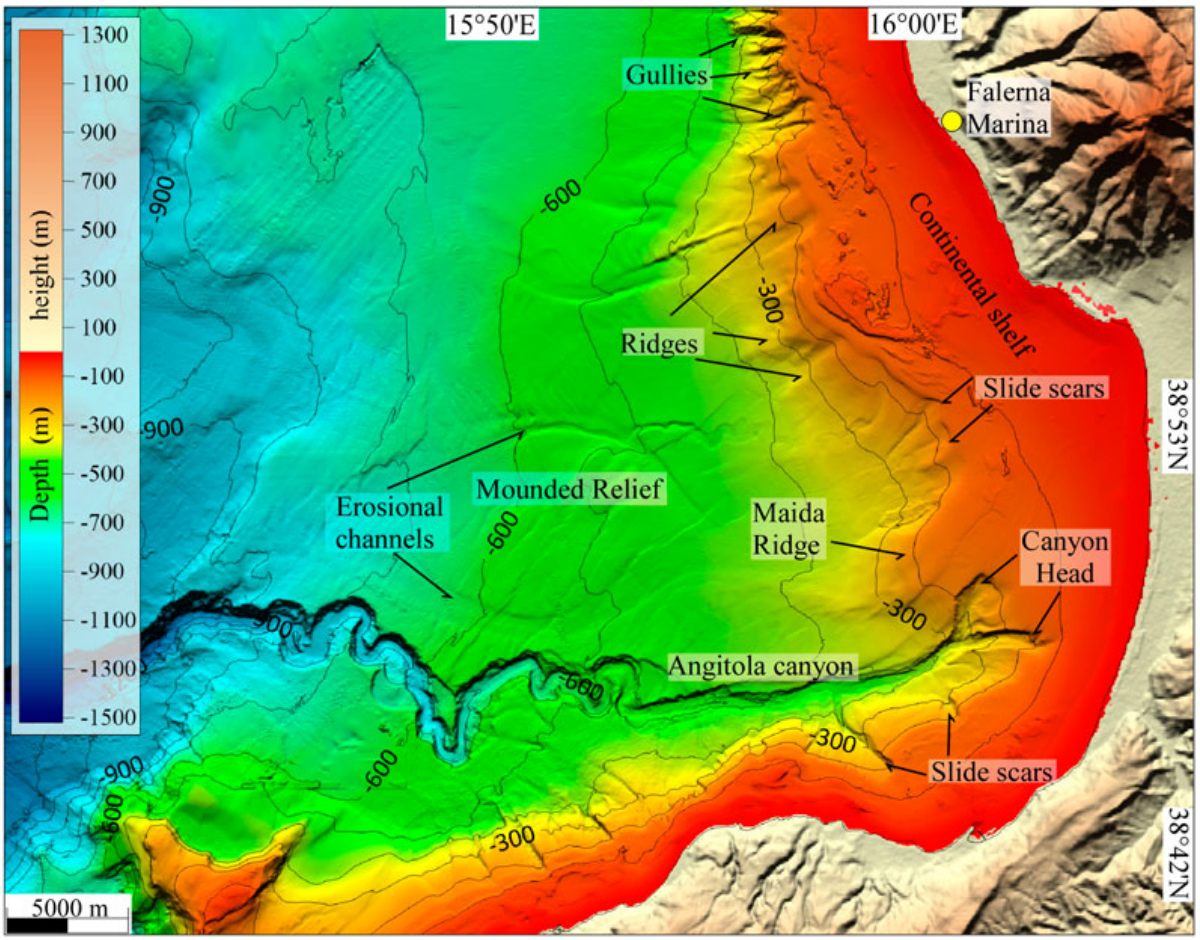

FIGURE 3. Morphobathymetric map of the Sant'Eufemia Gulf.

4.1 Morpho-bathymetry analysis

The multibeam bathymetry of the study area shows a 1-9 km wide continental shelf, with the edge located between 140 and 160 m water depth. The shelf edge is irregular in plan-view because of the alternation of erosive features (canyon heads, gullies and landslide scars in Figure 3), carving the shelf, and submarine ridges developed on the continental slope. One of the prominent ridges, hereafter named Maida Ridge, is located just to the north of the Angitola Canyon between 120-400 m water depth (Figure 3). The Maida Ridge is a NE-SW-trending morphological high over 12 km long, has an average width of ~4 km, and a morphological relief of ~150 m. Smaller ridge-like structures are also developed in the northern part of the study area, just below the shelf facing the Falerna Marina village. As a whole, the continental slope has a mean gradient of 3-4° and displays an overall uneven morphology both in its upper and lower part. Notably, the main morphology recognisable in the slope between 450 and 700 m water depth is a mounded relief located in the center of the study area (Mounded relief in Figure 3). This feature is about 11 x 8 km in size and has a morphological relief of about 20 m with respect to the surrounding seafloor; two shallow and narrow erosional channels laterally bound it. In particular, a set of SW-NE elongated scarps affects the morphological high and its surroundings; these scarps are 2-8 km long and 2-10 m high.

The Angitola Canyon is the main bathymetric feature of the Sant'Eufemia Gulf. Its head lies at a water depth of about 100 m, along the offshore prolongation of the Angitola River. The canyon pattern is roughly rectilinear from the canyon head to ~560 m water depth. Below this depth, the pattern abruptly becomes meandering. Such a meandering pattern extends down to a regional NE-SW-trending scarp, which crosses the canyon at roughly 900 m water depth. After that, the canyon resumes a sub-rectilinear pattern.

4.2 Seismo-stratigraphic characterisation and interpretation

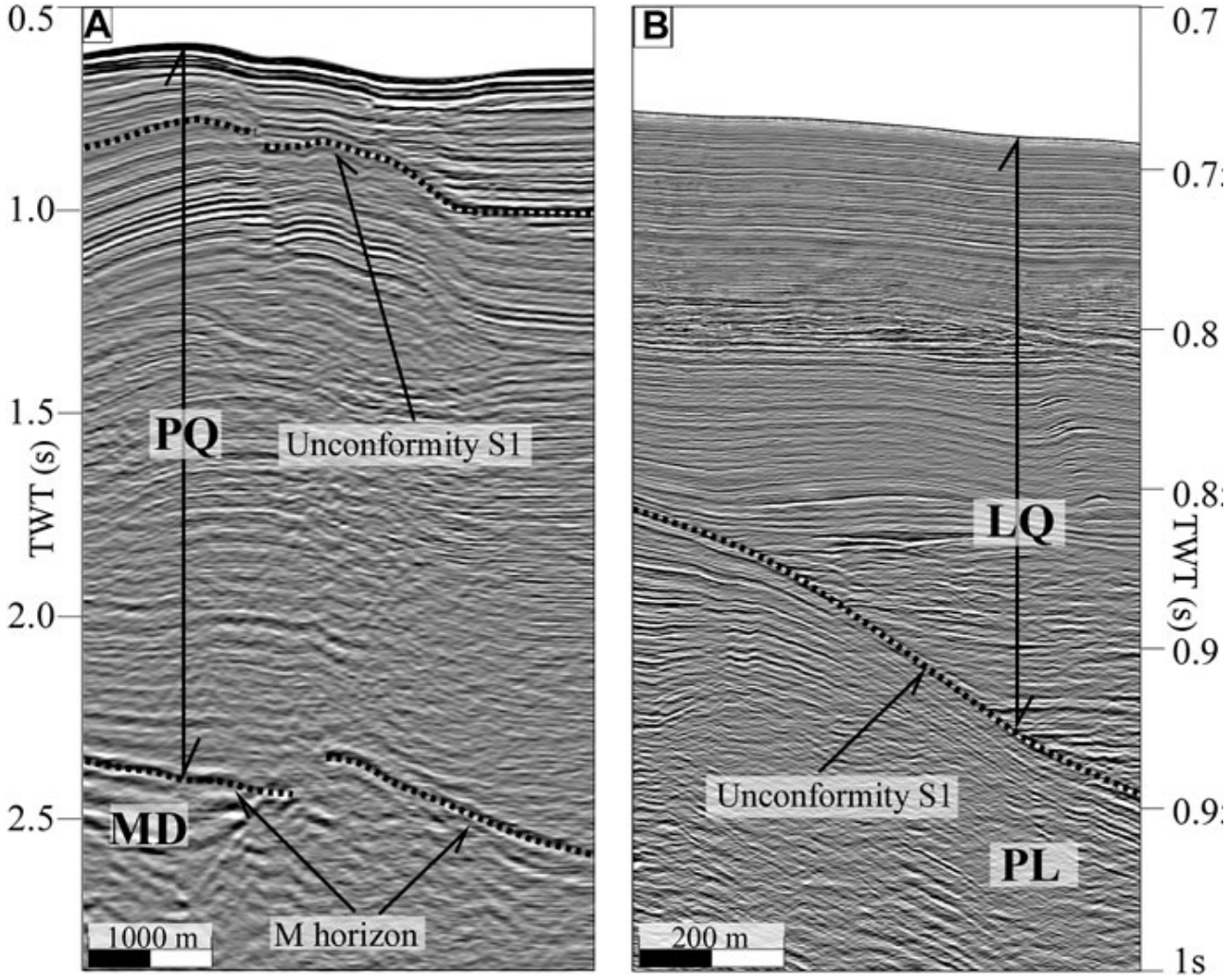

FIGURE 4. (A) Seismostratigraphic units (MD and PQ) recognised on the high-penetration seismic profile "Line Sister—12". (B) Seismostratigraphic subunits (PL and LQ) recognised on the HR seismic profile "Line—04." See Figure 5A for location.

In the high-penetration seismic profiles, two seismo-stratigraphic units, labelled from bottom to top as MD and PQ (Figures 4a, 5a and b), were defined by their bounding unconformities and described based on their architecture and seismic characters (e.g., amplitude, lateral continuity, and frequency of internal reflectors). Seismic profiles were calibrated using well-log data (Cosentino et al., 2017; Ms and Mt in Figure 1g).

Unit MD is characterised by relatively discontinuous, medium frequency, and medium- to high-amplitude reflectors. It is bounded upwards by a well-defined, high-amplitude unconformity (M horizon in Figure 4a), associated with the top of evaporites deposited during the late Messinian salinity crisis or to an erosional unconformity formed during the late Messinian sea-level fall (Malinverno et

al., 1981, and references therein). We correlate unit MD with the Upper Miocene deposits based on the seismic signature and well log data (Figures 5b).

Unit PQ overlays the M horizon and shows continuous, high- to medium-frequency and medium- to high-amplitude reflectors (Figure 4a). We correlate unit PQ with the Plio-Quaternary sedimentary succession widespread in the Tyrrhenian Sea based on its seismic signature and well log data.

Two subunits, named PL and LQ from bottom to top, were distinguished based on the occurrence of a well-defined unconformity that separates them (S1 in Figures 4a and b, 5a and b). Well-seismic calibration indicates that the unconformity S1 formed during the Early Pleistocene (Calabrian).

Subunit PL is characterised by subparallel and well-defined laterally continuous reflectors with an aggradational internal pattern. The strata are sub-horizontal in the central and northern sectors of the line Sister-12 and show northwards directed onlap terminations onto the M horizon (Figure 5a). In the southern part of the seismic profile, reflectors exhibit a variable inclination from bottom to top, defining a fan geometry (FSD in Figure 5a). Subunit PL is also sub-horizontal in the southeastern sector of line ER-77-502, whereas it exhibits slightly seaward dipping reflections moving towards the north-west (Figure 5b).

The subunit LQ consists of a series of layered and generally sub-horizontal reflectors with an aggradational structure (Figure 5a and b). The strata terminate with onlap geometry onto the unconformity S1 in the central sector of the gulf (Figures 4b, 5a, 6a and b) and in the eastern one (Figures 5b, and 7). Conversely, strata paraconformably overlay subunits PL deposits towards both the north and the south. Another unconformity surface was detected within subunit LQ only in the southeastern sector of the Gulf, along the north-western flank of the Maida Ridge (S2 in Figure 7). Subunit LQ is bounded upwards by the seafloor.

4.3 The Sant'Eufemia fault system

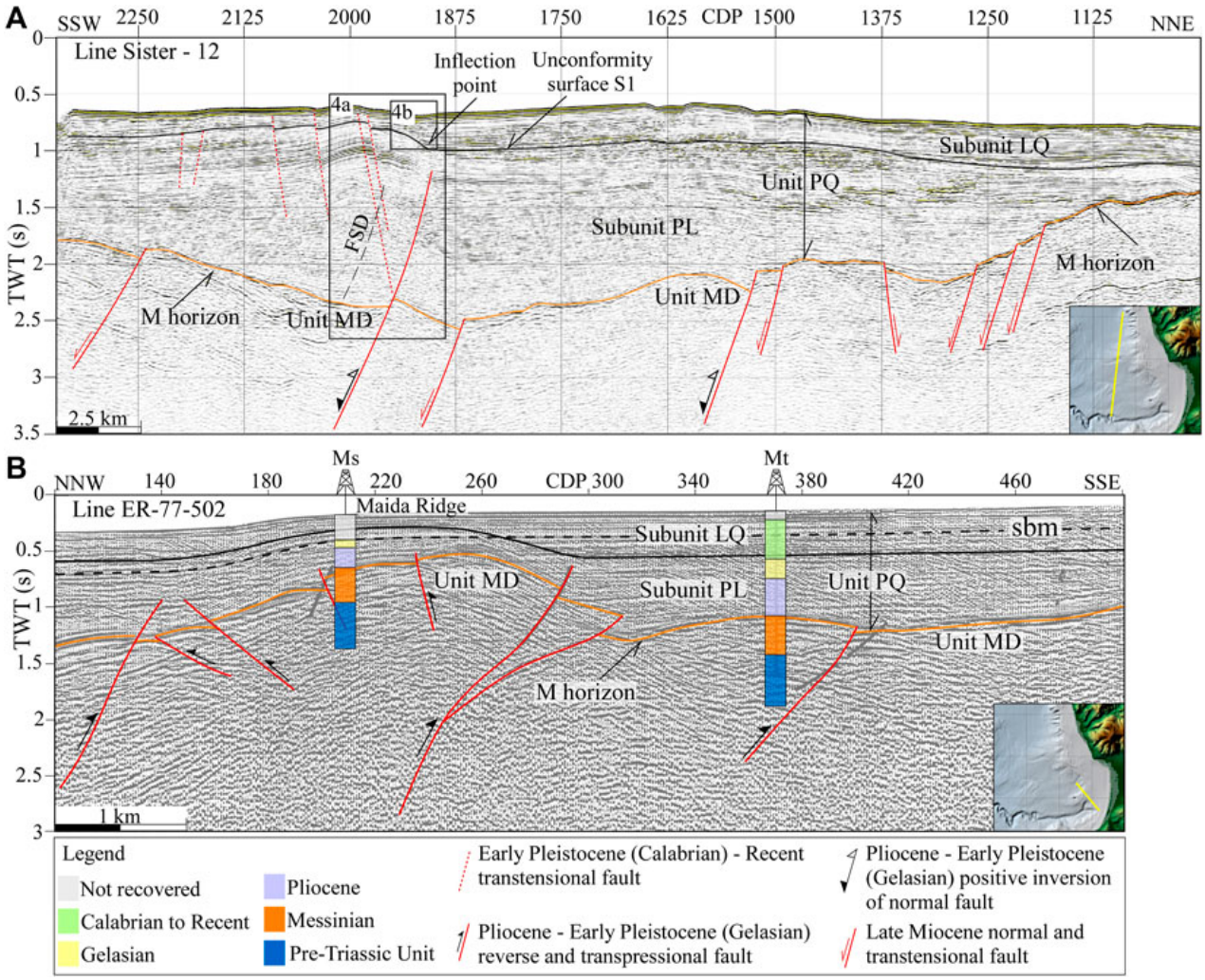

FIGURE 5. (A) Seismic profile "Line Sister—12" and its interpretation. Boxes 4a and 4b are displayed in Figure 4. (B) Seismic profile "Line ER-77-502" and its interpretation. Insets show the location of the profiles. Ms, Marisa well; Mr, Marta well; FSD, fan-shaped deposits; sbm., seabed multiple; Unit MD, Upper Miocene deposits; Unit PQ, Plio Quaternary deposits; PL and LQ, subunits of the Plio Quaternary deposits.

A series of normal faults that offset the deposits of Unit MD are observed on the high-penetration seismic profiles. Faults generally dip towards the south and bound horst (CDPs 1250-1500, Figure 5a) and half-graben (CDPs 1600 – 2300, Figure 5a) structures. Some faults are sealed by Pliocene deposits but younger activity is locally observed (e.g. CDPs 1800-2100 in Figure 5a). In this area, the deposits of subunit PL show a fan-shaped geometry (FSD) with the thicker deposit in the hanging wall of a SSW-dipping fault (Figure 5a). We interpret these deposits as syn-tectonic strata associated with the development of a normal or transtensional fault that offset rocks deeper than 3 km (using 2000 m/s for the time to depth conversion). However, this fault shows a reverse feature in its upper part; thus, we interpret it as a positive inversion structure (probably due to transpression)

involving subunit PL and older deposits. The inversion is partial (sensu Williams et al., 1989) because the deeper fault still retains an apparent normal displacement. Another positive partial inversion structure is observed towards the north (CDPs 1500-1700 in Figure 5a). The transpressional reactivation of both faults leads to the uplift of the earlier basin fill and bending of the upper part of PL. Towards the east, sub-unit PL was also involved in shortening along steep transpressional ramps (Figure 5b). Seismic and well-log data suggest that the transpressional structures were active until the Calabrian. Thus, the unconformity S1 that limits the subunit PL deposits upward has a tectonic origin. Above this surface, LQ deposits show onlap reflectors terminating on top of unit PL (CDPs 1900 - 1950, Figure 5a).

The deep inversion structures involving subunit PL are not detectable on the high-resolution seismic profiles. Considering that the positive inversion structure was traced in correspondence of the inflection point of the unconformity S1 in the high-penetration seismic lines (Figure 5a and b), we used this inflection point to infer the shallow position of transpressional faults on the high-resolution seismic profiles (Figure 6a). In the central sector of the Sant'Eufemia Gulf, the transpressional faults show NE-SW orientations. NNE-SSW to NE-SW trending transpressional structures were also detected in the eastern sector of the Sant'Eufemia Gulf in correspondence with ridges (Figures 3, 5b, 7 and 8a). The most prominent structure is associated with the formation of the Maida Ridge (see paragraph 4.1), and has a south-eastward asymmetric shape indicating its vergence (Figures 7 and 8a). A secondary unconformity S2 was identified along the north-western flank of this transpressional structure above the main unconformity S1 (Figure 7). The formation of this unconformity is probably linked to the tectonic activity of the structure associated with the development of the Maida Ridge.

NNE- SSW trending, closely-spaced, high-angle normal to transtensional faults offset the upper part of subunit PL and younger deposits (Figure 6a, b and c). Some of the faults reach the seafloor, whereas others propagate upwards, affecting the LQ deposits. The maximum depth at which these structures can be traced is generally less than 1.5 km (using 2000 m/s for the time to depth conversion). The transtensional faults show an anastomosing pattern in the central sector of the Sant'Eufemia Gulf, with individual segment length typically of a few km and rarely approaching 10 km (Figure 8a). Seafloor vertical offset along these faults vary from few meters to a few dozen meters, and, consequently, these faults have a mild morphological expression.

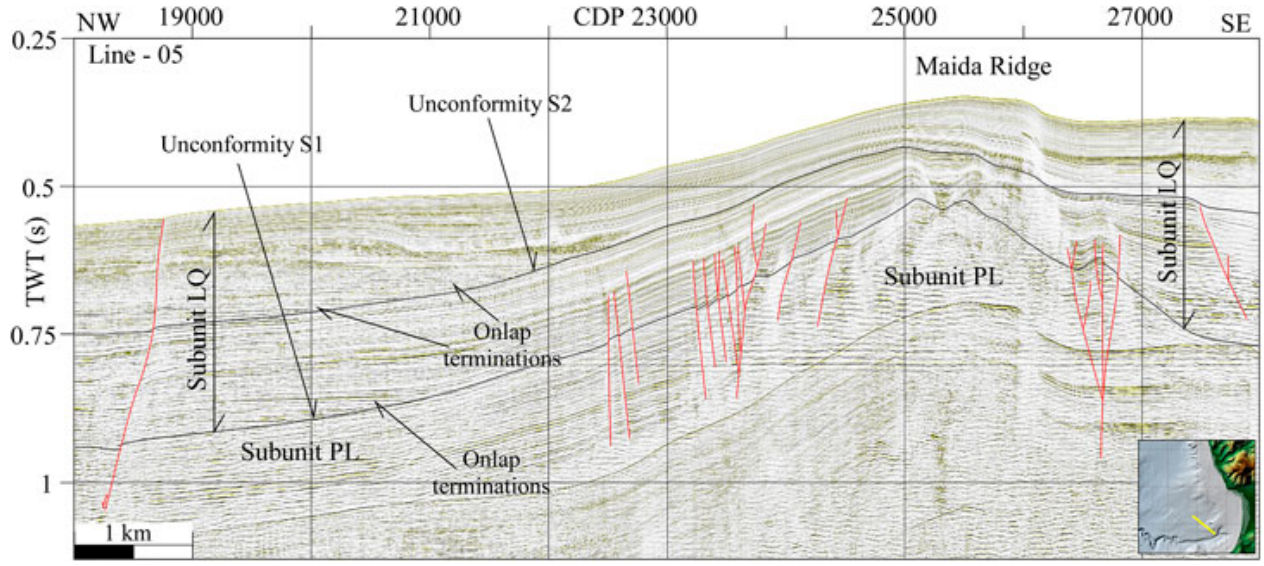

FIGURE 6. (A) Seismic profile "Line—04" and its interpretation. Inset shows the location of the profile. (B and C) Parts of Line—04 that show high-angle trastensive faults. Blue line marks the south-westernmost part of the anticline associated to the development of the Maida Ridge. Black dashed line represents the anticline axis. Red lines indicate transtensional faults. PL and LQ are the subunits recognised in the Plio Quaternary deposits.

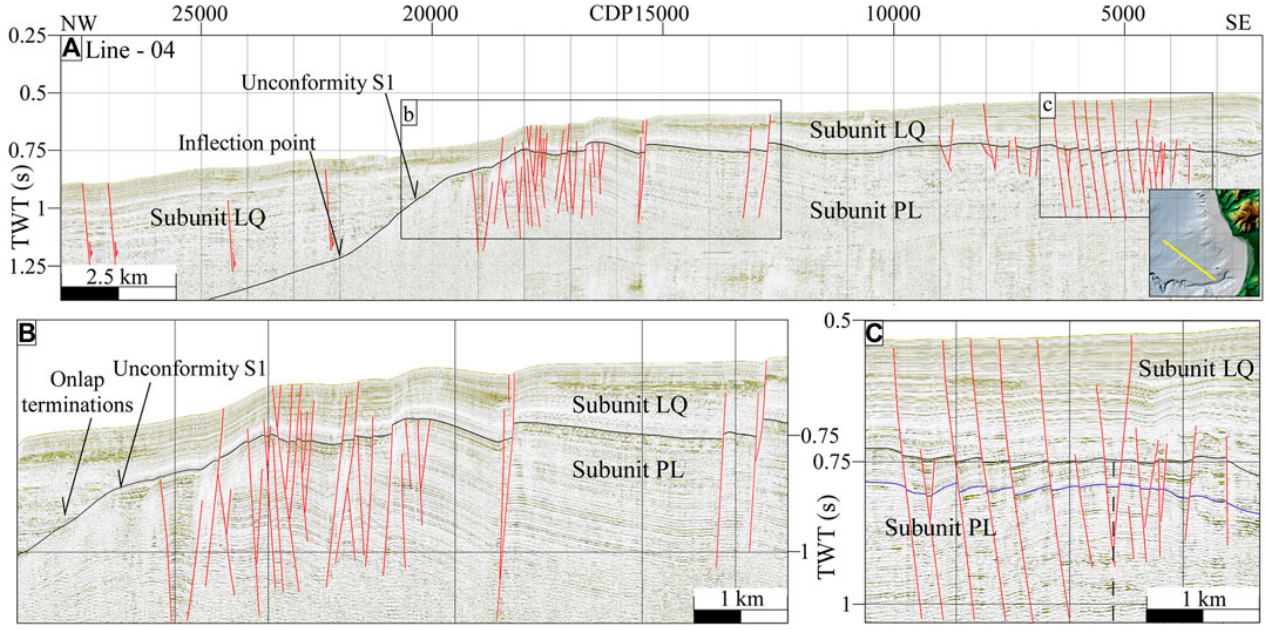

FIGURE 7. Seismic profile "Line—05" and its interpretation. Inset shows the location of the profile. PL and LQ are the subunits recognised in the Plio Quaternary deposits. Red lines indicate transtensional faults.

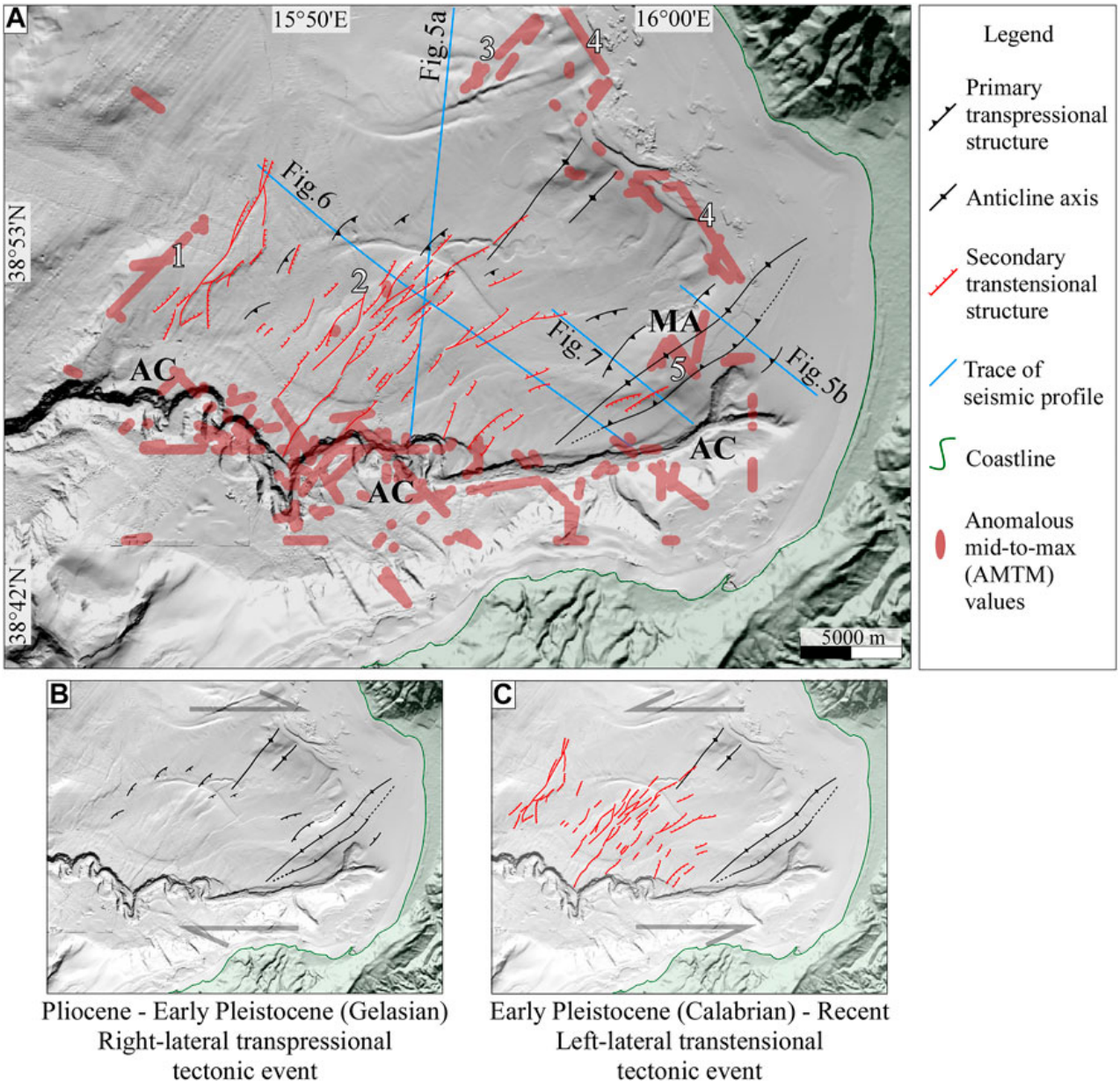

FIGURE 8. (A) Structural map of the Sant'Eufemia Gulf. Red dots are the AMTM values localised at the intersection points of their related swath profiles. MA, Maida Ridge; AC, Angitola Canyon; 1, 2, 3, 4, and 5, sectors with alignments of AMTM values. (B and C) Schematic structural maps showing the active structures during the Pliocene—Early Pleistocene (Gelasian) and Early Pleistocene (Calabrian)—Recent tectonic events that affected the Sant'Eufemia Gulf. The activity of the structures is inferred from the analysis of seismic profiles and swath profiles (AMTM values).

4.4 Morphotectonic anomalies

The qualitative analysis of swath profiles shows morphological anomalies (relief anomalies, topography excesses, terraced surfaces, asymmetrical valleys, and counter-slope areas; Figures 2e and f) that suggest a transient landscape state due to a tectonic forcing.

The quantitative analysis of the swath profiles highlights AMTM values in distinct sectors of the gulf. In the western sector, an alignment of AMTM values is observed along a NE-SW

morphological scarp (1 in Figure 8a). Few AMTM values were detected in the central sector of the gulf, whereas several alignments of AMTM were computed towards the east. In particular, AMTM values are observed in the north-eastern sector in correspondence of a roughly NE-SW striking bathymetric scarp (3 in Figure 8a) along the shelf-upper slope transition (4 in Figure 8a) and above the NE-SW trending transpressional Maida Ridge (5 in Figure 8a). Towards the south, many AMTM values are observed along the Angitola Canyon (AC in Figure 8a).

The longitudinal profile of the upper 22 km sublinear part of the thalweg of the Angitola Canyon and the cross profiles allowed the detection of three different reaches characterised by different Stream Length-gradient (SL) index and H/W values and trends (Figure 9a and 9b). The roughly constant negative trend of H/W and the correlative flat SL trend (avg. 125, st. dev. of 52), extending from the canyon head to roughly 9 km, describes the steady-state and concave upward shape of the Reach 1 of the profile (Figures 9a and b). The average canyon width is roughly 303 m, and its standard deviation is about 72 m. We detect the minimum SL (avg. 116, st. dev. 187) and H/W values in Reach 2, ranging from 9 to 16 km (Figure 9c). Such low values, corresponding to an average width of 574 m (st. dev. 90 m), can be interpreted as an increase of the canyon width relative to its height or a change to a less erodible bedrock of the thalweg. Differently, a positive trend of the H/W curve and a high-amplitude SL curve (avg. 826, st. dev. 1308) distinguish Reach 3, extending till the first meander that characterises the deeper part of the Angitola Canyon.

The positive trend of the H/W curve of the Reach 3, together with the average canyon heights (~ 81, 83 and 100 m with a standard deviation of 7, 4, and 17 m for Reach 1, Reach 2 and Reach 3, respectively), highlights a growing stream power moving towards the canyon outlet.

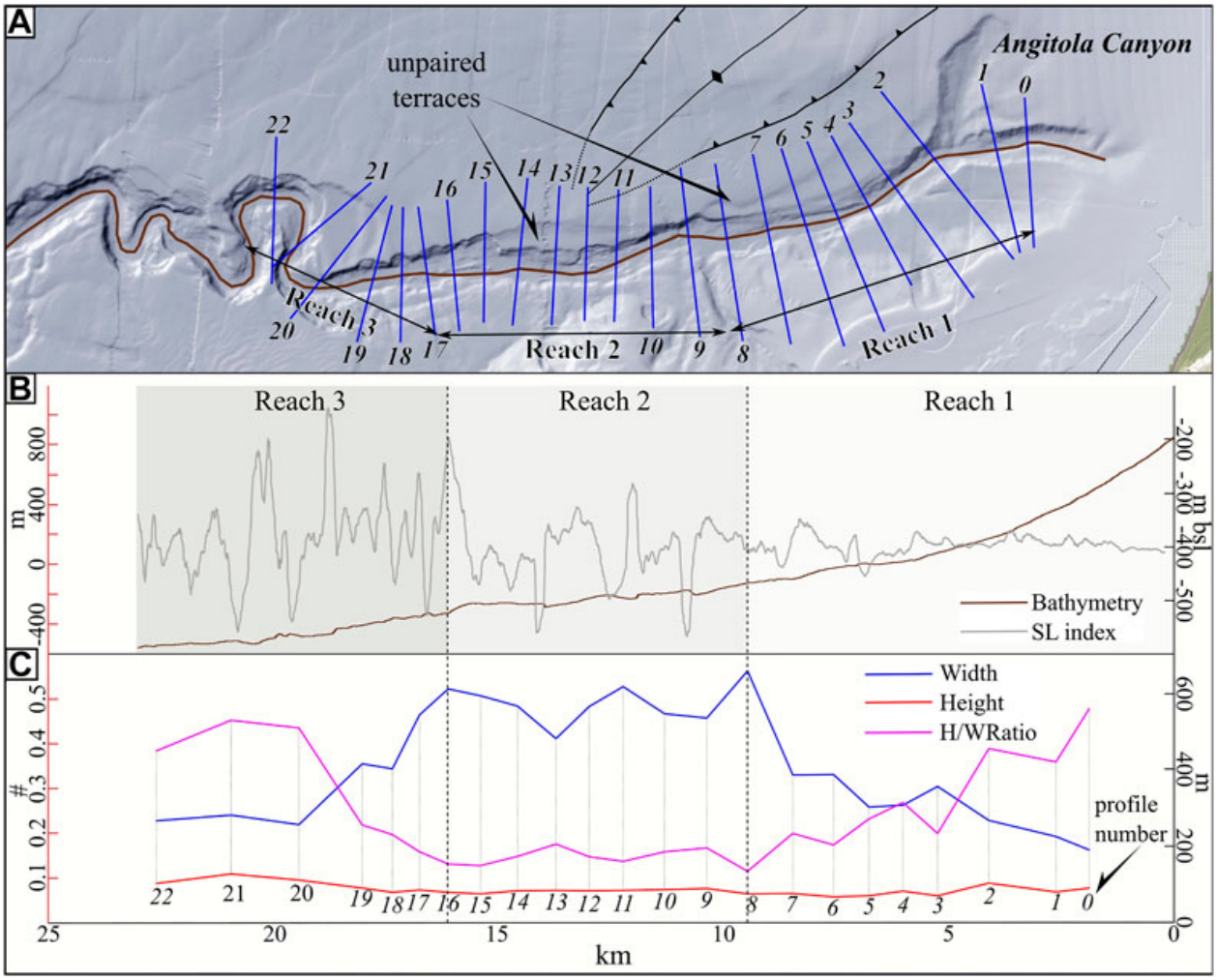

FIGURE 9. A) Map view of the upstream portion of the Angitola Canyon. In black, the southern part of the Maida Ridge. In blue, the location of 23 bathymetric cross-profiles. In brown, the trace of the thalweg. The three double-arrowed black lines show the length of the three reaches. (B) The brown line and the black vertical axis relate to the long profile of the Angitola Canyon, while the grey curve and the red vertical axis represent the SL index computed values. (C) In red and blue, the canyon height and width curves, respectively; both curves refer to the black vertical axis. In magenta, the H/W ratio curve which values relate to the red vertical axis.

5. Discussion

5.1 From deep to shallow: tectonic interpretation of the Sant'Eufemia Gulf

The structural investigation results integrated with the geomorphic analysis pinpoint three major tectonic events in the structural evolution of the Sant'Eufemia Gulf from Late Miocene to Recent times. We propose to frame these tectonic events within the kinematics of a deep-seated slab tear drawn from previous geodynamic analysis of the region (Lucente et al., 1999; Rosenbaum et al., 2008) and interpreted as a regional, first-order structure.

Seismic reflection profiles show that the first tectonic event was characterised by the development of extensional faults during the Late Miocene (Figure 5a). The second tectonic event was characterised by the positive inversion of deep (>3 km) extensional faults inherited from the previous event (Figure 5a). During this stage, we also document the formation of transpressional faults and NNE-SSW to NE-SW oriented anticlines (e.g. the Maida Ridge), involving Upper Miocene to Lower Pleistocene (Gelasian) deposits, in the central and eastern sector of the gulf, respectively (Figures 5b, and 8a and b). The orientation of the anticlines and their en-echelon arrangement suggest that they developed within a roughly E-W oriented right-lateral transpressional zone, located above the deep-seated slab tear fault (red line in Figure 1d). The last tectonic event began in the Early Pleistocene (Calabrian). It was characterised by the onset of shallow (less than 1.5 km), NNE- SSW trending, high-angle normal to oblique faults (Figure 5a, 6, and 7). The orientation of these younger faults (Figure 8a and c) suggests that they formed in a left-lateral strike-slip regime along the E-W oriented shear zone. This interpretation is consistent with the deep-seated structural setting documented by Guarnieri, 2006, suggesting a current left-lateral wrenching develops between Sant'Eufemia Gulf and Squillace Gulf, and with seismological data that highlight left-lateral focal mechanisms in this sector of Calabria (e.g. Presti et al., 2013).

Data and interpretation highlight a change from right-lateral to left-lateral kinematic since the Calabrian. A kinematic change for the second and third tectonic event was proposed by Brutto et al. (2016) based on field data collected in the western Catanzaro Trough and on the interpretation of seismic profiles collected in the Sant'Eufemia Gulf. Conversely, the evolutionary model proposed by Brutto et al. (2016) suggests that the last extensional stage is governed by a sub-vertical P-axis similarly to what occurs slightly to the south, from the Messina Straits to the Mesima Valley. In the northern sector of the Catanzaro Trough and adjacent Squillace Gulf, an ESE-WNW trending strike-slip fault system (Figure 1a and e; Lamezia-Catanzaro line, Tansi et al., 2007) and an E-W trending transtensional basin connected to a negative flower structure (Del Ben et al., 2008) developed since the Late Miocene, respectively. The strike-slip fault system offsets the Middle Miocene to Lower Pleistocene deposits on-land (van Dijk et al., 2000; Tansi et al., 2007) and Plio-Quaternary sequences in the Squillace Gulf (Del Ben et al., 2008). Their orientation confirms that a roughly E-W oriented crustal strike-slip fault can be traced from the Sant'Eufemia Gulf to the Squillace Gulf. On a lithospheric scale, the western part of the crustal fault lies over an ESE-WNW trending, shallow (< 100 km) slab tear fault (red line in Fig. 1d, Rosenbaum et al., 2008). Because a slab tear fault develops in the correspondence of two adjacent parts of the lower plate that move at different rollback velocities (Rosenbaum et al., 2008), the formation of the crustal faults can be considered as the upper plate

response to the tearing of the lower plate (Fig. 10). Considering the age of the older deposits affected by the upper plate deformation, we infer that the formation of the tear fault started in the Late Miocene.

The slip-sense inversion from right-lateral to left-lateral of the roughly E-W oriented crustal strike-slip fault traced from the Sant'Eufemia Gulf to the Squillace Gulf could be the result of a deceleration of the eastward motion of the northern part of the Calabrian Arc with respect to the southern sector during the Quaternary transition from the tectonic event 2 to 3, as a consequence of the collision of the northern sector of the Calabrian Arc with the continental crust of the Apulian foreland (Guarnieri, 2006). This event has partially inhibited the propagation of the northern part with respect to the southern sector that continued to migrate southeastwards (Figure 10). The same effect could have resulted from the slab detachment (~ 700 ka) that caused the end of the subduction beneath the northern Calabrian Arc (Neri et al., 2009; Scarfì et al., 2018).

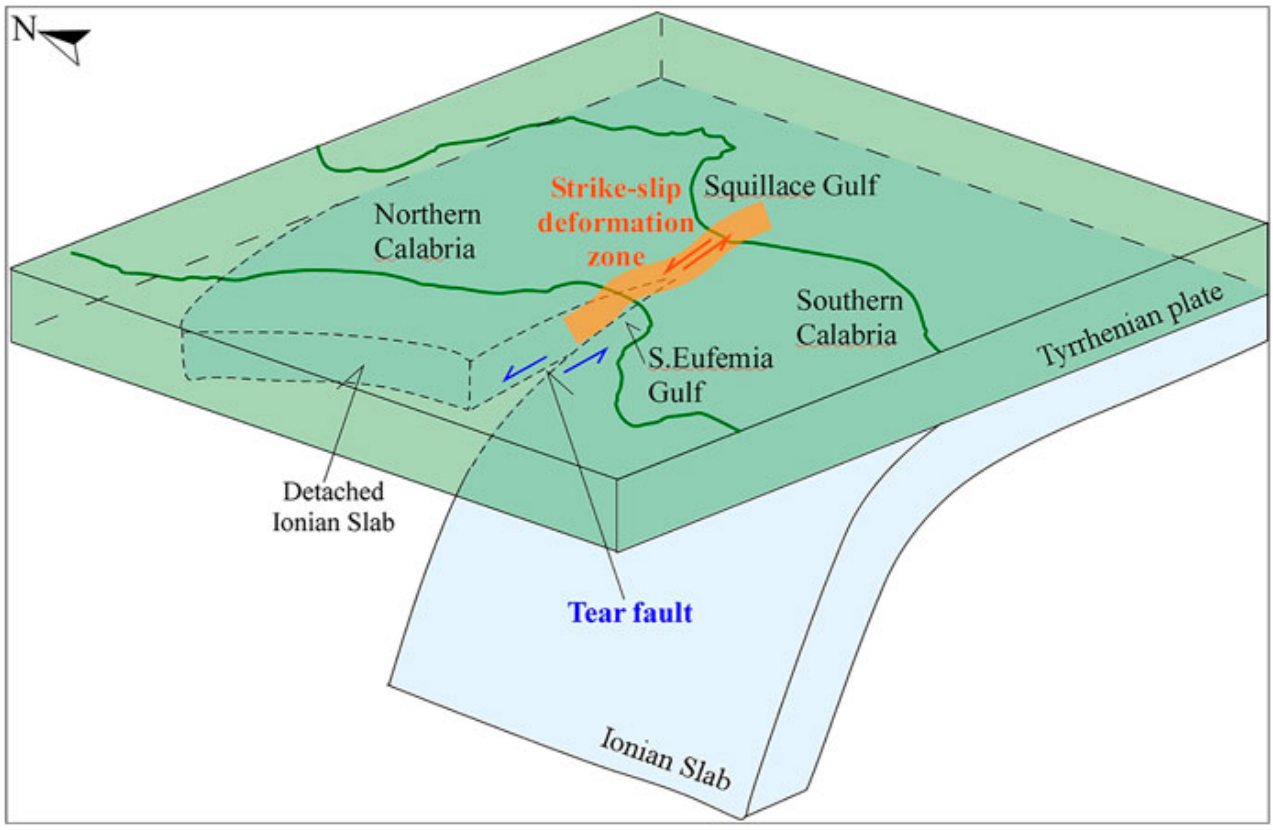

FIGURE 10. Geodynamic sketch of the Tyrrhenian-Ionian subduction system illustrating the strike-slip deformation zone extending from Sant'Eufemia Gulf to Squillace Gulf formed above the tear fault inferred between two segments of the Ionian slab.

5.2 Landscape response of the Sant'Eufemia Gulf to tectonic forcing

The alignment of the AMTM values in correspondence with a NE-SW seafloor scarp developed in the western sector of the gulf (1 in Figure 8a) suggests a recent morphostructural control

on its formation. The geometrical and stereological characteristics of this N15°E striking, 10 km long and 200 m high scarp, make this morphological feature compatible with the deep structures detected on the high-penetration seismic profiles.

A few AMTM values were detected in the central sector of the Gulf (2 in Figure 8a), where a number of NNE-SSW-trending shallow normal to transtensional faults offset the seafloor. The limited occurrence of AMTM values indicates that the wavelength of the topographic signature of the normal to transtensional faults is smaller than the width of the swath profiles. Thus, the morphometric analysis confirms that these faults are basically shallow structures, whose roots do not reach the same depth as the transpressional faults. No AMTM values were found in correspondence to the deep transpressional faults in the central sector of the Gulf, suggesting that this structure is probably inactive.

In the eastern sector of the Gulf, AMTM values were detected in correspondence of the NNE-SSW to NE-SW trending anticlines (e.g. Maida Ridge, MA in fig. 8a), indicating that these structures controlled the morphology of the eastern sector of the Gulf in recent times. Thus, the analysis of swath profiles suggests that deep transpressional faults (e.g. CDPs 260-300 in Figure 5b), associated with the development of the anticlines during the second tectonic event (see paragraph 5.1), were reactive in the left-lateral transtensional regime that characterises the last tectonic event.

In the southern sector of the Gulf, several AMTM values are detected along the Angitola Canyon. However, in this case, the tectonic forcing probably has triggered multiple geomorphological processes (e.g., gravitational processes, changes in slope and drainage patterns, sediment density flows that travel down the canyon, etc.) able to produce AMTM values. Thus, we have integrated the analysis of swath profiles with the bathymetric analysis of the Angitola Canyon to better understand the possible tectonic forcing of the 22 km long upstream section of the channel. The longitudinal profile of the canyon (Figure 9) shows that Reach 1 follows a steady-state evolution process as attested by its concave upward bathymetric profile and the flat SL trend. Along Reach 1, the canyon progressively increases its width in the downstream direction and approaches the Maida Ridge. Reach 2 responds to a tectonic landward tilt process and to the lateral tectonic forcing, as shown by the minimum SL value, the maximum width of the channel, and the corresponding minimum value of the H/W ratio associated with a steady H value. Finally, the morphology of the Reach 3 evolves following a growing stream power, as inferred by higher SL values and an increasing H/W ratio.

The change in the longitudinal slope of the canyon between Reach 2 and Reach 3 and the asymmetric shape of the canyon, expressed by the active channel flowing near the southern wall and the presence of unpaired terraces along the northern flank (Figure 9a), suggest that Reach 2 and Reach 3 underwent differential uplift. Considering that the south-western prolongation of the Maida Ridge

roughly lies below the boundary between the Reach 2 and Reach 3 of the canyon, we infer that the differential uplift of the two reaches represents the topographic response to the Late Quaternary activity of the Maida Ridge.

5.3 Seismotectonic implications

The 1905 earthquake, one of the largest seismic event in Italy, was widely felt along the whole Tyrrhenian coastline of Calabria, with maximum macroseismic intensities documented in the northern part of the Capo Vaticano promontory (CFTI5Med, Guidoboni et al., 2018; CPTI15, Rovida et al., 2021). The earthquake also triggered a tsunami wave that flooded the coastline of central Calabria (Piatanesi and Tinti, 2002; Loreto et al., 2017; Maramai et al., 2019). Shaking scenarios suggest that the seismogenic fault is located in the Sant'Eufemia Gulf (Sandron et al., 2015). Two different structures located south of the Capo Vaticano promontory (Cucci and Tertulliani 2010) and in the Sant'Eufemia Gulf (Loreto et al., 2013) were proposed as seismogenic faults. The different hypothesis on the source of the 1905 seismic event is due to the difficulty of identifying offshore structural lineaments able to produce high-magnitude seismic events.

Some consideration on the age and stratigraphy of the deformed units is necessary to infer the seismogenic potential of the two sets of faults mapped in the Sant'Eufemia Gulf. The Pliocene to Early Pleistocene (Calabrian) transpressional faults (primary fault set) deform highly competent rocks of the Kabilian-Calabrian units, including imbricate sheets of the Hercynian basement, Alpine poly-metamorphic rocks, and Mesozoic sedimentary units. Conversely, the faults of the shallower transtensional deformation zone (secondary fault set) dissect less competent Pliocene fine-grained (mudstone and claystone) and Quaternary coarser (sandstone and siltstone) rocks. Based on the depth and geometry of the faults (i.e. dimension derived from mapped fault length and width) and on the lithology of the deformed rocks, we suggest that the potential source of large magnitude earthquakes should be related to the primary fault set.

The anticline axis of the Maida Ridge was mapped for a length of about 15 km (MA in Figure 8a). This value is probably underestimated due to the lack of seismic data at the NE and SW terminations of the structure, close to the coastline and the Angitola Canyon, respectively. Geomorphic analysis of the upper reach of the canyon indicates that its evolution was controlled by tectonic forcing compatible with the growth of the anticline. Thus, the length of the deep fault, associated with the development of the anticline, possibly extends south-westward for an additional 3-4 km. The deep structure evolved during the second tectonic stage (Pliocene - Gelasian) as a transpressional fault (Fig. 5b and 8b). Successively, it was active during the last tectonic event (Calabrian – Recent, Figure 8c) in a

left-lateral transtensional regime, as suggested by a) the distribution of the AMTM values indicating that the tectonic activity of the deep fault, responsible for the formation of the Maida Ridge, controlled the seafloor morphology in recent time (see paragraph 5.2), b) the bathymetric analysis of the upper reach of the Angitola Canyon indicating that the growth of the Maida Ridge controlled the evolution of the canyon in the Late Quaternary (see paragraph 5.2), and c) the NNE-SSW orientation of the deep fault that is compatible with its reactivation in a left-lateral transtensional regime (see paragraph 5.2, Figure 8c). Considering the length and depth of this deep fault, its recent activity, and its location close to the epicentre of the 1905 event as inferred by Camassi et al., (1997) (red square-3 in Figure 1f), we suggest that the deep primary fault, associated with the growth of the Maida Ridge, is likely the seismogenic source of the 1905 earthquake.

The seismogenic fault proposed by Loreto et al., (2013) and Brutto et al. (2016) (SEF in Figure 1e, included in the DISS database as the "ITIS139 Sant'Eufemia", DISS Working Group, 2018) is an extensional, SE-dipping fault, formed along the southeastern flank of the Maida Ridge. This fault offsets shallow reflectors (at a depth less than 2s, Figure 13 in Brutto et al., 2016). Based on its depth and its direction, parallel to the shallow transtensional faults documented in our study, we interpret this fault as a secondary structure.

Our suggested seismogenic fault also differs from an intra-plate rupture at the bending zone of the Ionian subduction slab, proposed by Presti et al., (2017), that implies a deeper seismogenic source at a depth of several tens of kilometres. However, the tectonic model we suggest does not exclude the formation of a structure in the subducting lithosphere of the lower plate along or near the slab tear fault.

6. Conclusions

A multiscale approach based on the interpretation of multichannel seismic profiles with different resolution/penetration and quantitative morphometric analysis of multibeam bathymetry provides new insights into the characterisation of active faults in offshore areas. The results of this work allowed to reconstruct the structural setting and the kinematic evolution of surficial and deeper faults developed in the Sant'Eufemia Gulf (Tyrrhenian offshore of the Calabrian Arc) since the Late Miocene, and to detect their morphological signature at the seafloor. The main conclusions can be summarised as follows:

1. Three tectonic events controlled the evolution of the Sant'Eufemia Gulf since the Late Miocene. The first one is an extensional or transtensional phase that occurred during the Late Miocene. Following, a right-lateral transpressional tectonic event developed from the Early

Pliocene to the Early Pleistocene. It caused the positive inversion of deep (>3 km) extensional/transtensional tectonic features and the formation of NNE-SSW to NE-SW trending anticlines (e.g. Maida Ridge). Since the Early Pleistocene (Calabrian), a left-lateral transtensional regime induced the formation of shallow (less than 1.5 km), NNE- SSW oriented, high-angle normal to transtensional faults.

2. The integration of seismic reflection and quantitative morphometric analysis provides evidence that the NNE-SSW to NE-SW trending anticlines, formed during the Pliocene to Early Pleistocene (Gelasian), were reactivated during the Calabrian to Recent left-lateral transtensional event. Also, the bathymetric analysis of the Angitola Canyon suggests a differential uplift between two reaches of the canyon. We infer that the south-western prolongation of the Maida Ridge lies below the canyon and, thus, the differential uplift may be regarded as a topographic response of the Late Quaternary negative inversion of the fault that has controlled the growth of the Maida Ridge.
3. Based on the length (>15 km), and recent tectonic activity, the deep structure controlling the development of the Maida Ridge can be considered a potential candidate for the seismogenic source of the 1905 earthquake.
4. Our results, integrated with previous literature, support the hypothesis that the transpressional/transtensional structures detected in the study area correspond to a ~E-W oriented crustal strike-slip fault zone extending from the Sant'Eufemia Gulf to Squillace Basin (Ionian Sea). This zone may be regarded as a crustal response to the development of a tear fault in the lower plate.

Acknowledgements

This study has been partly funded by the joint projects of Ministero degli Affari Esteri e della Cooperazione Internazionale in collaboration with the Israeli Ministry of Science and Technology grant no. 3-14333 in the frame of the EPAF Project (principal investigators Pepe F. and Kanari M.) and MUSE 4D-Overtime tectonic, dynamic and rheologic control on destructive multiple seismic events -Special Italian Faults and Earthquakes: From real 4-D cases to models, in the frame of PRIN 2017. High resolution multichannel seismic reflection data (Geo-Source Sparker) were acquired by the "Geo Marine Survey Systems" company (Rotterdam, The Netherlands) and processed by the "GeoSurvey" company (Aveiro, Portugal). Interpretation of seismic profiles was performed within the GeoSuite AllWork software package. Bathymetric data were collected in research projects funded by the National Research Council. We acknowledge Andrea Zanchi, an anonymous reviewer and the

associate editor Paola Vannucchi for their critical reading and useful comments that allowed us to improve the manuscript.

References

Argnani, A. (2009). Evolution of the southern Tyrrhenian slab tear and active tectonics along the western edge of the Tyrrhenian subducted slab. Geol. Soc. London, Spec. Publ. 311, 193–212.

Baes, M., Govers, R., and Wortel, R. (2011). Subduction initiation along the inherited weakness zone at the edge of a slab: Insights from numerical models. Geophys. J. Int. 184, 991–1008.

Barreca, G., Bruno, V., Cocorullo, C., Cultrera, F., Ferranti, L., Guglielmino, F., Guzzetta, L., Mattia, M., Monaco, C. and Pepe, F. (2014). Geodetic and geological evidence of active tectonics in south-westernSicily (Italy). J. Geodyn., 82, 138–149. http://dx.doi.org/10.1016/j.jog.2014.03.004

Barreca, G., Corradino, M., Monaco, C. and Pepe, F. (2018). Active Tectonics along the South East Offshore Margin of Mt. Etna: New Insights from High-Resolution Seismic Profiles. Geosciences, 8, 62; doi:10.3390/geosciences8020062.

Billi, A., Barberi, G., Faccenna, C., Neri, G., Pepe, F., and Sulli, A. (2006). Tectonics and seismicity of the Tindari Fault System, southern Italy: Crustal deformations at the transition between ongoing contractional and extensional domains located above the edge of a subducting slab. Tectonics 25.

Bonardi, G., Cavazza, W., Perrone, V., and Rossi, S. (2001). "Calabria-Peloritani terrane and northern Ionian sea," in Anatomy of an orogen: The Apennines and adjacent Mediterranean basins (Springer), 287–306.

Bonini, L., Bucci, D. D., Toscani, G., Seno, S., and Valensise, G. (2011). Reconciling deep seismogenic and shallow active faults through analogue modelling: the case of the Messina Straits (southern Italy). J. Geol. Soc. London. 168, 191–199. doi:10.1144/0016-76492010-055.

Brutto, F., Muto, F., Loreto, M. F., Paola, N. De, Tripodi, V., Critelli, S., et al. (2016). The Neogene-Quaternary geodynamic evolution of the central Calabrian Arc: A case study from the western Catanzaro Trough basin. J. Geodyn. 102, 95–114. doi:10.1016/j.jog.2016.09.002.

Burbank, D. W., and Anderson, R. S. (2011). Tectonic Geomorphology. Wiley Online Library Available at: http://search.ebscohost.com/login.aspx?direct=true&db=edsebk&AN=408384&site=eds-live.

Camassi, R., Stucchi, M., and Molin, D. (1997). NT4. 1 un catalogo parametrico di terremoti di area italiana al di sopra della soglia del danno. Consiglio Nazionale delle Richerche, Gruppo Nazionale per la Difesa dai ….

Carafa, M. M. C., Kastelic, V., Bird, P., Maesano, F. E., and Valensise, G. (2018). A "Geodetic Gap" in the Calabrian Arc: Evidence for a Locked Subduction Megathrust? Geophys. Res. Lett. 45, 1794–1804. doi:10.1002/2017GL076554.

Carminati, E., and Doglioni, C. (2005). Mediterranean tectonics. Encycl. Geol. 2, 135–146.

Carminati, E., Wortel, M. J. R., Spakman, W., and Sabadini, R. (1998). The role of slab detachment processes in the opening of the western-central Mediterranean basins: Some geological and geophysical evidence. Earth Planet. Sci. Lett. 160, 651–665. doi:10.1016/S0012-821X(98)00118-6.

Chatelain, J., Molnar, P., Prévot, R., and Isacks, B. (1992). Detachment of part of the downgoing slab and uplift of the New

Hebrides (Vanuatu) Islands. Geophys. Res. Lett. 19, 1507–1510.

Chiarabba, C., De Gori, P., and Mele, F. M. (2015). Recent seismicity of Italy: Active tectonics of the central Mediterranean region and seismicity rate changes after the Mw 6.3 L'Aquila earthquake. Tectonophysics 638, 82–93.

Chiarabba, C., De Gori, P., and Speranza, F. (2008). The southern Tyrrhenian subduction zone: deep geometry, magmatism and Plio-Pleistocene evolution. Earth Planet. Sci. Lett. 268, 408–423.

Chiarabba, C., and Palano, M. (2017). Progressive migration of slab breakoff along the southern Tyrrhenian plate boundary: Constraints for the present day kinematics. J. Geodyn. 105, 51–61. doi:10.1016/j.jog.2017.01.006.

Corradino, M., Pepe, F., Bertotti, G., Picotti, V., Monaco, C., and Nicolich, R. (2020). 3D Architecture and Plio-Quaternary evolution of the Paola Basin: Insights into the Forearc of the Tyrrhenian-Ionian Subduction System. Tectonics. doi:10.1029/2019tc005898.

Corradino, M., Pepe, F., Sacchi, M., Solaro, G., Duarte, H., Ferranti, L., et al. (2021). Resurgent uplift at large calderas and relationship to caldera-forming faults and the magma reservoir: New insights from the Neapolitan Yellow Tuff caldera (Italy). J. Volcanol. Geotherm. Res., 107183.

Cosentino, C., Molisso, F., Scopelliti, G., Caruso, A., Insinga, D.D., Lubritto C., Pepe F. and Sacchi M. (2017). Benthic foraminifera as indicators of relative sea-level fluctuations: Paleoenvironmental and paleoclimatic reconstruction of a Holocene marine succession (Calabria, southeastern Tyrrhenian Sea). Quat. Int. 439, 79-101. http://dx.doi.org/10.1016/j.quaint.2016.10.012

Cucci, L., and Tertulliani, A. (2010). The Capo Vaticano (Calabria) coastal terraces and the 1905 M7 earthquake: the geomorphological signature of regional uplift and coseismic slip in southern Italy. Terra Nova, 22(5), 378-389.

Cultrera, F., Barreca, G., Ferranti. L., Monaco, C., Pepe, F., Passaro, S., Barberi, G., Bruno, V., Burrato, P., Mattia, M., Musumeci, C., Scarfì, L. (2017a). Structural architecture and active deformation pattern in the northern sector of the Aeolian-Tindari-Letojanni fault system (SE Tyrrhenian Sea-NE Sicily) from integrated analysis of field, marine geophysical, seismological and geodetic data. Ital. J. Geosci., 136, 3, 399-417. https://doi.org/10.3301/IJG.2016.17

Cultrera, F., Barreca, G., Burrato, P., Ferranti, L., Monaco, C., Passaro, S., Pepe, F., and Scarfì L. (2017b). Active faulting and continental slope instability in the gulf of patti (Tyrrhenian side of NE sicily, Italy): A field, marine and seismological joint analysis. Nat. Hazards 86, S253–S272. doi:10.1007/s11069-016-2547-y.

De Ritis, R., Pepe, F., Orecchio, B., Casalbore, D., Bosman, A., Chiappini, M., et al. (2019). Magmatism along lateral slab edges: Insights from the Diamante-Enotrio-Ovidio volcanic-intrusive complex (Southern Tyrrhenian Sea). Tectonics 38, 2581–2605.

De Ritis, R., Ventura, G., Chiappini, M., Carluccio, R., and von Frese, R. (2010). Regional magnetic and gravity anomaly correlations of the Southern Tyrrhenian Sea. Phys. Earth Planet. Inter. 181, 27–41. doi:10.1016/j.pepi.2010.04.003.

Del Ben, A., Barnaba, C., and Taboga, A. (2008). Strike-slip systems as the main tectonic features in the Plio-Quaternary kinematics of the Calabrian Arc. Mar. Geophys. Res. 29, 1–12.

Devoti, R., D'Agostino, N., Serpelloni, E., Pietrantonio, G., Riguzzi, F., Avallone, A., et al. (2017). A combined velocity field of the mediterranean region. Ann. Geophys. 60, S0215. doi:10.4401/ag-7059.

Di Bucci, D., Ridente, D., Fracassi, U., Trincardi, F., and Valensise, G. (2009). Marine palaeoseismology from very high resolution seismic imaging: the Gondola Fault Zone (Adriatic foreland). Terra Nov. 21, 393–400.

DISS Working Group (2018). Database of Individual Seismogenic Sources (DISS), Version 3.2.1: A compilation of potential

sources for earthquakes larger than M 5.5 in Italy and surrounding areas. http://diss.rm.ingv.it/diss/, Istituto Nazionale di Geofisica e Vulcanologia; DOI:10.6092/INGV.IT-DISS3.2.1.

Doglioni, C., Innocenti, F., and Mariotti, G. (2001). Why Mt Etna? Terra Nov. 13, 25–31.

Dunbar, P.K., Lockridge, P.A., and Whitewide, L.S. (1992). Catalog of Significant Earthquakes 2150 B.C. to the present. NGDC Report SE, 49.

Faccenna, C., Becker, T. W., Lucente, F. P., Jolivet, L., and Rossetti, F. (2001). History of subduction and back-arc extension in the central Mediterranean. Geophys. J. Int. 145, 809–820. doi:10.1046/j.0956-540X.2001.01435.x.

Faccenna, C., Funiciello, F., Civetta, L., D Antonio, M., Moroni, M., and Piromallo, C. (2007). Slab disruption, mantle circulation, and the opening of the Tyrrhenian basins. Spec. Pap. Soc. Am. 418, 153.

Ferranti, L., Burrato, P., Pepe, F., Santoro, E., Mazzella, M. E., Morelli, D., et al. (2014). An active oblique-contractional belt at the transition between the Southern Apennines and Calabrian Arc: The Amendolara Ridge, Ionian Sea, Italy. Tectonics 33, 2169–2194. doi:10.1002/2014TC003624.

Ferranti, L., Santoro, E., Mazzella, M. E., Monaco, C., and Morelli, D. (2009). Active transpression in the northern Calabria Apennines, southern Italy. Tectonophysics 476, 226–251. doi:10.1016/j.tecto.2008.11.010.

Fracassi, U., Di Bucci, D., Ridente, D., Trincardi, F., and Valensise, G. (2008). Activity of the Gondola Fault Zone and potential earthquake sources offshore the Gargano Promontory (Adriatic Sea).

Gallais, F., Graindorge, D., Gutscher, M.-A., and Klaeschen, D. (2013). Propagation of a lithospheric tear fault (STEP) through the western boundary of the Calabrian accretionary wedge offshore eastern Sicily (Southern Italy). Tectonophysics 602, 141–152.

Galli, P., and Molin, D. (2009). Il terremoto del 1905 in Calabria: Revisione della distribuzione degli effetti e delle ipotesi sismogenetiche. Quat. Ital. J. Quat. Sci. 22, 207–234.

Galli, P. A., and Peronace, E. (2015). Low slip rates and multimillennial return times for Mw 7 earthquake faults in southern Calabria (Italy). Geophys. Res. Lett., 42(13), 5258-5265.

Govers, R., and Wortel, M. J. R. (2005). Lithosphere tearing at STEP faults: Response to edges of subduction zones. Earth Planet. Sci. Lett. 236, 505–523. doi:10.1016/j.epsl.2005.03.022.

Guarnieri, P. (2006). Plio-Quaternary segmentation of the south Tyrrhenian forearc basin. Int. J. Earth Sci. 95, 107–118. doi:10.1007/s00531-005-0005-2.

Guidoboni, E., Ferrari, G., Mariotti, D., Comastri, A., Tarabusi, G., Sgattoni, G., et al. (2018). CFTI5Med, Catalogo dei Forti Terremoti in Italia (461 aC-1997) e nell'area Mediterranea (760 aC-1500).

Guidoboni, E., Ferrari, G., Mariotti, D., Comastri, A., Tarabusi, G., and Valensise, G. (2007). Catalogue of Strong Earthquakes in Italy (461 BC-1997) and Mediterranean Area (760 BC-1500).

Gutscher, M. A., Dominguez, S., De Lepinay, B. M., Pinheiro, L., Gallais, F., Babonneau, N., et al. (2016). Tectonic expression of an active slab tear from high-resolution seismic and bathymetric data offshore Sicily (Ionian Sea). Tectonics 35, 39–54. doi:10.1002/2015TC003898.

Gutscher, M.A., Kopp, H., Krastel, S., Bohrmann, G., Garlan, T., Zaragosi, S., et al. (2017). Active tectonics of the Calabrian subduction revealed by new multibeam bathymetric data and high-resolution seismic profiles in the Ionian Sea (Central Mediterranean). Earth Planet. Sci. Lett. 461, 61–72. https://doi .org /10 .1016 /j.epsl.2016.12.020.

Knott, S. D., and Turco, E. (1991). Late Cenozoic kinematics of the Calabrian arc, southern Italy. Tectonics 10, 1164–1172.

ISIDe Working Group. (2007). Italian Seismological Instrumental and Parametric Database (ISIDe). Istituto Nazionale di Geofisica e Vulcanologia (INGV). https://doi.org/10.13127/ISIDE

Lallemand, S., Font, Y., Bijwaard, H., and Kao, H. (2001). New insights on 3-D plates interaction near Taiwan from tomography and tectonic implications. Tectonophysics 335, 229–253.

Levin, V., Shapiro, N., Park, J., and Ritzwoller, M. (2002). Seismic evidence for catastrophic slab loss beneath Kamchatka. Nature 418, 763.

Loreto, M. F., Fracassi, U., Franzo, A., Del Negro, P., Zgur, F., and Facchin, L. (2013). Approaching the seismogenic source of the Calabria 8 September 1905 earthquake: New geophysical, geological and biochemical data from the S. Eufemia Gulf (S Italy). Mar. Geol. 343, 62–75. doi:10.1016/j.margeo.2013.06.016.

Loreto, M. F., Pepe, F., De Ritis, R., Ventura, G., Ferrante, V., Speranza, F., Tomini, I., and Sacchi, M. (2015). Geophysical investigation of Pleistocene volcanism and tectonicsoffshore Capo Vaticano (Calabria, southeastern Tyrrhenian Sea). J. Geodyn. 90, 71-86. http://dx.doi.org/10.1016/j.jog.2015.07.005

Loreto, M. F., Pagnoni, G., Pettenati, F., Armigliato, A., Tinti, S., Sandron, D., et al. (2017). Reconstructed seismic and tsunami scenarios of the 1905 Calabria earthquake (SE Tyrrhenian sea) as a tool for geohazard assessment. Eng. Geol. 224, 1–14. doi:10.1016/j.enggeo.2017.04.018.

Loreto, M. F., Zitellini, N., Ranero, C. R., Palmiotto, C., and Prada, M. (2021). Extensional tectonics during the Tyrrhenian back-arc basin formation and a new morpho-tectonic map. Basin Res. 33, 138–158.

Lucente, F. P., Chiarabba, C., Cimini, G. B., and Giardini, D. (1999). Tomographic constraints on the geodynamic evolution of the Italian region. J. Geophys. Res. Solid Earth 104, 20307–20327.

Maesano, F. E., Tiberti, M. M., and Basili, R. (2017). The Calabrian Arc: three-dimensional modelling of the subduction interface. Sci. Rep. 7, 1–15.

Maesano, F. E., Volpi, V., Civile, D., Basili, R., Conti, A., Tiberti, M. M., et al. (2020). Active Extension in a Foreland Trapped Between Two Contractional Chains: The South Apulia Fault System (SAFS). Tectonics 39. doi:10.1029/2020TC006116.

Malinverno, A., Cafiero, M., Ryan, W. B. F., and Cita, M. B. (1981). Distribution of messinian sediments and erosional surfaces beneath the tyrrhenian sea-geodynamic implications. Oceanol. Acta 4, 489–495.

Malinverno, A., and Ryan, W. B. F. (1986). Extension in the Tyrrhenian Sea and shortening in the Apennines as result of arc migration driven by sinking of the lithosphere. Tectonics 5, 227–245.

Maramai, A., Graziani, L., and Brizuela, B. (2019). Italian Tsunami Effects Database (ITED): the first database of tsunami effects observed along the Italian coasts. Nat. Hazards Earth Syst. Sci. Discuss., 1–21.

Margottini, C., Ambraseys, N.N., and Screpanti, A. (1993). La magnitudo dei terremoti italiani del XX secolo. ENEA, 57.

Mariucci, M. T., and Montone, P. (2020). Database of Italian present-day stress indicators, IPSI 1.4. Sci. data 7, 1–11.

Michelini A., Lomax A., Nardi A. and Rossi A. (2006). La localizzazione del terremoto della Calabria dell'8 settembre 1905 da dati strumentali. In: Guerra I. and Savaglio A. (eds), 8 settembre 1905: terremoto in Calabria, Università della Calabria, pp. 225-240.

Miller, M. S., Gorbatov, A., and Kennett, B. L. N. (2006). Three-dimensional visualisation of a near-vertical slab tear beneath

the southern Mariana arc. Geochemistry, Geophys. Geosystems 7.

Monaco, C., and Tortorici, L. (2000). Active faulting in the Calabrian arc and eastern Sicily. J. Geodyn. 29, 407–424. doi:10.1016/S0264-3707(99)00052-6.

Neri, G., Caccamo, D., Cocina, O., and Montalto, A. (1996). Geodynamic implications of earthquake data in the southern Tyrrhenian sea. Tectonophysics 258, 233–249.

Neri, G., Orecchio, B., Totaro, C., Falcone, G., and Presti, D. (2009). Subduction beneath southern Italy close the ending: Results from seismic tomography. Seismol. Res. Lett. 80, 63–70.

Nijholt, N., and Govers, R. (2015). The role of passive margins on the evolution of Subduction-Transform Edge Propagators (STEPs). J. Geophys. Res. Solid Earth 120, 7203–7230.

Orecchio, B., Presti, D., Totaro, C., and Neri, G. (2014). What earthquakes say concerning residual subduction and STEP dynamics in the Calabrian Arc region , south Italy. Geophys. J. Int., 1929–1942. doi:10.1093/gji/ggu373.

Pepe, F., Bertotti, G., Ferranti, L., Sacchi, M., Collura, A. M., Passaro, S., et al. (2014). Pattern and rate of post-20 ka vertical tectonic motion around the Capo Vaticano Promontory (W Calabria, Italy) based on offshore geomorphological indicators. Quat. Int. 332, 85–98. doi:10.1016/j.quaint.2013.11.012.

Pepe, F., Sulli, A., Bertotti, G., and Cella, F. (2010). Architecture and Neogene to Recent evolution of the western Calabrian continental margin: An upper plate perspective to the Ionian subduction system, central Mediterranean. Tectonics 29, 1–24. doi:10.1029/2009TC002599.

Piatanesi, A., and Tinti, S. (2002). Numerical modelling of the September 8, 1905 Calabrian (southern Italy) tsunami. Geophys. J. Int. 150, 271–284.

Piromallo, C., and Morelli, A. (2003). P wave tomography of the mantle under the Alpine-Mediterranean area. J. Geophys. Res. Solid Earth 108.

Polonia, A., Torelli, L., Artoni, A., Carlini, M., Faccenna, C., Ferranti, L., et al. (2016). The Ionian and Alfeo–Etna fault zones: New segments of an evolving plate boundary in the central Mediterranean Sea? Tectonophysics 675, 69–90.

Polonia, A., Torelli, L., Mussoni, P., Gasperini, L., Artoni, A., & Klaeschen, D. (2011). The Calabrian Arc subduction complex in the Ionian Sea: Regional architecture, active deformation, and seismic hazard. Tectonics, 30(5).

Pondrelli, S., F. Visini, A. Rovida, V. D'Amico, B. Pace, C. Meletti (2020). Style of faulting of expected earthquakes in Italy as an input for seismic hazard modelling. Nat. Hazards Earth Syst. Sci., 20, 3577–3592, doi:10.5194/nhess-20-3577-2020.

Presti, D., Neri, G., Orecchio, B., Scolaro, S., and Totaro, C. (2017). The 1905 Calabria, southern Italy, earthquake: Hypocenter location, causative process, and stress changes induced in the area of the 1908 Messina Straits earthquake. Bull. Seismol. Soc. Am. 107, 2613–2623.

Presti, D., Billi, A., Orecchio, A., Totaro, C., Faccenna, C., Neri, G. (2013). Earthquake focal mechanisms, seismogenic stress, and seismotectonics of the Calabrian Arc, Italy. Tectonophysics 602, 153–175.

Riuscetti, M., and Schick, R. (1975). Earthquakes and tectonics in southern Italy. Boll. Geof. Teor. Appl 17, 59–78.

Rizzo, G. B. (1906). ... Sulla velocità di propagazione delle onde sismiche nel terremoto della Calabria del giorno 8 settembre 1905. C. Clausen.

Rosenbaum, G., Gasparon, M., Lucente, F. P., Peccerillo, A., and Miller, M. S. (2008). Kinematics of slab tear faults during subduction segmentation and implications for Italian magmatism. Tectonics 27, 1–16. doi:10.1029/2007TC002143.

Rovida A., Locati M., Camassi R., Lolli B., Gasperini P. (2020). The Italian earthquake catalogue CPTI15. Bulletin of Earthquake Engineering, 18(7), 2953-2984. https://doi.org/10.1007/s10518-020-00818-y

Rovida, A. N., Locati, M., Camassi, R. D., Lolli, B., and Gasperini, P., Antonucci A. (2021). Catalogo Parametrico dei Terremoti Italiani CPTI15, versione 3.0. Istituto Nazionale di Geofisica e Vulcanologia (INGV). https://doi.org/10.13127/CPTI/CPTI15.3

Sacks, P. E., and Secor Jr, D. T. (1990). Delamination in collisional orogens. Geology 18, 999–1002.

Sandron, D., Loreto, M. F., Fracassi, U., and Tiberi, L. (2015). Shaking scenarios from multiple source models shed light on the 8 September 1905 M<inf>w</inf> 7 Calabria earthquake (Southern Italy). Bull. Seismol. Soc. Am. 105, 912–927. doi:10.1785/0120140044.

Scarfì, L., Barberi, G., Barreca, G., Cannavò, F., Koulakov, I., and Patanè, D. (2018). Slab narrowing in the Central Mediterranean: The Calabro-Ionian subduction zone as imaged by high resolution seismic tomography. Sci. Rep. 8, 1–12. doi:10.1038/s41598-018-23543-8.

Schwanghart, W., and Scherler, D. (2014). Short Communication: TopoToolbox 2 - MATLAB-based software for topographic analysis and modeling in Earth surface sciences. Earth Surf. Dyn. 2, 1–7. doi:10.5194/esurf-2-1-2014.

Scrocca, D., Doglioni, C., and Innocenti, F. (2003). Constraints for an interpretation of the Italian geodynamics: a review. Mem. Descr. della Cart. Geol. d'Italia 62, 15–46.

Tansi, C., Muto, F., Critelli, S., and Iovine, G. (2007). Neogene-Quaternary strike-slip tectonics in the central Calabrian Arc (southern Italy). J. Geodyn. 43, 393–414. doi:10.1016/j.jog.2006.10.006.

Tiberti, M. M., Vannoli, P., Fracassi, U., Burrato, P., Kastelic, V., and Valensise, G. (2017). Understanding seismogenic processes in the Southern Calabrian Arc: A geodynamic perspective. Ital. J. Geosci. 136, 365–388. doi:10.3301/IJG.2016.12.

Tortorici, L., Monaco, C., Tansi, C., and Cocina, O. (1995). Recent and active tectonics in the Calabrian arc (Southern Italy). Tectonophysics 243, 37–55. doi:10.1016/0040-1951(94)00190-K.

Totaro, C., Orecchio, B., Presti, D., Scolaro, S., and Neri, G. (2016). Seismogenic stress field estimation in the Calabrian Arc region (south Italy) from a Bayesian approach. Geophys. Res. Lett. 43, 8960–8969. doi:10.1002/2016GL070107.

van Dijk, J., and Okkes, M. (1991). Neogene tectonostratigraphy and kinematics of Calabrian basins; implications for the geodynamics of the Central Mediterranean. Tectonophysics 196, 23–60.

van Dijk, J. P. (1992). Late Neogene fore-arc basin evolution in the Calabrian Arc (central Mediterranean); tectonic sequence stratigraphy and dynamic geohistory. Faculteit Aardwetenschappen.

van Dijk, J. P., and Scheepers, P. J. J. (1995). Neotectonic rotations in the Calabrian Arc; implications for a Pliocene-Recent geodynamic scenario for the Central Mediterranean. Earth-Science Rev. 39, 207–246.

van Dijk, J. P., Bello, M., Brancaleoni, G. P., Cantarella, G., Costa, V., Frixa, A., et al. (2000). A regional structural model for the northern sector of the Calabrian Arc (southern Italy). 324. doi:10.1016/S0040-1951(00)00139-6.

Williams, G. D., Powell, C. M., and Cooper, M. A. (1989). Geometry and kinematics of inversion tectonics. Geol. Soc. London, Spec. Publ. 44, 3–15.

Wortel, M. J. R., and Spakman, W. (2000). Subduction and slab detachment in the Mediterranean-Carpathian region. Science (80-.). 290, 1910–1917. doi:10.1126/science.290.5498.1910.

Thesis Conclusions

The above-presented case studies testify how the multidisciplinary approach, combining morphometry, structural and geophysics methodologies, allowed to detect evidence of active faulting even where standard techniques usually fail. Such an approach grants the overcoming of the main factors that hamper the detection of "elusive" faults, such as:

a) A prominent structural inheritance:
   As in the first chapter, a morphometric approach allows detecting evidence of deformation even in an area where the youngest field stratigraphic and structural evidence of deformation can be ascribed to the Miocene period.
b) Fault slip rate of the same order of magnitude as the erosion rate:
   As in the first chapter, a morphometric approach allows detecting evidence of deformation even in lithologies not capable of preserving any fault morphological signature.
c) Active structures can be blind:
   As in the third chapter, a morphometric approach allows detecting evidence of deformation of blind structures.
d) Partially offshore active structures:
   As in the fourth chapter, a morphometric approach proved to be applicable even in offshore landscapes.

It is essential to state that no standard, easily followable set of instructions allows the detection of active structure in every landscape and environment, even if some approaches are better than others. Nevertheless, some "suggestions" can be used as *good practice*, such as:

a) Always look for active deformation instead of active tectonics.
   Evidence of deformation is almost always evidence of active processes in the area, and mainly if characterized by long wavelengths, the chances of misinterpretation are considerably lower than stratigraphic-structural field evidence of active faulting.
b) Always know the erosive and sedimentary processes of the studied environment.
   The key to deciphering the deformation evidence in the studied landscape lies in its active erosive and sedimentary processes and in the "anomalous" areas that are not characterized by such processes.

Finally, the use of independent variables to verify the results to look at the same process from different points of view is almost the only way to discover the "smoking gun" that testify active faulting processes in an area.